DEPARTMENT OF RADIOLOGY – UNIVERSITY OF SOUTHERN CALIFORNIA

2009 Annual Report

Image Processing and Informatics Laboratory

1450 San Pablo Street, DEI 2100, Los Angeles, CA 90033. Tel: (323) 442-7050. Fax: (323) 442-7021

SUMMARY

With the backdrop of historical change that our nation is encountering, the Image Processing and Informatics Laboratory (IPILab) has also undergone change this last year – although not as dramatic but equally as significant related to medical imaging research. The lab has traded gorgeous sunset views of Marina del Rey for a more closer integration on the Health Science Campus, USC and its clinical academic research activities in April of 2008. Our new lab location is housed in the Doheny Eye Institute located in the hub of major clinical healthcare and research facilities such as the University Hospital, Healthcare Consultation Centers I and II, Norris Cancer Center, and the Zilka Neurogenetic Institute. We held an Open House event shortly after moving in and if you missed it, you are still welcome to drop by anytime for a personalized tour. Details about our new location and the Open House event are included in the succeeding pages of this annual report. In 2008, with the new location, IPILab has continued to receive research support; encountered expanded growth in scientists and new clinical collaborations while solidifying and bridging the gap between clinical and engineering sciences. Some of the accomplishments are detailed:

1. Education and Training

In June 2008, past and present trainees from our T32 Training Grant from the National Institute of Biomedical Imaging and Bioengineering (NIBIB), National Institutes of Health (NIH), DHHS entitled: "Biomedical Imaging Informatics Training Program" effective September, 1, 2005 – August 31, 2010, totaling about US$1.6 million, attended the biennial conference for all T32 training programs across the country in Washington, DC. Dr. Brent Liu, coordinator of the training program and all current trainees also participated in the conference. They presented their research work and networked with other faculty and trainees from the various programs. The PI and Co-PI are Dr. H.K. Huang of Radiology and Biomedical Engineering Departments (BME) and Dr. Michael Khoo of BME, respectively. Dr. Huang was invited to speak on the significance and impact of Medical Imaging Informatics in research and education. Existing trainees continue receiving national recognition as first author in national presentations, proceedings papers and peer-reviewed chapters and papers. We successfully recruited two additional T32 Postdoctoral Fellows, 1) Richard Lee, graduating from our own neighborhood of the Keck School of Medicine and is applying to the USC Radiology Residency Program and 2) Murali Krishna Meka, M.D., who received his residency training in Nuclear Medicine from St. Luke's Roosevelt Hospital, New York and is now completing a Fellowship in Nuclear Medicine, USC. Two current USC BME Ph.D. students are continuing the program. Two Postdoctoral Fellows from the USC Radiology Residency Program, Drs. Paymann Moin and James Fernandez and one USC BME Ph.D. student, Anika Joseph, M.S. have completed their training. The two MD's plan to continue their research while finishing up their Radiology Residency while the Ph.D. student will take her training and continue her work at Cedars Sinai Hospital by applying it to her thesis topic in the field of optical imaging.

The USC Summer Undergraduate Research Programs continue to fund our efforts to recruit and to foster bright young undergraduate students searching for future academic research directions. This last summer we were able to recruit four undergraduate students from the BME program. This program continues to be important bedrock for the future of Medical Imaging Informatics research. Two of them have remained as Student Assistants in IPILab after the summer.

Other new additions to our lab, which are a direct result of being closer on the Health Science Campus include, Robert Leiberman, a medical student intern, Gautham Raghavendhar, Ruchi Deshpande, and Hanyi Chrisman, all Master's student interns from the BME graduate program.

In addition to the milestones mentioned above in the T32 training program, Dr. Aifeng Zhang completed her Ph.D. in BME and a Post Doctoral fellowship with IPILab and has taken a research scientist position at UC San Francisco. Dr. Brent Liu has accepted the position as co-Chair for the "Advanced PACS-based Imaging Informatics and Therapeutic Application" Conference of the SPIE Medical Imaging Conference.

2. Research Projects

We have continued in our new areas of Medical Imaging Informatics research: 1) a DICOM-RT based ePR system with Decision Support for Managing patients treated with Proton Beam Therapy; 2) CAD for Neurological Pathologies including Multiple Sclerosis detection and management on MRI, small Acute Intracranial Hemorrhage detection on CT, and image-based in characterization of ischemia and hemorrhage in stroke patients; 3) CAD-PACS Integration Toolkit; 4) A surgical ePR system for Image-Assisted Minimally Invasive Spinal Surgery (MISS), the prototype system is under clinical evaluation; and 5) Clinical validations of bone age assessment of children. The DICOM-RT ePR system had two papers accepted for publication in Radiographics, and CAD bone age assessment work were published in Radiology directly resulted from 2007 RSNA presentations. We enjoyed another successful RSNA conference in November 2008 with a total of twelve presentations. Other existing long term research projects such as the Data Grid have continued to progress, and have expanded clinical applications in imaging-based clinical trials, small animal imaging, and Breast Cancer imaging. We have participating clinical sites for the Bone Age Assessment research including children from Women's and Children Hospital, USC; Hong Kong; Pisa, Italy; Tehran, Iran; and Taiwan. Some of the research work continues to be supported by extramural finds including NIH, U.S. Army Medical Research and Materiel Command, and the private industry.

3. Industrial Collaborations

IPILab has continued R & D collaborations with the private industry including but not limited to: Fujifilm, USA in the development of PACS tools; Cedara in their PACS workstation display software; Calgary Scientific, Inc. in 3-D thin-client server system; and SurgMatix, USA in the development of an ePR System for minimally invasive spinal surgery; and Global Care Quest, Inc. in providing PACS and DICOM expertise for product validation. We are also in communication with multiple manufacturers for collaborations in our various existing research products.

As described in the Table of Contents, this 2009 Annual Report includes materials related to the new IPILab location, IPI R & D plans and current results, selected published and in-press peer-reviewed papers during the year, as well as preprints to appear in the Proceedings of the International Society for Optical Engineering (SPIE) in Medical Imaging, Orlando, Florida, February 8-13, 2009.

Our research has been supported by:

- NIH/NIBIB R01 EB 00298
- NIH/NLM Training Grant T15 LM07356
- NIH/NIBIB Biomedical Imaging Informatics Training Grant T32 EB 00438
- USAMRMC/Henry M. Jackson Foundation Subaward 53-5149-5600
- USAMRMC/TATRC AAMTI Subaward 2007011185
- USC Undergraduate Research Award No. 22-2149-6044
- USCRA Research Fund 3051-00
- Array Corporation, Japan
- Fujifilm, USA
- MI2, USA
- SurgMatix, USA
- Global Care Quest, Inc, USA

TABLE OF CONTENTS

STAFF AND COLLABORATORS

Faculty and Administrative	
Edward V. Grant, M.D., FACR. Professor and Chairman, Department of Radiology **H.K. Huang, D.Sc., FRCR (Hon.), FAIMBE** Professor of Radiology and BME Chair Professor of Medical Informatics, Hong Kong Polytechnic University; and Honorary Professor, Shanghai Institute of Technical Physics, The Chinese Academy of Sciences Director, IPILab **James William Hill, M.D., J.D.** Clinical Assistant Professor Department of Radiology **James Sayre, Ph.D.** Professor of Biostatistics and Radiological Science, University of California, Los Angeles (UCLA) Consultant **Cammy Huang, Ph.D.** Lecturer, Computer Science Dept, Director of Scientific Outreach, WGLN Stanford University Consultant **Angelica Virgen** Administrative Assistant	**Michael C.K. Khoo, Ph.D.** Professor and Chairman, Department of Biomedical Engineering (BME) **Brent J. Liu, Ph.D.** Associate Professor of Radiology and BME Deputy Director, IPILab **Greg T. Mogel, M.D.** Associate Professor of Radiology, Asst Prof. of BME **Ewa Pietka, Ph.D. D.Sc.** Professor, Technical University of Silesia, Poland Visiting Professor of Radiology **Jianguo Zhang, Ph.D.** Professor, Shanghai Institute of Technical Physics, The Chinese Academy of Science Visiting Professor of Radiology **Maria YY Law, MPhil, BRS, Ph.D.** Associate Professor, Hong Kong Polytechnic University President, Hong Kong College of Radiography and Radiation Therapy Visiting Associate Professor of Radiology **Heinz U. Lemke, Ph.D.** Technical University Berlin Visiting Research Professor of Radiology
Post Doctoral/Visiting Fellows	**NIH T32 Post/Pre Doctoral Fellows**
Aifeng Zhang, Ph.D. **Tao Chan, M.D., Ph.D.** Assistant Professor, Department of Radiology Hong Kong University **Marco A. Gutierrez, Ph.D.** Invited Professor Heart Institute of University of San Paulo Visiting Distinguished Research Fellow **Christina Chia-Fen Tsai, M.D.** Department of Psychiatry, Taipei Veterans General Hospital Visiting Scholar, Department Neurology **Mark W. Haney, M.D.** USC Provost Fellow, Ph.D. Candidate	**Paymann Moin, M.D.** Radiology Fellow **James Fernandez, M.D.** Radiology Resident **Jasper Lee, M.S.** Ph.D. Candidate **Kevin Ma, B.S.** Ph.D. Candidate **Anika Joseph, M.S.** Ph.D. Candidate
Research Assistants	**Medical/Graduate Students**
Anh Le, M.S., Ph.D. Candidate **Sinchai Tsao, M.S.,** Ph.D. Candidate **Heston K. Kwong, M.D., MBA. M.S.,** Ph.D. Candidate Hong Kong Polytechnic University **Jorge Documet, M.S.,** Ph.D. Candidate Lab Manager	**Richard Lee, B.S.** Medical Student **Robert Lieberman, M.S., MBA** Medical Student, Saint Louis University **Hanyi Chrisman,M.S.** Graduate Student
2008 USC Summer Students	
Jessica Liu **Ashley Sullivan**	**Mariam Fleshman** **Bharat Reddy**

IPILAB NEW LOCATION @ HEALTH SCIENCE CAMPUS

1450 San Pablo Street, Suite DEI 2100, Los Angeles, CA 90033

NETWORK CONFIGURATION & COLABORATIONS

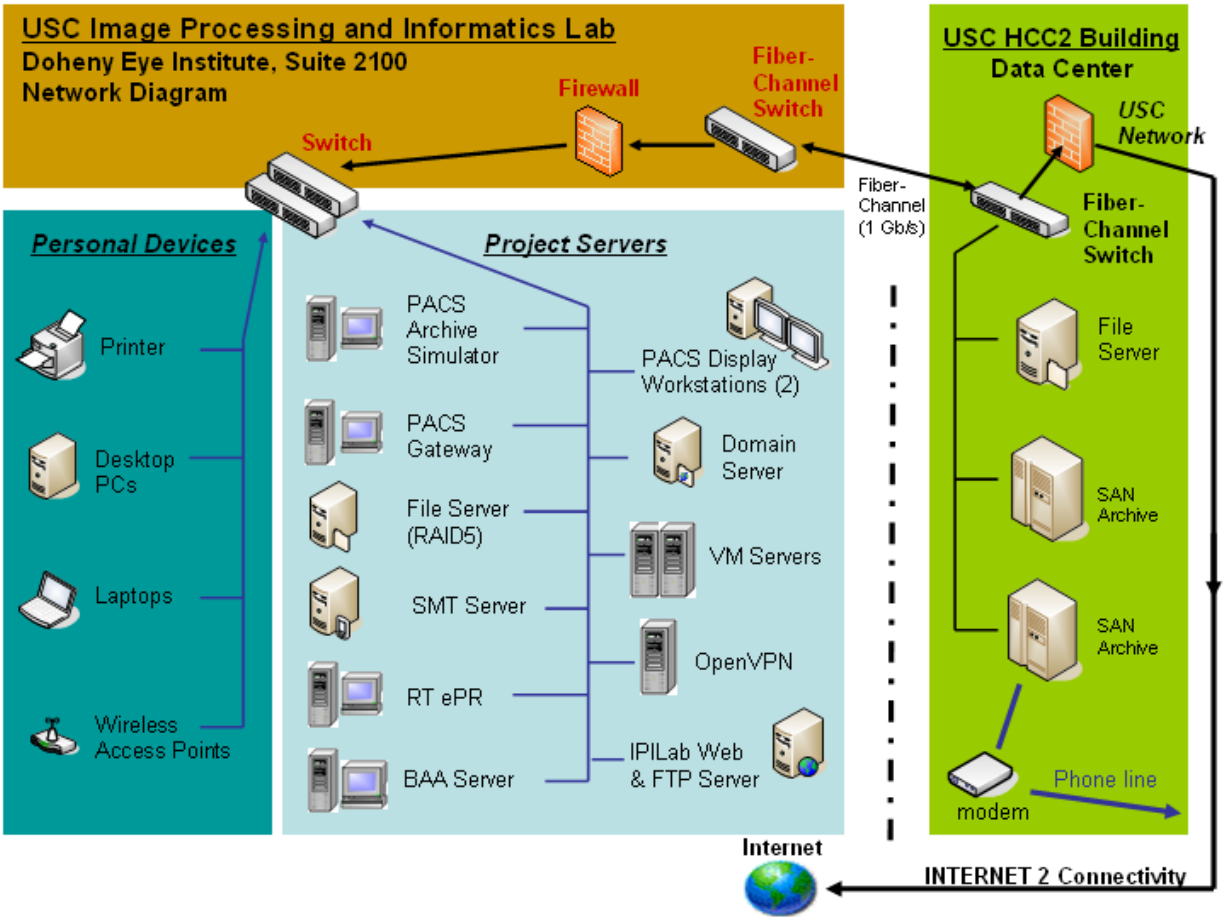

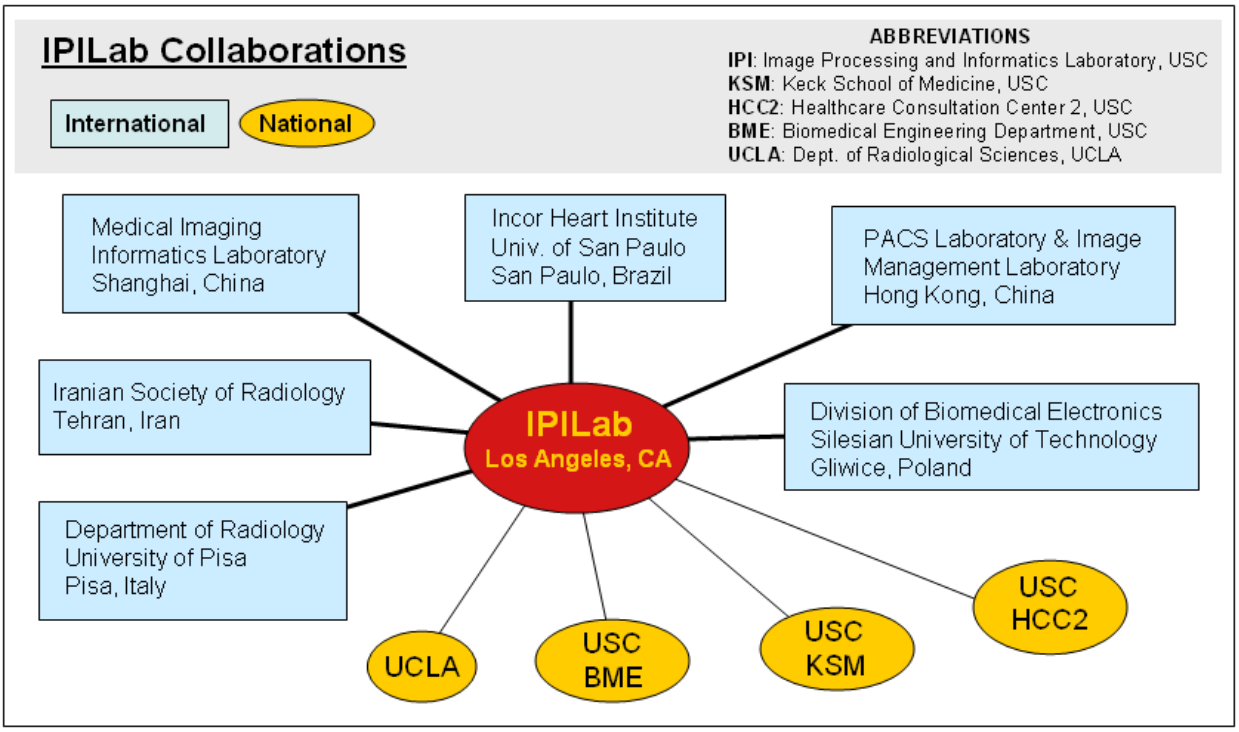

IPILAB WEBSITE

http://www.ipilab.org

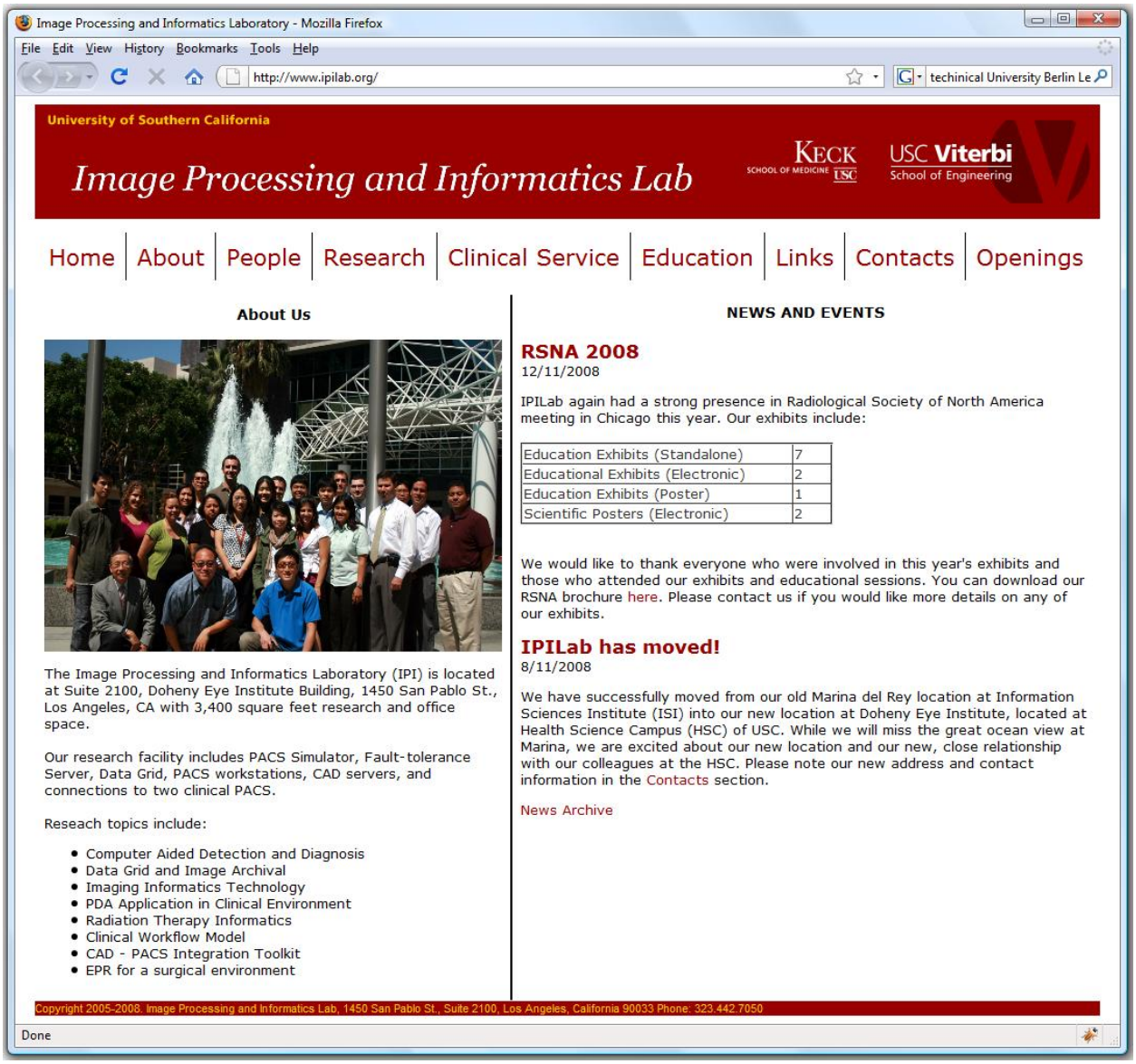

RSNA 2008 POSTERS & PAMPHLET

USC UNIVERSITY OF SOUTHERN CALIFORNIA

Image Processing and Informatics Lab

Extending Imaging Informatics beyond Radiology: The Development of an Image-intensive ePR for Image-guided Minimally Invasive Surgery Applications Including Real-time Intraoperative Image Acquisition, Archival, and Display

B Liu, PhD[1]; J Documet, MS[1]; MW Haney, MD[1]; A Le, MS[1]; S Tsao, MS[1]; K Wang[1], BS; John Chiu, MD, DSc[2]; HK Huang, DSc[1]

1 – Department of Radiology, Keck School of Medicine University of Southern California, Los Angeles, CA, USA

2 – California Spine Institute, Thousand Oaks, CA, USA

Learning Objectives:

1) **Integrate key imaging and informatics data during the pre, intra, and post-operative phases of clinical workflow.**
2) **Apply the ePR concept to Image-Guided Minimally Invasive Spinal Surgery (IG-MISS) cases.**
3) **Demonstrate a one-stop source system that improves clinical workflow efficiency and serves as a platform for future training and patient outcomes analysis.**
4) **Integrate a variety of still and real-time acquisition systems including X-Ray, CT, MRI, digital fluoroscopy and digital endoscopic video, and waveforms into the ePR.**

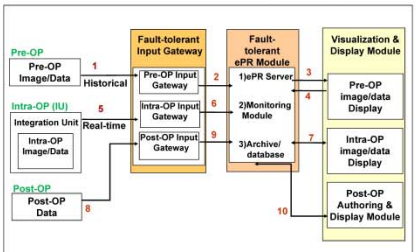

Dataflow of the IG-MISS ePR System

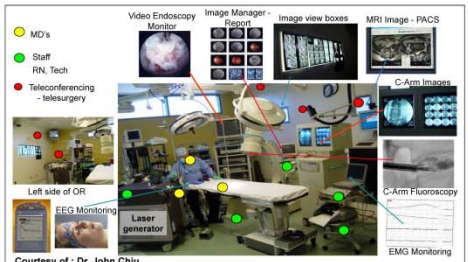

Existing Operating Room (OR) Layout

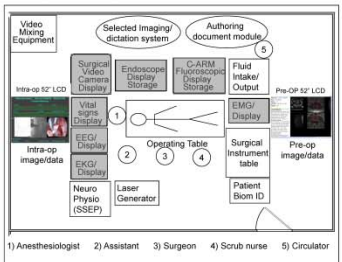

Future OR Layout w/ ePR System

Workflow Stages

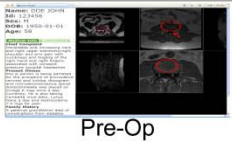

Pre-Op

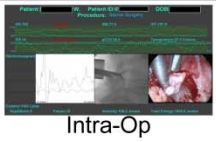

Intra-Op

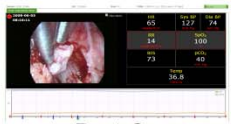

Post-Op

This project is supported by SurgMatix

USC UNIVERSITY OF SOUTHERN CALIFORNIA

Image Processing and Informatics Lab

theViewbox.com: A Tool for Radiology Web-based Content Management and Personalization

P Moin, MD[1]; J Documet, MS; JF Fernandez, MD[1]; BJ Liu, PhD

IPILab, Department of Radiology, Keck School of Medicine, University of Southern California, Los Angeles, CA, USA

1 - Trainee of NIH T32 EB00438 "Biomedical Imaging Informatics Training."

- organized format
- several content types
- social network features

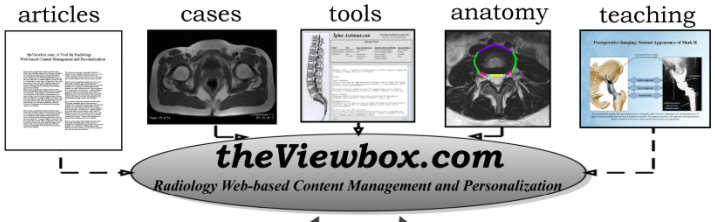

- web-based
- intelligent bookmarks
- customizable

BACKGROUND

Educational material, reference resources, articles, images, cases, and radiology search engines have made for a rich, but dizzying volume of web-based resources. We introduce a website to manage and personalize the growing number of resources. Web resources are organized by modality and body region. Within each subheading are descriptive bookmarks for several content types.

Individual user personalization and management

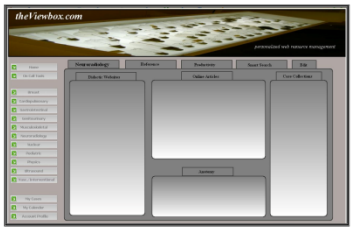

THIS PROJECT

This organized, customizable website is presented as a tool for **radiology residents** and those in **private practice** to gather, manage, learn from and reference the growing number of internet-based radiology resources. A standard template is provided for each user with the ability to add, remove, or change any listing within their profile to better fit their needs.

USC UNIVERSITY OF SOUTHERN CALIFORNIA — IPILab Data Grid Project

Image Processing and Informatics Lab

Integration of Content-based DICOM-SR for CAD in a Medical Imaging Informatics Data Grid

Examples in CT Chest, Mammography, and Bone-Age Assessment

OVERVIEW

To utilize CAD radiological reporting, the Medical Imaging Informatics Data Grid incorporates CAD findings and DICOM key image referencing into its DICOM-compliant databases and services in the form of DICOM-Structured Report (SR) data objects. By supporting DICOM-SR of CAD algorithms, content-based query and retrieval of DICOM imaging studies can be performed based on quantitative findings rather than patient identification and/or disease category. The advantages of query/retrieving anonymized yet content-based imaging data from a virtualized grid infrastructure can be a great benefit for medical imaging research and imaging-based clinical trials.

BACKGROUND

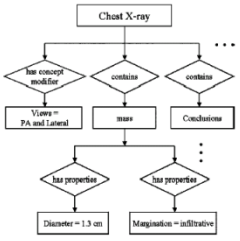

A DICOM Structured Report for Chest CAD (ref. PS 3-16 2008)

The Image Processing and Informatics Lab at the University of Southern California does research in radiological computer-aided detection and medical imaging informatics research. To archive, distribute and utilize results generated by multiple CAD algorithms, a standard reporting format and archiving method was needed. The DICOM Structured Report, defined in 2001, has established templates for Chest and Mammography CAD-generated reports, and is adopted into our lab as a flexible solution.

The Medical Imaging Informatics Data Grid is a DICOM file archiving and distribution infrastructure based on the Globus Toolkit. It incorporates DICOM compatibility with grid-based file management and secure file transfers for multi-site collaboration in medical imaging informatics research as well as imaging-based clinical trials.

METHODOLOGY

1) Support CAD Structured Reports in the DICOM-Services layer of the Data Grid.
2) Extend Data Grid's database for CAD SR content within a DICOM-modeled schema.
3) Design a recursive algorithm to extract content-of-interest from CAD Structured Reports using a novel knowledge-based approach and the DICOM standard.
4) Implement web-based client interfaces to allow **remote data-mining for Structured Reports and Images** archived in the Data Grid by quantitative findings, rather than patient identifiers or study UID's.

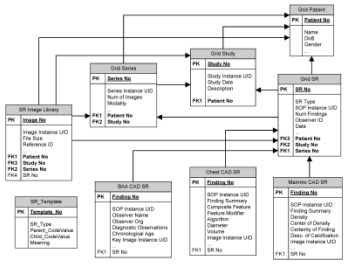

DICOM Metadata & Structured Report Database Schema

SYSTEM WORKFLOW

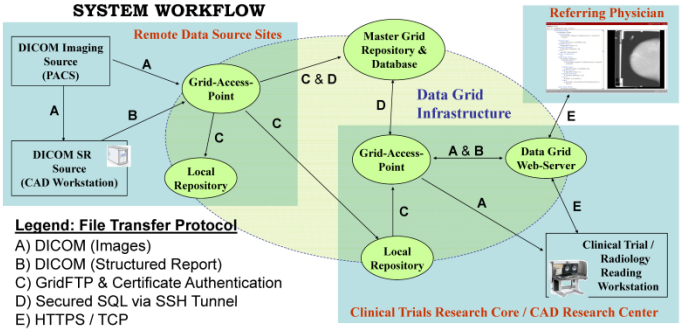

Legend: File Transfer Protocol

A) DICOM (Images)
B) DICOM (Structured Report)
C) GridFTP & Certificate Authentication
D) Secured SQL via SSH Tunnel
E) HTTPS / TCP

RSNA 2008, McCormick Center – Lakeside Learning Center

This Research is Funded in Part by T32 EB00438 and MII Corp.

USC UNIVERSITY OF SOUTHERN CALIFORNIA

A Radiology Dashboard Integrated with RFID Location System

J Documet, BS[1]; B Liu, PhD[1]; K Wang[1]; R Lee, BS[1]

1 - Department of Radiology, Keck School of Medicine University of Southern California, Los Angeles, USA

Learning Objectives:

- **Real-time clinical and workflow metrics.**
- **Display of related reports from the RIS.**
- **Display of the location of patients with the waiting times that were collected in the different areas inside a clinical facility while a procedure was performed.**
- **Display of the location of staff to more quickly assess who is the most appropriate person to contact in the clinical facility, ie. tech support.**

Track the patient while procedure is performed

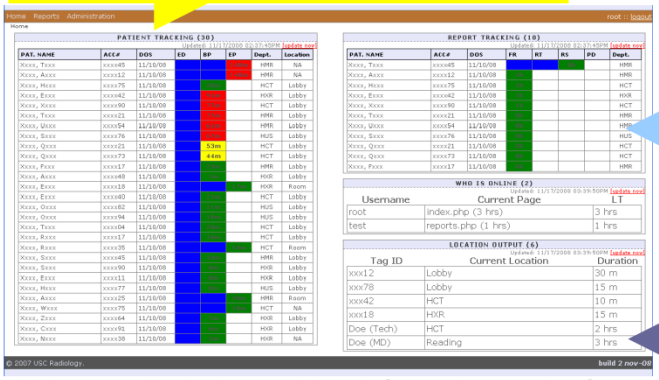

Track the status of the reports

Location Module for patients and staff

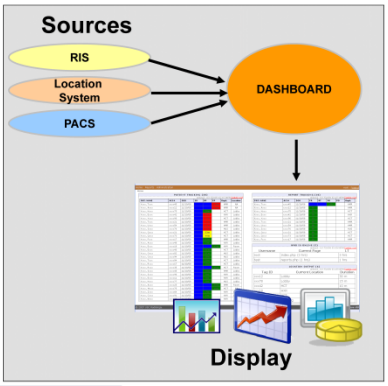

Main page displaying real-time information coming from different systems

USC UNIVERSITY OF SOUTHERN CALIFORNIA

Image Processing and Informatics Lab

Computer-Aided Detection System for Acute Ischemic Stroke on CT in Emergency Environment

K Ma, BS; A Le, MS; J Fernandez, MD; T Chan, MBChB; B Liu PhD; HK Huang DSc, J. Liu.
Image Processing and Informatics Lab, Department of Radiology, Keck School of Medicine, University of Southern California, Los Angeles, CA 90033

Background:

• A patient suspected of stroke arrives in ER and needs a timely diagnosis (within 6 hours)

• CT is used to rule out hemorrhagic stroke, but non-neuroradiologists may not correctly diagnose acute ischemia from CT non-contrast brain images.

• IPILab's AIH CAD is able to detect hemorrhages, but only 20% is hemorrhagic, while around 80% of stroke is ischemic

• Neuroradiologists may not be readily available in ER to correctly diagnose ischemic stroke

Proposed Solution:

A CAD system to detect subtle signs of acute ischemic stroke on CT images to aid emergency physicians and non-specialized radiologists during the first hours of the Patient encounter for timely diagnosis

• Algorithm is based on the existing AIH CAD program in IPILab, and can be integrated later for a complete brain CT CAD package

Potential Stroke signs:

- •Hyperdensity of MCA
- •Sulci effacement
- •Regional Hypodensity
- •Midline shift
- •Symmetry matching
- •Loss of insular ribbon

Results:

• Algorithm is designed from confirmed subacute and acute ischemia cases

• Detection is currently focusing on micro-infarct changes

• Suspected small ischemic changes are marked and displayed

Lessons Learned:

• Computer–aided Detection of acute or subacute infarction, while useful, is not enough in diagnosing stroke on CT

• Future work include collecting confirmed ischemic stroke cases and their matched normal cases. Algorithms will be trained to detect positive stroke signs that are confirmed by neuroradiologists

Generalized CAD Workflow:

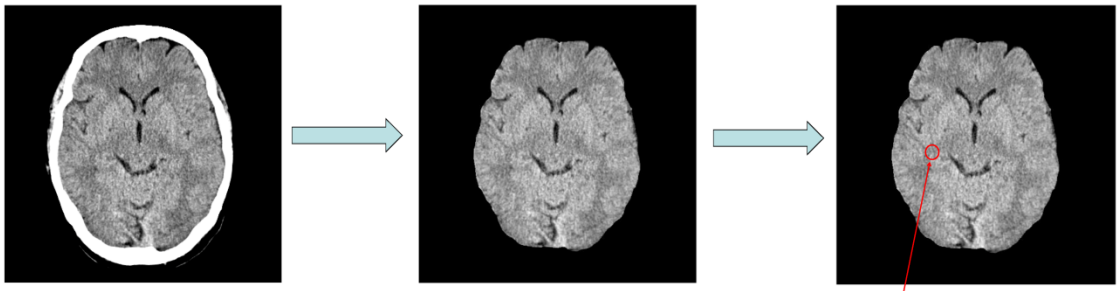

Original brain CT image — Segmented CT image — Identifying and locating micro-infarction

This project has been supported by NIH NIBIB T32 Training Grant EB00438

USC UNIVERSITY OF SOUTHERN CALIFORNIA

Image Processing and Informatics Lab

Automated Quantitative Analysis of MR Images of the Pelvic Hindgut and Its Correlation with Fecal Incontinence and Interventional Outcomes

Mark W. Haney, MD, MS, Anika Joseph, MS, Haig Dudugian, MD, Brent J. Liu, PhD

Learning Objectives

•Identify Anal Canal Structure
•Understand mechanisms underlying fecal incontinence
•Understand how MRI may be used to find fecal incontinence pathology
•Learn how Computer-Aided Diagnosis may be used to quantify function from MRI
•Understand how fluid mechanics can predict potential regions of weakness

Background: The second leading cause of elderly admission to long-term care facilities is fecal incontinence and it effects between 0.3 to 5% of the general population. Prior studies have evaluated imaging techniques including 3D ultrasound (US) and computed tomography (CT) to define gross anatomic defects such as tears in the wall but thus far have been unable to better delineate patients who will have a successful outcome. Recently, some magnetic resonance imaging (MRI) techniques appear to be able to delineate greater soft tissue specificity compared with US and CT.

CAD Algorithm Workflow:

Stage 1: DICOM Loaded. Candidate slices selected based on slices beginning with the presence of Acetabula until the beginning of the coccyx.

Stage 2. The location of interest is narrowed by an assumption that the canal lies midline and approximately 2/3 posterior.
Stage 3: Image is analyzed with Zero Crossing edge detection to find inner and outer edges of the canal.

Stage 4: Image Histogram analyzed to create thresholds for background, adipose / other tissue and muscle. Thresholds used to further refine edges. A missing inner or outer ring is recreated based on gradient edge detection filtered by the muscle threshold value.

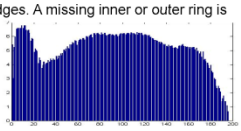

Stage 5a: Rays are projected from the center out for 360 degrees to determine mean wall thickness and radius. Wall thickness is weighted by a Gaussian distribution with a mean halfway between the muscle threshold and the maximum intensity.

Stage 5b: Wall pressure is calculated for the inner wall by Navier-Stokes Equation derived for a cylinder. Muscle Force is calculated by the weighted value and the known force of muscle.

General Equation

$$\rho\left(\frac{\partial \mathbf{v}}{\partial t} + \mathbf{v}\cdot\nabla\mathbf{v}\right) = -\nabla p + \mu\nabla^2\mathbf{v}$$

Cylinder Equation $\frac{1}{r}\frac{\partial}{\partial r}(ru_r) + \frac{1}{r}\frac{\partial u_\theta}{\partial \theta} + \frac{\partial u_z}{\partial z} = 0.$

Stage 6: Possible weakness is determined by a mismatch of force and pressure by at least 10mmHg. Incontinence is determined to be a region of weakness of at least 90 degrees continuously or a mean mismatch in 50% of the canal area. Either must be in two contiguous slices.

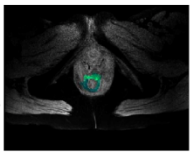

Discussion: This study illustrates the feasibility of combining the soft tissue sensitivity of MRI with the consistent measurement by a computer to measure the forces which are exerted on the anal canal. By using the forces generated against the wall compared to the estimated physiological force generated by the sphincters, the system is able to demonstrate regions which are prone to weakness.

These measurements are being followed to determine whether they are predictive of surgically confirmed pathology and subsequent successful anoplasty

Conclusion: MRI, with its greater soft tissue specificity, in conjunction with computer analysis of the anal canal's muscular features can help predict between successful and non successful outcomes.

Acknowledgement: Supported by University of Southern California Provost Fellowship and NIH T32 Medical Imaging Informatics Grant EB00438

USC UNIVERSITY OF SOUTHERN CALIFORNIA

Image Processing and Informatics Lab

Spine Assistant: *A Tool to Efficiently Generate Spine Reports*

P Moin, MD[1]; AH Le, MS[1]; J Documet, MS[1]; BJ Liu, PhD[1]
SK Antani, PhD[2]; LR Long, MA[2]
1- IPILab, Department of Radiology, Keck School of Medicine, University of Southern California, Los Angeles, CA, USA
2- Communications Engineering Branch, National Library of Medicine, Bethesda, MD, USA

clickable structures open anatomy-specific menus to **reduce repetitive reporting**

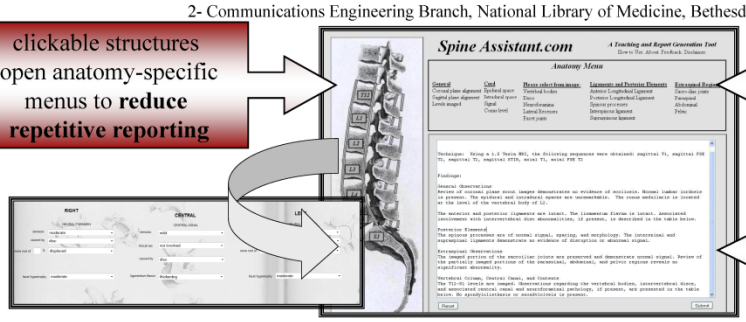

interactive anatomy menu as a **guide to study interpretation**

real-time report generation and editing using **Task Force accepted terms**

OBJECTIVES

1)To increase the correct use of accepted descriptions of disc pathology through use as an **educational tool** in the training of radiology residents and as a **reference** for those in practice.

2)To quickly and efficiently **generate well-organized reports** that clearly communicate pathology. Simple measurement and classification tools in graphical format with easily referenced schematics to teach or clarify preferred correct disc nomenclature and pathology are provided. Early results with our institution's fellows are promising.

BACKGROUND

Evaluation and reporting of spine imaging is a tedious process with specific reporting requirements. In practice, accepted descriptive terminology is not always followed in reporting. This creates the potential for miscommunication and errors both in reporting and clinical management. We introduce a web-based report generation tool to quickly, systematically, and efficiently produce spine reports that are compliant with accepted nomenclature and classification of disc pathology.

Paymann Moin, MD is a trainee of NIH T32 EB00438 "Biomedical Imaging Informatics Training."

PROJECT DESIGN

In 2001, the Combined Task Force of the North American Spine Society, American Society of Spine Radiology, and American Society of Neuroradiology released a consensus document entitled "Nomenclature and Classification of Lumbar Disc Pathology" in an effort to standardize the language of reporting spinal imaging findings. We use the definitions and guidelines set forth in this paper to construct a web-based program in a graphical format to quickly generate reports compliant with Task Force descriptions. This site can currently generate lumbar spine reports and is available at www.SpineAssistant.com.

Optimization and Management of User Registration and HIPAA-Compliance in a Clinical PACS Environment by integration with a HIPAA-Compliant Auditing Toolkit

B Guo, MD[1] (bguo@usc.edu); J Lee,MS[2]; B J Liu[2], PhD; K Wang[1]
1 Department of Radiology
2 Image Processing and Informatics Lab, Dept. of Biomedical Engineering
University of Southern California, Los Angeles, CA

BACKGROUND

USC Health Science Campus is supported by an enterprise PACS with four hospital sites – UH (University Hospital), Norris (Cancer Center), HCC2 (Healthcare Consultation Center 2), LAC+USC (Los Angeles County General Hospital). The radiology staff and referring physicians require log-in access to any of the PACS data. However, policies and procedures dictate a written HIPAA Form to the PACS IT support team before log-in access is granted. This HIPAA Form is mandated to expire within a given period of time.

The workflow for requesting accounts for PACS log-in access are as follows:

1) The user contacts a PACS administrator via phone or email to request login access.
2) The PACS administrator emails an electronic copy or faxes a HIPAA form (Figure A) to the requesting user.
3) The user fills out form with required information, then obtains a signature from his/her supervisor, and faxes the form back to the PACS administrator.
4) Upon receipt, the PACS administrator creates a username and password for that user and emails the log-in access information including additional system user guide back to the requesting user.
5) The paper form is stored for records.

Figure A

With the myriad of user types and hundreds of users for the PACS support team to manage across the department's multiple healthcare systems, it is difficult to process these HIPAA Forms in a timely fashion and keep user accounts valid upon expiration. Furthermore, the turn around time for users to obtain a username and password for access into the PACS is about 72 hours. If the form gets lost in the workflow, or there is some delay in the workflow, it may take even longer for the user to have access to the PACS. In another scenario, the PACS administrator may need to spend additional time to decipher a user's first name and last name due to poor handwriting and/or missing information. These kinds of problems may seem very minimal but actually become a major challenge when multiplied by the many daily requests (about 30 requests per month). This slows down turn around time for creating the username and password and potentially violating HIPAA requirements.

In order to address these problems, an online registration GUI has been designed and developed. The online registration GUI is integrated into a HIPAA-Compliant Auditing Toolkit which extracts information from log files of various PACS components into an auditing database. The challenges of user registration efficiency, HIPAA authorization and auditing are presented in this electronic workflow solution.

WORKFLOW

The following steps demonstrates the electronically improved registration workflow ,

1) User goes to the registration GUI page, and chooses either to request a new PACS log-in account or to request an existing username and password by email. (Figure B).
2) If the user requests a new account, they enter in their personal information and supervisor's name and USC email address, and submits the form online (Figure C).

Figure B

3) If that account does not yet exist, the registration database gets updated with the user's information.
4) A USC-only email is sent to the supervisor with a link to verify their approval, which is reflected into the database via a server-side script.
5) PACS administrator receives an email upon supervisor approval and logs into the registration GUI page (Figure D) where a table of supervisor-approved requesting users can be seen.
6) If valid, the PACS administrator will create an account in the PACS system, and click the "create" button to input the username, password and expiration date into the GUI for record. The insert date and PACS administrator name will also be recorded automatically.
7) Upon creation, an email will be sent to the requesting user with the username, password, and electronic copy of the PACS user guide.
8) A HIPAA-Compliant Auditing System (H-CAS) developed at the Image Processing and Informatics Lab, USC is integrated with this web-based registration system's database and will confer user log-in accounts with the expiration dates to generate audits and alerts (Figure F). Furthermore, emails will be sent out to users and PACS administrators of expired users trying to log-in.

Figure E

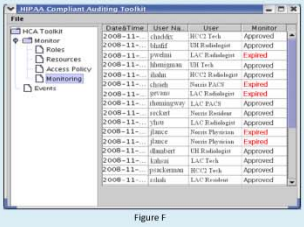

Figure F

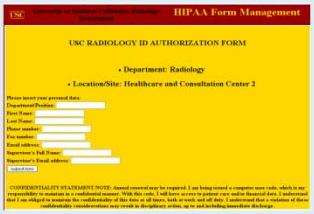

Figure C

Figure D

CONCLUSION

A web-based HIPAA authorization and auditing system allows the PACS support staff in a large radiology environment to manage new user requests online rather than via faxed sheets of paper. Furthermore, the system database allows the staff to monitor account privileges and user activity across multiple healthcare information systems. Automatic email notification is also developed for users with expiring HIPAA authorization forms to make sure periodic renewals of PACS account passwords and HIPAA rules are actually met. This saves the PACS administrators from going through hundreds of paper forms to keep passwords HIPAA-complaint. In addition, this GUI integrates with an auditing system to provide rules-based alerts based on actual PACS user log-in activity.

Current evaluation of the this web-based HIPAA authorization and auditing system is on-going for considering average turn-around-time, the number of lost requests for PACS accounts, and the number of PACS account expirations per month. The statistical analysis data will be collected from the H-CAS database which is integrated with the GUI.

This poster proposed an electronic system and workflow that can help a PACS support team to better communicate, monitor and manage its healthcare information system. by allowing PACS users to submit their HIPAA statements of confidentiality forms online, paper-work is reduced, PACS account creation turn-around-time is reduced, and HIPAA-compliance is increased. In addition, the HIPAA authorization and auditing system is linked to a HIPAA-Compliant Auditing System (H-CAS), which is a rules-based alert generation system that sends out automatic email notifications to users and PACS administrators when expired users tries to log into PACS .

RSNA 2008 – McCormick Convention Center, Chicago, IL

UNIVERSITY OF SOUTHERN CALIFORNIA

Image Processing and Informatics Laboratory

Department of Radiology, Keck School of Medicine

Education Exhibits & Presentations RSNA 2008

November 30 – December 5, 2008
McCormick Place, Chicago, Illinois

RSNA2008 Personal Learning in the Global Community

USC Viterbi School of Engineering

KECK SCHOOL OF MEDICINE USC

1450 San Pablo St. Suite 2100
Los Angeles, CA 90033
Tel: (323) 442-7050
Fax: (323) 442-7021
http://www.ipilab.org

WELCOME

Dear Colleagues and Friends of IPILab,
Welcome to another exciting year of IPILab's presentations and exhibits at RSNA 2008.

This year we are presenting:

Education Exhibits (Standalone Presentation)	7
Education Exhibits (Electronics Presentation)	2
Education Exhibits (Poster)	1
Scientific Posters (Electronics Presentation)	2

Two large screen presentation:

Tuesday December 02, 2008 - Scientific Poster
12:15PM - 1:15PM ROOM Lakeside Learning Center 07
An Online Real-time DICOM Web-based Computer-aided Dagnosis (CAD) System for Bone Age Assessment (BAA) of Children in a PACS Environment: Clinical Validation Cross-Racial Discrepancies of Growth Patterns in Bone Age Assessment
Kevin C Ma, BS, Los Angeles, CA; A Zhang, PhD; M Fleshman; L A Vachon, MD; B J Liu, PhD; H K Huang, DSc; et al.

Wednesday, December 03, 2008 - Scientific Poster
12:15PM - 1:15PM ROOM Lakeside Learning Center 07
RadSearch: A RIS/PACS Integrated Retrospective Medical Image Retrieval Tool
Sinchai Tsao, MS, Los Angeles, CA; J Documet, MS; P Moin, MD; K Wang; B J Liu, PhD

Contents

STAFF AND COLLABORATORS

Faculty and Administration	
Edward V. Grant, MD, FACR Professor and Chairman, Department of Radiology	**Michael C.K. Khoo, PhD,** Professor and Chairman, Department of Biomedical Engineering (BME)
H.K. Huang, DSc, FRCR (Hon.) Professor of Radiology and BME Director, IPI	**Brent J. Liu, PhD** Associate Professor of Radiology and BME
Vicente Gilsanz, MD Professor of Radiology and Pediatrics	**Greg T. Mogel, MD** Assistant Professor of Radiology and BME
James William Hill, MD, J.D. Clinical Assistant Professor, Department of Radiology	**Ewa Pietka, PhD, DSc** Professor, Technical University of Silesia, Poland *Visiting Professor of Radiology*
James Sayre, PhD Professor of Biostatistics and Radiological Science, UCLA *Consultant*	**Jianguo Zhang, PhD** Professor, Shanghai Institute of Technical Physics, The Chinese Academy of Science *Visiting Professor of Radiology*
Cammy Huang, PhD Director of Scientific Outreach, Wallenberg Global Learning Network, Wallenberg Hall *Consultant*	**Maria YY Law, MPhil, BRS, PhD** Associate Professor, The Hong Kong Polytechnic University *Visiting Associate Professor of Radiology*
Angelica Virgen Administrative Assistant	**Heinz U. Lemke, Professor** Technical University Berlin *Research Professor of Radiology*
Postdoctoral and Visiting Fellows	
Paymann Moin, MD **Mark W. Haney, MD** **Tao Chan, MD, PhD** Hong Kong Polytechnic University	**Marco A. Gutierrez, PhD** Invited Professor, Heart Institute of University of San Paulo **Heston K. Kwong, MD, MBA, MS** PhD Candidate, Hong Kong Polytechnic University
Research Assistants & PhD Candidates	*Graduate Students/Medical Students*
Jorge Documet, MS **Anh Le, MS** **Jasper Lee, MS** **Kevin Ma, BS**	**Hanyi Wang, MS** PhD Student **Robert Liberman, MS, MBA** Medical Student **Richard Lee, BS** Medical Student
Undergraduate Trainees	
Meriam Fleshman	**Ashley Sullivan**
Past Research Collaborators	
Zheng Zhou, PhD ***Arkadiuz Gertych, PhD*** ***Alfeng Zhang, PhD***	**Anika Joseph, MS** **Sinchai Tsao, MS**

IPILAB NEW LOCATION @ HEALTH SCIENCE CAMPUS

1450 San Pablo Street, Suite DEI 2100, Los Angeles, CA 90033

IPILAB NETWORK LAYOUT & COLLABORATIONS

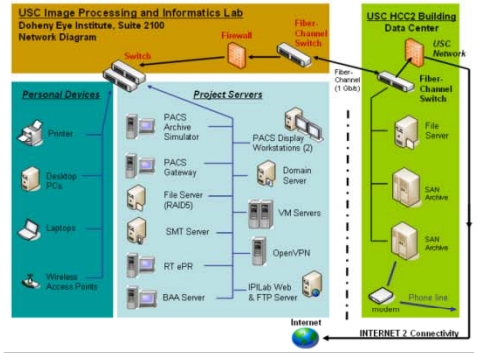

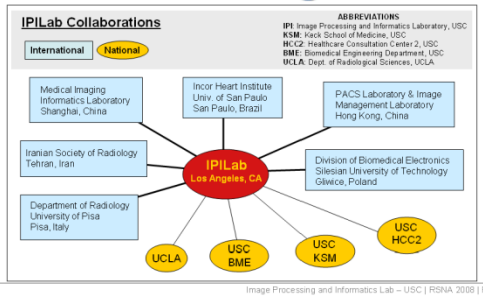

EDUCATION EXHIBITS – STAND ALONE PRESENTATIONS

LL- IN1062: Extending Imaging Informatics beyond Radiology: The Development of an Image-intensive ePR for Image-guided Minimally Invasive Surgery Applications Including Real-time Intraoperative Image Acquisition, Archival, and Display

B J Liu, PhD, Marina del Rey, CA; J Documet, MS; M W Haney, MD; A H Le, MS; S Tsao, MS; K Wang; et al.(brentliu@usc.edu)

BACKGROUND: Recent developments in medical imaging informatics have improved clinical workflow in Radiology enterprise. However, there still remains gaps in the clinical continuum from diagnosis to surgical treatment through post-operative follow-up that can be addressed by a variety of advanced technologies. One solution is the development of an electronic patient record (ePR) that integrates key imaging and informatics data during the pre, intra, and post-operative phases of clinical workflow. One application is in image-guided minimally invasive spinal surgery (MISS) where spinal discectomy procedures are performed for decompressing nerve roots affected by spinal disc protrusions. This procedure utilizes a variety of still and real-time acquisition systems including X-Ray, CT, MRI, digital fluoroscopy and digital endoscopic video. The integration of these data together with waveform and other related informatics data is necessary during the entire surgical procedure for evaluation, treatment planning, and review.

EVALUATION: An ePR system prototype has been developed based on lessons learned from imaging informatics research in Radiology applications including: clinical and data workflow modeling, system user requirements, DICOM compliance, and clinical evaluation. The ePR prototype has been implemented at a clinical site that performs image-guided MISS and evaluated for three months with over 100 patient cases.

DISCUSSION: The imaging informatics approach includes the development of such ePR system features as pre and post-operative authoring toolkits, intra-operative live displays, acquisition devices connectivity, and database storage management of imaging, waveform, and patient-centric informatics data. Results and statistical analysis of the 3 month clinical evaluation will be presented.

CONCLUSION: Extending the imaging informatics approach has yielded the development of an ePR that integrates emerging image-guided technologies for diagnosis and treatment of MISS surgical operations and acquisition of key data during the clinical continuum. The result is a one-stop source system that improves clinical workflow efficiency and serves as a platform for future training and patient outcomes analysis.

LL-IN1068: A Viewbox.com: A Tool for Radiology Web-based Content Management and Personalization

P Moin, MD, Los Angeles, CA; J Documet, MS; J F Fernandez, MS; B J Liu, PhD (pmoin@usc.edu)

BACKGROUND: There has been a rapid proliferation of medically related websites, especially those with a focus upon radiology. Many of these contain content designed for use by radiologists. Educational materials, reference resources, articles, images, practice cases, and radiology-centric search engines have made for a rich, but dizzying volume of resources. We introduce a web-based program to manage and personalize the continually growing number of informational resources.

EVALUATION: Web resources are organized by modality and body region. Within each subheading, applets contain descriptive bookmarks for several content types provided in an organized format for review including sites that highlight relevant anatomy, key articles, reference resources, unknown (practice) cases, reference cases, and search tools. A standard template is provided for each user with the ability to add, remove, or change any listing within their profile to better fit their needs. Radiology-centric sites as well as relevant sites from related specialties (eg. Wheeless' Textbook of Orthopeadics for the musculoskeletal radiology section) will be included.

DISCUSSION: The internet and the methods of organizing and communicating information which it allows are a valuable tool to learn or reference when learning more about a topic or reading a difficult case on call. As these resources proliferate and become more complex, a management tool is needed in order to organize and effectively use them. Radiologists in training and practice are increasingly incorporating web-based resources for learning and decision-support. TheViewbox.com is developed with the intent of being a tool to facilitate the management of these resources and to allow the continued expansion and complexity of these resources while still maintaining quick access to promote their use.

CONCLUSSION: We introduce an organized, customizable web-based program to allow radiology residents and those in private practice to easily manage and reference the growing number of radiology internet resources. To our knowledge, this is the first attempt to allow individual tailoring of the management and organization of access to desired web-based radiology resources.

LL-IN1105: A Timely Computer-aided Detection System for Acute Ischemic and Hemorrhagic Stroke on CT in an Emergency Environment

K C Ma, BS, Los Angeles, CA; A H Le, MS; J F Fernandez, MS; T Chan, MBChB; B J Liu, PhD; H K Huang, DSc; et al. (kevincma@usc.edu)

BACKGROUND: *When a patient is accepted in the emergency room suspected of stroke, time is* of the most importance. The infarct brain area suffers irreparable damage as soon as three hours after the onset of stroke symptoms. Non-contrast CT scan is the standard first line of investigation used to identify hemorrhagic stroke cases. However, CT brain images do not show hyperacute ischemia and small hemorrhage clearly and thus may be missed by emergency physicians. We reported a timely computer-aided detection (CAD) system for small hemorrhages on CT that has been successfully developed as an aid to ER physicians to help improve detection for Acute Intracranial Hemorrhage (AIH). This CAD system has been enhanced for diagnosis of acute ischemic stroke in addition to hemorrhagic stroke, which becomes a more complete and clinically useful tool for assisting emergency physicians and radiologists. In the detection algorithm, brain matter is first segmented, realigned, and left-right brain symmetry is evaluated. As in the AIH system, the system confirms hemorrhagic stroke by detecting blood presence with anatomical and medical knowledge-based criteria. For detecting ischemia, signs such as regional hypodensity, blurring of grey and white matter differentiation, effacement of cerebral sulci, and hyperdensity in middle cerebral artery, are evaluated.

EVALUATION: 25 confirmed cases with acute ischemic or/and hemorrhagic stroke with match normals have been collected for this study. For each case, the CAD results are matched with the initial diagnoses.

DISCUSSION: The CAD system is able to successfully detect signs of acute ischemia and hemorrhage in brain CT images. Potentially, the CAD system increases stroke detection speed and improves sensitivity and specificity in detecting acute ischemic and hemorrhagic stroke. The system provides opportunities for better timely stroke detection for patients in the emergency environment when a neuroradiologist may not be readily available.

CONCLUSION: The CAD system for acute stroke detection is can increase the accuracy of stroke detection by emergency physicians on CT. It can be useful for both clinical applications and educational purposes.

LL-IN1106: Automated Quantitative Analysis of MR Images of the Pelvic Hindgut and its Correlation with Fecal Incontinence and Interventional Outcomes

Mark W. Haney, MD; Anika Joseph, MS, Haig Dudukgian, MD, Brent J. Liu, PhD (mhaney@usc.edu)

BACKGROUND: The second leading cause of elderly admission to long-term care facilities is fecal incontinence which has a prevalence of 0.3 to 5%. Addressing the pathology of the fecal incontinence, an anoplasty may be performed but patient outcomes are highly variable. Prior studies have evaluated imaging techniques including 3D ultrasound and computed tomography to define gross anatomic defects in the wall but thus far have been unable to better delineate patients who will have resolution of their incontinence. Magnetic resonance imaging (MRI) techniques appear to be able to delineate soft tissue more specifically than US and CT. We discovered that in some cases, combining MRI with computer aided image analysis of the tissue components (adipose, fibrosis and specifically, the anal canal muscle and sphincters) has shown an indication of patients who were more likely to have a successful outcome after anoplasty. This paper describes this preliminary study.

METHODS: Thirty patients were retrospectively collected who underwent MR imaging of the pelvis as part of an evaluation of pelvic floor disorders. An image analysis system was developed which identifies the anal canal via local anatomy and anatomic characteristics of the canal itself. The program segmented the muscle from adipose external to the canal and feces internal to the canal. Radial projects from the canal's center are used to calculate a mean and variance of the thickness of the muscular wall. A second set of projects then identify regions which exist outside two standard deviations of the mean as muscularly weak regions. Finally, a 3-D plot combines the canal's muscle thickness along with the fluid stress exerted on the wall to provide the clinician with a visual means of identifying regions of muscle which are less likely to contribute to continence.

DISCUSSION: Wall thickness and fluid stress were analyzed with respect to the presence of confirmed anal canal muscle pathology and known patient outcome after anoplasty.

CONCLUSION: MRI, with its greater soft tissue specificity, in conjunction with computer analysis of the anal canal's muscular features can help predict between successful and non successful outcomes.

Acknowledgements: Mark W. Haney, MD is supported by the USC Provost Fellowship, and was a former trainee of the NIH T32 EB00430 "Biomedical Imaging Informatics Training". Anika Joseph, MS is supported by the NIH T32 EB00438: "Biomedical Imaging Informatics Training"

LL-IN1116: A Radiology Dashboard Integrated with RFID Location System

J Documet, MS, Los Angeles, CA; B J Liu, PhD; K Wang; R J Lee, BS (documet@usc.edu)

PURPOSE/AIM:

To develop a Physician's dashboard that will help improve the workflow processes in a radiology department, monitoring every stage of the clinical care process within radiology. An integrated location tracking interface using RFID (Radio Frequency Identification) will permit to know location of patients and staff inside the clinical facility.

CONTENT ORGANIZATION:

The development of an extensible, scalable and secure web-based Physician's Dashboard; that allows access to display:

- real-time clinical and workflow metrics,
- related reports from the RIS,
- the location of patients with the waiting times that were collected in the different areas inside a clinical facility while a procedure was performed,
- the location of staff to more quickly assess who is the most appropriate person to contact in the clinical facility, ie. tech support.

SUMMARY:

This exhibit implements a Physician's Dashboard for the Radiology Department that monitors ongoing clinical and workflow metrics. The real-time monitoring of the flow of the patient in the radiology department will use data entered in the RIS. Combining the above with the location of patients will add more powerful spatial information to better measure true waiting times for examinations. The primary users of the application will be administrative staff, technologists and PACS administrators.

LL-IN1123: Integration of Content-based DICOM-SR for CAD in the Medical Imaging Informatics Data Grid with Examples in CT Chest, Mammography, and Bone-Age Assessment

J Lee, MS, Marina del Rey, CA; A H Le, MS; B J Liu, PhD (jasperle@usc.edu)

BACKGROUND: The Medical Imaging Informatics Data Grid started at the IPILab in 2005 as a secure and DICOM-compliant Data Grid for backing up medical imaging exams in multi-site research and radiological environments. The Data Grid includes DICOM-compliant services and SQL databases to handle storage, query and retrieve requests from the radiological environment. It also utilizes middleware from the Globus Toolkit 4.0 for file transmission, replica location, and grid security. Additional features include HIPAA-compliant events auditing, data resource failover and recovery, requests buffering, and a web-based GUI for user access and Data Grid management. The Data Grid currently extends its application to support DICOM Structured Reports (SR) generated by select CAD methods.

EVALUATION: The Medical Imaging Informatics Data Grid has been deployed at the USC Health Science campus and also among international medical imaging research laboratories and hospitals. The DICOM-SR for CAD is being evaluated using examples in CT chest, mammography, and bone-age assessment within the lab environment for comprehensiveness of its content extraction algorithm and database, as well as the user GUI.

DISCUSSION: The integration of DICOM-SR into the Data Grid involves new database schemas, a DICOM-SR receiver, content extraction algorithms, and updated DICOM services. Storing DICOM-SR in the same Data Grid repository as the original DICOM images allows the Data Grid to extend its benefits of fault-tolerant replication and federated storage towards CAD development and potentially complex radiological reports.

CONCLUSION: Due to the more complex CAD and radiological reporting, the Medical Imaging Informatics Data Grid seeks to incorporate CAD findings and DICOM key image referencing into its DICOM-compliant databases and services in the form of DICOM-SR data objects. By supporting DICOM-SR of CAD algorithms, content-based query/retrieval of DICOM imaging studies can be performed based on quantitative findings rather than patient identification and/or disease category. The advantages of query/retrieving anonymized yet content-based imaging data can be a great benefit for medical imaging research and imaging-based clinical trials.

LL-IN1130: Spine Assistant: A Tool to Efficiently Generate Cervical and Lumbar Spine Reports

P Moin, MD, Los Angeles, CA; A H Le, MS; J Documet, MS; S Antani; R Long; B J Liu, PhD (pmoin@usc.edu)

BACKGROUND: Evaluation of the anatomy and pathology of cervical and lumbar spines is a tedious process with specific reporting requirements for each level. In practice, accepted descriptive terminology is not always followed in reporting. This creates the potential for miscommunication and errors both in reporting and subsequent clinical management.

EVALUATION: In 2001, the Combined Task Force of the North American Spine Society, American Society of Spine Radiology, and American Society of Neuroradiology released a consensus document entitled "Nomenclature and Classification of Lumbar Disc Pathology" in an effort to standardize the language of reporting spinal imaging findings. We use the definitions and guidelines set forth in this paper to construct a web-based program in a graphical format to quickly generate reports compliant with Task Force descriptions. Analogous terminology is then used in the generation of cervical spine reports.

DISCUSSION: Aims:
1) To increase awareness and correct use of accepted descriptions of disc pathology through use as an educational tool in the training of radiology residents and as a refresher for those already in practice.
2) To quickly and efficiently generate well-organized reports that clearly communicate pathology. Simple measurement and classification tools in graphical format with easily referenced schematics to teach or clarify preferred correct disc nomenclature and pathology are provided. Pertinent descriptions of discs at each level including selections for normal, developmental variants, degenerative lesions, herniations, etc. are generated.
3) To gather data for computer aided diagnosis (CAD). Imaging studies and the reports generated from them is being collected to develop a CAD function to identify and characterizedisc pathology to facilitate the quick and efficient generation of reports. The second step will be to put the report in DICOM-SR data format for integrating CAD results into a PACS-based clinical workflow.

CONCLUSION: We introduce a web-based report generation tool to quickly, systematically, and efficiently produce cervical and lumbar spine reports that are compliant with accepted nomenclature and classification of disc pathology.

EDUCATION EXHIBITS – ELECTRONIC PRESENTATIONS

LL-MK5234: Review of Hemipelvectomy Endoprostheses: What the Orthopedic Oncologist Wants to Know

P Moin, MD, Los Angeles, CA; C Allison, MD; E Ahlmann, MD; L R Menendez, MD; T J Learch, MD; E White, MD (pmoin@usc.edu)

PURPOSE/AIM:

The purposes of this exhibit are:
1) To understand the indications, various treatment methods, contraindications, and complications of endoprostheses used for pelvic reconstruction after tumor resection, with orthopedic oncologist input.
2) To highlight the Mark II saddle prosthesis, a new type of peri-acetabular reconstruction endoprosthesis.

CONTENT ORGANIZATION:

1) Anatomy, including surgically important structures.
2) Indications and contraindications for hemipelvectomy endoprostheses.
3) Review of endoprosthesis types with emphasis upon the Mark II saddle prosthesis
4) Radiologically important outcomes, including complications such as dislocation, loosening, and recurrence of tumor. Examples will be presented using multimodality images and intraoperative photos

SUMMARY:

The major teaching points of this exhibit are:
1) To provide the radiologist with a detailed understanding of pelvic reconstruction after tumor resection.
2) To highlight different types of pelvic reconstruction endoprostheses with particular attention to a new type of peri-acetabular reconstruction endoprosthesis.
3) The accurate recognition of post-operative complications is crucial to preventing long-term patient morbidity.

LL-IN2060-B06: Optical Imaging of Melanoma Mimics: An Imaging Informatics Tool Kit Using Discriminant Analysis, Optical Properties, and Histological Characteristics

A Joseph, MS, Los Angeles, CA; G Galliano, MD; S Bose, MD; D Farkas, PhD (anikajos@usc.edu)

PURPOSE/AIM:

The long term objective of this study is to evaluate optical imaging methods that could be applied clinically to distinguish between aggressive and benign forms of cutaneous melanoma in humans. In this study, we would like to apply an optical imaging method, specifically, spectral imaging, to image mimics, of human melanoma to determine if distinct imaging markers can be found that are not present in human melanoma with metastatic potential.

CONTENT ORGANIZATION:

These research efforts have focused on both the detection of melanoma mimics and the in-depth evaluation of pigmented lesions for propensity to develop melanoma. We have developed an imaging informatics tool kit with vendor supplied software packages and in-house customized software applied on reflectance imaging spectroscopy in the range of 400–1000 nm. The tool kit has been applied to discriminate and characterize melanoma mimics. Images were acquired for 20 primary biopsies of suspected melanomas and 20 re-excisions of tissues suspected to be reoccurrences of melanoma in patients, later confirmed by histology to be negative for melanoma. The images of melanomas mimics were processed semi-automatically through two software packages in the tool kit that spectrally separate and characterize tissue features from hematoxylin and eosin stained and unstained tissue. A Least Mean Square and Mahalanobis method based in-house customized algorithm in the tool kit was used to classify the lesions. The "gold standard" for training and testing these classifiers were verified by a dermatopathologist.

SUMMARY:

From each spectral image, corresponding to a selected wavelength, four parameters were derived to quantify color, pigment distribution, dimension and boundary of each lesion. A statistical analysis performed on the selected parameters shows that the mean effective reflectance, pigment distribution and lesion area are significantly different with the different pathological imitators of melanoma.

EDUCATION EXHIBITS – POSTER

LL-IN1052: Optimization and Management of User Registration and HIPAA-Compliance in a Clinical PACS Environment by Integration with a HIPAA-Compliant Auditing Toolkit

J Lee, MS, Marina del Rey, CA; B Guo, MD; B J Liu, PhD; K Wang (jasperlee@usc.edu)

BACKGROUND: USC Health Science Campus is supported by an enterprise PACS with four hospital sites. To access PACS, USC radiology staff and referring physicians must fax a written HIPAA Form to the PACS support team and wait for an email confirmation. However with the myriad of user types and hundreds of users to manage across the department's multiple healthcare systems, not all forms are processed in a timely fashion and not all user accounts are kept up-to-date. An online registration GUI will be integrated into a HIPAA-Compliant Auditing Toolkit which extracts pertinent auditing information from the logs of various PACS components into an auditing database. The challenges of user registration efficiency, HIPAA authorization and auditing are presented in an electronic workflow solution.

EVALUATION: A Web-based Radiology ID Authorization System will be evaluated for users in the Internal Medicine and Orthopedics departments within HCC2 because they currently have the largest number of new referring physician requests per month. Evaluation will be based on average user registration turn-around time and analysis of user activities by integrating the user authorization list with the HIPAA-Compliant Auditing System.

DISCUSSION: A web-based HIPAA authorization and auditing system allows the PACS support staff in a large radiology environment to manage new user requests online rather than via faxed sheets of paper. Furthermore, the system database allows the staff to monitor account privileges and user activity across multiple healthcare information systems. Automatic email notification is also done for users with expiring HIPAA authorization to make sure annual renewals of HIPAA rules are actually met.

CONCLUSION: An electronic HIPAA authorization and auditing system allows the PACS support team to better communicate and manage its healthcare information system users by allowing them to submit their HIPAA statements of confidentiality forms online. Furthermore, the user accounts system can be linked to a HIPAA-Compliant Auditing System for user-based events monitoring. The system hopefully reduces turn-around time while improving HIPAA-compliance of users in the PACS and healthcare information systems.

SCIENTIFIC POSTERS – ELECTRONICS

LL-IN2087-L07: RadSearch: A RIS/PACS Integrated Retrospective Medical Image Retrieval Tool

Wed Dec 03 2008 12:15PM - 1:15PM ROOM Lakeside Learning Center 07

S Tsao, MS; Los Angeles, CA; J Documet, MS; P Moin, MD; K Wang; B J Liu, PhD (stsao@usc.edu)

BACKGROUND: Radiology Information Systems (RIS) hold text reports that contain a wealth of information that can be used for research, education, and practice management. However, there are currently very few tools available that query specific data from these reports from an existing RIS database and also allow for query/retrieval of relevant image studies from the Picture Archival and Communications System (PACS). This project aims to create a software tool that integrates a Radiology text report query tool with PACS' abilities to view and move images within the clinical workplace. RadSearch allows users to seamlessly data mine the radiology reports whilst previewing and moving related medical images.

EVALUATION: As a means of evaluation, RadSearch is integrated into University of Southern California's Health Consultation Center's Two's PACS and RIS system to allow clinical user feedback on the tool. Two versions of the tool is available, one that uses only mysql database's built in full text searching tool and another hybrid version that searches based on all related terms defined within the RadLex lexicon. Feedback is presented in the form of suggestions in improving ease of use as well as requests for future features.

DISCUSSION: RadSearch relates data fields in the RIS such as Current Procedure Terminology 4 (CPT 4) codes and the Radiology Report text back to the PACS study. This allows RadSearch to implement the new paradigm of performing retrospective studies or generating teaching files by leveraging existing data within the clinical practice. This project will also discuss the utility of the different strategies in integrating RadLex as well as CPT-4 codes as a means to provide synonymity and structure into the searching algorithm. The potential problems and pitfalls in adoption as well as implementation of such a system will also be discussed.

CONCLUSION: RadSearch illustrates a development of a data mining tool built using open source components such as CPT-4, RadLex, mySQL and PHP that allows research institution to maximally utilize and data mine existing clinical data for knowledge discovery and scientific research.

LL-PD4093-H07: An Online Real-time DICOM Web-based Computer-aided Dagnosis (CAD) System for Bone Age Assessment (BAA) of Children in a PACS Environment: Clinical Validation

Tue Dec 02 2008 12:15PM - 1:15PM ROOM Lakeside Learning Center 07

K C Ma, BS, Los Angeles, CA; A Zhang, PhD; M Fleshman; L A Vachon, MD; B J Liu, PhD; H K Huang, DSc; et al. (azhang@usc.edu)

PURPOSE: During the past 10 years, 1,390 hand images of normal children, both male and female from Asian, African American, Caucasian and Hispanic descends were collected and a digital hand atlas (DHA) was formed. Based on the DHA, a fully automatic, objective, racial, and gender specific computer-aided-diagnosis (CAD) method has been developed within the Image Processing and Informatics Lab (IPILAB), USC. To bring the DHA and CAD method to clinical environment for daily use in assisting radiologist to achieve higher accuracy in BAA, a web-based client-server system is designed as a novel clinical implementation approach for online and real-time BAA. This paper presents the clinical integration of the CAD system with the PACS at the Los Angeles County Women's and Children's Hospital (LAC WCH) for clinical validation.

METHOD AND MATERIALS: In the CAD system clinical implementation workflow, a second copy of the hand image from CR modality is sent to the CAD server with secure intranet connection. The CAD server includes the following major components: DICOM receiver, BAA CAD engine, web service and clinical database. The DICOM receiver listens and receives the hand image from CR modality. The CAD engine is then triggered to segment the hand images, extract bony features for automatic bone age assessment by fuzzy logic. The CAD report, including assessed bone age, best match image from DHA and patient displayed on the normal development graph for the specific racial group, was then generated automatically at CAD server as a DICOM SR (Structure Report). The radiologist at the clinical site can log into the website and review CAD results from a PACS WS and the assessment will be uploaded back to the server and stored in the final SR file of the clinical database.

RESULTS: The CAD server and PACS integration has been successfully implemented in LAC WCH. A fully automatic workflow is achieved without manual intervention. More than 60 prospective clinical cases have been evaluated.

CONCLUSION: This paper presents a novel clinical implementation approach for a CAD system using web technology for online and real time BAA. The success of the prototype can be easily extended to multiple clinical sites and will provide the foundation for broader use of the CAD system for BAA.

CLINICAL RELEVANCE/APPLICATION: To bring the DHA and CAD method to the clinical environment as a useful tool in assisting radiologist to achieve higher accuracy in BAA.

SPIE 2009 PREPRINTS

Evaluation of a computer-aided detection algorithm for timely diagnosis of small acute intracranial hemorrhage on computed tomography in a critical care environment

Joon K. Lee[a], Tao Chan[b], Brent J. Liu[a], H.K. Huang[a]
[a]Image Processing and Informatics Laboratory, Department of Radiology
University of Southern California, Doheny Eye Institute Building,
1450 San Pablo Street, Suite 2100, Los Angeles, CA, USA 90033;
[b]Dept. of Health Technology and Informatics, The Hong Kong Polytechnic University,
Hong Kong, SAR, China

ABSTRACT

Detection of acute intracranial hemorrhage (AIH) is a primary task in the interpretation of computed tomography (CT) brain scans of patients suffering from acute neurological disturbances or after head trauma. Interpretation can be difficult especially when the lesion is inconspicuous or the reader is inexperienced. We have previously developed a computer-aided detection (CAD) algorithm to detect small AIH. One hundred and thirty five small AIH CT studies from the Los Angeles County (LAC) + USC Hospital were identified and matched by age and sex with one hundred and thirty five normal studies. These cases were then processed using our AIH CAD system to evaluate the efficacy and constraints of the algorithm.

Keywords: CAD, Brain, Computed Tomography, CT, Intracranial Hemorrhage, Algorithm

1. INTRODUCTION

Intracranial hemorrhage within the brain can be divided into intraaxial and extraaxial categories. Intraaxial hemorrhages include intraparenchymal hemorrhages (IPH) and intraventricular hemorrhages (IVH) while extraaxial hemorrhages encompass epidural hemorrhages (EDH), subdural hemorrhages (SDH), and subarachnoid hemorrhages (SAH).

AIH is often a sequela of head trauma and can result in acute neurological disturbances. Identification of AIH is of paramount clinical importance as its presence and nature dictates distinct management and treatment strategies. However, clinical signs, symptoms, and other parameters are insufficient to accurately differentiate AIH from other etiologies of neurologic disturbance [1,2]. Therefore, CT has long been the primary modality for detection and characterization of AIH due to its wide availability, quick performance, and ready depiction of AIH.

In most parts of the world, emergency department physicians, internists, or neurosurgeons are often the first to read CT studies, particularly when a radiologist's expertise is not immediately available. The skill of such acute care physicians has been shown to be imperfect based on receiver operating characteristic (ROC) studies [3]. Further, radiology residents have been shown to infrequently overlook hemorrhage on brain CT [4]. Among even the best human observers, errors in image interpretation are inevitable [5].

It is envisioned that CAD will help improve the accuracy of detecting AIH and decrease the risk of misdiagnosis and mismanagement. The ultimate goal of this study is to develop a CAD system to integrate within the clinical environment and to evaluate and refine a CAD algorithm [6] developed to detect small AIH. However, this system differs from other CAD products in that it is intended to be used by clinicians other than radiologists and that the likelihood of true AIH in identified candidate lesions is rated based on anatomical positions and imaging features.

In 2007, we presented a CAD system for the detection of small AIH. The purpose of this study is to validate the efficacy of that system and use the results to develop a CAD system for clinical implementation and evaluation using a larger data set derived from an acute care setting.

2. METHODOLOGY

2.1 Study Population

Final reports signed by staff radiologists for all non-contrast CT's of the head performed from 2005 to 2008 were extracted from the LAC+USC hospital information systems, parsed, and imported into a custom database for data mining. One hundred thirty eight patients were identified who were reported to have AIH and whose studies were available for export. Each patient was matched by age, sex, and ethnicity with a control patient who was reported to have a normal study. Available studies were exported out of the Department of Radiology PACS as DICOM files and the headers were anonymized. This retrospective study was approved by our institutional review board.

2.2 CT Acquisition

All CT studies included in the present study were acquired employing a Picker PQ 5000 or 6000 single-slice CT scanner. Acquisition parameters include 5 mm collimation, 130 kV, and beam currents of 30 mA.

2.3 CAD System

The CAD system was developed using MATLAB (The MathWorks, Inc., Natick, MA, USA) and modified from an earlier iteration to run in batch mode without any user intervention. The system ran on a 1.8 Ghz Intel Core 2 Duo laptop with 2 megabytes of RAM. A flowchart of the CAD algorithm is illustrated in Figure 1. Image processing and analysis methods used by the system are listed in Table 1.

Intracranial contents are segmented by global thresholding and morphological operations followed by contiguity analysis. Noise reduction using median filter and adjustment for CT cupping artifacts are performed. The intracranial contents are realigned into the conventional orientation after automatic localization of the mid-sagittal plane and boundaries of the series of images. Then, high attenuation components are segmented as candidate AIH from each of the axial sections based on top-hat transformation and subtraction between the two halves of the images. Image features of the candidate regions are then quantified. The candidate AIH are given anatomic context by registration against a normalized coordinate system developed for this project. Then, the features and coordinates are used in a rule-based classification system to reduce false positives due to normal variants and artifacts.

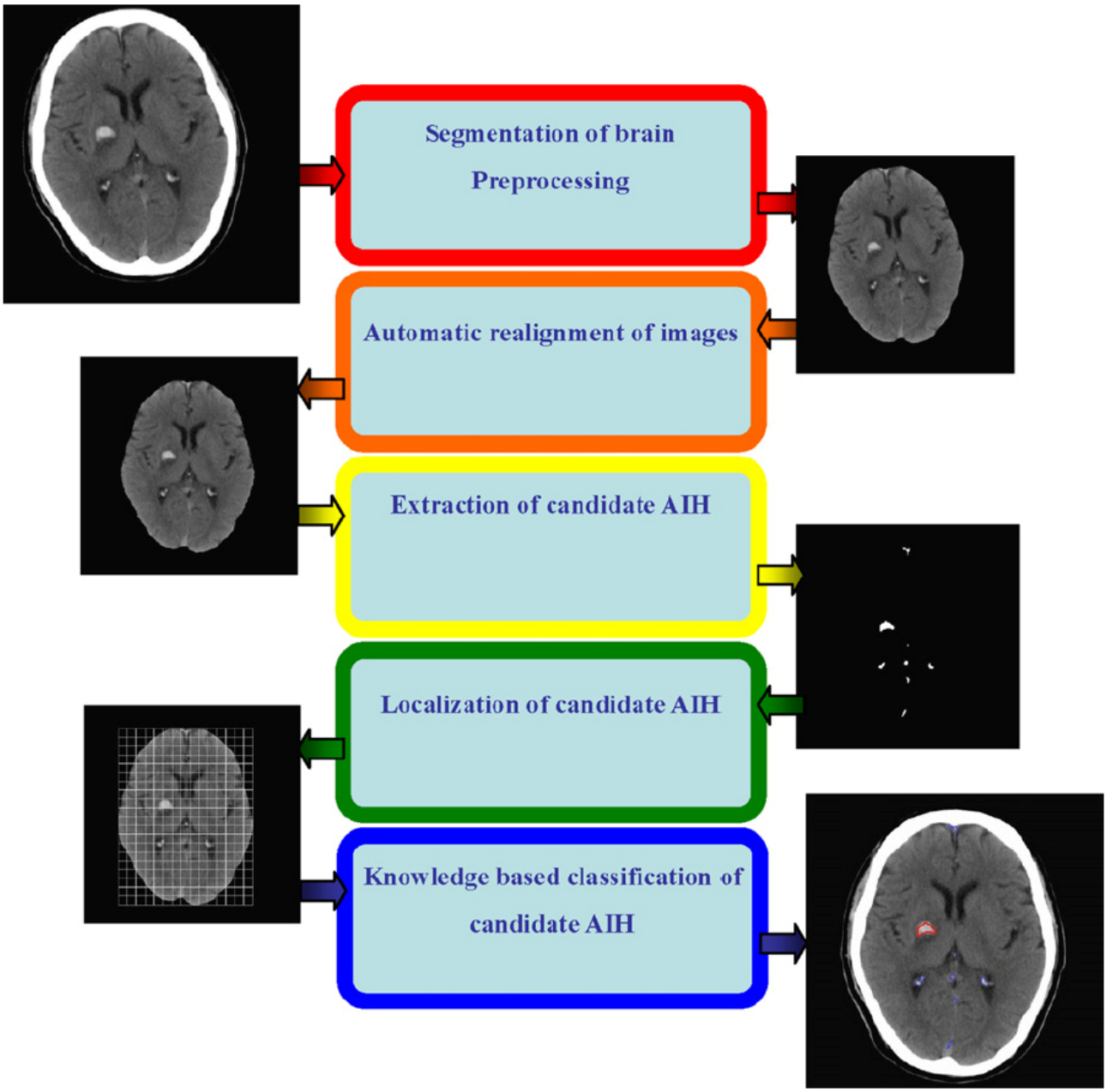

Fig. 1. Schematic diagram of the CAD system. Intermediary outputs of an image showing right basal ganglia hemorrhage illustrate the effect of individual steps.

Table. 1. Details of individual image processing and analysis steps in the CAD system as outlined in Fig. 1.

Steps	Methods	Purposes
Segmentation of intracranial contents	Global thresholding and morphological operations Remove structures not contiguous with the main central bulk of intracranial contents	Remove bones of skull and face Remove scalp, orbits, and other head and neck soft tissue
Preprocessing of intracranial contents	Median filtering Adjustment of intensity according to distance from the skull	Denoising Correction for CT cupping artifacts

Automatic realignment of images	Automatic localization of limits of brain, ventricles, floor of anterior intracranial fossa, mid-sagittal plane	Align the brain into normal position
Extraction of candidate AIH	Top-hat transformation Subtraction between the two sides	Highlight local high density regions Extract asymmetrically high density regions
Localization of candidate AIH	Registration of the brain in question against a normalized coordinate system	Render the candidate AIH anatomical information
Knowledge-based classification of AIH	Rule-based system with inputs of image features and anatomical coordinates of the extracted candidates	Distinguish genuine AIH from false positives resulting from noise, artifacts, and normal variants

2.4 Display of output

The contours of potential and genuine AIH are overlaid in different colors onto a duplicate of the original images. This permits juxtaposition of original input and CAD output images. A custom visualization tool was developed to facilitate inspection and to record analysis. A screenshot of the graphical interface is shown in Figure 2.

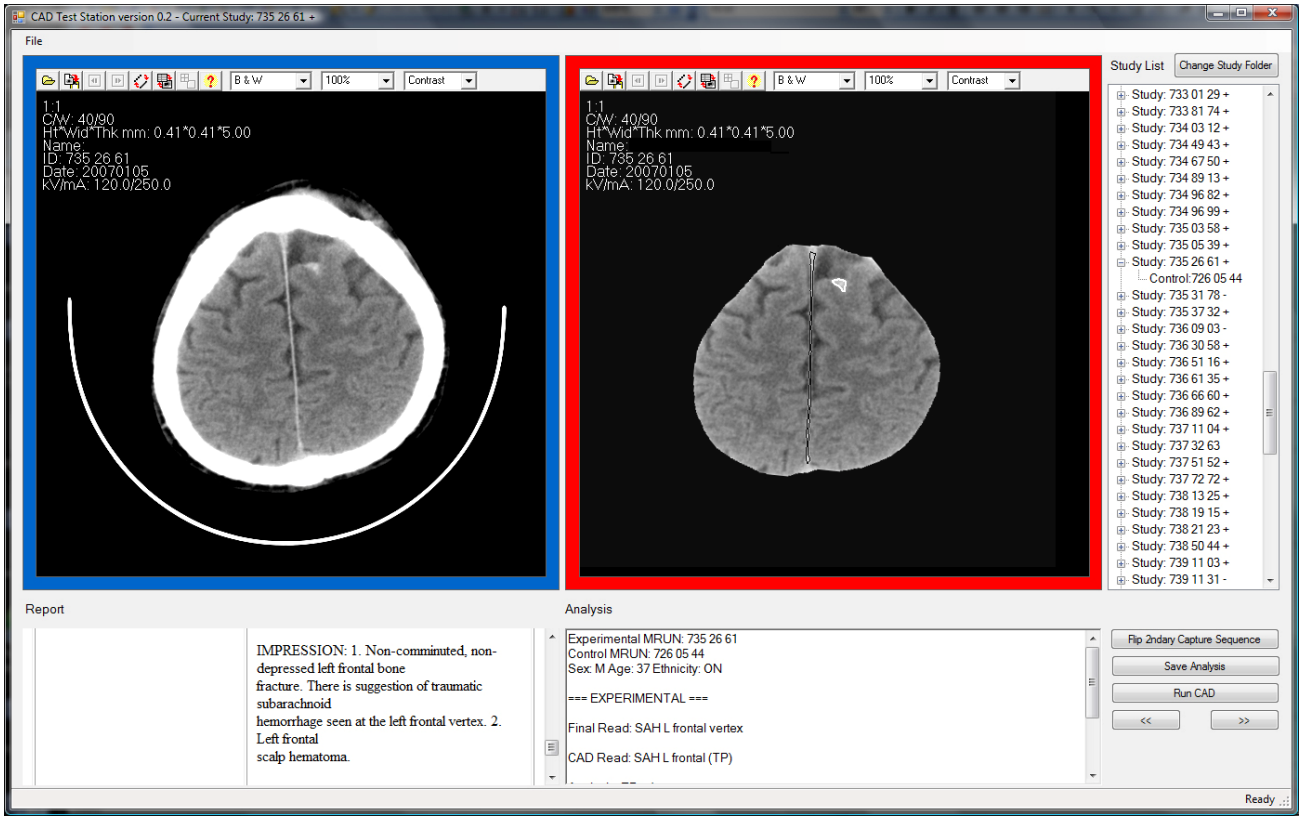

Fig. 2. Screenshot of CAD visualization tool. The original images are displayed in the left window while the output images with overlay of the outlines of AIH are displayed on the right.

3. RESULTS

The performance of the system was described by sensitivity and specificity pairs on both per lesion and per case bases. The per lesion descriptors are more informative when number or size of lesions need to be quantified, or when the performance of detecting some particular type of lesion is of interest. On the other hand, the performance on a per patient or per case basis is of more clinical relevance for the diagnosis of AIH as management options depend on the presence or absence or lesions rather than the quantity of lesions.

In the following section, a CAD output is counted as true positive if it overlaps at least part of the true AIH as determined by radiologists.

The actual presence of a lesion was based on the gold standard of the final report signed by a staff neuroradiologist. For each combination of lesion and location, a unique lesion was noted to exist in this study. Thus, a single study could possibly represent multiple AIH categories at multiple locations. The success or failure of the CAD system was based on whether such lesions derived from the final report were correctly identified. Specifically, all distinct lesions described in the final report were compared against CAD-identified candidate lesions by visual inspection. A successful detection was confirmed if any region of the lesion, regardless of the size, was correctly outlined by the CAD system. A logical next step would be establishment of an ROC study.

On a per patient basis, if any one of the CAD outputs for a particular patient is a true positive, then the case is counted as true positive, disregarding whether the other outputs are true or false positive. If there are one or more CAD output(s), none of which are true positives, the study is considered a false positive. On the contrary, if there is no CAD output for a particular patient, but there is a genuine AIH, the case is considered a false negative. If there is no CAD output for a patient in whom an AIH exists, the case is counted as a true negative.

Represented in the 135 studies were 20 studies with IPH, 14 with IVH, 91 with SAH, 53 with SDH, and 13 with EDH. The overall sensitivity in lesion detection was 69.6% (167/240) (Table 2). However, in some cases, the system correctly identified the location of the AIH but subsequently categorized the candidate lesion as not being a true AIH. With this in consideration, the overall sensitivity in lesion identification was 84.2% (202/240).

Table 2. Summary of CAD results according to type of individual AIH on a per lesion basis. TP: True positive; TP » FN: Correctly identified lesion but incorrectly classified as not being true AIH; FN: False negative.

	IPH	**IVH**	**SAH**	**SDH**	**EDH**	**Total AIH**
Studies	20	14	91	53	13	191
TP	20	10	72	53	12	167
TP » FN	5	6	17	5	2	35
FN	3	6	19	10	0	38

On a per patient basis, the overall sensitivity was 77.0% (104/135) (Table 3). Similar to the per lesion basis, when correctly identified but incorrectly classified AIH is taken into consideration, the overall sensitivity in lesion identification was 89.6% (121/135).

Table 3. Summary of CAD results on a per patient basis.

	AIH Cases
Studies	135
TP	104
TP » FN	17
FN	14

Our control cases returned 100% false positive results primarily originating around the falx most likely due to an error in the registration of the brain against the internal, normalized coordinate system used by the CAD system. Incorrect application of the coordinate system would apply inconsistent or erroneous rules-based logic in determining the nature of a candidate lesion. Interestingly, corresponding false positives around the falx were not replicated in the CAD output of true AIH cases. To address this possible source of error, we will have to audit that segment of the algorithm to determine whether the coordinate system is being oriented properly and consistently.

The current system has not been optimized for speed and continues to take an average of approximately 15 s per image to produce the CAD output. Actual times vary substantially for each case and depend on the number of images and candidate AIH regions to be evaluated by the classification system. This can mean that the time required to perform the CAD can be an important factor in the design of an integrated CAD system.

4. CONCLUSIONS

4.1 Detection of AIH

In a departure from our prior assessment, we selected random AIH cases to test against the CAD system from an institution in the United States as opposed to the original study that was performed in Hong Kong. It appears that some component of the CAD system may not be functioning optimally in response to these differences which is a normal outcome in CAD when changing population groups. That the core of the algorithm has not changed suggests that the performance decrement may stem from discrepancies in acquisition protocols between the two sites, in the knowledge-based classification system, or the combination thereof. More investigation is needed and is ongoing.

If we compare the sensitivity of the CAD system on a per lesion basis from our previous study [6] (training cases with 84.4% and validation cases with 82.6%) to the sensitivity of candidate lesion identification in this study (84.2%), we find that the performance of the identification component of the CAD system appears consistent. This may suggest that the source of our underlying performance issue lies in the elements associated with the classification system.

This dataset of random AIH cases included studies in which multiple AIH lesions existed concurrently and throughout the entire brain. The CAD system identifies candidate AIH regions in part by comparing pixel intensity in presumably normal contralateral anatomic regions. This process is particularly useful in identification of lone AIH. However, when multiple AIH exist in bilateral distributions across hemispheres, this procedure can be compromised yielding unexpected results. These conditions may account for some the false negative results.

4.2 Future Development

CAD systems development continues to be a major activity in the field of radiology. Recently, CAD systems have been applied to polyp detection in CT colonoscopy [7], mammography [8], pulmonary nodule detection [9], and traumatic brain injury [10]. Detection of small AIH continues to be an area amenable to the development of computer algorithms and CAD systems accurate enough to assist clinicians in emergent conditions. The combination of the results of this study and our prior study still support the idea that our CAD system can be refined into an integrated practice aid.

In the near term, we will need to isolate the source of the performance decrement in the CAD system to re-attain the levels established in our prior study. The success of AIH lesion identification seems unaltered lending support to the overall approach. A more in depth comparison of the captured images from LAC+USC versus Princess Margaret hospital in Hong Kong [6] and a review of the knowledge-based classification system may yield a quick solution to this current issue and a resolution to our false positive controls. We will likely rerun these acquired cases and controls through a new iteration of the CAD algorithm before continuing with our plan to perform a multisite assessment of the system.

Next, as most institutions upgrade their equipment to multislice CT scanners, the adaptation of this CAD algorithm to thin-slice images generated from these new machines may yield more accurate results. Such images are less prone to artifact and the contrast between AIH and normal parenchyma is higher as thinner sections make volume averaging less of a problem, even for small lesions. Furthermore, AIH may be better characterized in these newer acquisitions by their three dimensional morphology or interrelation. This is planned for the near future as we collect more cases during the clinical evaluation.

The design of a fully integrated CAD system will need to take into consideration the current processing time of the algorithm. The MATLAB code is currently not optimized for speed and takes an average of 15 s per slice. This means that the aggregate time to completion for the CAD algorithm can extend into the minutes. Such duration affects workflow considerations, particular when we consider the intended audience and role of this tool within the clinical milieu. The future incarnation of the CAD system will need to reflect either code migration to a better performing programming language or optimized MATLAB code to achieve gains in speed. If these remedies and/or hardware investment do not decrease the latency, the architecture of the CAD system may require non-real time or parallel processing prior to a study's arrival at a reading station.

We continue to envision a CAD system that can be implemented into daily clinical practice in the emergency department. It is believed that the system can be used as a triage tool for patients suffering from minor neurological disturbances or head trauma. After CT is performed, clinicians can read the images with support from the CAD system and make the appropriate treatment and management decisions.

REFERENCES

[1] Perry JJ, et al., “Attitudes and judgment of emergency physicians in the management of patients with acute headache,” Acad Emerg Med 12(1), 33-7 (2005).

[2] Mader TJ, Mandel A., “A new clinical scoring system fails to differentiate hemorrhagic from ischemic stroke when used in the acute care setting,” J Emerg Med 16(1), 9-13 (1998).

[3] Schriger DL, et al., “Cranial computed tomography interpretation in acute stroke: physician accuracy in determining eligibility for thrombolytic therapy,” JAMA 279(16), 1293-1297 (1998).

[4] Mysoki MG, et al., “Head trauma: CT scan interpretation by radiology residents versus staff radiologists,” Radiology 208(1), 125-128 (1998).

[5] Erickson BJ, Bartholmai B., “Computer-aided detection and diagnosis at the start of the third millennium,” J Digit Imag 15(2), 59-68 (2002).

[6] Chan T., “Computer aided detection of small acute intracranial hemorrhage on computer tomography of brain,” Computerized medical Imaging and Graphics 31, 285-298 (2007).

[7] Baker ME, et al., “Computer-aided detection of colorectal polyps: can it improve sensitivity of less-experienced readers? Preliminary findings,” Radiology 245, 140-149 (2007).

[8] Fenton, JJ, et al., “Influence of computer-aided detection on performance of screening mammography,” N. Engl. J. Med 356, 1399-1409 (2007).

[9] Beyer F, et al., “Comparison of sensitivity and reading time for the use of computer-aided detection (CAF) of pulmonary nodules at MDCT as concurrent or second reader,” Eur. Radiol. 17, 140-149 (2007).

[10] Yuh EL, et al., “Computer-aided assessment of head computed tomography (CT) studies in patients with suspected traumatic brain injury,” J. Neurotrauma 25, 1163-1172 (2008).

Computer-assisted detection (CAD) methodology for early detection of response to pharmaceutical therapy in tuberculosis patients

Robert Lieberman[a], Heston Kwong[b], Brent Liu[a], HK Huang[a]
[a]Image Processing and Informatics Laboratory, 1450 San Pablo St., Suite 2100, Los Angeles, CA, USA 90033;
[b]Principal Medical Officer, Department of Health Hong Kong Special Administrative Government

ABSTRACT

The chest x-ray radiological features of tuberculosis patients are well documented, and the radiological features that change in response to successful pharmaceutical therapy can be followed with longitudinal studies over time. The patients can also be classified as either responsive or resistant to pharmaceutical therapy based on clinical improvement. We have retrospectively collected time series chest x-ray images of 200 patients diagnosed with tuberculosis receiving the standard pharmaceutical treatment. Computer algorithms can be created to utilize image texture features to assess the temporal changes in the chest x-rays of the tuberculosis patients. This methodology provides a framework for a computer-assisted detection (CAD) system that may provide physicians with the ability to detect poor treatment response earlier in pharmaceutical therapy. Early detection allows physicians to respond with more timely treatment alternatives and improved outcomes. Such a system has the potential to increase treatment efficacy for millions of patients each year.

Keywords: CAD Development, Lung, Directly Observed Treatment Short Course (DOTS), Tuberculosis, Chest X-rays, Outcomes

1. INTRODUCTION

With a prevalence of one-third of the world's population, tuberculosis (TB) is the leading cause of infectious disease in the world [1]. Eight million people annually become infected with TB, and two million people die each year from disease caused by TB. According to the World Health Organization (WHO), disease burden caused by TB disproportionately affects developing countries where many essential medical services are limited or non-existent, especially China [2].

TB is caused by Mycobacterium tuberculosis, a bacterium that spreads via inhalation. Although 90% of people infected with mycobacterium tuberculosis are asymptomatic (referred to as latent TB infection), 10% of people infected with the bacterium go on to develop tuberculosis disease in their lifetime. Although it can attack the central nervous system, the lymphatic system, the circulatory system, the genitourinary system, the gastrointestinal system, bones, joints, and even the skin, tuberculosis primarily infects the lung tissue. Such lung infection with mycobacterium tuberculosis is referred to as pulmonary TB.

The definitive diagnosis of TB requires the positive identification of cultured mycobacterium tuberculosis in a clinical sample, commonly of patient sputum. However, when the culture method of diagnosis is not possible, a probable diagnosis can be made using a tuberculin skin test or using imaging, most commonly chest radiography [3]. Furthermore, the sensitivity of the particular strain of mycobacterium tuberculosis to the various anti-TB drugs can be determined by checking for growth of the particular bacterial strain on agar plates prepared with the anti-TB medications in question.

1.1 Radiologic Features of TB Infection

Given that TB primarily infects the lung tissue, chest radiography has become the primary modality used around the world to aid in the diagnosis and management of TB patients. The general pathology of TB infection is often described as exudative, proliferative, caseating, and often calcifying. Radiographically, the initial parenchymal focus of TB presents as granulomatous tissue or mature fibrous tissue appearing as a lung nodule. Lymph node enlargement is one of the most common presenting abnormalities on chest radiograph, most commonly unilateral and in the hilum or paratracheal region. Airspace consolidation is also common and is usually unilateral. Pleural effusion is often found unilaterally on the same side as the primary focus of TB. Other common radiographic findings include but are not limited to focal or patchy heterogeneous consolidation of the apical and posterior segments of the upper lobes and the superior segments of the lower lobes, as well as poorly defined nodules and linear opacities, cavitary lesions, and tuberculomas [4].

1.2 TB Treatment: Directly Observed Therapy – Short Course

The standard pharmaceutical treatment for tuberculosis infection involves directly observed therapy [5]. Directly observed therapy treatment for TB was created because, although TB is curable in almost all cases, most experts agree that patients' inability to adhere to sufficient uninterrupted therapy has prevented the total elimination of TB infection in the world. Directly observed therapy treatment requires the observation of the patient by a health care provider or other responsible person as the patient ingests anti-TB medications [5]. In Hong Kong, the directly observed treatment – short course (DOTS) is the preferred form of TB treatment. Patients undergo treatment with Isoniazid, Rifampicin, Pyrazinamide and either Ethambutol or Streptomycin in the initial 2 months, followed by two drugs, Isoniazid and Rifampicin, in the subsequent four months. Timely radiological evaluation, using a time series of chest x-rays, is useful in following the progression or resolution of TB disease in patients undergoing DOTS therapy.

1.3 Drug Resistant Tuberculosis

Even with the implementation of DOT treatment for TB, drug resistance is common. Various isolates of mycobacterium tuberculosis exist that are resistant to one or more of the commonly used anti-TB drugs. Disease manifested as a result of infection with one of the resistant TB strains is referred to as drug-resistant tuberculosis. When the particular TB strain is resistant to at least Isoniazid and Rifampicin, it is more specifically referred to as Multidrug-Resistant Tuberculosis (MDR-TB). It is estimated that China and India together represent approximately 50% of the total number of MDR-TB cases in the world [6].

Although drug-resistance can be diagnosed during the initial sputum culture, they are often inaccurate and take six to eight weeks for drug sensitivity results to be determined. By the time the culture and sensitivity results are known, the patient has most likely been taking DOT therapy for almost two full months or almost one-third of the total duration of DOT therapy. Furthermore, the medical supplies needed to perform culture and sensitivity tests on patients being tested for TB are not available at all medical facilities. More commonly, TB patients are not diagnosed with drug-resistant tuberculosis or MDR-TB until it is recognized that the patient's symptoms continue to worsen while undergoing DOT therapy.

In the context of recognizing drug resistance based on patient response to DOT therapy, chest radiography in conjunction with clinical, laboratory, and microbiological parameters play an invaluable role in the monitoring of TB patients undergoing DOT therapy. Because many of the sophisticated medical supplies required to monitor the laboratory and microbiological parameters of TB patients are not readily available to many laboratories throughout the world [6], chest radiography can be used to monitor changes in the radiographic findings mentioned in section 1.1 of patients undergoing DOT therapy. The radiographic changes alert a physician to the possibility of treatment failure. However, patients responding to DOT therapy may not show favorable signs of improvement until four to six weeks following the initiation of treatment, and treatment failure may not be recognized for a significant period of time beyond this window. By the time treatment failure is recognized, the disease progression has occurred and valuable resources may have been wasted.

Therefore, timely and effective treatment of TB minimizes disease progression, decreases the contagiousness of a patient, and helps control the spread of the disease. However, the prevalence of drug-resistance and DOT treatment failure prevent the timely and effective treatment of TB and lead to poor outcomes. The chest radiographs of TB patients undergoing DOTS treatment will be used to develop a digital image analysis algorithm that utilizes subtraction images created from the original chest radiographs. Analysis of the subtraction images will be done in order to determine which

statistical parameters or image analysis correlates with a patient's response to DOTS therapy. Thresholds will be determined based on the patient subtraction images in order to assist in the early establishment of successful TB treatment response versus TB treatment resistance in future TB patients. A CAD system will be created utilizing the chest radiograph algorithm in order to provide early detection of treatment failure to physicians. With successful results, the CAD system may improve TB outcomes of millions of patients worldwide.

2. METHODS

2.1 Patient Selection

We selected 200 patients from TB clinics of the Department of Health in Hong Kong in the year 2004. The diagnosis of TB infection was determined by chest physicians specializing in TB management and confirmed with laboratory testing. Sensitivity tests were used to determine the drug sensitivity of the strain of mycobacterium tuberculosis in each patient.

2.2 TB Treatment Protocol and Image Collection

The patients underwent the six month DOTS treatment regimen for TB. Based on the sensitivity results, the appropriate anti-TB regimen was chosen. Typically, a patient took Isoniazid, Rifampicin, Pyrazinamide, and Ethambutol for two months. The patients subsequently took Isoniazid and Rifampicin for the remaining four months of treatment. During DOTS therapy, six longitudinal PA chest radiographs of each patient were taken and scanned into DICOM files. The first chest radiograph was taken at the onset of DOTS therapy (Fig. 1) and the subsequent radiographs were taken over the six month duration of the DOTS treatment. The number of days between the first chest radiograph and each subsequent radiograph was recorded.

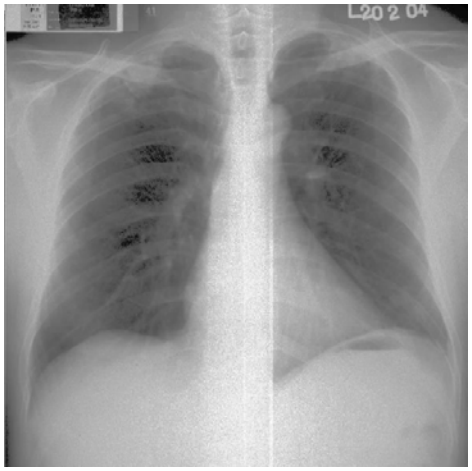

Fig. 1. A chest radiograph of a TB patient taken at the onset of DOTS therapy.

2.3 Chest Radiograph Subtraction Image Creation

As the patient responds to DOTS therapy, the pulmonary disease improves. Consequently, the chest radiographs show improvement in the lung disease over time in those patients that respond to treatment. As the pulmonary disease continues to improve towards the end of DOTS therapy, the improvement in the lung disease becomes more apparent. Subtraction images between the chest radiographs were created to emphasize the changes occurring in the level of pulmonary disease over time.

The subtraction images were created using the six original DICOM chest radiographs mentioned in the previous section. All the DICOM chest radiographs were converted to a jpeg format. The jpeg images were then used to create the chest subtraction images. The initial chest radiograph taken at the onset of DOTS treatment was used as the reference point that all subsequent chest radiographs were compared to. The six chest radiographs were then used to create five

subtraction images by subtracting the second image from the first, the third image from the first, the fourth image from the first and so forth.

The subtraction images were created in the following manner. First, the lung fields of each chest radiograph were isolated. Lung field isolation was done through several steps. Because the lung fields and background have densities and consequently pixel values lower than other tissues, the lung tissue was merged with the spine and other high density tissues to create a mask that allowed for the empty background to be removed. Once the background was removed, the next step involved isolating the lung tissue from the other tissues in the chest radiograph, such as the heart, spine, ribs, etc. Lung tissue isolation was done using the run length coding method that compares each pixel value to either eight or four neighboring pixel values. This run length coding method takes advantage of the fact that the lungs are fairly homogeneous organs in terms of tissue density. Consequently, pixels representing lung tissue in the chest radiograph have pixel values that are almost identical to neighboring lung tissue pixel values. A random pixel, called a seed, was chosen within one of the lung fields. The run length coding method states that if this pixel and its neighboring pixels shared the same pixel value, then it was concluded that the pixel was a part of the lung fields and was added to the lung image array. If the pixel was not identical to its neighboring pixels, it was assumed to not be lung tissue and was removed from the lung field array.

Because tissues other than lung tissue may share pixel values with neighboring pixels, areas outside of the actual lung fields may be included in the lung field array as false positives. However, lung tissue generally has a very low density compared to other homogeneous tissues in the chest. Therefore, once the lung field arrays were completed, the false positive tissue was removed by zeroing out pixel values above a certain threshold. The resulting lung field array contains only pixels representing lung tissue. The process of isolating the lung tissue by creating a lung field array was performed on all of a patient's chest radiographs.

Next, we created the subtraction images. Because it was difficult to have patients stand in the exact same location with identical levels of inspiration/expiration, the lung fields in two different chest radiographs did not completely overlap. To solve the issue of overlap, the lung field arrays of the later chest radiographs were warped to overlap as much as possible with the original chest radiograph lung fields. Once the images had been warped, the pixel values from the later chest radiograph were subtracted directly from the pixel values of the original chest radiograph lung field array. The resulting image was a subtraction image with pixel values emphasizing the differences between the chest radiographs (Fig. 2). Ideally, the differences between the chest radiographs represented improvement in pulmonary disease.

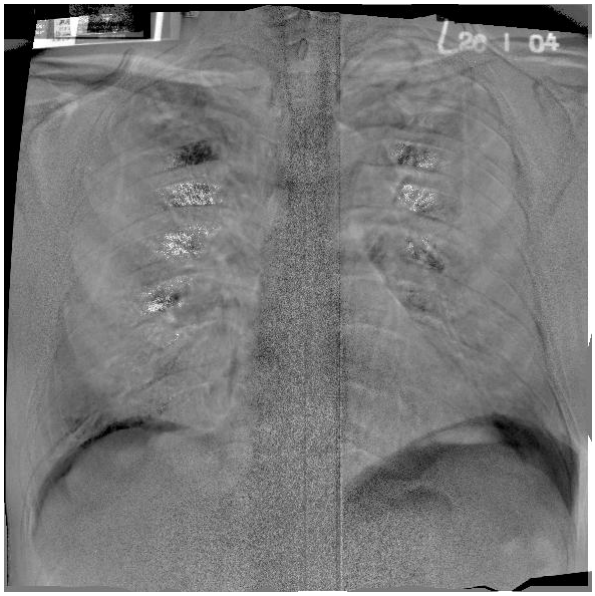

Fig. 2. An example of a subtraction image using the entirety of both the first and second chest radiographs of a TB patient undergoing DOTS therapy. Note that some anatomical structures can still be identified.

Each subtraction image was then further broken down into one subtraction image with only the left lung field (Fig. 3) and one subtraction with only the right lung field. Consequently, each patient had three groups of subtraction images: left lung subtraction images, right lung subtraction images, and subtraction images containing the entire chest. In order to minimize the effects of anatomy outside of the lungs, only the left lung and right lung subtraction images were analyzed. We subsequently analyzed various aspects of the subtraction images.

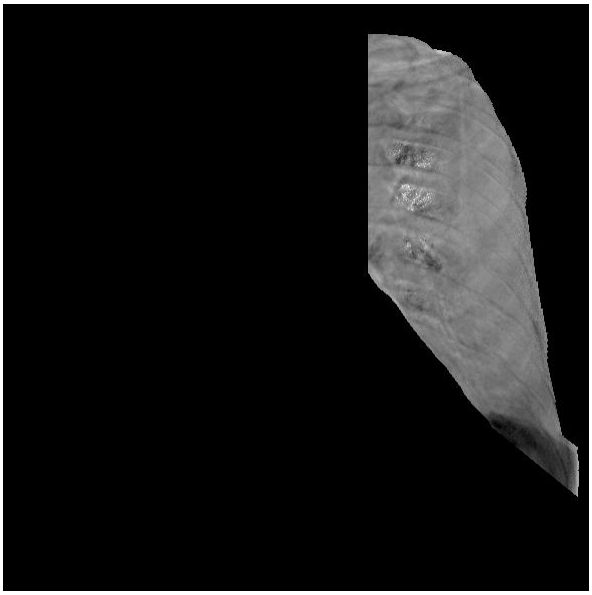

Fig. 3. The left lung tissue has been isolated from figure 2 and all pixel values outside the left lung have been zeroed out.

2.4 Subtraction Image Analysis

Several statistical parameters were calculated for each subtraction image. The image histogram for each subtraction image was created. Furthermore, seven statistical parameters - the image mean, uniformity (average entropy), 2^{nd} moment (variance), 3^{rd} moment (skewness), 4^{th} moment (relative flatness), correlation, and contrast - were calculated for each subtraction image [7]. Finally, the Fourier and power spectrum were created in order to evaluate the overall energy and the various frequencies, respectively, of each image.

Each individual lung subtraction image was then placed into one of three separate categories based on the lung's radiographic changes in response to DOTS therapy as confirmed by the physician interpreting the chest radiographs: an improved group, a worsening group, and an unchanged group. The improved group consisted of patients that showed radiographic signs of improvement in response to DOTS therapy. The worsening group consisted of patients that radiographic signs of worsening in response to DOTS therapy. Finally, the unchanged group consisted of patients that did not show radiographic signs of significant improvement or decline in response to DOTS therapy. A t-test was performed to determine any difference between the statistical parameters of the three groups.

Next, the time in days between the two images used to create each subtraction image was compared to the various statistical parameters. The time in days represents the number of days between the second chest radiograph used to create the subtraction image and the original chest radiograph taken at the onset of DOTS therapy. For example, if the fourth of six chest radiographs was taken 120 days after the original chest radiograph, then the time in days was recorded as 120 days. Regression analysis was done on the subtraction images for each patient using the time in days as the independent variable and the various statistical parameters as the dependent variables.

3. RESULTS

3.1 Subtraction Image Analysis

Each of the 200 patients had six chest radiographs taken for a total of 1200 chest radiographs. All the chest radiographs were digitized and subjected to the subtraction image algorithm. When subjected to the subtraction image algorithm, 101 of the patients' chest radiographs successfully produced subtraction images for a total of 390 subtraction images. The remaining 99 patients' chest radiographs did not produce subtraction images. The right and left lungs were isolated in each of the 390 subtraction images. 390 left lung and 390 right lung subtraction images were created for a total of 780 individual lung subtraction images.

Based on physician assessment of each lung in the original chest radiographs, the individual lung subtraction images were classified into three categories: improved, worsened, or unchanged. The number of subtraction images in each group is summarized below (Table 1). It is no surprise that the total number of left lung images, 390, is identical to the total number of right lung images. It is also important to note that the number of left and right subtraction images is not identical within each category. For instance, the number of right lung subtraction images that showed improvement, 150, is not the same as the number of left lung subtraction images that showed improvement, 102. This inequality is due to the fact that when TB is treated with DOTS therapy, the pathology in each lung may respond in different ways and at different speeds, resulting in different radiologic changes. It is also important to note that the number of combined right and left subtraction images – 252, 286, and 242 respectively - in each category are roughly the same.

Table 1. The number of individual subtraction images in each category.

	Improved	*Worsened*	*Unchanged*	*Total*
Left Lung	102	123	165	390
Right Lung	150	163	77	390
Combined	252	286	242	780

The mean and standard deviation were calculated for each of the seven statistical parameters mentioned above. The statistical parameters for the group of subtraction images that showed signs of radiological improvement were then compared to the statistical parameters of the other two groups. A t-test was performed in order to determine if there a statistical difference exists between the group that improved and the two groups that did not improve (Tables 2 and 3). It is important to notice that the t-test shows that a significant difference exists between the image mean and the uniformity when the group that improved is compared to either the group that worsened or remained unchanged ($p<0.05$). Furthermore, the t-statistic for the correlation of the subtraction images suggests that a significant difference between the mean correlation of the two groups likely exists ($p<0.20$), but may require more data to confirm. The image 2nd moment, 3rd moment, 4th moment, and contrast were not significantly different between the subtraction image groups.

Table 2. Comparison of subtraction images that improved vs. subtraction images that worsened including a t-stat for the various statistical parameters.

	Improved		***Unchanged***		
Parameter	**Mean**	**Standard Deviation**	**Mean**	**Standard Deviation**	**t-stat**
Image Mean	29.24	8.61	31.42	8.77	-2.68
Uniformity (entropy)	0.642	0.073	0.630	0.068	3.00
2^{nd} Moment (variance)	3889.8	1456.7	4196.7	1514.4	-0.04
3^{rd} Moment (skewness)	$1.2x10^{12}$	$1.4x10^{13}$	$1.1x10^{12}$	$1.3x10^{13}$	2.0×10^{-13}
4^{th} Moment (flatness)	$4.3x10^{17}$	$4.8x10^{18}$	$3.7x10^{17}$	$4.5 x10^{18}$	5.6×10^{-19}
Correlation	0.981	0.088	0.986	0.057	-1.45
Contrast	79.84	25.88	81.60	26.66	-0.42

Table 3. Comparison of subtraction images that improved vs. subtraction images that remained unchanged including a t-stat for the various statistical parameters.

	Improved		*Unchanged*		
Parameter	**Mean**	**Standard Deviation**	**Mean**	**Standard Deviation**	**t-stat**
Image Mean	29.24	8.61	31.05	8.81	-2.10574
Uniformity (entropy)	0.642	0.073	0.631	0.067	2.734344
2^{nd} Moment (variance)	3889.8	1456.7	4147.7	1571.2	-0.03026
3^{rd} Moment (skewness)	$1.2x10^{12}$	$1.4x10^{13}$	$1.3\ x10^{12}$	$1.42\ x10^{13}$	$-6.7\ x10^{-14}$
4^{th} Moment (flatness)	$4.3x10^{17}$	$4.8x10^{18}$	$4.42\ x10^{17}$	$4.85\ x10^{18}$	$-2\ x10^{-19}$
Correlation	0.981	0.088	0.982	0.090	-0.07709
Contrast	79.84	25.88	80.44	27.36	-0.13619

3.2 Computer-Assisted Detection System

A computer-assisted detection (CAD) system was created that utilizes the subtraction image algorithm and statistical analysis results. The CAD utilizes a graphical user interface (GUI) that allows the user to load the patient's original chest radiographs using "load images" button (Figure 4).

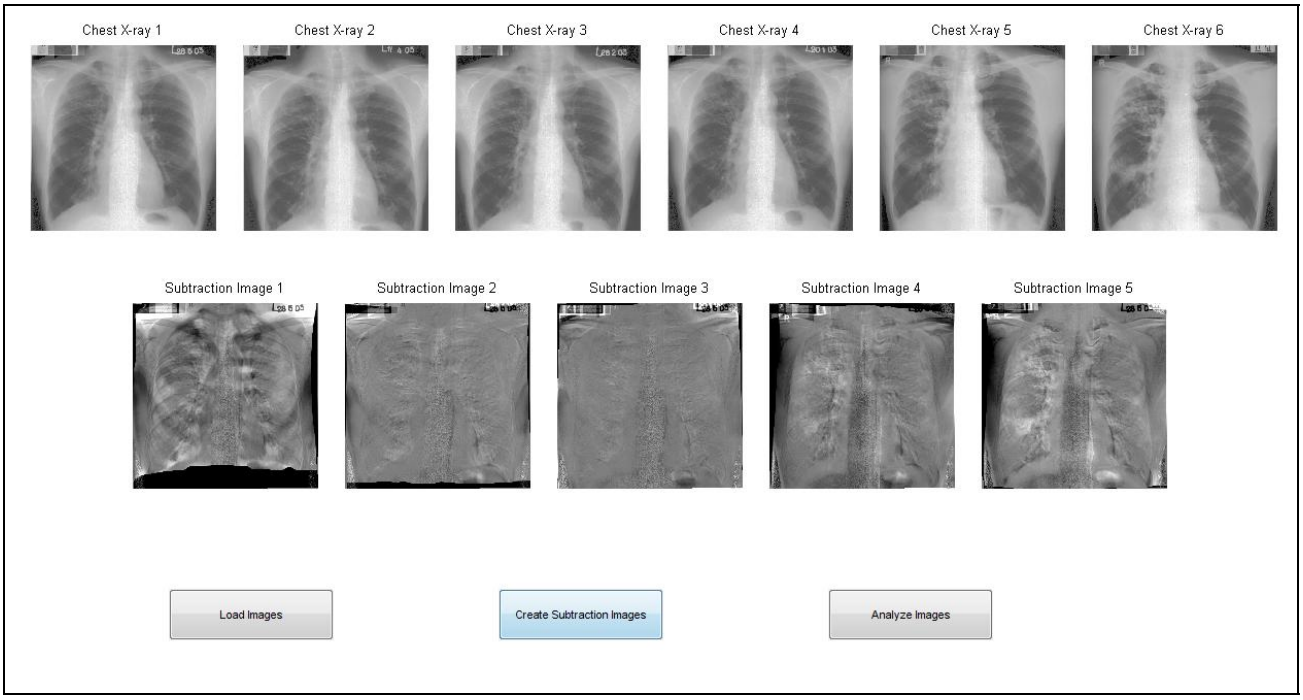

Fig. 4. GUI utilized by the CAD system. All six chest radiographs are displayed on the top row in order of oldest to most recent. The subtraction images are displayed on the second row. The three buttons are displayed on the bottom row.

The original chest radiographs are displayed side-by-side in order from earliest to most recent so that the physician can get a visual feel for the radiographic findings that may be changing over time as a result of DOTS therapy. Once the original chest radiographs have been loaded, the "create subtraction images" button allows the user to create subtraction images using the subtraction image algorithm. The subtraction images are displayed below the original chest radiographs in order. The subtraction images emphasize the areas of greatest difference between a more recent chest radiograph and the original baseline chest radiograph. Finally, the "analyze images" button allows the user to calculate the statistical

parameters of each subtraction image. The statistical parameters are then used to determine whether the chest radiographs suggest that the patient is improving, worsening, or not changing in response to DOTS therapy. The physician may use this CAD in order to determine whether or not to change to an alternate anti-TB pharmaceutical regimen before the patient's condition worsens.

4. CONCLUSION

Currently, TB poses a serious health threat worldwide, especially in many areas of the world that have insufficient medical supplies. The treatment regimen proved to be difficult to follow and led to increased non-compliance. DOTS therapy was developed to increase the effectiveness of the anti-TB treatment regimen. However, drug resistance among various strains of mycobacterium tuberculosis has decreased the effectiveness of DOTS therapy. As a result, TB continues to cause a significant amount of preventable morbidity, mortality.

200 TB patients from Hong Kong were identified. The 200 patients were treated for six months and followed with time-series chest radiographs over that time for a total of 1200 chest radiographs. 390 subtraction images were created from the 1200 original chest radiographs using a subtraction image algorithm. Each lung was isolated and seven statistical parameters were measured on each subtraction image. Image mean and Image uniformity proved to be statistically different between those patients who showed radiological signs of improvement and those patients that did not.

A CAD system was successfully created. The CAD system utilizes a GUI that allows the user to load patient chest radiographs and creates subtraction image using the subtraction image algorithm. Finally, the CAD uses the subtraction images to determine whether or not the patient is showing signs of improvement in response to DOTS therapy. Physicians can use the CAD system to respond earlier to TB treatment failure, potentially leading to improved outcomes.

REFERENCES

[1] Cegielski JP, Chin DP, et al. "The global tuberculosis situation: progress and problems in the 20th century, prospects for the 21st century," Infect Dis Clin North Am 2002; 16:1-58.

[2] Corbett EL, Watt CJ, et al. "The growing burden of tuberculosis: global trends and interactions with the HIV epidemic," Arch Intern Med 2003; 163:1009-1021.

[3] Diagnostic standards and classification of tuberculosis in adults and children. This official statement of the American Thoracic Society and the Centers for Disease Control and Prevention was adopted by the ATS board of directors, July 1999. This statement was endorsed by the Council of the Infectious Disease Society of America, September 1999. Am J Respir Crit Care Med 2000; 161:1376.

[4] Jeong YJ, Lee, KS. "Pulmonary Tuberculosis: Up-to-Date Imaging and Management," American Journal of Roentgenology 2008; 191:834-844.

[5] Chaulk, CP, Kazandjian, VA. Directly observed therapy for treatment completion of pulmonary tuberculosis. Consensus statement of the public health tuberculosis guidelines panel. JAMA 1998; 279:943.

[6] Sharma, SK, Mohan, A. "Multidrug-resistant tuberculosis," Indian J Med Res 2004. 120:354-376.

[7] Gonzalez, R. and Woods, R., [Digital Image Processing Second Edition], Prentice Hall, Upper Saddle River, New Jersey, 665-669 (2002).

An Online Real-Time DICOM Web-based Computer-Aided Diagnosis System for Bone Age Assessment of Children in a PACS Environment

Kevin C. Ma*[a], Aifeng Zhang[a], Paymann Moin[a], Mariam Fleshman[a], Linda Vachon[b], Brent Liu[a], H.K. Huang[a],
[a]Image Processing and Informatics Lab, Dept. of Radiology, Univ. of Southern California, 1450 San Pablo St. Suite 2100 Los Angeles, CA 90033;
[b]LAC+USC Medical Center, Dept. of Radiology, Univ. of Southern California, Los Angeles, CA 90033

ABSTRACT

Bone age assessment is a radiological procedure to evaluate a child's bone age based on his or her left-hand x-ray image. The current standard is to match patient's hand with Greulich & Pyle hand atlas, which is outdated by 50 years and only uses subjects from one region and one ethnicity. To improve bone age assessment accuracy for today's children, an automated race- and gender-specific bone age assessment (BAA) system has been developed in IPILab. 1390 normal left-hand x-ray images have been collected at Children's Hospital of Los Angeles (CHLA) to form the digital hand atlas (DHA). DHA includes both male and female children of ages one to eighteen and of four ethnic groups: African American, Asian American, Caucasian, and Hispanic. In order to apply DHA and BAA CAD into a clinical environment, a web-based BAA CAD system and graphical user interface (GUI) has been implemented in Women and Children's Hospital at Los Angeles County (WCH-LAC). A CAD server has been integrated in WCH's PACS environment, and a clinical validation workflow has been designed for radiologists, who compare CAD readings with G&P readings and determine which reading is more suited for a certain case. Readings are logged in database and analyzed to assess BAA CAD performance in a clinical setting. The result is a successful installation of web-based BAA CAD system in a clinical setting.

Keywords: bone age assessment, computer-aided diagnosis, clinical validation, web-based GUI, clinical workflow

1. INTRODUCTION

1.1 Bone Age Assessment

Bone Age Assessment is a clinical procedure in pediatric radiology to evaluate skeletal maturity based on a frontal left hand and wrist radiograph. It is a common practice to evaluate normality of children's growth and development. The workflow of BAA includes the radiologist examining the left-hand radiograph, and then comparing it to a hand atlas to give a final diagnosis of the patient's bone age. The current gold standard for BAA is the Greulich & Pyle Hand Atlas, which was compiled more than 50 years ago with only Caucasian subjects from the mid-west. To get the BAA process up-to-date for children today, IPILab has proposed a new hand atlas with subjects of multiple ethnicities and an automatic and objective computer-aided diagnosis program to evaluate bone age based on the new hand atlas.

1.2 Digital Hand Atlas and CAD Program

During the past 10 years, 1,390 hand images of normal children, both male and female from Asian, African American, Caucasian and Hispanic ethnic groups were collected and a digital hand atlas (DHA) was formed. Based on the DHA, a fully automatic, objective, race- and gender-specific computer-aided diagnosis (CAD) method has been developed within the Image Processing and Informatics Lab (IPILAB), USC.

The program uses image processing techniques to analyze three major regions of interests of the hand: the phalangeal regions of the middle three fingers, the carpal region, and the wrist joint region. Features from the three analyses are congregated and bone age is calculated with a fuzzy logic system. The CAD workflow is displayed in Figure 1.

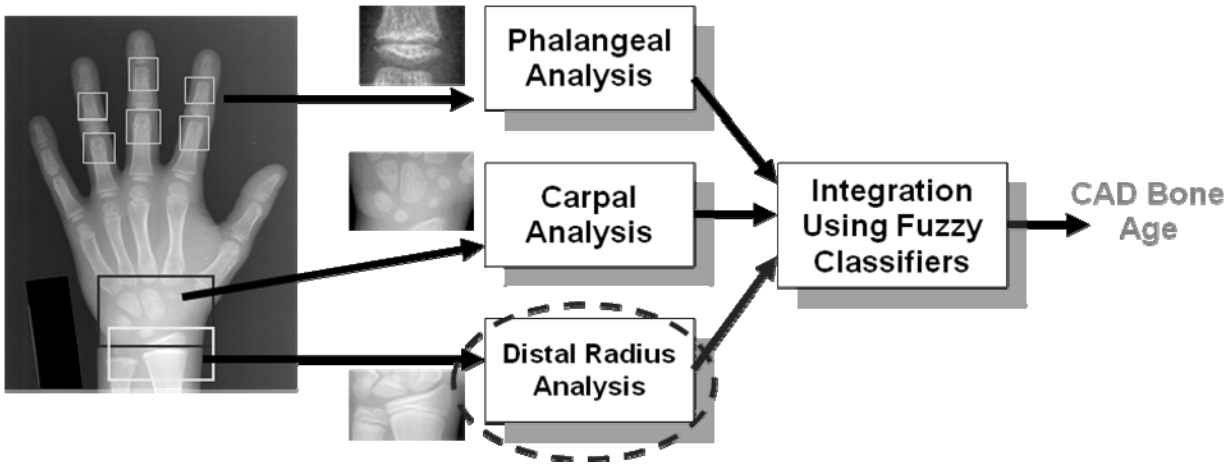

Fig. 1 Bone Age Assessment CAD program workflow. The distal radius region is specially marked because it is still under development, and thus is not incorporated in the clinical validation

The details of BAA CAD algorithms and design have been presented in previous papers and will not be elaborated here. The results from previous studies show that the CAD method with DHA has a higher accuracy to assess bone age of ethnically diverse subjects comparing to G&P hand atlas, the current standard.

1.3 BAA Clinical Validation

To bring DHA and BAA CAD system into a clinical setting to assist radiologists on a daily basis, a web-based client-server system is designed as a novel clinical implementation approach for online and real-time BAA. The Digital Hand Atlas is already available online in JPEG format at http://www.ipilab.org/BAAweb. The clinical validation system includes a stand-alone CAD workstation that is connected with the PACS, a web-based graphical user interface (GUI) at the workstation, and a CAD workflow designed specifically for the clinical environment. The system is integrated in the Radiology department at Los Angeles County Hospital, and cases are collected both in real-time and retroactively to analyze the CAD system's performance.

2. METHODOLOGY

2.1 Workflow Design

The clinical workflow of BAA CAD has been previously designed by IPILab and tested within the laboratory environment. Figure 2 shows the clinical workflow diagram.

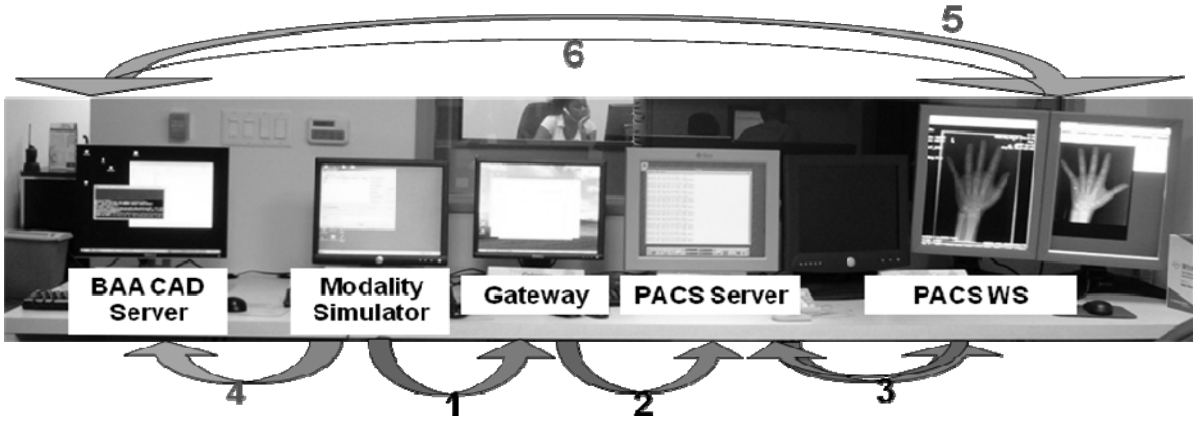

Fig. 2 Simulated Clinical Workflow diagram of BAA CAD system

This workflow design has been previously presented in SPIE and is now summarized here. The workflow has 6 steps, the first 3 steps include conventional PACS workflow in radiology and the last 3 steps detail how data is transmitted in the presence of a CAD workstation:

1. Hand image is sent from the modality simulator (which simulates a CR, DR, or film scanner) to the acquisition gateway
2. Acquisition gateway transmits the image into the PACS storage server
3. PACS workstation queries and retrieves the hand image from PACS and display the image
4. The modality sends a second copy of the hand image to the CAD workstation/server. The server processes CAD results and displays on the web GUI for viewing at PACS workstation
5. Radiologists review both the case and CAD results
6. Readings by radiologists are captured and send back to CAD server for storage

The actual clinical validation workflow is presented by Figure 3.

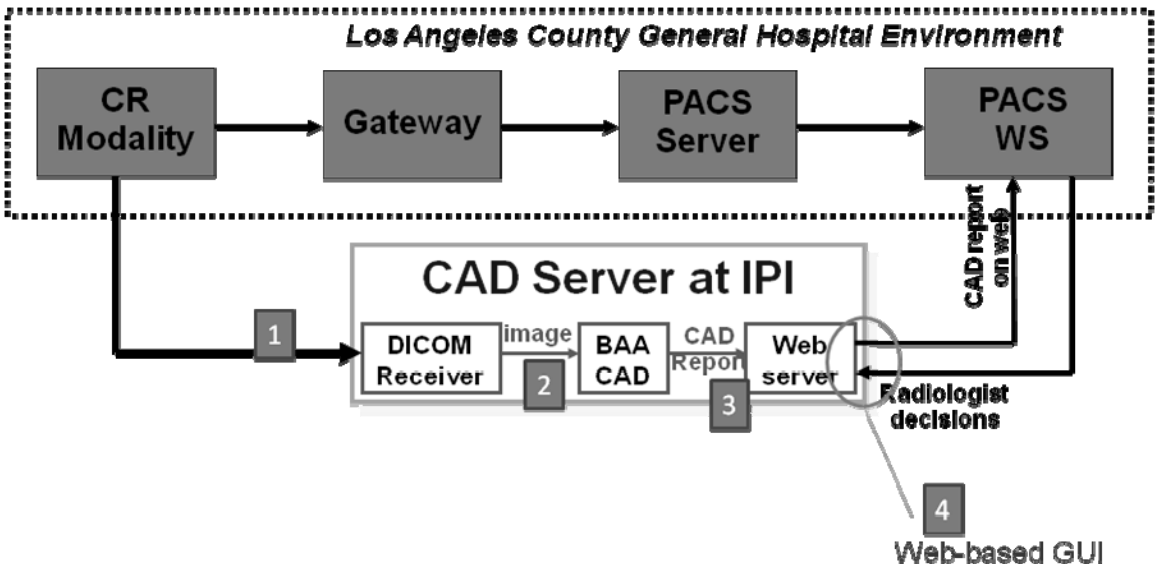

Fig. 3 Clinical Validation Workflow implemented in LAC

The implemented workflow largely corresponds to the proposed workflow:

1. CR sends a copy of the hand image to the CAD server located in the radiology reading room
2. CAD program receives the image, performs BAA and record results in database
3. Web server looks into the database to locate the original image and BAA results, as well as best-matched DHA image (determined by CAD)
4. GUI displays images and guides radiologists through validation steps

2.2 Web-based BAA Clinical Validation system

The BAA CAD server has two components: a CAD server that performs automated BAA, and a web server that serves as a database manager and a graphical user interface for display and a walkthrough of the clinical validation process.

2.2.1 CAD Server

The BAA CAD program is written in MATLAB® and then converted to an executable file for better integration and compatibility. The DICOM receivers and other necessary functions are handled by open-source DICOM Toolkit DCMTK®.

2.2.2 Web Server

The web server is set up such that the CAD results and the validation procedures can be accessed remotely via TCP/IP. A standard Apache® web server is used, and the web user interface is designed in PHP. The database is handled by MySQL.

The web user interface guides the radiologist through the validation process, which is separated into three steps. Figures 4, 5, and 6 are screenshots showing how the GUI works.

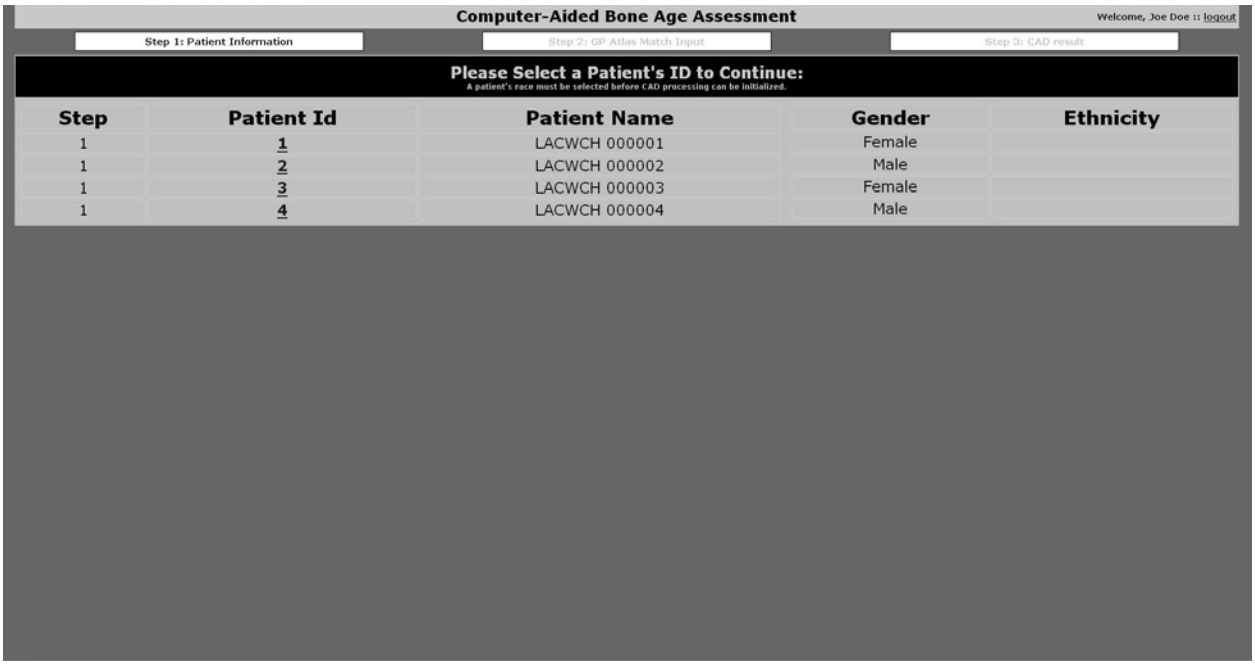

Fig. 4 BAA CAD Clinical validation web GUI - Step 1

During step 1, the GUI displays the list of patients waiting to be evaluated. CAD results have already been stored but are not displayed here. Each patient is anonymized, and patients' genders and ethnicities are displayed. Since ethnicities are not stored in the DICOM header, radiologists have to manually input patients' ethnicities. The radiologist clicks on a patient ID to continue the evaluation process. For example, in Figure 3, the user can select patient "00003 " from the work list….

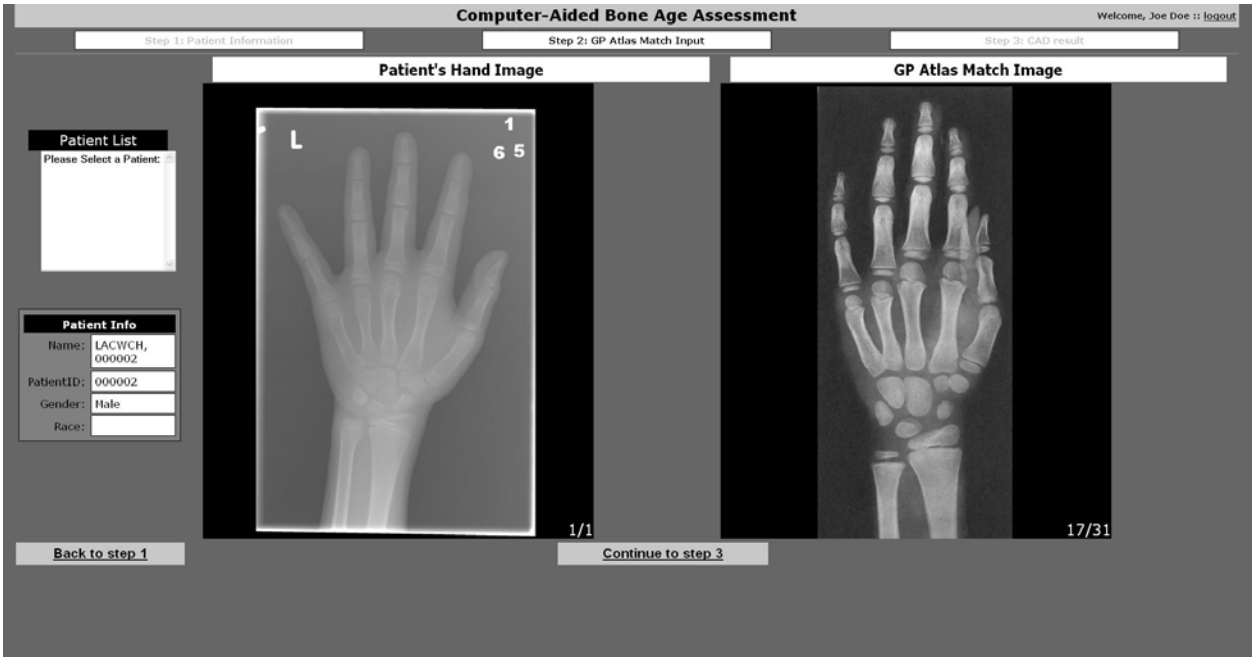

Fig. 5 BAA CAD Clinical validation web GUI - Step 2

Continue to step 2, the GUI displays the patient's hand image as well as scans of hang images from G&P hand atlas. The purpose of this stage is to let radiologists make an unbiased diagnosis using the current standard. After the best-fit atlas image is selected by the radiologist, the result is saved into the database when the user click on the link to go to step 3.

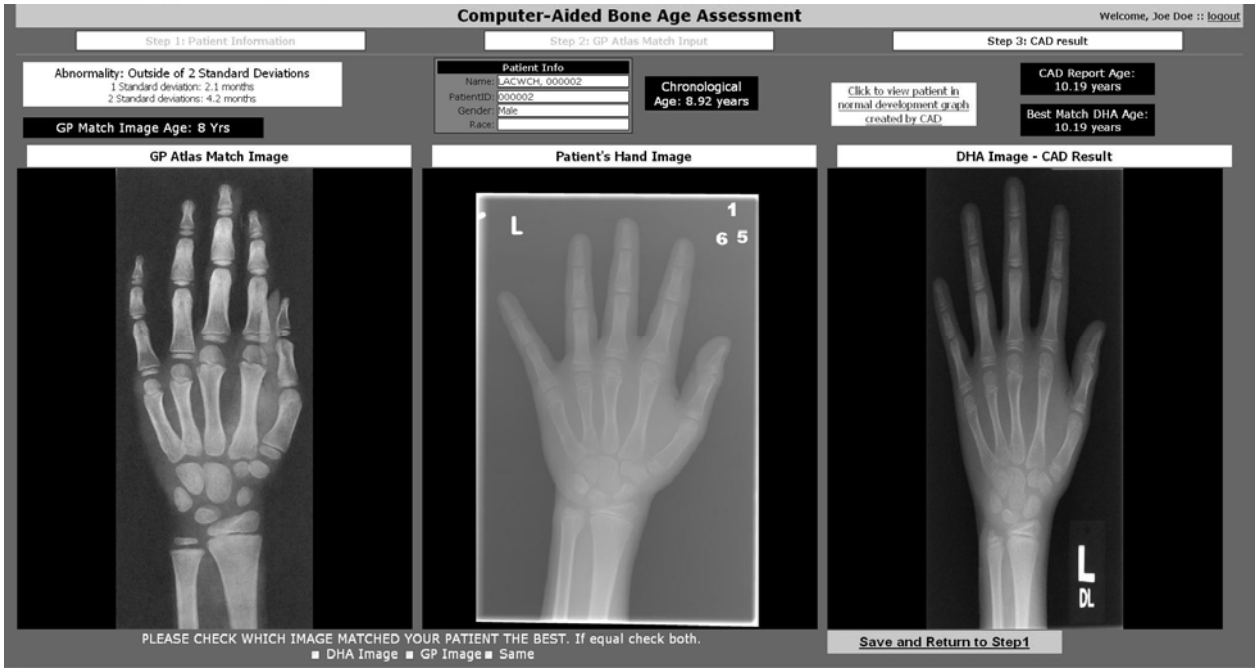

Fig. 6 BAA CAD Clinical validation web GUI - Step 3

During step 3, the GUI displays the patient's hand image in the middle of Figure 6, the G&P atlas hand image selected in Step 2 in the right of Figure 6, and the best-matched digital hand atlas image determined by CAD program in the left of Figure 6. The CAD result is displayed on the right top corner, as well as a normality graph (not shown here) that shows if the patient's BA falls within the range of normal (which is determined by mean and two stand deviations from the G&P atlas). Here, the radiologist can choose if the original diagnosis with G&P atlas is more accurate or if the CAD result is more accurate. When the radiologist clicks "Save and Return to Step 1" link on the right bottom corner of Figure 6, the validation for this patient is complete and the validation starts back from the beginning.

2.3 Integration with Los Angeles County General Hospital

The CAD system was installed in LAC Women & Children's Hospital in February 2008. A DICOM receiving node is created such that CR system on-site can send copies of acquired left-hand images to the CAD server. As of November 2008, the Los Angeles County Hospital has moved to a new location, and thus the system has to be reinstalled and integrated with PACS. Further work is needed for the addition of DRs at LAC, access to archives and historical cases, and access to the web server from remote workstations on-site.

2.4 Data Collection

Between the dates of Feb 2008 to Nov 2008, there have been 74 bone age cases collection from both real-time (directly from modality) and some archived cases hand-picked by Dr. Linda Vachon, radiologist at the Women and Children's Hospital. CAD readings and radiologists' diagnosis from book atlas are both recorded and data analysis is performed to evaluate CAD's performance.

3. RESULTS

The first stage of the clinical validation process is to test the success rate of the CAD program in obtaining a bone age output. CAD output is compared with radiologist readings. Table 1 lists the CAD results of the 74 cases collected.

Table 1. Cases collected at Los Angeles County

Case Description	Total Cases	Normal Cases	Abnormal Cases
Total Number of Cases	74	33	41
CAD successful outputs	35	16	19
CAD error: Unable to detect phalanges	14	3	11
CAD error: Unable to segment hand and fingers	13	8	5
CAD program crashes	12	6	6

"Successful outputs" means that the CAD program is able to output a bone age reading that does not deviate widely from the radiologists' readings. In the unsuccessful cases, the program may not be able to segment the hand correctly, may not be able to select the correct regions of interests, or experience unexpected crashes that requires reboot of the program. "Normal" and "Abnormal" are defined by radiologists' readings. Bone age normality is defined by the G&P Atlas as bone age falling in between plus and minus two standard deviations of the mean bone age. In most cases, radiologists' reports indicate if the patient is normal or not. Since patients' ethnicity data is not recorded, all cases are assumed to be Hispanic since most patients are of Hispanic origins at Los Angeles County. Figure 7 shows CAD results among the success/all cases and success/normal cases. Data analysis is discussed in the next section.

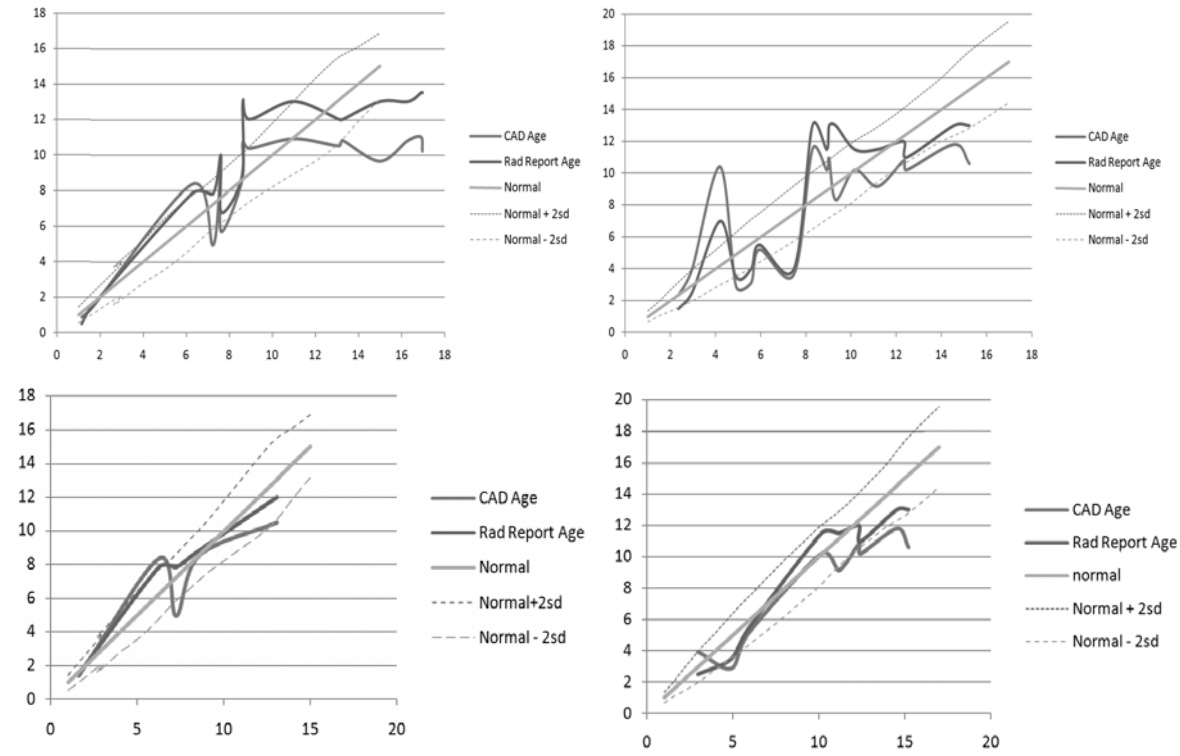

Fig. 7 Plots of CAD BAA readings for clinical validation
Top-left: All Female cases (16 cases) Top-right: All Male cases (19 cases)
Bottom-left: Normal Female cases only (5 cases) Bottom-right: Normal Male cases only (9 cases)

4. DISCUSSION

Connection between BAA CAD system and the clinical PACS environment has been established and tested with multiple cases. Cases stored on CR can be sent to the CAD server, and the CAD program can run successfully and output BAA results.

The success rate of CAD is less than 50%, which is below expectations. One of the reasons for the poor performance is the lack of a hand scanning protocol. The images collected from LAC differ in degrees of finger separation, image angle, wrong hand (right instead of left), and others irregularities that can be observed visually. These problems can be rectified by the enforcement of a standardized scanning protocol. Results of implementation of scanning protocol will be analyzed in a future study.

The preliminary validation results, presented in Figure 7, show that CAD BAA outputs roughly match radiologists' readings based on G&P atlas, especially for the normal cases. Since the CAD program is designed and trained on normal studies, the CAD results for abnormal cases are not used in evaluating CAD performance. Currently, the sample size is not yet large enough to draw definite conclusions regarding CAD performance.

CAD outputs generally agree with radiologists' readings for younger children, while the two readings differentiate more in older children. This can be explained by two reasons. First, the epiphysis and metaphysis fully closes after around 13-15 years of age, and thus the "degree of separation" feature from phalanges are no longer applicable, leading to underreading from CAD. This problem can be solved by including the distal radius analysis element into the CAD program. The second reason for the bigger difference in bone age readings for older children can be attributed to the nature of carpal features and phalangeal features. Younger children's bone age assessments depend mostly from the size and shape of carpal bones and epiphysis, which is more defined and easier to calculate. Older children's bone age analysis depends mostly on separation of epiphysis and metaphysis, a more difficult feature to compute.

The second stage of BAA CAD clinical validation, which is the utilization of web-based GUI for radiologists to evaluate CAD performance, is under development and will be deployed in the near future.

5. CONCLUSION

Bone Age Assessment Computer-aided Diagnosis system has been developed at the IPILab and is now in the clinical validation stage. A web-based BAA clinical validation system has been installed in Los Angeles County affiliated with University of Southern California, and the CAD system has been integrated with the PACS environment. A web-based GUI has been developed to aid radiologists in comparing CAD bone age results with results based on the Greulich & Pyle Hand Atlas. Some cases are collected and CAD performance has shown promising results. CAD program errors are observed and system performance can be further improved.

Future works include the completion of distal radius analysis and incorporating the third component of bone age analysis into the BAA CAD program. A standard scanning protocol for hand images is needed for improving CAD accuracy, and more cases will be evaluated along with the evaluation of a real-time validation result using the web-based GUI and related technologies.

REFERENCES

[1] Greulich W, Pyle S, *Radiographic Atlas of Skeletal Development of Hand and Wrist*, Stanford, CA: Stanford University Press, 1959

[2] Pietka E, Pospiech-Kurkowska S, Gertych A, Cao F, Huang HK, "Computer-Assisted Bone Age Assessment: Image Analysis And Fuzzy Classification", Radiology, 225(P), 751, 2002.

[3] Pietka E, Gertych A, Pospiech S, Cao F, Huang HK, Gilsanz V, "Computer Assisted Bone Age Assessment: Image Processing and Epiphyseal/Metaphyseal ROI Extraction,: IWWW Trans. Medical Imaging, 20, 715-729, 2001

[4] Pietka E, Pospiech S, Gertych A, Cao F, Huang HK, Gilsanz B, "Computer Automated Approach to the extraction of epiphyseal regions in hand radiographs," Journal of Digital Imaging, 14, 175-172, 2002.

[5] Gertych A, Zhang A, Sayre J, Pospiech-Kurkowska, S, Huang, HK, "Bone Age Assessment of Children using a Digital Hand Atlas,:" Computerized Medical Imaging and Graphics, May 2007.

[6] Huang HK, *PACS and Imaging Informatics: Basic Principles and Applications*, Wiley & Sons, NJ, p. 44, 504-507, 2004

[7] Zhang A, Zhou Z, Gertych A, Liu B, Zheng X, Huang HK, "Integration of Bone Age Assess,emt CAD Results with the PACS Diagnostic Workflow Utilizing DICOM Structure Report", Scientific Poster, RSNA 2006

[8] Zhang A, Uyeda J, Tsao S, Ma K, Vachon L, Liu B, Huang HK, "Web-based Computer-aided diagnosis (CAD) System for Bone Age Assessment (BAA) of Children" Medical Imaging 2008: PACS and Imaging Informatics. Proceedings of the SPIE, Volume 6919, 69190H (2008)

The Development of an MRI Lesion Quantifying System for Multiple Sclerosis Patients Undergoing Treatment

Paymann Moin[a], Kevin Ma[a], Lilyana Amezcua[b], Arkadiusz Gertych[c], Brent Liu[a]
[a]Image Processing and Informatics Lab, Department of Radiology, USC Keck School of Medicine, 1450 San Pablo Street, Suite 2100, Los Angeles, California 90033
[b]Multiple Sclerosis Comprehensive Care Center, Department of Neurology, USC Keck School of Medicine, 1520 San Pablo Street, Suite 3000, Los Angeles, California 90033
[c]Minimally Invasive Surgical Technologies Institute, Cedars-Sinai Medical Center, 8700 Beverly Boulevard, Davis 6062, Los Angeles, California 90048

ABSTRACT

Multiple sclerosis (MS) is a demyelinating disease of the central nervous system that affects approximately 2.5 million people worldwide. Magnetic resonance imaging (MRI) is an established tool for the assessment of disease activity, progression and response to treatment. The progression of the disease is variable and requires routine follow-up imaging studies. Currently, MRI quantification of multiple sclerosis requires a manual approach to lesion measurement and yields an estimate of lesion volume and interval change. In the setting of several prior studies and a long treatment history, trends related to treatment change quickly become difficult to extrapolate. Our efforts seek to develop an imaging informatics based MS lesion computer aided detection (CAD) package to quantify and track MS lesions including lesion load, volume, and location. Together, with select clinical parameters, this data will be incorporated into an MS specific e-Folder to provide decision support to evaluate and assess treatment options for MS in a manner tailored specifically to an individual based on trends in MS presentation and progression.

Keywords: imaging informatics, magnetic resonance imaging (MRI)**,** multiple sclerosis (MS), computer aided detection (CAD).

1. INTRODUCTION

The objective of our project is to determine if MRI and imaging informatics tools designed specifically for monitoring and treating multiple sclerosis improve the detection of treatment response in patients with MS. Specifically, we are developing an MS Lesion CAD system for quantifying lesion load, volume, and location. It is hoped that such a comprehensive imaging informatics based e-Folder system for MS Patients will provide a solid yet adaptable platform for treatment assessment, outcomes analysis and decision-support in both the clinical and research environments.

1.1. The need for a comprehensive multiple sclerosis database

Studies have shown that factors such as racial groups and environmental exposures can affect the manifestation of differing forms and patterns of disease progression in multiple sclerosis. These initial results demonstrate the importance of creating a comprehensive database to address the differing disease assessment and treatment needs of various patient populations as grouped by patient and environmental variables. In particular, Hispanics belong to a complex admixture of Caucasian and Asian ancestry that might lead to the reported complex form of MS prevalent in this group. In addition to the possibility that MS has a unique presentation and course in Hispanics, it is important to note that a steady rise in the prevalence of MS in Hispanics has been reported in Latin America that cannot be explained by better identification of the disease.

1.2. The need for imaging informatics tools as biomarkers for MS

Diagnosis is based upon clinical data and MRI, which is the strongest surrogate marker of MS disease. MRI is an established tool for the assessment of disease activity, progression and response to treatment. Following diagnosis, disease activity is indicated by the number of relapses per year (relapse rate), accumulation of disability as measured

by the expanded disability status scale (EDSS) and changes in MRI lesion characteristics. The progression of the disease is variable, and requires routine follow-up imaging studies to document disease exacerbation, improvement, or stability of the characteristic MS lesions. Currently, MS plaque quantification requires a time consuming manual approach to lesion measurement on MRI. The task of tracking MS lesion changes becomes more difficult if several MR studies of the same patient require quantitative comparison. Therefore, lesion detection and tracking could be greatly improved through the use of imaging informatics tools. Utilizing CAD (computer-aided-detection) methods is considered ideal for monitoring progression of MS.

1.3. The need for an imaging informatics-based e-Folder system

The concept of the electronic patient record (ePR) is a patient-based digital folder of clinical information obtained from various sources. The inclusion of imaging data and built-in decision support makes the ePR stand out amongst general clinical information systems. The e-Folder system differs from the ePR in two ways:

1) The e-Folder system is a subset group of patients, in this case, MS patients, with specifically tailored imaging informatics data together with diagnostic clinical data.

2) The e-Folder is designed to allow for data mining of specific disease characteristics across making it more powerful than the patient-centric ePR for use in longitudinal studies.

The e-Folder system serves as an adaptable, comprehensive tool to mine data and investigate complex associations such as cross-racial discrepancies and characteristics of MS patients from various ethnicities. There have been previous large-scale clinical databases tailored to MS patient outcomes, however there are no such systems that include powerful image quantifying and analysis tools to track MS lesion load. This platform holds the promise of providing decision support to evaluate and assess future drug treatment options.

2. STUDY METHODOLOGY

As an initial clinical application of this e-Folder system, the clinical disease expression in Hispanics is being investigated. The diversity of the Los Angeles area provides a unique opportunity to study the effects of ethnicity, genetic and environmental factors in MS. Several departments within the University of Southern California are working together in an effort to share data collection and results in both the private and public care settings.

The Department of Neurology is responsible for patient recruitment, management and treatment. Patients with clinical definite MS as defined by the newly revised McDonald criteria are offered the opportunity to participate in this study. Patients are ethnically defined as Caucasian, Asian, African American, or Hispanic.

Neuroradiology attending physicians and neuroradiology fellows review and annotate magnetic resonance imaging examinations selected for inclusion in this study. The fellows and attendings that review studies are within the Division of Neuroradiology, Department of Radiology, USC Keck School of Medicine. Using an overlay tool developed for this project, three physician reviewers manually outline lesions that are consistent with imaging findings suggestive of multiple sclerosis plaques. Results are compared among the reviewing attending staff and fellows to evaluate for significant discrepancies. The results, which are considered the gold standard for this study, are compared against the MS CAD results for sensitivity and specificity of lesion load and volume. The Image Processing and Informatics laboratory (IPILab) is responsible for the development of the automatic MS lesion quantification package with clinical input from the aforementioned collaborating departments.

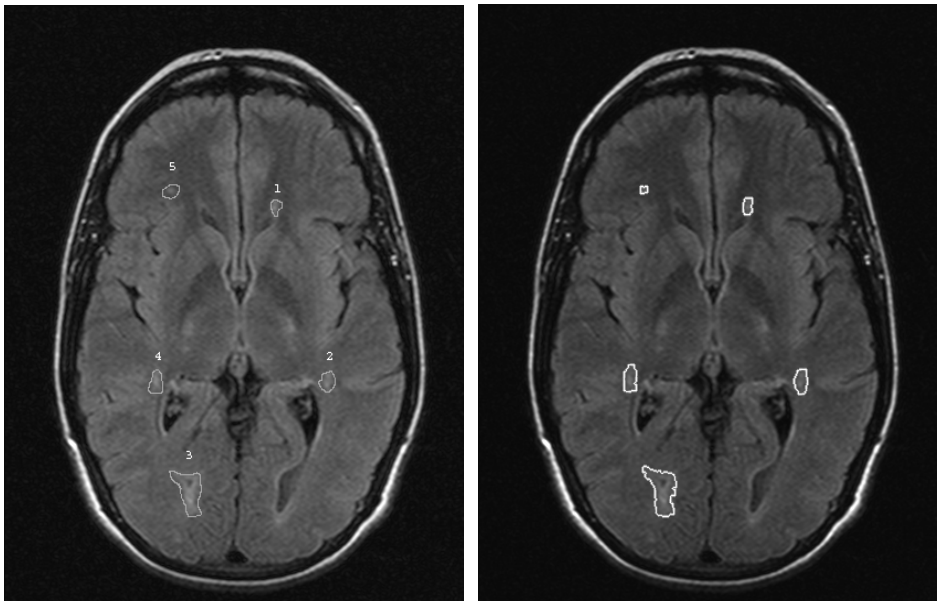

(a) (b)

Figure1.Neuroradiologist identification (a) and CAD result (b) of suspected MS related lesions on FLAIR sequence.

2.1. Two-Phase data collection and model development of MS Patients

Patients have been retrospectively selected from each of four specified ethnicities. In addition, twenty MS patient cases are to be prospectively selected for a small pilot study. Patients presenting to USC MS Clinics (USC+LAC Outpatient Clinics and the USC MS Comprehensive Care Center) are invited to participate in this study. Socio-demographic data and clinical MS characteristics are being collected. Patients are classified into Hispanic and non-Hispanic, with ethnicity information from both groups.

The following data are collected and cataloged: race, gender, migration history, age of disease onset, type of MS, initial presentation, duration of disease, expanded disability status scale (EDSS), current and past disease modifying treatment, exposure to a selected set of pathogens, family history of MS, and MRI data. MRI data is collected with attention to lesion distribution as defined by T2/FLAIR lesion volume and gadolinium enhancing lesions involving both the brain and spinal cord. In addition, MS lesion load, volume and location are extracted by the MS lesion CAD 3D tracking algorithm.

2.2. Development an e-Folder System to integrate collected data and construct a data model

An e-Folder System to integrate data collected for different racial groups is being designed and developed at IPILab based upon the developed data model. Analysis includes assessing the number, volume and location of inflammatory demyelinating lesions. The CAD results are compared with the gold standard based on manual outlines of neuroradiologists. A repeated measures analysis of variance is used to test the manual versus the CAD outline areas. In addition, data mining and visualization tools are being developed to assess the treatment and outcome analysis based on the cohort of MS patients. A user friendly Graphic User Interface (GUI) is being developed for better visualization of patient data and treatment planning.

2.3. Evaluation of the e-Folder system in a cohort of MS patients

Once complete, the e-Folder System is to be tested and evaluated on MS patients of Hispanic descent to seek statistically significant correlations such as cross-racial discrepancies. For now, our focus is the collection and analysis of data to uncover the potential association of treatment outcomes with imaging data. MRI scans are conducted prior to and following treatment with natalizumab, a relatively new disease modifying drug for MS. An automated quantification system for T2, FLAIR and T1 lesion volumes, load, and location in patients is being developed and validated.

3. CAD ALGORITHM

3.1. CAD algorithm for quantifying MS lesions

Multiple sclerosis is a disease well suited for automated analysis. A CAD algorithm using MRI T1 and FLAIR sequences has been developed to assist in making MS diagnoses. The T1 sequence is utilized for brain anatomy and the FLAIR sequence is employed to identify MS-related locations of demyelination.

The segmentation algorithm classifies normal and abnormal brain structures and then measures the volume of multiple sclerosis lesions using fuzzy c-means clustering with incorporated spatial (sFCM) information. First, using T1 image data, a mask of intracranial structures is localized and superimposed upon FLAIR image data. Locations with signal corresponding to foci of demyelination are identified using the sFCM method and quantified within a predefined volume.

Each lesion and all image slices are processed in preparation for volumetric segmentation. All related lesions are then combined to form a three-dimensional representation. A report is generated by the CAD system as a means of tracking MS lesions across the two dimensional image slices that are summed to form volumes. When comparison studies exist, a further step of comparing interval change in location and overall volume is also completed. The process is summarized in graphical format in Figure 2.

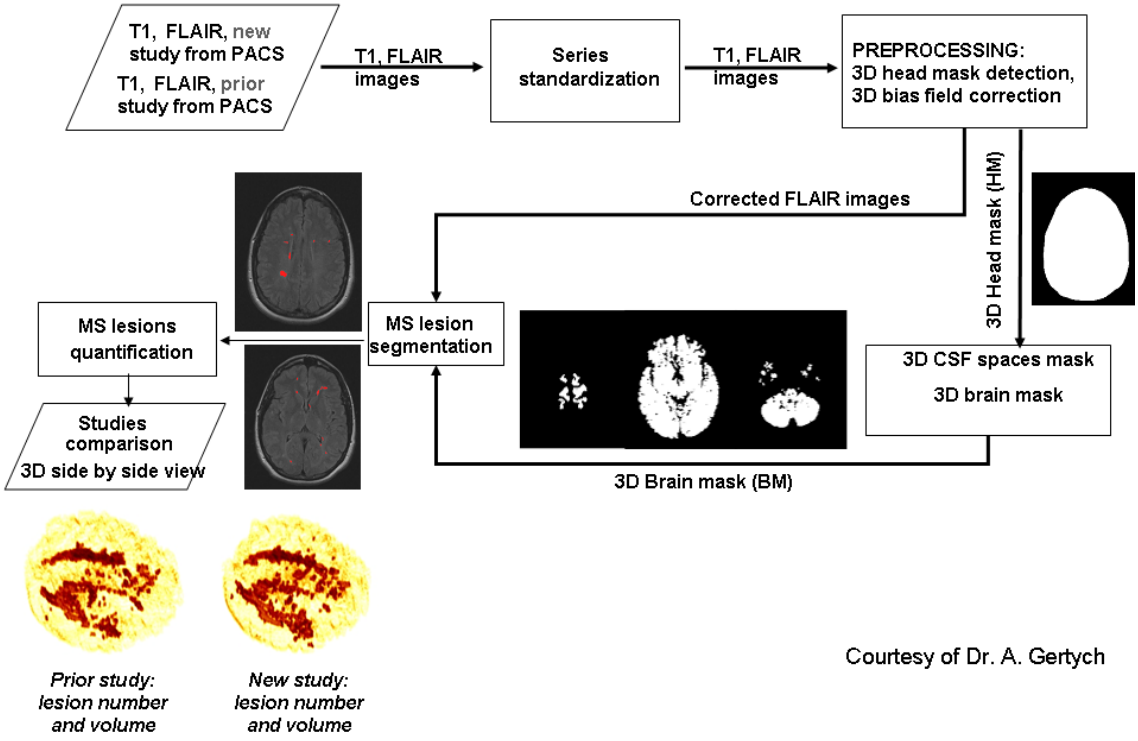

Figure 2. CAD workflow of MS lesion quantification

The detected lesions in each of the 2-D image slices are processed in order to link across multiple slices. A lesion is treated as a multi-slice lesion if areas of two detected lesions lying on neighboring slices overlap. Figure 3 demonstrates the methodology for 3-D volume segmentation of the MS lesions. Each lesion and all image slices are processed for volumetric segmentation. Referring to Figure 3, (a) demonstrates detected lesions in one axial plane FLAIR image (b) demonstrates an overlay of two contiguous axial plane FLAIR images where two of the lesions from both image slices overlap (c) demonstrates overlays for all axial plane image slices. Note that each color set of lesions represent MS lesions detected from a particular image slice. All related lesions are then combined to form the 3-D representation and the end results are shown in Figure 4 in the form of a CAD report. This report is generated by the CAD system as a means of tracking MS lesions across 2-D image slices that form 3-D volumes.

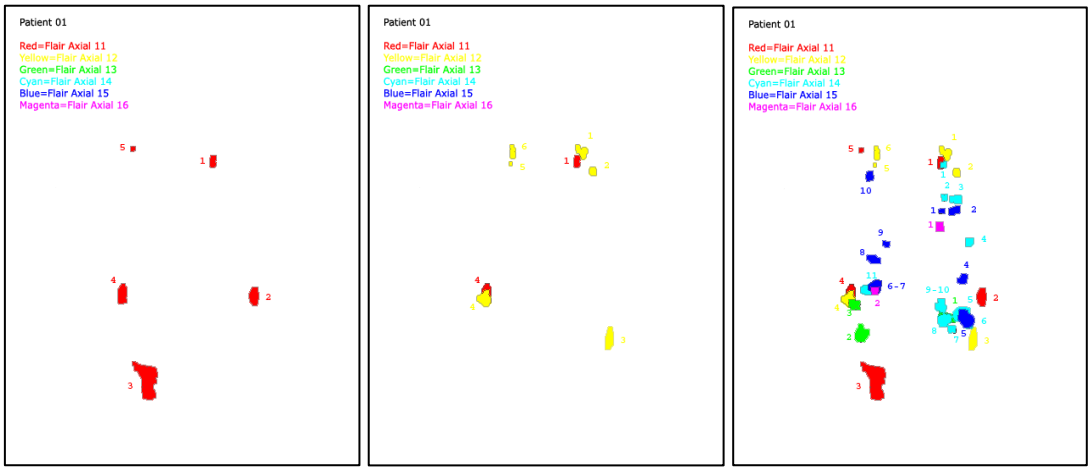

Figure 3. (a) MS lesions on one axial plane FLAIR image (b) MS lesion overlay of two axial FLAIR slices (c) color map of MS lesions on all FLAIR slices

Lesion Name	Slice areas included in lesion	Total Count	Red	Yellow	Green	Cyan	Blue	Magenta
A	red 1, yellow 1	213	82	131				
B	red 2	172	172					
C	red 3	617	617					
D	red 4, yellow 4, Green 3	501	188	212	101			
E	red 5	24	24					
F	yellow 2	65		65				
G	yellow 3	194		194				
H	yellow 5	16		16				
I	yellow 6	79		79				
J	Green 1, Cyan 5, 8, 9-10, 6*, Blue 5*	1058			143	634	281	
K	Green 2	250			250			
L	Cyan 1	50				50		
M	Cyan 2	50				50		
N	Cyan 3	120				120		
O	Cyan 4	82				82		
P	Cyan 6	58				58		
Q	Cyan 7	55				55		
R	Cyan11, Blue 6-7, Magenta 2	393				151	170	72
S	Blue 1	37					37	
T	Blue 2	111					111	
U	Blue 3	0					0	
V	Blue 4	102					102	
W	Blue 8	125					125	
X	Blue 9	52					52	
Y	Blue 10	88					88	
Z	Magenta 1	89						89

* Cyan 5 and 6 are not connected in slice 14 but join lesion J through Blue 5.

Figure 4. CAD report of identified suspected MS-related lesions.

3.2. Current challenges and future work

Most of the data collected thus far consists of studies conducted on a 1.5 Tesla MRI unit. In addition, each sequence acquired contains images that are 5mm thick with 5mm gaps between each sequential image. This study acquisition protocol has proven to be an early challenge in the compilation of segmented 2D images into 3D data sets. A trend that developed was a significant degree of variation of the calculation of lesion volumes due to the large gap between images. We are working to change the imaging protocol for future studies to include thinner sections with smaller or no gaps. We hope that this will resolve this issue.

In addition, our clinical site recently acquired a 3.0 Tesla MRI. We hope to perform some initial studies comparing segmentation and calculation results between 1.5 and 3.0 Tesla studies. We hope that the improved signal to noise ratio will result in more precise identification and delineation of MS-related lesions.

4. GRAPHICAL USER INTERFACE

4.1. Graphical user interface to manage data

A highly adaptable Graphical User Interface (GUI) is being designed to display and manage MS lesion tracking information derived from the MS CAD algorithm as well as relevant neurological and functional clinical data. Visualization of MS lesions will be available in multiple formats to allow display and organization of data in a manner most conducive to a specific need. Several image display options are being developed including two-dimensional MRI images with localized MS lesions as well as multiplanar three-dimensional volume and surface rendered images. Potentially innovative imaging informatics tools that combine data analysis and image display will also be available and include:

- a four-dimensional display for longitudinal temporal evaluation of the course of MS lesions
- localization of MS lesions by functional brain region and white matter tracts
- image fusion for individual patients and user defined cohorts (eg. different ethnic groups) for differentiation of potential patterns of lesion location, lesion volume, disease course, and treatment response
- tracking of imaging characteristics and plotting lesion load against clinical variables such as the EDSS
- an anatomically based frequency distribution map of lesion location and disease course with modifiable patient variables such as ethnicity to better characterize disease type, tailor treatment, and better predict outcome.

These sets of tools will allow for a powerful GUI with customizable toolbars to allow users to manage and evaluate data with the hope of highlighting and validating previously unidentified disease trends and characteristics.

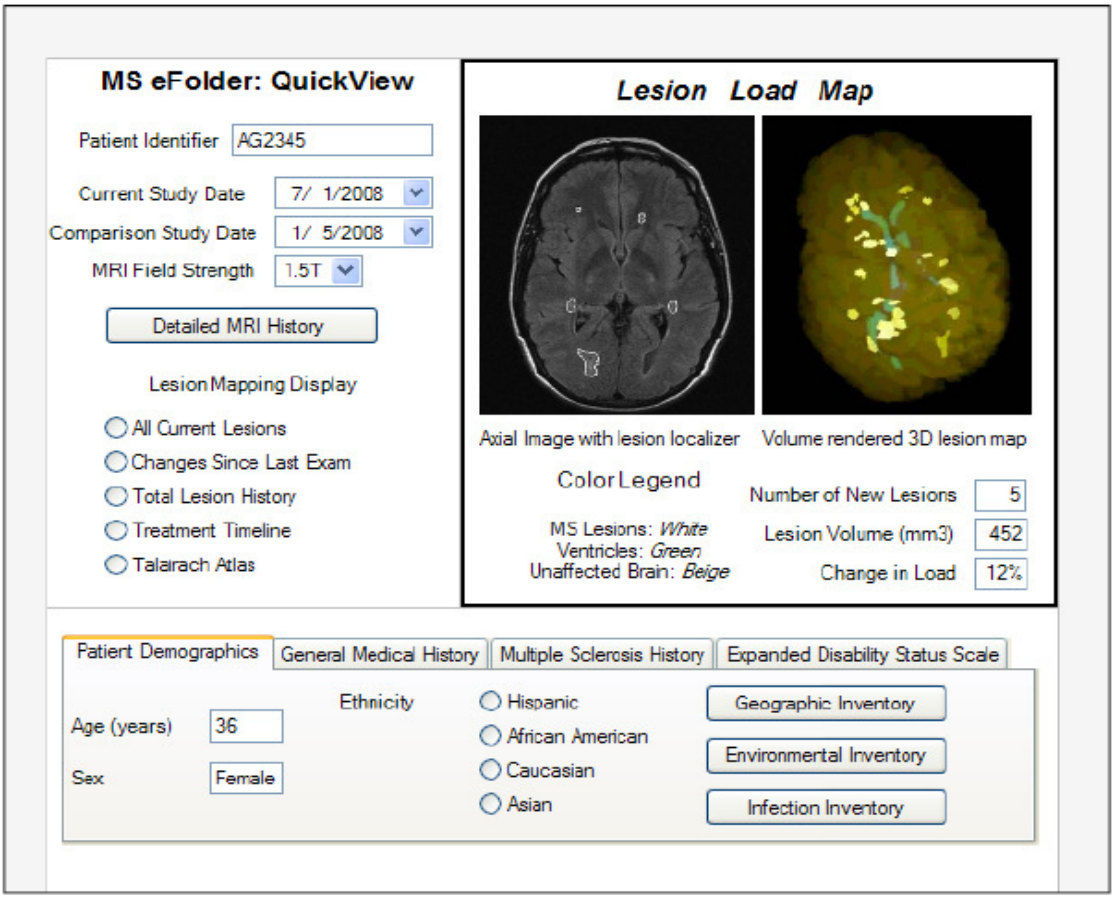

Figure 5: A page from an early prototype of the GUI designed for the e-Folder System. This is the QuickView page which contains an overview of some of the tools available for use. Access to patient data as well as several imaging and analytical tools are available to allow complex analyses utilizing user defined clinical and imaging parameters. All image results can be exported as DICOM format and can be utilized by any imaging applications that are DICOM-compliant. In this the case 2D views can be displayed side-by-side with the volumetric views. The user can navigate each accordingly.

5. CONCLUSIONS

A CAD algorithm for the detection and quantification of multiple sclerosis lesions has been developed. Work on the clinical incorporation of this algorithm to monitor and assist in the treatment of multiple sclerosis continues. It is hoped that the outcomes of this study will lead to an imaging-based automated quantification and classification/grading system for MS based upon lesion load, volumes, and location that can be utilized for treatment evaluation, disease associations, and future clinical trials.

ACKNOWLEDGEMENTS

Paymann Moin is partially supported by the NIH/NIBIB T32 EB014308 Biomedical Imaging Informatics Training Program

REFERENCES

[1] "Just the Facts," National Multiple Sclerosis Society, (2000-2001).
[2] Filipi M, Douset V, McFarland HF, Miller DH, Grossman RI, "Role of magentic resonance imaging in the diagnosis and monitoring of multiple sclerosis: consensus report of the White Matter Study Group," J Magn Reson Imaging 15(5), 449-509 (2002).
[3] Kurtzke JF, "Rating neurologic impairment in multiple sclerosis: an Expanded Disability Status Scale (EDSS)," Neurology 33, 1444-1452 (1983).

[4] McFarland HF, Barkhof F, Antel J, Miller DH, "The role of MRI as a surrogate outcome measure in multiple sclerosis," Mult Scler 8(1), 40-51 (2002).
[5] Moreu T, Thorpe J, Miller D, Moseley I, Hale G, Wladmann H, "Preliminary evidence from magnetic resonance imaging for reduction in disease activity after lymphocyte depletion in multiple sclerosis," The Lancet 344, 298-302 (1994).
[6] Filippi M, Horsfield MA, Morrissey SP, et al., "Quantitative brain MRI lesion load predicts the course of clinically isolated syndromes suggestive of multiple sclerosis," Neurology 44,635-641 (1994).
[7] Iannucci G, Minicucci L, Rodegher M, Sormani MP, Comi G, Filippi M, "Correlations between clinical and MRI involvement in multiple sclerosis: assessment using T1, T2 and MT histograms," J Neurol Sci. 171, 121-129 (1999).
[8] O'Connor PW, et al., "Randomized multicenter trial of natalizumab in acute MS relapses: Clinical and MRI effects," Neurology 62, 2038-2043 (2004).
[9] Miller DH, et al., "MRI outcomes in placebo-controlled trial of natalizumab in relapsing MS," Neurology 68, 1390-1401 (2007).
[10] Sicotte NL, Voskuhl RR, Bouvier S, et al., "Comparison of multiple sclerosis lesions at 1.5 and 3.0 T," Invest Radiol 38, 423-427.
[11] Pollman C, Reingold S, Edan G, et al., "Diagnostic Criteria for Multiple Sclerosis 2005 Revisions to the "McDonald Criteria," Ann Neurol 58, 840-846 (2005).
[12] Wong A, Gertych A, Zee CS, Guo B, Liu BJ, "A CAD system for assessment of MRI findings to track the progression of multiple sclerosis," Proceedings of SPIE Medical Imaging, 65142U-1-7 (2007).
[13] Bezdek J, Hall LO, and Clark L, "Review of MR, image segmentation techniques using pattern recognition," Medical Physics 20(4), 1033-1048 (1993).
[14] Noordam J, van den Broek W, and Buydens L, "Geometrically guided fuzzy c-means clustering for multivariate image segmentation," Proceedings 15th International Conference on Pattern Recognition IEEE, 462-465 (2000).
[15] Pachai C, Zhu Y, Grimaud J, Hermier M, Dromigny-badin A, Boudraa A, Gimenez G, Confavreux C, and Froment J, "A pyramidal approach for automatic segmentation of multiple sclerosis lesions in brain MRI," Comput Med Image Grap 22(5), 399-408 (1998).
[16] Mitchell J, Karlik S, Lee D, Eliasziw M, Rice G, and Fenster A, "The variability of manual and computer assisted of computer assisted quantification of multiple sclerosis lesion volumes," Med. Phys. 23(1), 85-97 (1996).
[17] Alfano B, Brunetti A, Larobina M, Quarantelli M, Tedeschi E, Ciarmiello A, Coveli E, and Salvatore M, "Automated segmentation and measurement of global white matter lesion volume in patients with multiple sclerosis," Journal of Magnetic Resonance Imaging 12(6),799-807 (2000).
[18] Shan Z, Yue G, and Liu J, "Automated histogram-based brain segmentation in t1-weighted threedimensional magnetic resonance head images," Neuroimage 17(3), 1587-1598 (2002).
[19] Ebers GC, "A genetic basis for familial aggregation in multiple sclerosis," Nature 377, 150-151 (1995).
[20] Islam T, et al., "Childhood sun exposure influences risk of multiple sclerosis in monozygotic twins," Neurology 69(4), 381-8 (2007).
[21] Ascherio A., et al., "Environmental risk factors in multiple sclerosis. Part I: the role of infection," Ann Neurol 61(4), 288-99 (2007).
[22] Barcellos LF., et al., "Heterogeneity at the HLA-DRB 1 locus and risk of multiple sclerosis," Hum Mol Genet 15(18), 2813-2824 (2006).
[23] Beebe GW, et al., "Studies on the natural history of multiple sclerosis. 3. Epidemiologic analysis of the army experience in World War II," Neurology 17(1), 1-17, (1967).
[24] Cree Ba, et al., "Clinical characteristics of African American vs Caucasian Americans with multiple sclerosis," Neurology 63(11), 2039-45 (2004).
[25] Kira J, "Multiple Sclerosis in the Japanese population," Lancet Neurol. 2(2), 117-27 (2003).
[26] Wingerchuck DM, et al., "The clinical course of neuromyelitis optica (Devic's syndrome)," Neurology 53(5), 1107-1114 (1999).
[27] Cordova J, et al., "Western and Asian features of multiple sclerosis in Mexican Mestizos," Clinical Neurology Neurosurgery 109(2), 146-51 (2007).
[28] Lisker R, et al., "Gene frequencies and admixture estimates in four Mexican urban centers," Human Biology 62(6), 791-801 (1990).
[29] Gonzalez O, Sotelo J, "Is the frequency of multiple sclerosis increasing in Mexico?" Journal of Neurology, Neurosurgery and Psychiatry 59(5), 528-30 (1995).

[30] Velazquez-Quintana M, et al., "Esclerosis multiple en Mexico: un studio multicentrico," Revista de Neurologia 36, 1019-22 (2003).
[31] Sotelo J, "On the viral hypothesis of multiple sclerosis: participation of varicella-zoster virus," Journal of Neurological Science 262(1&2), 113-6 (2007).
[32] Tarrtas R, et al., "Varicella, ephemeral breastfeeding and eczema as risk factors of multiple sclerosis in Mexicans," Acta Neurol Scand 105(2), 88-94 (2002).
[33] Pollman C, Reingold S, Edan G, et al., "Diagnostic Criteria for Multiple Sclerosis: 2005 Revisions to the McDonald Criteria," Ann Neurol 58,840-846 (2005).
[34] U.S. Census Bureau American fact finder. Available at: http://factfinder.census.gov/home/saff/main.html?_lang=en. Accessed April 3, 2008
[35] Kurtzke JF, "Rating neurologic impairment in multiple sclerosis: an expanded disabilitystatus scale (EDSS)," Neurology 33, 1444-1452 (1983).
[36] Butzkueven H, Chapman J, Cristiano E, Grand'Maison F, Hoffman M, Izquierdo G, Jolley D, Kappos L, Leist T, Pohlau D, Revera V, Trojano M, Verheul F, Malkowski J-P, "MSBase: an international, online registry and platform for collaborative outcomes research in multiple sclerosis," Multiple Sclerosis 12, 769-774 (2006).
[37] Gean-Marton AD, et al., "Abnormal corpus callosum: a sensitive and specific indicator of multiple sclerosis," Radiology 180, 215-221 (1991).
[38] Barkhoff F, Filippi M, Miller DH, et al., "Comparison of MR imaging criteria at first presentation to predict conversion to clinically definite multiple sclerosis," Brain 120, 2059-2069 (1997).
[39] Barkhoff F, "The clinio-radiological paradox in multiple sclerosis revisited," Curr Opin Neurol 15(3), 239-245 (2002).

A Virtualized Infrastructure for Molecular Imaging Research using a Data Grid Model

Jasper Lee, Al Gurbuz, Grant Dagliyan, Brent Liu
Image Processing & Informatics Laboratory, USC 90033, CA
Molecular Imaging Center, USC 90033, CA

ABSTRACT

The animal-to-researcher workflow in many of today's small animal imaging center is burdened with proprietary data limitations, inaccessible back-up methods, and imaging results that are not easily viewable across campus. Such challenges decrease the amount of scans performed per day at the center and requires researchers to wait longer for their images and quantified results. Furthermore, data mining at the small animal imaging center is often limited to researcher names and date-labelled archiving hard-drives. To gain efficiency and reliable access to small animal imaging data, such a center needs to move towards an integrated workflow with file format normalization services, metadata databases, expandable archiving infrastructure, and comprehensive user interfaces for query / retrieval tools - achieving all in a cost-effective manner.

This poster presentation demonstrates how grid technology can support such a molecular imaging and small animal imaging research community to bridge the needs between imaging modalities and clinical researchers. Existing projects have utilized the Data Grid in PACS tier 2 backup solutions, where fault-tolerance is a high priority, as well as imaging-based clinical trials where data security and auditing are primary concerns. Issues to be addressed include, but are not limited to, novel database designs, file format standards, virtual archiving and distribution workflows, and potential grid computing for 3-D reconstructions, co-registration, and post-processing analysis.

Keywords: Imaging Informatics, Data Grid, Small Animal Imaging, Molecular Imaging, Fault-Tolerance, Archiving

1. INTRODUCTION

1.1. Molecular Imaging and Small Animal Imaging Research

Personalized medicine in the 21st century describes a bottom-up approach in diagnostic and preventative healthcare. It is based on understanding biological and disease processes at the molecular level to better characterize a patient's physical condition and risks of disease. Imaging at the molecular level is largely used on small animal studies in disease studies pharmaceutical research to monitor molecular pathways non-invasively and at high spatial and temporal resolutions. As biology and disease increased, molecular imaging laboratories have become an integral part of translational research on academic and industrial campuses. Modalities such as optical imaging and autoradiography have coincided with a miniaturization of radiology modalities such as CT, PET, US and MRI to form these molecular imaging and small animal imaging labs. Each imaging modality type, with its own set of strengths and weaknesses, has provided various angles to observe sub-cellular enzyme, gene and protein activity without having to perform biopsies, thus reducing the number of animal sacrifices and enabling more accurate longitudinal biological experiments involving small animal trials.

The current infrastructure requirements of a small animal imaging lab are framed by the multiple modalities and vendor-provided workstations to run post-processing software. Due to proprietary data formats and vendor-provided dedicated workstations, it is difficult for small animal imaging labs to share, or federate its computing and archiving hardware into cross campus and multi-disciplinary resources. There is a one-machine-one-modality infrastructure in today's molecular imaging laboratories where post-processing and reporting features are all done on stand-alone computers dedicated to individual modalities. This infrastructure has apparent pitfalls for the future of personalized medicine in that:

1. High cost-per modality due to dedicated workstations limits work to one user per workstation.
2. Islands of non-compatible data stored on dispersed hard-drives are accessible only by proprietary software.
3. A lack of fault-tolerance in hardware as well as data makes reliable data mining an avoided feature.

4. Inaccessible data and workstations from remote locations limit multi-campus translational research.

Below is a diagram that demonstrates the multiple levels of today's medical and biological sciences research. It provides insight into personalized medicine's bottom-up approach to understanding disease and physiology. If a molecular imaging lab could bridge distances between its diverse imaging modalities with data normalization and its diverse users with an archiving and distribution system, more efficient interchange of knowledge within these biological organizations could make molecular imaging a more integral part of the 21st century's personalized medicine

Table 1. Levels of biological organization and research. Source from Medical Physics Nikiforidis, G., et al. [1]

	Organizational level	Focus on	Modalities	Analysis
Top-down approach	Organism	Clinical symptoms, signs, and behavior	Medical history, physical examination, laboratory exams, biochemical tests,[a] forensics	Statistical analysis
	Organ and organ systems	Morphology, anatomy, and physiology	CT, SPECT, PET, MRI, U.S., x rays, fMRI, perfusion, diffusion, hybrid imaging, computational fluid dynamics (characterization of hemodynamics), organ biopsy[a]	Anatomical and functional imaging
	Tissue	Epithelium, connective, muscle, nervous	fluorescence spectral imaging, optical[a] and electron microscopy,[a] flow cytometry[a]	Immunohistochemistry, histopathology
	Cell	Function of proteins and metabolic pathways	SPECT, PET, MRI, optical imaging, CT with specific probes	Molecular imaging, quantum dots
Bottom-up approach	Proteomic	Level and patterns of expression of many proteins or protein fragments	Microarrays,[a] western blot[a] (proteins), autoradiography[a]	Proteomics, NMR
	Genomic	Level and patterns of transcription and expression of many genes and chromosomes	Microarrays,[a] *in situ* hybridization,[a] autoradiography,[a] microfluidics[a]	Genomics, bioinformatics
	Genetic	Presence, absence, or mutation status of a few genes, nucleic acids analysis, SNPs	PCR,[a] microarrays,[a] mass[a] spectrometry, southern blot[a] (DNA), northern blot[a] (RNA)	Genetics, (DNA sequencing, linkage maps, genetic maps)

[a]*In vitro*.

1.2. The Medical Imaging and Informatics Data Grid

At the IPILab, the Medical Imaging Informatics Data Grid project utilized grid technology developed by the Globus Alliance to archive and serve clinical radiology images in the DICOM format. It includes all radiology imaging modalities that comply with the DICOM standard, meaning the outputted images can be transmitted, viewed, and processed all according to a set of formatting guidelines defined by the DICOM committee. Current modalities covered by DICOM are most commonly seen in CT, MRI, US, PET, DR, CR, and mammography. As a clinical archiving system for these modalities, the Data Grid acts similarly to a PACS. It has a DICOM listener at all grid-access-points; it is able to receive the DICOM file and extrapolate its header information into a DICOM-modeled database; and it provides DICOM query/retrieve functionality for other DICOM nodes or workstations. The Data Grid is different from a PACS, however, because it has built-in fault-tolerant replication of data and hardware that spans multiple geographic sites, it federates databases permitting user-specific enterprise access to the DICOM data, and it utilizes grid technology to retrieve files from remote sites quickly and securely.

In 2005, the Medical Imaging Informatics Data Grid was first presented at the Radiological Society of North America conference as a solution for enterprise PACS Tier 2 backup. The application was to develop a solution for creating a physical copy of the PACS solution at an off-site location, in case the primary PACS goes down or the hardware holding the data becomes unavailable. In the following year, the Data Grid project was adopted for imaging-based clinical trials in collaboration with the UCLA Thoracic Imaging Research Group. The rigorous patient privacy requirements of clinical trials allowed the Data Grid system to focus on features such as HIPAA-compliant user access control and auditing. In these previous Data Grid applications, the infrastructure was based on DICOM-compliance of the incoming data format, a need for web-based user interfaces for management and customized accessibility, and a reporting format to archive

non-image documentation. This manuscript will discuss how file format normalization can be achieved in molecular imaging, what features of the web-based user interface need apply, and how the Data Grid can support the reports generated in the molecular imaging realm.

2. METHODOLOGY

The scope of this discussion covers steps towards integrating a Data Grid model into molecular imaging labs – data format normalization, user-interface requirements, and structured reporting of non-image type data. At the University of Southern California are the Image Processing and Informatics Lab (IPILab) and the Molecular Imaging Center which has collaborated for purposes of development and implementation of a Molecular Imaging Informatics Data Grid system. Both located on the Health Sciences Campus, the IPILab provides the infrastructure and software development resources for the project and the Molecular Imaging Center provides the small animal imaging laboratory environment and data with which this project was implemented.

2.1 Molecular Imaging Informatics Data Grid Architecture

The software architecture of the Data Grid system is shown in figure 1 below. At the top of the four layer hierarchy are three DICOM services that interact with the users, presumably DICOM-compatible workstations that either have images to be archived into the Data Grid, or are requesting DICOM images existing from within the Data Grid system. At the next user-level are three services that interact with the core grid components of the Globus Toolkit. It includes an indexing service that maintains where files are archived in the Data Grid, a metadata catalog service that extracts DICOM header information and updates the DICOM-modeled database for future querying, and lastly a DICOM-Structured Reporting (DICOM-SR) catalog service that extracts textual content from the tree-like structure of a Structured Report defined by the DICOM Standard. The Core Middleware layer that these previous services interact with are primarily constituted by the technology provided in the Globus Toolkit. These include the Replica Location Service (RLS), Reliable File Transfer service (RFT), Database Access Interface (DAI), security measures such as certificate authentication, and GridFTP which is the file transfer method across public domain much like FTP. The bottom-most layer called Fabric describes the archiving storage system, networking, and database systems needed to house the Data Grid model.

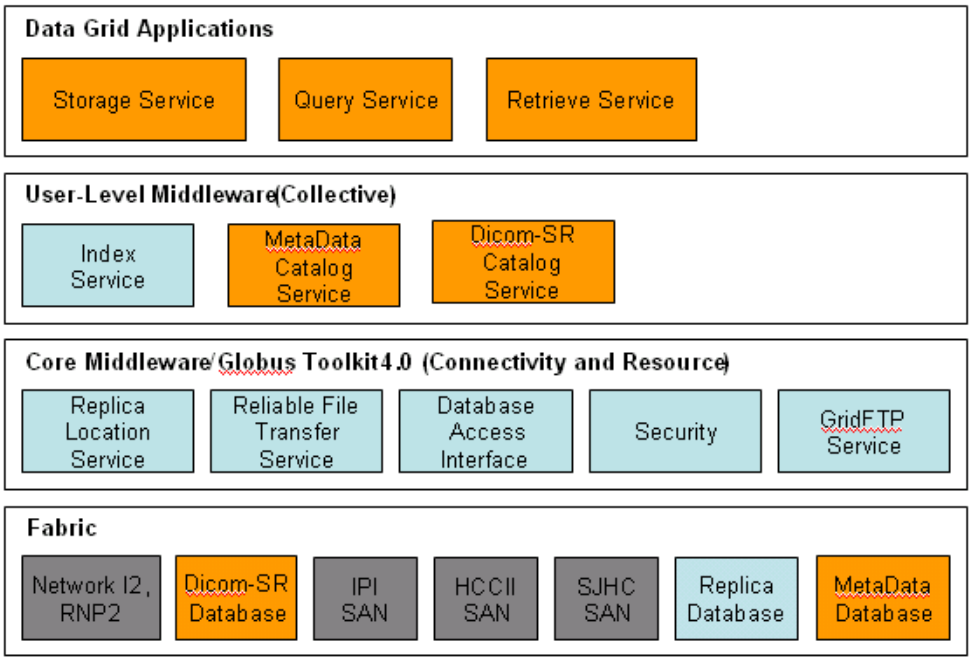

Figure 1. Overview Architecture of Medical Imaging Informatics Data Grid
Orange: developed at IPILab, Blue: Globus Toolkit, Grey: hardware

The physical computer components that make up the Data Grid architecture are grid-access-points (GAP), web servers, database servers, and high-capacity SAN or NAS storage silos. The grid-access-points are servers (one at each participating site) that function as the gateway into the Data Grid. It houses the top three layers of the Data Grid architecture seen in figure1, which makes the grid-access-point the primary component of the Data Grid system. It is both DICOM-compatible and utilizes the Globus Toolkit to transfer incoming files to SAN storage, other site nodes or directly to on-site user workstations. The next component is the web-server, which provides user interface pages such as log-in, uploading of DICOM files, and report viewing capabilities to on-site users. Access from users outside of a local network is not permitted for security purposes. For this reason, the web-server can also be hosted on the grid-access-point if the hardware so permitted. The database servers are unlike the previous two and do not require to be hosted at every site, but need to be redundant and available to all grid sites. It can be made secure by using firewall filtering and SSL secured connections from the grid-access-points. Redundancy of the databases is done via mirroring and monitoring services on each database server that guarantee updated data synchronization. The last physical components are high-capacity SAN or NAS storage silos. For fault-tolerance, there is a minimum requirement of two participating silos, but can be expanded depending on the storage space requirements and back-up policies. These storage silos require the Globus Toolkit to be installed to permit GridFTP transfers and certificate authentication. They too should be protected behind firewalls to limit access to only known remote grid-access-points.

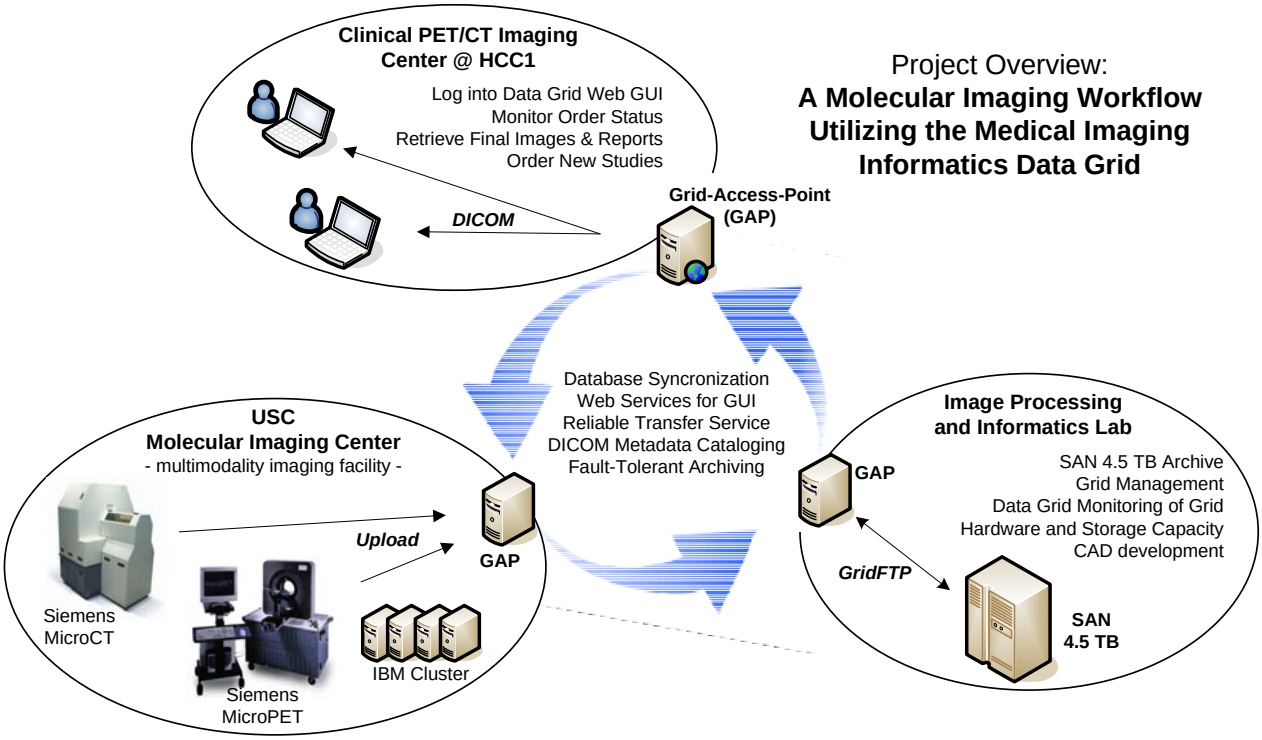

Figure 2. Overview of the Data Grid model for Molecular Imaging Center at USC

Figure 2 is a workflow overview of the USC Molecular Imaging Center (MIC) utilizing the Molecular Imaging Informatics Data Grid to archive and disperse its findings to other research facilities at USC. The USC Molecular Imaging Center receives requests for small animal imaging studies from faculty and research groups on campus. After the MIC staff perform the planned set of imaging studies and generate reports of their findings, they upload the post-processed images and reports to the grid-access-point through the on-site Data Grid web server. In Figure 2, the web server is located on the same machine as the grid-access-point. Upon receiving files, the GAP recognizes the file format and converts images and textual data into DICOM if they are not already in the "dcm" format for archiving and distribution. For example, TIFF images generated in autoradiography and the region-of-interest files generated by a microCT modality are converted to DICOM at the GAP before being archived via GridFTP to a remote SAN at the IPILab. The DICOM header information that holds the metadata for these images and reports are entered by users on the

Data Grid web-based user interface (UI) when the files are initially uploaded at attached during the DICOM conversion. At the third site, a clinical PET/CT radiology center for example, a GAP is also set up for researchers and participating radiologists who would benefit from access to imaging and report data generated at either the MIC or IPILab. They would be able to query/retrieve these cases of interest directly from the local GAP without having to access remote archives or licensed workstations just for viewing purposes.

2.2 File Format Normalization

The preliminary step in adopting a data grid model at a molecular imaging lab is file format normalization of images and findings so that they can be comprehended and viewable in non-proprietary systems. Because significantly more post-processing is done using original raw data in the molecular imaging lab as compared to clinical radiology, not all raw data formats can nor should be converted into standardized formats such as DICOM. For these raw data formats a different type of archiving method is required, but will not be discussed here. However, the final results, generated by post-processing reconstructions and ROI analysis, are almost always viewable in 2-D images or transcribed into textual reports and excel sheets. Therefore the first step towards supporting the diverse modalities' data in the Molecular Imaging Informatics Data Grid is to convert final output images and textual reports into DICOM with header information specifying the researcher and experimental metadata. Some image conversions needed are exhibited in table 2 below. Note that ultrasound machines used in small animal imaging labs are similar to the ones used for clinical radiology so their output screen captures are already in DICOM format.

Table 2. Imaging conversion methods for molecular imaging modalities.

Modality	Output Format	Final Format	Method
MicroPET	TIFF	DCM	Java Advanced Imaging
MicroCT	CT	DCM	Linear Transform
Optical Imaging	PNG	DCM	ImageIO
Autoradiograph	TIFF	DCM	Java Advanced Imaging
Ultrasound	DCM	DCM	None

As for textual documents and excel sheets, a language parser is required to extract specified content of interest and constructed into a DICOM Structured Report using DCM4CHE. This will be discussed in the following section 2.4.

2.3 Web-based User-Interfaces

There are two methods to access images and reports stored in the Molecular Imaging Informatics Data Grid: a DICOM node such as a PACS workstation and DICOM viewer with query/retrieve functionality could pull studies from a local grid-access-point via DICOM protocol; or a user could log-in to the web-based interface hosted by an on-site web-server and view the images and reports there based on their user privileges. The benefit of the former option is compatibility with existing clinical PACS applications to allow radiologist to work in a familiar environment while doing their research. The benefit of the later is portability, customizable input and functionality, and grid management tools.

The web-server could be located on the same server as the grid-access-point, but regardless, it interacts with the grid-access-point as just another DICOM node. Figure 3 demonstrates the workflow of the Data Grid system with the web-based user interface. The staff at MIC are able to upload images and text reports to the web server via HTTP to a local web server where file format normalization is performed before being archived into the Data Grid. The grid-access-point has a DICOM receiver, a Metadata Catalog Service, and a Structured Report Catalog Service that communicates with the database server before the actual files are archived in replicated storage silos. On the other end, researchers can access these images and reports also from the web-based user interface by logging in and giving requests to their grid-access-points in the form of HTTP forms and buttons. The web page translates those requests into DICOM query/retrieve actions.

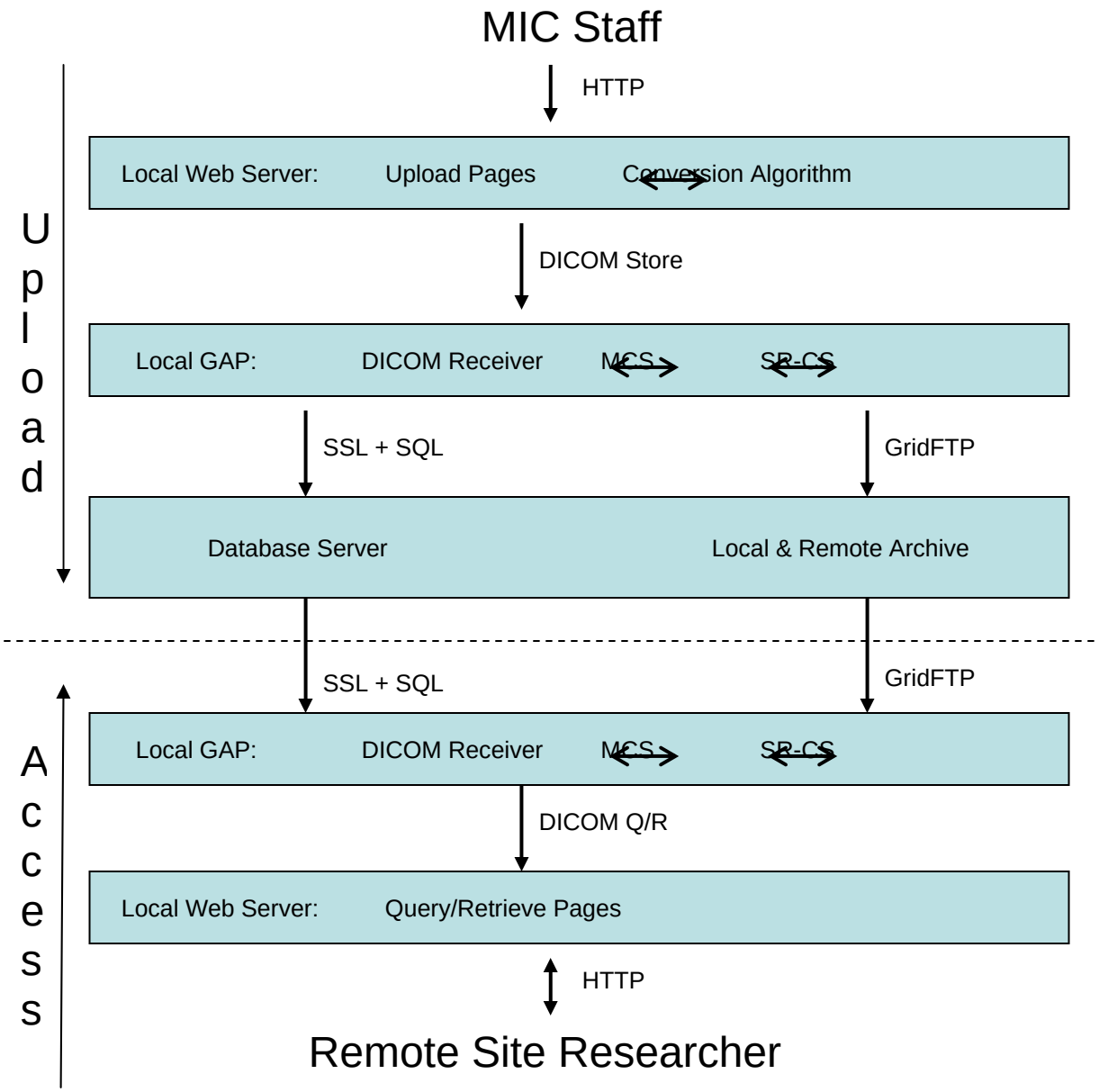

Figure 3. Workflows for uploading and accessing molecular imaging images and findings using the web-based user interface, provided in the Molecular Imaging Informatics Data Grid.

2.4 Structured Reporting

A method is needed to normalize textual reports being generated by the various molecular imaging modalities. The current model is to generate reports by the small animal imaging lab staff using a simple copy-paste routing. Though this method is efficient for getting results to the researchers, it is not the efficient for data mining purposes and archiving. Thus the file format normalization is also required for report creation by conforming to the DICOM Structured Report standard. The benefits of this standard are not only compliance to DICOM header metadata, but are also seen in the tree-like structure that allows content to have relational meaning rather than implicit containment of objects. To achieve compliance, the conversion algorithm requires knowledge of modality type and a language parser that can extract desired content from the various txt or excel files. The conversion algorithm will use dcm4che to construct the DICOM-SR file after the content of interest has been extracted. The result is a report can be managed in the metadata catalog service in

much the same way as a DICOM image file. The DICOM Standard currently has the Supplement 23 that defines general SR attributes such as observer information, completion flags, procedure description, and references to other SR files that the creator may find important for reference. Below is a diagram taken from Supplement 23 that describes the general structure of an SR report. Each content item can take the form of a various value types such as text, code, date, image, coordinate, uidref, waveform, etc. Each relationship can take the form of "contains", "has properties", "inferred from", "has observation context", etc. With such descriptive flexibility, DICOM-SR is a great mechanism to be adopted for reports generated in molecular imaging labs.

Below in figure 4, is a sample viewer that can display an SR file. Such viewers can easily be integrated into the web-based user interface for researchers to see their findings.

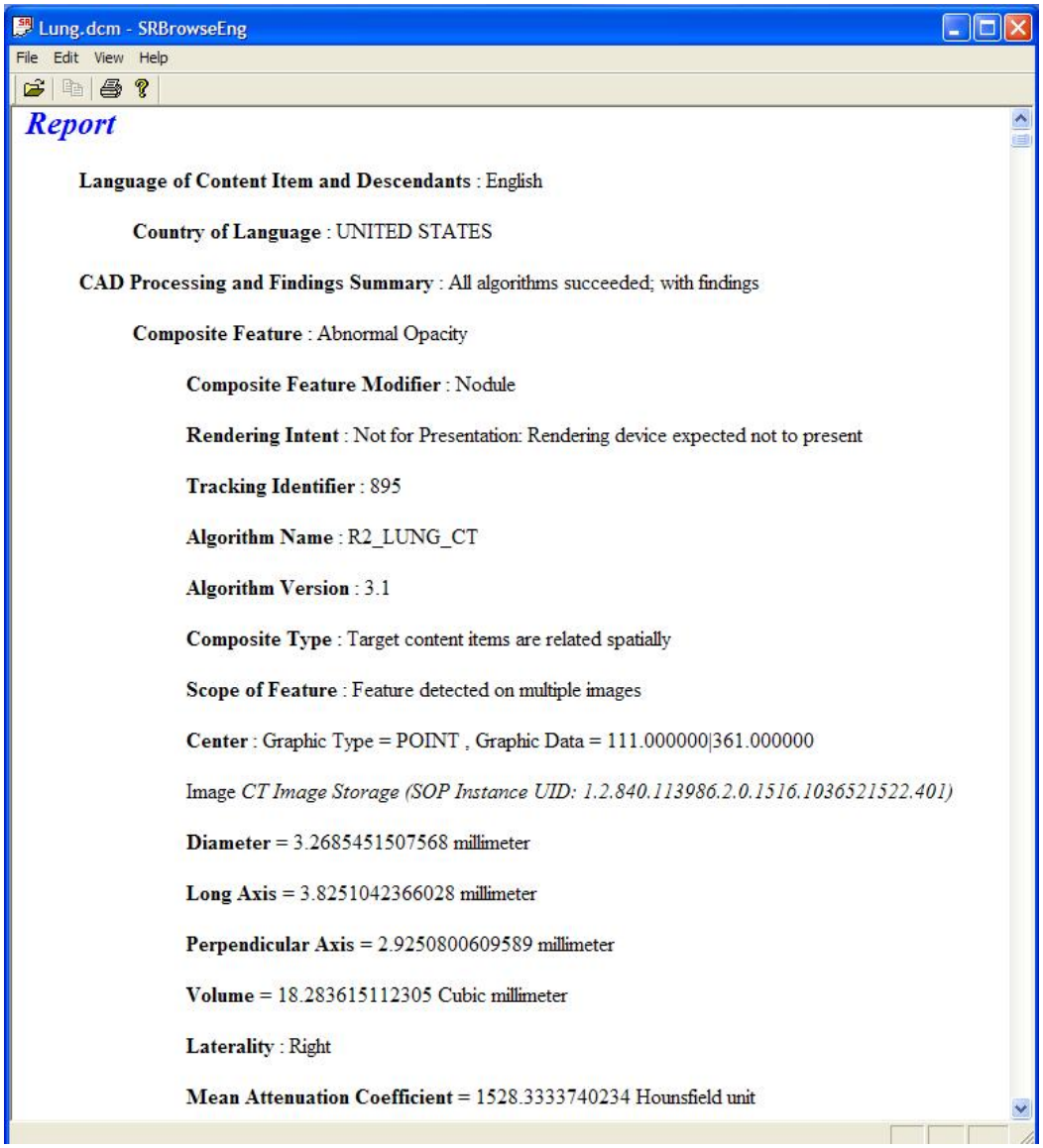

Figure 4. Sample DICOM-SR document provided by IPILab, USC. Courtesy R2 Technology, Inc.

3. RESULTS and DISCUSSION

The Molecular Imaging Informatics Data Grid is currently being implemented at the USC Health Sciences Campus. Prior imaging studies that have been published and archived at the USC Molecular Imaging Center are being migrated into the Data Grid system. A total of 4 TB has been allocated on two separate storage silos for this initial phase. TIFF images have been converted to DICOM and certain text reports have been manually converted to the DICOM-SR format. A web-based user interface has been developed to manage grid services, to allow users to log-in and upload DICOM imaging studies and SR files, query, retrieve and view DICOM images and structured reports, and to allow customized anonymization of incoming DICOM files before archiving into the Molecular Imaging Informatics Data Grid. The next steps are to provide real-time support for imaging studies being generated at the MIC, to archive non-DICOM data, and to allow remote researchers to create their own SR reports, and to plan and manage their experimental studies online.

4. CONCLUSION

Adopting a Data Grid model into the molecular imaging and small animal imaging research community is a significant step towards molecular level research and a bottom-up understanding of medical diagnosis and treatment methods. Some challenges of multi-modal imaging infrastructure have been discussed to demonstrate the need for improved workflow and virtualized archiving, distribution and computational infrastructure for molecular imaging labs. Existing work in applying the Data Grid model towards PACS tier 2 backup solutions, where fault-tolerance is a high priority, and imaging-based clinical trials, where data security and auditing are primary concerns, have strengthened the understandings and approaches of applying a similar model into molecular imaging. Nonetheless this new arena of research and imaging presents its own set of challenges for the Data Grid project to explore. Novel database designs, file format standardization, archiving and distribution workflows are fundamental engineering steps toward a virtualized infrastructure in molecular imaging research.

REFERENCES

[1] Nikiforidis G, Sakellaropoulos G, Kagadis G. Molecular Imaging and the Unification of Multilevel Mechanisms and Data in Medical Physics. Medical Physics, Vol. 35, No. 8:3444-3452. August 2008.

[2] DICOM. "Supplement 23 : Structured Reporting Storage SOP Classes," <www.nema.org> (accessed Dec. 08)

[3] Tulipano PK, Tao Y, Zanzonico P, Kolbert K, Lussier Y, Friedman C. Natural Language Processing and Visualization in the Molecular Imaging Domain. AMIA Annual Symposium Proc 2005, 1143.

[4] Mabry PL, Olster DH, Morgan GD, Abrams DB. Interdisciploinarity and Systems Science to Improve Population Health. Am J Prev Med 2008; 35.

[5] DCM4CHE. <www.dcm4che.org> (accessed Jan. 2009)

[6] Delaloye AB, et al. White Paper of the European Association of Nuclear Medicine (EANM) and the European Society of Radiology (ESR) on Multimodality Imaging. Eur J Nucl Med ol Imaging (2007) 34:1147-1151

[7] Globus Toolkit. <http://www.globus.org/toolkit/> (accessed Jan 2009)

SELECTED PEER REVIEWED REPRINTS AND PREPRINTS

Int J CARS (2008) 3:27–39
DOI 10.1007/s11548-008-0199-4

ORIGINAL ARTICLE

Utilization of medical imaging informatics and biometrics technologies in healthcare delivery

H. K. Huang

Received: 11 January 2008 / Accepted: 29 April 2008 / Published online: 22 May 2008

Abstract
Purpose With the large amount of image data accumulated daily from medical imaging modalities and picture archiving and communication systems (PACS) in hospitals and from healthcare biometrics related databases, we can take advantage of these data resources to investigate innovative clinical service, research and education using the concept of imaging informatics. In this paper we present five independent concepts and technologies in their own right and their intertwined relationship in achieving some goal-oriented healthcare applications.
Methods The five independent concepts and technologies with goal-oriented healthcare applications include medical imaging informatics infrastructure; Data Grid for image fault tolerant backup and disaster recovery; integration of computer-assisted detection and diagnosis (CAD) in daily clinical practice; biometrics technology for patient location and identification in an enterprise Hospital/Radiology information system (HIS/RIS/PACS) integrated environment; and the concept of in vivo image-guided diagnosis and real-time surgical treatment.
Conclusion The success of implementing these novel technologies and concepts would have tremendous impact to better present and future healthcare delivery as illustrated by examples in the paper.

Keywords PACS · Medical imaging · Imaging informatics · Medical biometrics · Data grid · CAD · Minimally invasive spinal surgery

Abbreviations

API	Application programming interface
BAA	Bone age assessment
CAD	Computer-assisted detection and diagnosis
CSI	California Spine Institute
DICOM	Digital imaging and communications in medicine
ePR	Electronic patient record
FRS	Facial biometric recognition system
FT	Fault tolerance
G & P	Greulich and Pyle bone development Atlas
GT4	Globus Toolkit Version 4, open source software for Grid Computing
GUI	Graphical user interface
HCC II	Healthcare consultation center II
HIPAA	Health insurance portability and accountability act
HIS	Hospital information system
HL-7	Health level seven
IHE	Integrating the healthcare enterprise
InfoRAD	A group of scientific sessions dedicated to radiology informatics in the RSNA Scientific Assembly and Annual Meeting

Portions of the materials were presented at the 24th International EuroPACS Conference, Trondheim, Norway, June 14–17 2006; and the 21st International CARS Congress, Berlin, Germany, June 27–30 2007.

H. K. Huang (✉)
Departments of Radiology and Biomedical Engineering,
Image Processing and Informatics Laboratory (IPI),
University of Southern California, 1450 San Pablo Street,
Suite 2100, Los Angeles, CA 90033, USA
e-mail: hkhuang@aol.com

H. K. Huang
Department of Health Technology and Informatics,
Hong Kong Polytechnic University, Hong Kong, China

H. K. Huang
Shanghai Institute of Technical Physics,
Chinese Academy of Sciences, Shanghai, China

IPILab	Image processing and informatics laboratory, USC
LTVS	Location tracking and verification system using biometric technologies
MIII	Medical imaging informatics infrastructure
MISS	Minimally invasive spinal surgery
PACS	Picture archiving and communication system
Perl	Practical extraction and report language
RIS	Radiology information system
ROI	Region of interest
RSNA	Radiological society of North America
SAN	Storage area network
SC	DICOM screen capture service
SJHC	Saint Johns Healthcare Center
SR	DICOM structured report service
USC	University of Southern California
WS	Workstation

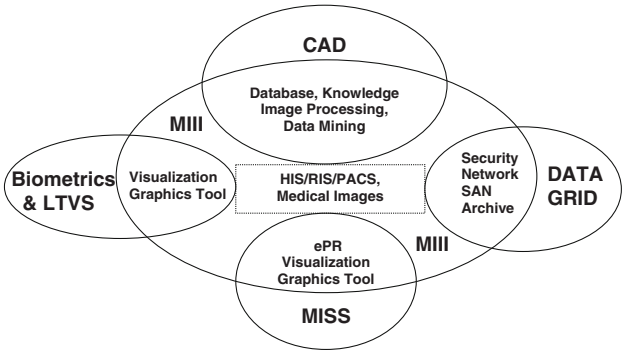

Fig. 1 The relationship of five concepts and technologies (*large and small ellipses*) discussed in this paper. *MIII* Medical imaging informatics infrastructure (*large ellipse* the fundamental infrastructure used by others); Data Grid is for fault tolerance medical image archive, *SAN* storage area network; *CAD* computer-aided detection and diagnosis; *LTVS* location tracking and verification system using biometric technologies; *MISS* minimally invasive spinal surgery, *ePR* electronic patient record; HIS/RIS/PACS and medical images are data components of MIII used by all others

Introduction

We select five independent concepts and technologies in medical imaging informatics and medical biometrics to discuss their intertwined relationship and utilization in healthcare delivery. The first concept is medical imaging informatics infrastructure (MIII) which lays the foundation of medical imaging informatics. The second is Data Grid technology and its application in medical imaging which provides a fault-tolerant storage method for the longevity of medical imaging and biometric data. The other three topics are applications which utilize various components in MIII for applications. They are: integration of computer-assisted detection and diagnosis (CAD) in daily clinical practice; biometrics technology for patient tracking and identification in an enterprise HIS/RIS/PACS (Hospital/Radiology information system/Picture archiving and communication system) integrated environment; and in vivo image-guided diagnosis and real-time surgical treatment. Figure 1 shows the relationship and utilization of these five concepts and technologies, the details of each are discussed in following sections.

Although these five concepts and technologies are independent, a different application would take them intertwining with others to accomplish the targeted task. Section "Five independent concepts and technologies in imaging informatics and biometrics" presents five theme interconnected ellipses each of which describes a concept or technology. Each Example given in Section "Summary" first describes the application, components used in the theme ellipse followed by the utilization of components from other ellipses depending on the application under consideration.

Among imaging informatics components and technologies, Data Grid would benefit the HIS/RIS/PACS and electronic patient record (ePR) integration, minimally invasive spinal surgery (MISS) data retrieval and outcomes analysis, and data mining of CAD results for improvement in radiology diagnosis. HIS/RIS/PACS integration allows for a better ePR with image distribution design and implementation, which in turn, provides the cornerstone for the development of efficient and effective MISS operation. In biometric technologies, HIS/RIS integration provides patient registration and procedural time stamp data to the location tracking and verification system (LTVS) to track, locate and identify the patient is actually in the pre-assigned procedure room within a given time period after registration. Currently, there is no single player, either at the research laboratory and hospital (customer), or any manufacturer or company (provider) would have enough resources to research and develop all these technologies. The customer and the provider have to work together in order to achieve fruitful results. The Summary section describes roles of the customer and providers would have to play in each application.

Five independent concepts and technologies in imaging informatics and biometrics

HIS/RIS/PACS as the infrastructure for medical imaging informatics research

HIS/RIS/PACS-based medical imaging informatics

HIS/RIS/PACS-based medical imaging informatics is to use existing integrated hospital information system (HIS), radiology information system (RIS), and picture archiving and

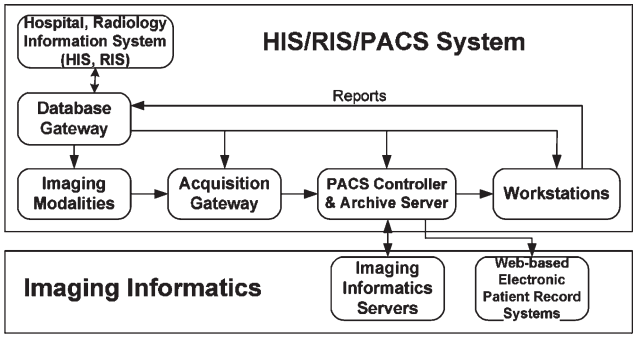

Fig. 2 The relationship between HIS/RIS/PACS and medical imaging informatics. Electronic patient record (ePR) systems are application specific Web-based patient object oriented database with image distribution. Imaging informatics servers are application specific

communication system (PACS) resources including images and related data for systematic large-scale horizontal and longitudinal clinical service, education, and research applications that could not have been performed individually because of insufficient data and unavailable tools. HIS/RIS/PACS integration shown in Fig. 2 relies on the digital imaging and communications in medicine(DICOM) standard for imaging format and communication protocols, and health level (HL-7) standard for textual format, and integrating the healthcare enterprise (IHE) for workflow profiles (Upper rectangle in Fig. 2). Medical imaging informatics infrastructure (MIII) extracts relevant images and data from HIS/RIS/PACS to form the database (Lower rectangle in Fig. 2), and in doing so, becomes the vehicle to facilitate the utilization of HIS, RIS and PACS data for informatics applications in addition to their daily clinical service. Three applications, CAD bone age assessment, LTVS, and MISS mentioned above will be discussed in details in the Section "Five independent concepts and technologies in imaging informatics and biometrics" utilizing different components and servers inside the two rectangles. MISS is based on the electronic patient record system (ePR), LTVS uses HIS and RIS data of the patient to facilitate patient location and verification, and bone age assessment relies on the HIS/RIS/PACS integration. Figure 2 shows the relationship between HIS/RIS/PACS and imaging informatics. Figure 3 illustrates MIII components and their logical relationship [1].

Data Grid for medical images

Data Grid basic

Data Grid is a service in the Grid Computing technology situated in the third layer of the MIII. Several large-scale Data Grid architectures, such as TeraGrid and Data Replication for LIGO, and Globus tool kit have been developed by the Grid community for fast movement of large amount of data among multiple research institutes. In this section, we describe the Globus in more detail. Data Grid is important for storing large-scale imaging informatics and biometric data because of its fault-tolerant nature of design.

Fault-tolerant backup archive and disaster recovery for medical images

A Data Grid specifically designed for clinical image backup and disaster recovery has been developed at the image processing and informatics laboratory (IPILab), USC using the Globus Toolkit 4 (GT4) [2]. This Data Grid was designed to utilize the strengths of grid technology along with PACS/DICOM (Digital Imaging and Communications in Medicine) technology for storing and distributing medical images. In particular, some PACS/DICOM resources were embedded within the five layer grid computing architecture: fabric, connectivity, resource, collective, and applications (See Fig. 4). DICOM services included Storage services, Query services, and Retrieve services in the DICOM protocols, which were integrated with other Data Grid Services shown in the shaded boxes in Fig. 4 [3]. Figure 5 shows a Data Grid architecture for backup and disaster recovery of three PAC systems. The Data Grid is now being used at IPILab for three applications: backup archive of the clinical PACS at HCC II (Healthcare Consultation Center II, see Fig. 5 the rightmost column), USC; IPILab research data backup; and experimental radiology core backup in several image-based clinical trials.

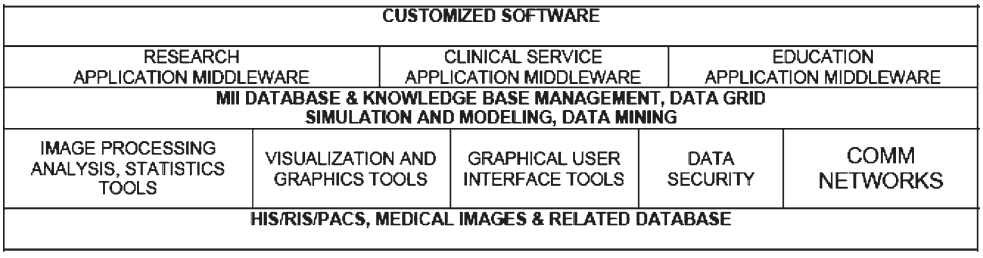

Fig. 3 Five MIII layers and their logical relationship. The *first layer* from bottom contains HIS/RIS/PACS data, the *second layer* consists of common tools in MIII; the *third layer* is general databases including knowledge base, simulation and modeling, and data mining software packages; the *fourth layer* is application specific software; and the top layer is customized software

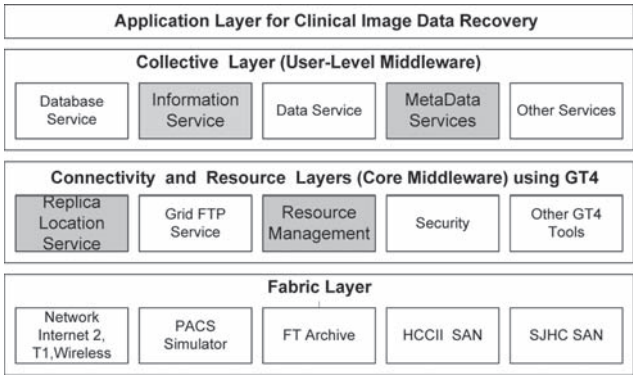

Fig. 4 Five-layer architecture and components of the Data Grid Globus toolkit 4, *shaded areas* are integrated components with DICOM services developed at IPI embedded in the Globus. Application Layer (*top*) software is designed for clinical image data recovery. See also Fig. 5 caption for symbols

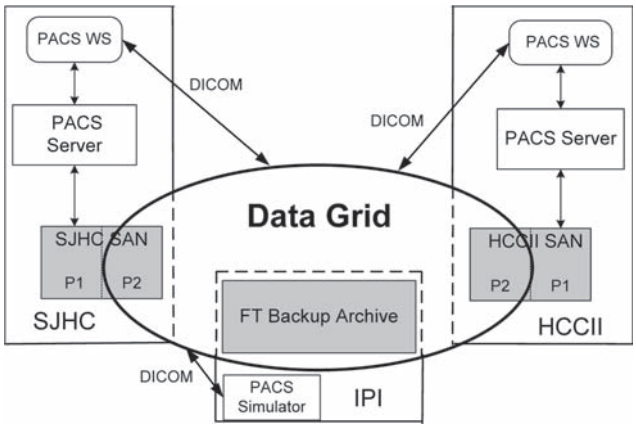

Fig. 5 Configuration of three PACS sites data storage systems (*shaded boxes*) which contribute to the image data shared storage resources in the Data Grid. Each SAN (storage area network) has two partitions, partition P1 at each site is used to store its own PACS images, whereas P2 becomes a shared resource of the Data Grid. Failure of any PACS server and/or archive in the P1 of SAN storage can be recovered by the Data Grid automatically after the failed equipment are up and running. Workstations (WS) outside of the Data Grid can access the grid for image query/retrieve service to continue clinical operation when its own PACS fails. Saint Johns Healthcare Center (SJHC), Santa Monica, CA; Healthcare Consultation Center II (HCCII), University of Southern California (USC); Image Processing and Informatics Laboratory (IPI), USC; Fault tolerance (FT)

Integration of computer-aided detection/diagnosis (CAD) with PACS operation

The first two concepts and technologies, HIS/RIS/PACS integration and Data Grid discussed above, are components of the MIII infrastructure, they serve both as building blocks and for value-added imaging clinical applications. The next three topics to be discussed on CAD, LTVS and MISS are concepts and technologies outside the realm of radiology. However, these applications use data derived from HIS/RIS/PACS.

CAD is a computer method to obtain quantitative measurements from medical images along with clinical information to assist clinicians and radiologists to assess the clinical state of a patient under consideration more objectively. CAD software can be in a stand-alone CAD workstation, or be integrated in the PACS as PACS-based CAD. In order to utilize the CAD results more efficiently and timely, CAD should be integrated with daily clinical HIS/RIS/PACS operation. Currently, some PACS and CAD companies have some success of integrating several CAD applications, but either in a CAD specific workstation, or in a close environment PACS operation through proprietary software. In this section we present the integration of PACS with CAD using an open architecture PACS–CAD integration toolkit based on DICOM and HL 7 standards and IHE workflow profiles. One CAD on bone age assessment under clinical validation is used as an example.

CAD–PACS integration toolkit

CAD–PACS© is a software toolkit using DICOM and HL 7 standards and IHE profiles for the integration of CAD results with the PACS workflow. This CAD software toolkit is modularized and can be installed in a standalone CAD workstation, a CAD server, a PACS workstation, a PACS server or a mixture of some of the above. In general, a CAD company would be in favor of the first two approaches so that they don't have to get into the PACS software which is extreme complex, whereas a PACS company would prefer to acquire the CAD and integrate it with its own PACS using the latter three approaches. Figure 6 depicts the architecture of the CAD–PACS© which has three versions DICOM-SC™, DICOM-PACS-IHE™, and DICOM-CAD-IHE™ [4,5]. The first version uses the DICOM Screen Capture (SC) service which is simple to design and implement but with limitation in clinical research. It uses screen capture to store CAD results for viewing purpose only. The second version uses the DICOM Structured Report (SR) service and several IHE Workflow Profiles, the methodology is elegant but requires several modules of the toolkit to be installed in the PACS server which would need intensive collaboration of the PACS manufacturer during the integration. The integration would require patience and perseverance from the integrator because of the protective culture of PACS business. The third version also uses DICOM SR and Key Image Note IHE Profile, this method reduces the necessity of altering the current PACS Server, but CAD results are stored in the CAD server and not in PACS. This version is favored by CAD manufacturers because they have the ability to install the toolkit in their CAD server and integrate CAD results with the clinical workflow. DICOM SR provides the data format allowing CAD results, text, images, graphics and annotations to be directly store in the DICOM SR compliance PACS or CAD server. The last two versions are the correct methods of

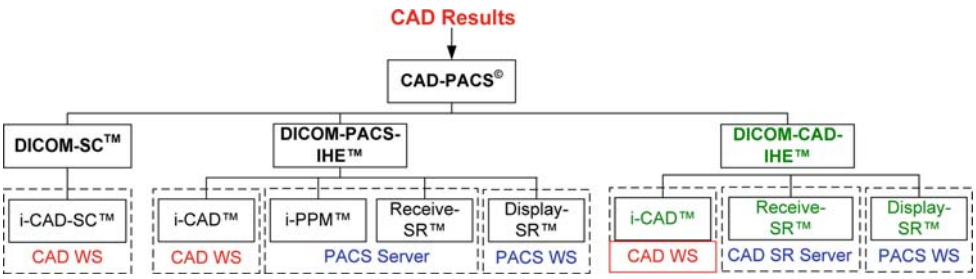

Fig. 6 *Left and middle* The original design of CAD–PACS© integration toolkit has two versions: The DICOM–SC™, and the DICOM-PACS-IHE™. *Right* DICOM-CAD-IHE™ (*Green*) version is a modification from the second version (*middle*) by extending the toolkit to the CAD Server. Each version consists of modules. The DICOM-CAD-IHE™ (*Green*) is independent from the PACS manufacturer as long as the PACS workstation is complied with the DICOM SR, the third (*right*) version is favored by the CAD manufacturers or research laboratories for integration. The three modules i-CAD™, Receive-SR™, and Display-SR™ are the same in both DICOM-PACS-IHE™ and DICOM-CAD-IHE™ versions. Post-processing manager (PPM) allows the integration of CAD results with the PACS server which is PACS specific and would require PACS vendor's assistance for implementation

integrating CAD with PACS because direct CAD results in clinical workflow would enhance future PACS research capability and improve the utility of medical imaging informatics infrastructure.

An example—bone age assessment of children

This application describes the integration of the CAD for bone age assessment of children with a clinical PACS for daily operation using the CAD–PACS@ integration toolkit. Clinical bone age assessment for children has been based on the 1950 Greulich and Pyle Atlas (G & P) from a homogeneous population. With today's diverse ethnicities in the US and around the world, the atlas may no longer be a good reference. A digital hand atlas is described here as a means to possibly replace the classic P & G Atlas for bone age assessment.

We have collected 1,400 normal children hand images from Caucasian (CA), African American (AA), Hispanic (HI), and Asian (AS); male (M) and female (F), ranging from 0 to 18 years. The validation of normal was determined with three standards: body mass index, Tanner Maturity Index, and chronological versus skeletal age from the 1,940 Brush Foundation Study. Each image was read by two to four pediatric radiologists. A computer-aided diagnosis (CAD) based on phalangeal and carpal bone growth has been developed to assess the bone age. 50% of the collected images were used for training the CAD, and the other 50% for evaluation. The data from 0 to 18 years was categorized into eight categories (CAM, CAF, AAM, AAF, HIM, HIF, ASM, and ASF) for comparison. These data together with the CAD algorithm form the basis of the digital hand atlas [6,7]. Figure 7a describes the workflow of using the digital hand atlas in the PACS environment for bone age assessment of children. Figure 7b shows the graphical user interface page of bone age assessment results depicted on a PACS workstation. The system integration methodology and the accuracy of the radiologists' readings without CAD compared to those with CAD are under clinical validation [8,9].

Integrating HIS/RIS/PACS data with biometric technologies in healthcare environment

Background

Most healthcare facilities currently struggle with protecting medical data privacy, mis-identification of patients, and long patient waiting times [10]. With the explosion of digital imaging and medical records, more and more medical data are managed and stored electronically in different Medical Information Systems, for example, HIS, RIS, PACS, and ePR. In order to protect the privacy of personal health information, Health Insurance Portability and Accountability Act (HIPAA) [11] privacy rules regarding national standards were published on 11 April 2003 and mandated on 11 April 2006. Great care should be taken to protect patient confidentiality to meet partial HIPAA requirement.

A location tracking and verification system (LTVS) for patient in clinical environment

This section describes a location tracking and verification system (LTVS) which integrates biometric technologies, and HIS/RIS/PACS data in the MIII core infrastructure (see Fig. 1) to automatically monitor and identify staff and patients in healthcare image-based environment as a means to partially conform to HIPAA requirement. Biometric technologies used in this application include facial features recognition and fingerprint recognition. HIS/RIS/PACS data required are not the patient history, diagnosis, treatment, and outcomes; but the time stamps of patient registration, procedure workflow, examination duration, and patient discharge.

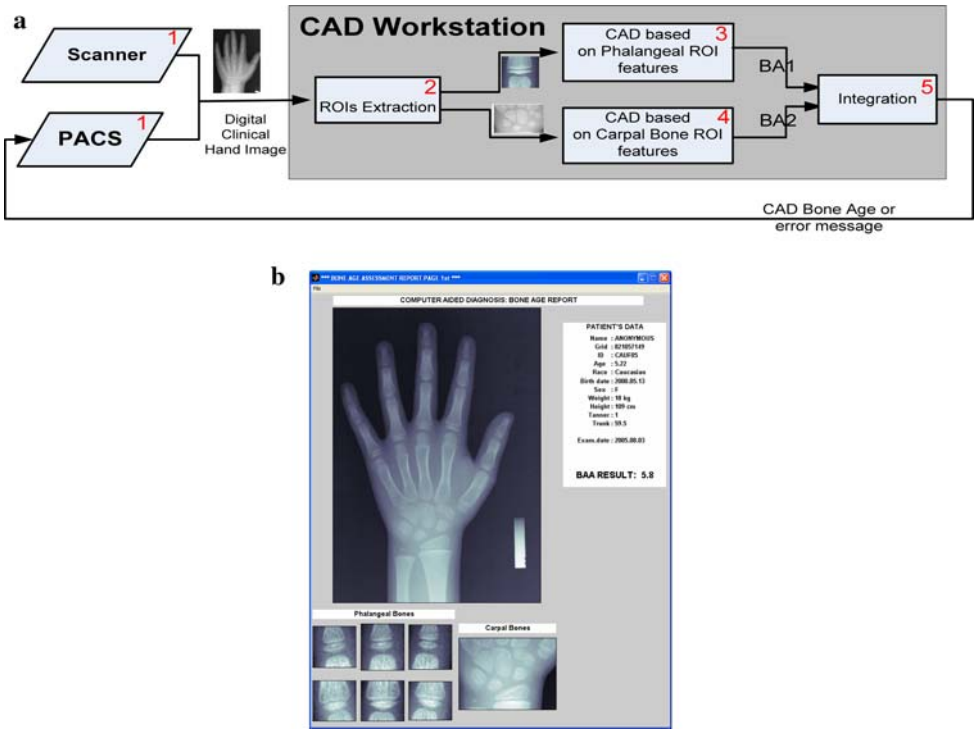

Fig. 7 **a** The workflow (numerals) of using the digital hand atlas with CAD integrated in PACS environment for bone age assessment (BA) of children. **b** Results of the bone age assessment of a child using the digital hand atlas are shown on a PACS workstation (WS). *Upper left* Hand image of the child; *upper right* results; *bottom left* Phanlangeal bone regions of interest (ROIs); *bottom middle* Carpal bone ROI. CAD results (images in the *bottom row* and text in the *right column*) stored in DICOM SR format allow the PACS WS to retrieve and pair them with the hand image (image in the *upper left*) archived in the PACS database and display them all on the WS monitor as shown

The design of the LTVS requires a workflow study to observe the physical location and movement of patient and staff in the clinical environment. The environment includes floor space and set up, various operating clinical information systems like HIS, RIS, PACS, ePR, and imaging equipment. Based on the analysis of this workflow study, a LTVS can be designed using a wireless real-time location system, and a facial biometric system or a finger print recognition system integrated with the RIS. The LTVS uses wireless technology for tracking the location of patients and staff [12] and facial (discussed in this section) [13] or fingerprint biometric technology for automatically identifying staff and patients [14–16]. By integrating these two technologies, LTVS system provides a simple yet systematic solution to monitor and automatically identify staff and patients in order to streamline the patient workflow, protect against erroneous examinations and create a security zone to prevent and audit unauthorized access to patient healthcare data for partial compliance of the HIPAA mandate.

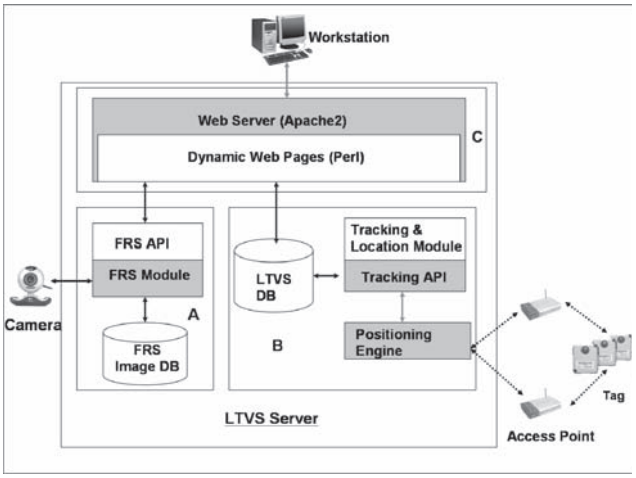

Fig. 8 System architecture shows the location tracking and verification system (LTVS) Server which consists of a web server application that runs the LTVS web-based Graphical User Interface (GUI). **a** Facial biometrics verification module with cameras. **b** Wireless Location Tracking module with tags. **c** Web server with GUI for clients to access. *Perl* Practical extraction and report language; *FRS* Facial biometric recognition system; *API* Application programming interface ([14], Fig. 2)

Location tracking and verification system (LTVS) design

As an example, the design of the LTVS prototype system in the outpatient radiological imaging center of the Healthcare Consultation Center II (HCCII), Radiology Department, USC is described. The components for the LTVS consists of a facial biometric or a fingerprint recognition module (Fig. 8a, in this example, the facial biometric is used), and a Wi-Fi (wireless fidelity) based tracking module (Fig. 8b) integrated into a web-based application (Fig. 8c). "Wi-Fi" stands for certain types of wireless local area networks (WLAN) that use specifications conforming to IEEE 802.11 network.

The facial biometrics recognition module (Fig. 8a) uses software that calculates and analyzes landmark positions and features on a face to verify a person's identity. High resolution USB video cameras are used for identity verification purpose.

Table 1 Hardware and software components of the LTVS system

Hardware	Software
Dedicated LTVS Server (PC Workstation, DELL DIMENSION 3000)	LTVS GUI web application Web server (Apache)
Wi-Fi tracking devices Wireless Access Points (D-Link Xtreme G Router) Ekahau Wi-Fi tags	LTVS Tracking API PostGreSQL Database Ekahau Wi-Fi Positioning Engine
Client Workstations (PC Workstation, DELL DIMENSION 3000)	LTVS Facial Verification API (Neven Vision) Image-Capturing software
Logitech USB Video cameras	
System design and implementation were completed in-house	

The facial biometrics recognition module has a database for image storage. The tracking module (Fig. 8b) consists of a wireless radio frequency solution that utilize IEEE 802.11 b/g access points and Wi-Fi tags to track the current and historical location of patients and staff stored in the LTVS database which is a local database located at HCCII. LTVS can be connected to any Wi-Fi network, as a result it complies with the IEEE 802.11 b/g network standard described above. In addition to location information, the integrated web-based application (Fig. 8c) stores data inputs into the LTVS database from both the facial biometric recognition module as well as other data from the tracking module.

The LTVS application can be installed in any standard PC workstation with a web browser. A web-based browser capable Personal Digital Assistant (PDA) can also be utilized as a mobile application for users to monitor patient and staff and verify patient and staff identities [15]. Table 1 lists all the hardware and software components of the LTVS system. Based on the workflow, system integration design and the Graphical User Interface (GUI) would allow healthcare providers to extract real-time location information and verify the identity of the patient and staff. The tracking and biometrics module runs independently and synchronously using the Windows 2000 Professional operating system. The design of the LTVS server is modular in design to facilitate any improvements and replacements in the future. The system was demonstrated at the InfoRAD Exhibit, ninety first Scientific Assembly and Annual Meeting of the Radiological Society of North America Conference 2005 and received Certificate of Merit Award [16].

LTVS operation

Patient registration First, a patient photo is captured at the registration desk by the video camera, correlated with patient information from RIS/HIS, and stored in the database of the LTVS.

Tag assignment Then, the patient is assigned a Wi-Fi tag which links the patient information, such as the patient name and patient birth date. It is important to include a passive biometric ID because tracking devices can be easily lost or stolen and used to impersonate in order to gain access to the environment.

Patient tracking Once the tags have been assigned to patients or staff, the system allows the staff to access patient location records including when, where and who. It also provides the ability to locate patients on a real-time location tracking page in the Graphic User Interface (GUI) window. In addition, the application provides a warning message to the staff if a particular patient has been in one location (e.g., waiting room) beyond the time limit.

Information security

The system can trigger an alert if an unauthorized person enters a pre-defined restricted area, (e.g. a reading room). These pre-defined rules are set not only for areas within the system coverage but also base on authorized and unauthorized staff. For example, a technologist would be allowed within the Reading Room, but a patient would not. Predefined rules could be re-configured within the LTVS to reflect these restrictions.

Patient safety In order to prevent patient mis-identification, before the patient enters the procedure room for an exam, the technologist can verify the identity of the patient by capturing the patient's facial image, and the software verifies and confirms the patient information including the patient ID, name, and original photos.

User interface examples Figure 9 (*left upper corner*) shows four user interface menus of the LTVS report system in which the "Report" menu is being chosen (arrow) depicting the tracking of patient John Doe. Figure 10 shows the LTVS "Monitoring page" menu from where the real-time location of patients and staff can be located in the image map of the HCCII environment. Patients John Doe 1, staff 2, and staff 3 assigned with tags (Fig. 10, *top middle*) are tracked on

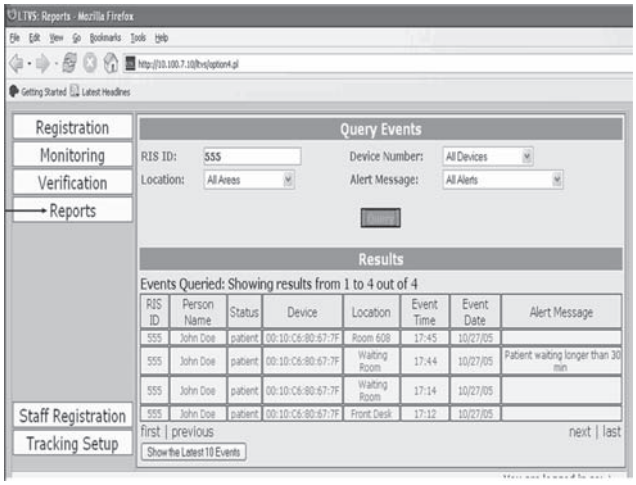

Fig. 9 The Report Page" provides multiple choices for querying the report from the database (see *left column, arrow*). For example, in the figure, the GUI displays a window of patient John Doe, with RIS ID, name, status tracking device number, location, event time, event date, and system message saying "Patient waiting longer than 30 min" ([14], Fig. 3)

Fig. 10 The GUI showing a window of the floor plan of the clinical evaluation site, USC Healthcare Consultation Center II (HCC II). This example depicts that patient John Doe 1, staff 2 and staff 3 each had been assigned a tracking tag. Their names, tag accession number, status, and physical location are shown in event list table above the floor plan ([14], Fig. 4)

the map in real-time with their names displayed next to the locations. The real-time walking movement can be tracked on the map as well.

Benefits of LTVS

Based on the HCCII prototype system, LTVS demonstrates the following benefit:

1. A patient can be clearly identified and tracked through the course of examinations if the patient with a photograph taken during the registration carries a Wi-Fi tag. It allows users to understand the operational bottlenecks at HCCII and recommend an improved workflow.
2. Healthcare providers can know the patient location and the overall time a patient spent during the examination. Prompts can be put in place when the patient has remained in the waiting room for more than a specific amount of time to decrease the waiting time as to track workflow inefficiencies throughout the time the patient is within the department (See Fig. 9, *lower right* Alert Message).
3. From a security standpoint, facial recognition will provide instantaneous and highly reliable biometric identity information, to be certain that the examination was being performed on the right patient. It helps to prevent misidentification of patients undergoing a radiological procedure.
4. It improves the overall clinical management of policies and procedures in a clinical environment in order to partially fulfill HIPAA requirements for patient electronic data security.

Integration of image-based diagnosis with treatment—minimally invasive spinal surgery (MISS)

Diagnosis and treatment

This section discusses the concept of bridging the gap between diagnostic images and surgical treatment in the sense that real-time images are obtained continuously guiding the surgeon to perform the operation. Figure 11 left and right show the diagnostic image domain and the treatment domain, respectively. The arrow in the bottom bridging the chasm between these two domains creates a continuum between diagnosis and treatment. In this discussion, minimally invasive spinal surgery (MISS) is used as an example to explain the steps involved. The two real-time imaging techniques used are digital fluoroscopic (DF or DR, see Fig. 11) and endoscope video images (Endo). The underlining informatics technologies are data collection and depository in the ePR data base, and patient outcomes analysis based on data in the ePR database. Data collection and depository include from ePR with images distribution, PACS data and other relevant medical images not included in PACS, pre-surgical images and data during patient consultation, intra-surgical real-time images and vital signs data, and post-surgical observation and vital signs data.

MISS

Back and neck pain is the price human beings pay for poor posture, prolonged sitting, lifting, repeated bending, obesity,

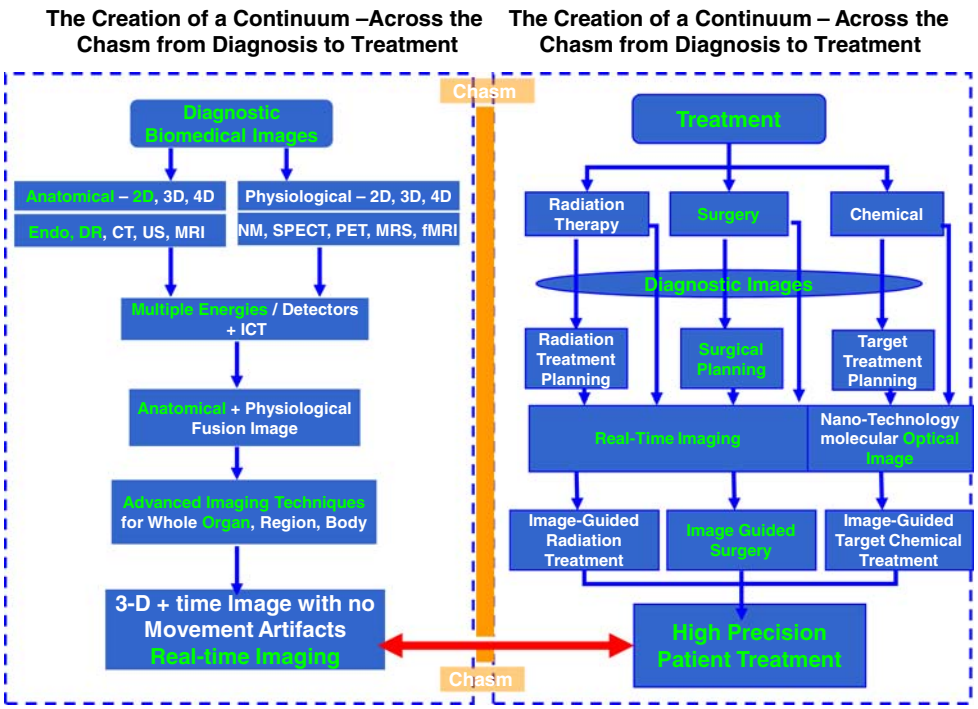

Fig. 11 The creation of a continuum across the chasm from diagnosis to treatment. The traditional patient workflow is that the patient was first diagnosis with imaging techniques, then surgeon performs the surgery based on the diagnosis. It is rarely happened that the surgeon performs image-guided surgery until very recently. The example in MISS illustrates that now the surgeon performs the spinal surgery under the guidance of two real-time imaging techniques: Endoscope and DR (*left* second row)

and injury from accidents. This ailment gives the United States with a massive economic headache. Approximately 85% of inhabitants of the Western world are afflicted with some degree of back or neck pain at some point in their lives. About 25% of our population has been incapacitated for two weeks or more due to back pain and an estimated 8–10 million people have a permanent disability from it. The economic impact is obvious. In most cases, simple treatments such as bed rest, exercise, physiotherapy, and pain medication bring relief. Many sufferers are not so fortunate. If one or more of their vertebral discs ruptures and presses on nerve roots, the pain radiating from the back or neck and down the limbs can be incapacitating and severe. Until recently, the only treatment was surgical removal of part of the ruptured disc, a major operation that required general anesthesia, the dissection of muscle, removal of bone, manipulation of nerve roots, and, at times, bone fusion. In an effort to overcome the disadvantages of traditional surgical techniques, the scientific medical community began exploring the use of endoscopy (arthroscopy) for MISS operation.

An endoscope provides clear visualization and magnification of deep structures in real time. With the advancement of scientific technology and miniaturization, including fiber optics, video imaging technology, laser treatment and experience gained through minimally invasive spinal surgery, there is a less traumatic discectomy procedure for some patients with disc problems. In the recent years, development of image-guided surgery has improved the precision and reduced surgical tissue trauma [17].

The MISS procedure

Depending on the type of spinal surgery, the MISS procedure is done with the patient under either a local anesthesia or in some situations, a brief general anesthesia. External real-time minimal exposure digital fluoroscopy (DF) is used to guide the surgeon to pinpoint the exact location of the disc under consideration based on pre-surgical evaluation of MRI spinal scans. After the location of the problematic disc is marked on the skin, a small hollow tube (about 6 mm) is inserted by the surgeon into the disc space. An endoscope and a variety of MISS surgical instruments can be inserted through the hollow tube including mini-forceps, curettes, trephines, rasps, burrs, cutters, and other types of probes for disc decompression guided by real-time continuous endoscopic video images. Lasers are also used to shrink and tighten the disc and to remove portions of the protruded disc. The procedure takes about 30 min per disc on the average. The discectome, a hollow probe, is used to cut, suction and remove small pieces of disc material until enough disc material is removed for decompression of the nerve root. A laser is used to shrink and to tighten the disc. The supporting structure of the disc is not affected. Upon completion, sutures and a small band-aid are applied to the external incision. This endoscopic procedure is also used currently for bony decompression in spinal stenosis. [18,19] Based on a 4,000 patient study at the California Spine Institute (CSI) [20], endoscopic spine surgery has a patient satisfaction score of 91%, and a 94% success rate (for a single level of disc problem). The complication

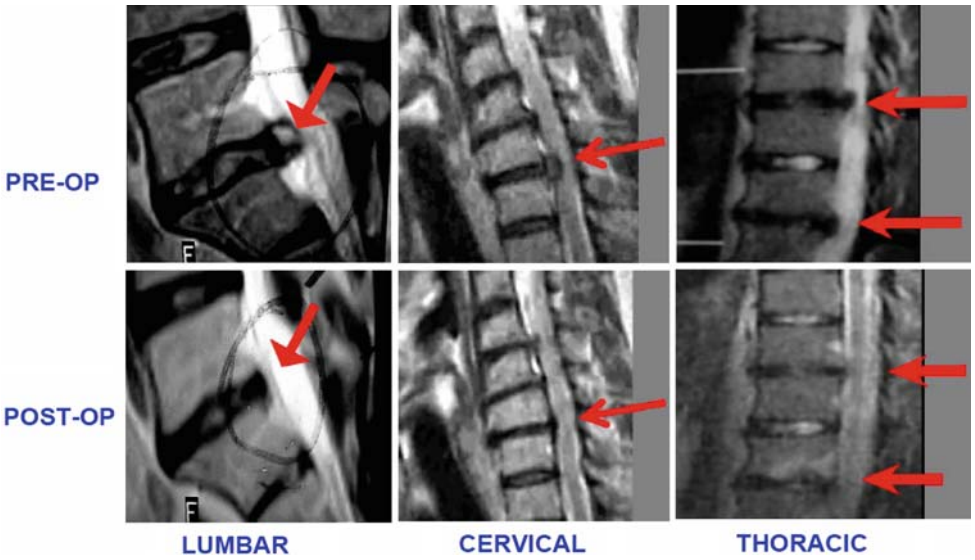

Fig. 12 MISS on Lumbar, cervical, and thoracic spines. Pre-operation arrows (*upper row*) show the areas where the disc protrudes the spine. *Lower row* post MISS operation (Courtesy of Dr. John Chiu, CSI)

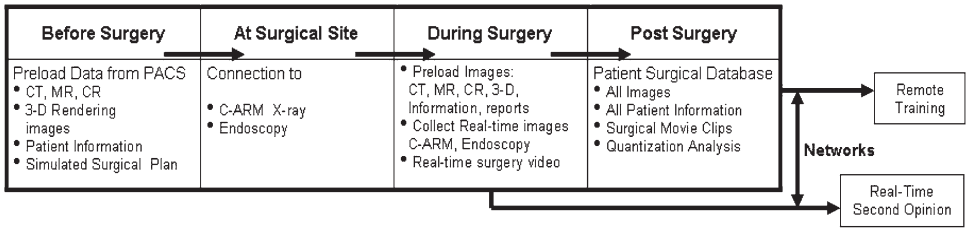

Fig. 13 Minimally invasive spinal surgery workflow

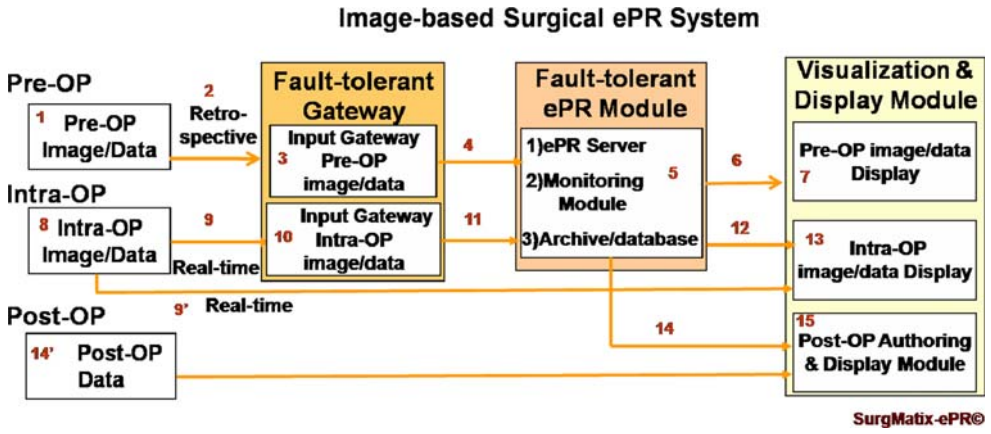

Fig. 14 Infrastructure, components, and workflow of the ePR system (SurgMatix 1©) supporting the MISS operation. Numerals are steps in the MISS workflow

rate is much less than 1% and mortality rate directly from spinal disc surgery is zero [21]. Figure 12 shows a cervical, thoracic and lumbar spine before and after MISS operations.

Integration of diagnosis with treatment—an ePR system for MISS operation

The design of an ePR System combining the aforementioned imaging techniques and surgical methods is being developed at CSI which integrates diagnosis and treatment as one continuum supporting MISS operation. A patient oriented ePR with integrated image acquisition, display, manipulation, management, distribution and documentation supporting MISS operation is important to facilitate and improve operation efficient and patient outcome.

The MISS operation workflow starting from pre-surgical consultation, pre-operation preparation, intra-operation image and vital signs acquisition and display, post-surgery documentation to patient recovery monitoring is shown in Fig. 13 [22]. Figure 14 is the infrastructure and components in the MISS ePR system [23].

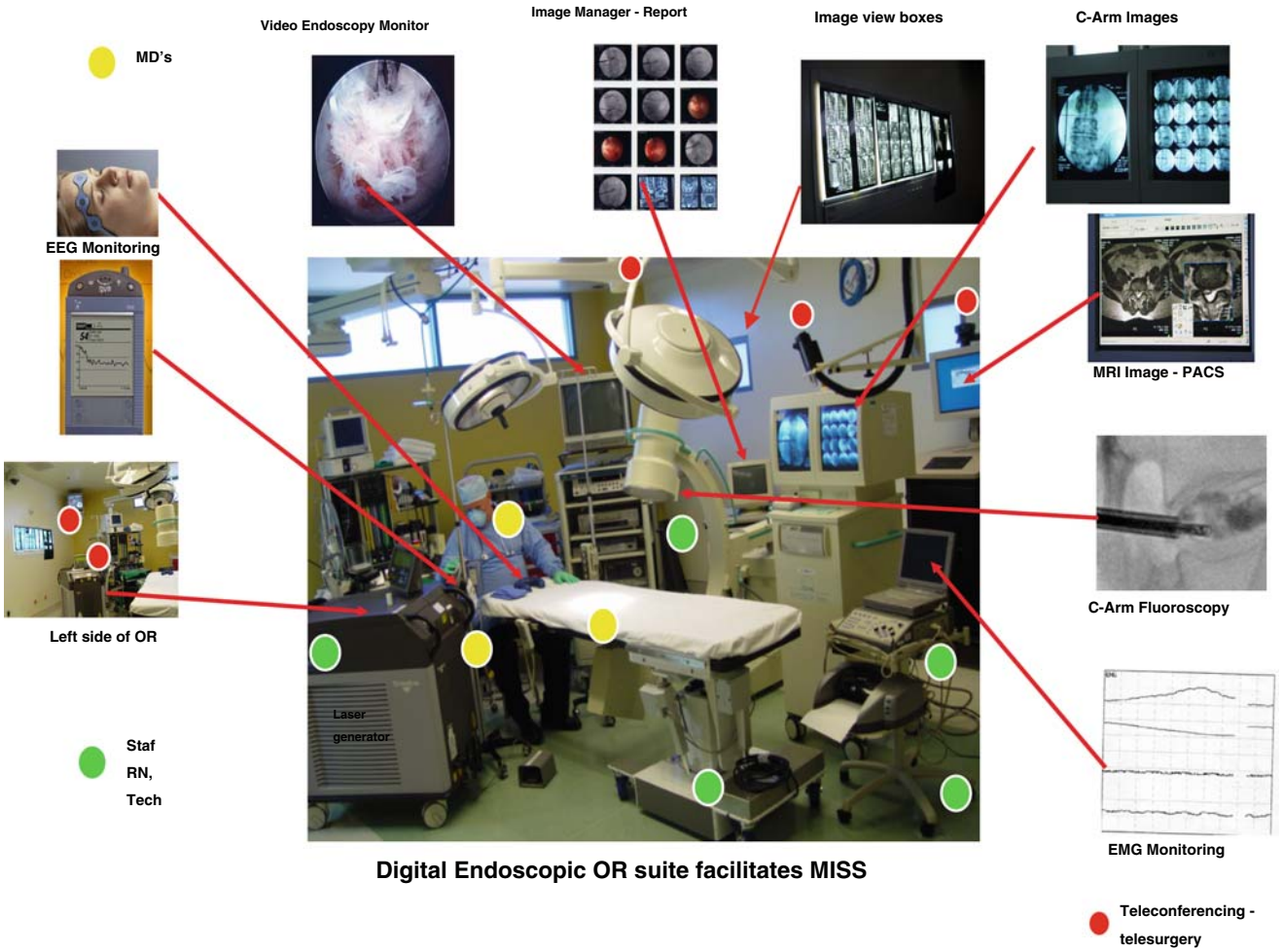

Fig. 15 A Digital endoscopic OR suite for MISS operation of today with manually controlled endoscopic systems, and images and waveform data scattering in the suite. With the design and implementation of the ePR described here, the today's suite will become a real-time image-guided MISS OR of the future shown in Fig. 16. (Courtesy of Dr. John Chiu) [24]

The MISS operation suite of today and future

Figure 15 shows a MISS surgical suite of today, which describes surgical equipment and required pre-op images, intra-op images and life-supported wave forms to support the surgical operation [24]. Figure 16 depicts a mock-up version of the future MISS OR with the ePR system supporting the surgery in which the pre-op (right) and intra-op (left) image data are shown in two organized large LCD monitors based on the database in the ePR system. The prototype, SurgMatix 1©, is being implemented at CSI.

Summary

We have discussed five topics related to medical imaging informatics and biometrics. Medical imaging informatics infrastructure is the fundamental concept of integrating medical imaging and informatics technologies logically for healthcare applications. Data Grid for image fault tolerant backup and disaster discovery technology is an indispensible tool for maintaining the integrity of medical images and biometric data. Integration of computer-assisted detection and diagnosis in daily clinical practice addresses the issue of integrating specific CAD methods into daily PACS operation to assist and improve the accuracy of imaging related diagnosis. Using biometric technologies including facial and fingerprint recognition for patient location and identification in an enterprise HIS/RIS/PACS integrated environment minimizes the possibility of mis-identification of the patient and protects data access right. The concept of in-vivo image-guided diagnosis and real-time treatment is the current trend of performing outpatient surgical operation to minimize suffers of and the cost to the patient resulting in a better healthcare delivery system.

These five concepts and technologies are independent in their own right but possess certain intertwined relationship to complement each other. In order for them to be useful

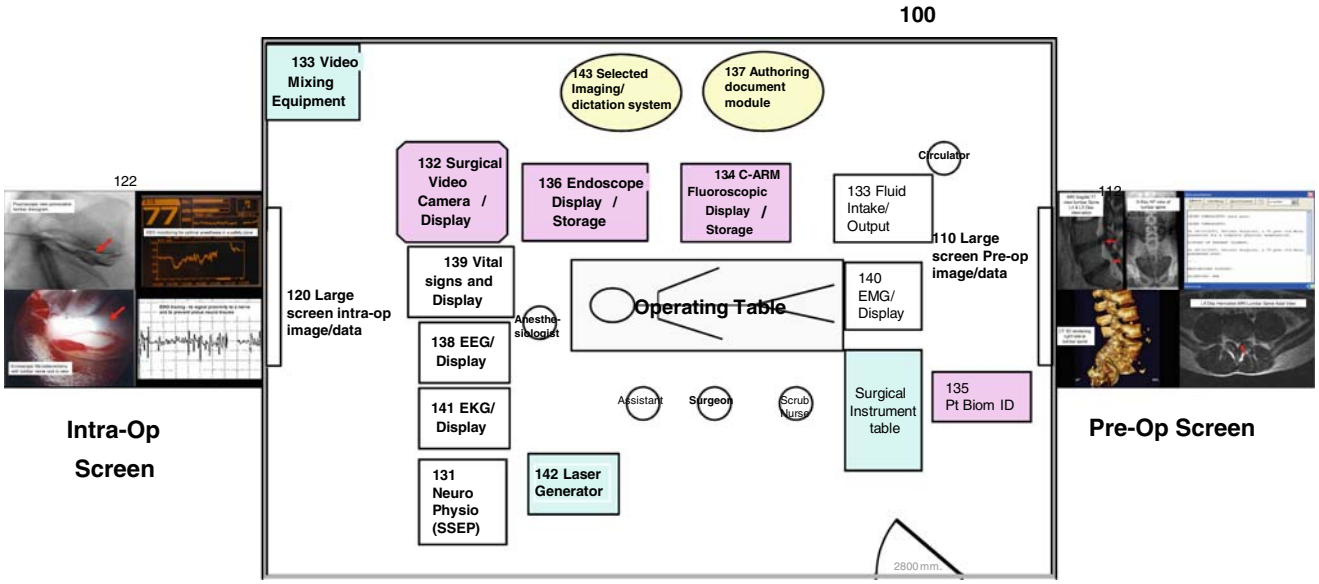

Fig. 16 Future MISS OR with organized pre- and real-time intra-surgical image/data in the ePR system displayed on two 52″ LCD monitors during surgery [23,24]

in medical imaging informatics applications, two projecting players, that is, the customers and the providers, have the responsibility to contribute their own shares. In this case, customers are research laboratories, radiology departments and hospitals; and providers are medical imaging and PACS manufacturers, communication network and software companies. Figure 1 can be used as an example on how these two players share the responsibility of developing components and the infrastructure in a three-step process.

The first step is to design and implement components and their connectivity within the large ellipse. Customers first work together with network and PACS manufacturers to establish the HIS/RIS/PACS integration which form the MIII core of the clinical operation and informatics infrastructure. The extensiveness of each component is not crucial, but the potential of its future expansion is. The customers with technological information from the providers should develop a long-term strategic roadmap of future expectations.

In the second step, the customers should look into certain components within the MIII core which are HIS/RIS/PACS clinical relevant, i.e. those components have immediately add-on values to HIS/RIS/PACS operation. In this example, they are the two small ellipses of ePR and visualization graphics tool, and network security and storage archive components. Customers working with providers during the HIS/RIS/PACS integration should consider including ePR and SAN in the infrastructure with potential expansion to link to ePR with image distribution, and Data Grid. If the budget is allowed and the provider's technology is available, they can be implemented as well.

The third step is for the customer to develop special applications. Figure 1 illustrates three examples, each of which requires a special provider(s). MISS is for the hospital to expand ePR with image distribution to minimally invasive spinal surgery application with the contribution from surgical device companies. CAD application is for the radiology department to work with a computer-aided-diagnosis software company to integrate CAD into daily clinical operation. LTVS is the collaboration of the hospital working with a biometrics location tracking and verification hardware company and an application software company to develop a patient location and identification system to fulfill a partial requirement from HIPAA.

Utilization of medical imaging informatics and biometrics technologies in healthcare delivery based on HIS/RIS/PACS data is still in its infancy, in this paper we provide certain concepts and the infrastructure to stimulate their future growth. We expect this field will continue to expand rapidly.

Acknowledgments B. Liu, A. Zhang, J. Documet, B. Guo, A. Le at IPI contributed substantially in projects described in this paper, which have been partially supported by the National Institutes of Health (NIH), USA: R01 EB 00298, R01 LM 07606, T32 EB00438; MI^2 Corp. ; and SurgMatix Corp. Dr. John Chiu provided materials used in the MISS operation.

References

1. Huang HK (2004) PACS and imaging informatics: principles and applications. Wiley, Hobokens
2. Huang HK, Zhang A, Liu B, Zhou Z, Documet J, King N, Chan LWC (2005) Data Grid for large-scale medical image archive and analysis. In: Proceedings of the 13th annual ACM international conference on multimedia (Hilton, November 06–11, 2005). MULTIMEDIA '05. ACM, New York, pp 1005–1013

3. Zhou Z, Gutierrez MA, Documet J, Chan L, Huang HK, Liu BJ (2007) The role of a data grid in worldwide imaging-based clinical trials. J High Speed Netw 16(1):21–33
4. Zhou Z, Le A, Liu B, Huang HK (2007) PACS-CAD toolkit for integrating an independent cad workstation to diagnosis workflow. Proceedings of SPIE medical imaging 6516:651609
5. Zhou Z, Liu BJ (2007) CAD-PACS integration tool kit—based on DICOM screen capture (SC) and structured report (SR) and IHE workflow profiles. Comput Med Imaging Graph 31(4–5):346–352
6. Pietka E, Gertych A, Pospeich S, Cao F, Huang HK, Gilsanz V (2001) Computer assisted bone age assessment: image preprocessing and epiphyseal/metaphyseal ROI extraction. IEEE Trans Med Imaging 20(8):715–729
7. Zhang A, Gertych A, Tsao S, liu BJ, Huang HK (2007) Bone age assessment for young children from new born—7 year old using carpal bones, 2006. J Comput Med Imaging Graph 31(4–5):299–310
8. Zhang A, Huang HK, Sayre J, Vachon, L (2007) Cross-racial discrepancies of growth patterns in bone age assessment. RSNA 2007, Scientific Paper: VP32–08
9. Zhang A, Gertych A, Tsao, S, Liu BJ, Huang HK (2007) Fuzzy system design for bone age assessment of children in multiple regions of the hand. RSNA 2007, Scientific Poster: LL-PD2098-R09
10. Thomas P, Evans C (2004) An identity crisis? aspects of patient misidentification. Clin Risk 10(1):18–22
11. HIPAA, http://www.hhs.gov/ocr/hipaa/ (2006)
12. Ekahau Inc., http://www.ekahau.com/ (2006)
13. NevenVision, http://www.nevenvision.com/ (2006)
14. Guo B, Documet J, Lee J, Liu B, King N, Shrestha R, Wang K, Huang HK, Grant EG (2007) Experiences with a prototype tracking & verification system implemented within an imaging center. Acad Radiol 14(3):270–278
15. Guo B, Documet J, Lee J et al (2006) A tracking and verification system implemented in a clinical environment for partial HIPAA compliance. Proceedings of SPIE medical imaging 6145:184–191
16. Guo B, Document J, King N (2005) Patient tracking and facial biometrics integrated in a clinical environment for HIPAA security compliance. Presented at the 91st scientific assembly and annual meeting of RSNA (Inforad Exhibit)
17. Chiu J, Savitz MH (2005) Use of laser in minimally invasive spinal surgery and pain management. In: Kambin P (ed) Arthroscopic and endoscopic spinal surgery—text and atlas, 2nd edn. Humana Press, New Jersey, pp 259–269
18. Savitz MH, Chiu JC, Yeung AT (2000) The practice of minimally invasive spinal technique, Millennium Edition, AAMISMS Education, Richmond, ISSN 1531–6084
19. Savitz MH, Chiu JC, Rauschning W, Yeung AT (2005) The practice of minimally invasive spinal technique, 2005 edn. AAMISS Press, NY
20. Chiu J (2006) Technological developments for computer assisted endoscopic minimally invasive spinal surgery (MISS). In: Proceedings of computer assisted radiology and surgery, 20th International Congress, Osaka, Japan, June 28–July 1
21. Chiu J, Savitz M (2005) Multicenter study of percutaneous endoscopic discectomy. In: Savitz M, Chiu J, Rauschning W, Yeung A (eds) The practice of minimally invasive spinal technique. AAMISS Press, New City, pp 622–626
22. Huang HK (2001) PACS, informatics, and the neurosurgery command module. J Mini Invasive Spinal Technique 1(1):62–67
23. Huang HK (2007) The role of imaging informatics in MISS. In: Proceedings of 21st CARS intern congress in computer assisted radiology and surgery, Berlin, Germany, June 27–30
24. Chiu JC, Savitz MH (2005) Operating room of the future for spinal procedures. In: Savitz MH, Chiu JC, Rauschning W, Yeung AT (eds) The practice of minimally invasive spinal technique. AAMISS Press, New York, pp 645–648

Racial Differences in Growth Patterns of Children Assessed on the Basis of Bone Age[1]

Aifeng Zhang, PhD
James W. Sayre, PhD
Linda Vachon, MD
Brent J. Liu, PhD
H. K. Huang, DSc

Purpose: To collect up-to-date data in healthy children to create a digital hand atlas (DHA) that can be used to evaluate, on the basis of the Greulich and Pyle atlas method, racial differences in skeletal growth patterns of Asian, African American, white, and Hispanic children in the United States.

Materials and Methods: This retrospective study was HIPAA compliant and approved by the institutional review board. Informed consent was obtained from all subjects or their guardians. From May 1997 to March 2008, a DHA containing 1390 hand and wrist radiographs obtained in male and female Asian, African American, white, and Hispanic children with normal skeletal development was developed. The age of subjects ranged from 1 day to 18 years. Each image was read by two pediatric radiologists working independently and without knowledge of the subject's chronologic age, and evaluation was based on their experience with the Greulich and Pyle atlas. Statistical analyses were performed with the paired-samples *t* test and analysis of variance to study racial differences in growth patterns. $P \leq .05$ indicated a significant difference.

Results: Bone age ($P \leq .05$) was significantly overestimated in Asian and Hispanic children. These children appear to mature sooner than their African American and white peers. This was seen in both male and female subjects, especially in girls aged 10–13 years and boys aged 11–15 years.

Conclusion: Ethnic and racial differences in growth patterns exist at certain ages; however, the Greulich and Pyle atlas does not recognize this fact. Assessment of bone age in children with use of the Greulich and Pyle atlas can be improved by considering the subject's ethnicity.

[1] From the Image Processing and Informatics Lab, Department of Radiology, University of Southern California, 1450 San Pablo St, Suite 2100, Los Angeles, CA 90292 (A.Z., B.J.L., H.K.H.); Department of Biostatistics and Radiological Sciences, University of California, Los Angeles, School of Public Health, Los Angeles, Calif (J.W.S.); and Department of Radiology, Los Angeles County Hospital and University of Southern California Medical Center, Los Angeles, Calif (L.V.). From the 2007 RSNA Annual Meeting. Received March 10, 2008; revision requested May 1; revision received April 3; accepted June 20; final version accepted July 9. Supported by National Institutes of Health grants R01 LM 06270 and R01 EB 00298: 97-08. **Address correspondence to** A.Z. (e-mail: *aifengz@gmail.com*).

Assessment of bone age is a clinical procedure used in pediatric radiology to evaluate skeletal maturity on the basis of bone growth in the left hand and wrist, as seen on a radiograph. The determination of skeletal maturity (also referred to as bone age) plays an important role in the diagnosis and treatment of endocrinologic abnormalities and growth disorders in children (1,2). In clinical practice, the method most commonly used to assess bone age is matching of a radiograph of the left hand and wrist with the Greulich and Pyle atlas (3), which contains a reference set of standard hand images collected in the 1950s in healthy white children who were members of the middle or upper class population.

Over the past 30 years, many authors have questioned the appropriateness of using the Greulich and Pyle atlas for bone age assessment in contemporary children. In 1975, Roche et al (4) showed that the average child in the United States was less physically mature than the children in the Greulich and Pyle atlas. In 1996, Ontell et al (5) examined the applicability of the Greulich and Pyle standards to ethnically diverse children. However, these studies and various others (6–8) did not provide a large-scale systematic method for validation. Thus, the purpose of our study was to collect up-to-date data in healthy children to create a digital hand atlas (DHA) that can be used to evaluate, on the basis of the Greulich and Pyle atlas method, racial differences in skeletal growth patterns of Asian, African American, white, and Hispanic children in the United States.

Advances in Knowledge

- A digital hand atlas (DHA) of 1390 hand-wrist radiographs obtained in Asian, African American, white, and Hispanic boys and girls with normal skeletal development has been developed to provide an up-to-date standard with which to assess growth and development and is accessible at *http://www.ipilab.org/BAAweb*.
- Radiologists assigned a bone age that was relatively close to the chronologic age in African American and white children; however, cross-racial differences indicated that Asian and Hispanic children mature sooner than do African American and white children, especially between 10 and 13 years of age in girls and between 11 and 15 years of age in boys.

Materials and Methods

The protocol of this retrospective study was approved and has been renewed annually by the institutional review boards of our institutions, and written informed consent was obtained from all subjects or their legal guardians. This study was compliant with the Health Insurance Portability and Accountability Act. Subject anonymity was achieved by replacing the subject name and other traceable information with a data encryption method.

Subject Recruitment

During the past 10 years (May 1997 to March 2008), a DHA has been developed that contains 1390 hand and wrist radiographs obtained in healthy Asian, African American, white, and Hispanic boys and girls. All subjects (age range, 1 day to 18 years) were recruited from public schools in Los Angeles County, California, starting in the late 1990s (9–15).

Case Selection Criteria

Before the hand was examined with radiography, a physical examination was performed to determine the health and Tanner maturity index (16) of the subject to ensure that he or she was healthy and that his or her skeletal development was normal. Height, trunk height, and weight were measured and used to calculate the body mass index.

Implication for Patient Care

- The discovery of cross-racial differences at different age ranges sheds light on the possibility that bone age assessment in children can be improved by considering a child's ethnicity, especially when accurate assessment of bone age is crucial to patient care (optimal surgical intervention in children with leg length discrepancies).

Image Acquisition

Each radiograph of the hand and wrist was obtained with a rigorous data collection protocol (9). The radiographs were obtained with an x-ray generator (Polyphos 50; Siemens, Erlangen, Germany) at 55 kVp and 1.2 mAs. The radiation dose delivered per image was less than 1 mrem (0.01 mSv), which is equivalent to approximately 1 day of natural background radiation. The hand was adjusted to the correct position, which required the subject to keep his or her fingers spread apart and maintain hand straightness as much as possible; no hand jewelry was worn. The distance between the x-ray tube and the image cassette was 40 inches. The hand of a normal child was less than 1 inch thick; therefore, the magnification factor was approximately 1.

Image Interpretation

After a radiograph of the hand was acquired in each subject, two experienced pediatric radiologists (each with more than 25 years of experience in bone age assessment) performed independent

Published online before print
10.1148/radiol.2493080468

Radiology 2009; 250:228–235

Abbreviations:
DHA = digital hand atlas
DICOM = Digital Imaging and Communications in Medicine

Author contributions:
Guarantors of integrity of entire study, A.Z., B.J.L., H.K.H.; study concepts/study design or data acquisition or data analysis/interpretation, all authors; manuscript drafting or manuscript revision for important intellectual content, all authors; manuscript final version approval, all authors; literature research, A.Z., B.J.L., H.K.H.; clinical studies, A.Z., L.V., B.J.L., H.K.H.; statistical analysis, A.Z., J.W.S., B.J.L., H.K.H.; and manuscript editing, A.Z., L.V., B.J.L., H.K.H.

Funding: This research was supported by National Institutes of Health (grant nos. R01 LM 06270, R01 EB 00298:97-08).

Authors stated no financial relationship to disclose.

readings based on Greulich and Pyle atlas standards. During reading, radiologists were blinded to the subject's chronologic age, race, and other pertinent information.

The subject's bone age, as determined by the radiologist, was compared with the subject's chronologic age. The image was selected and accepted to the DHA only if the difference between the subject's bone age, as determined by the radiologist, and the subject's chronologic age was less than 3 years. The acceptance rate was higher than 90%.

Image Digitization

For data analysis, Web-based image and data distribution, and communication in the clinical environment and public domain, each accepted radiograph (subject name and identification were covered with black tape) was digitized into the Digital Imaging and Communications in Medicine (DICOM) format by using a laser film digitizer (Array, Tokyo, Japan); furthermore, each subject's information (excluding his or her name and identification, as well as any other traceable data) was put in the DICOM header (17–19). We used the following parameters: 12 bits per pixel, optical density of 0.0–4.0, and 100-μm pixel spacing. The size of the image corresponded to the size of the original radiograph. Table 1 contains the pertinent information of four 14-year-old boys of different races. The corresponding radiographs of their hands are shown in Figure 1.

Data Collection Summary

There were two cycles of data collection, each of which had eight categories (Asian boys, Asian girls, African-American boys, African-American girls, white boys, white girls, Hispanic boys, and Hispanic girls). Each category contained 19 age groups (one for subjects younger than 1 year and 18 set at 1-year intervals for subjects aged 1–18 years). The two pediatric radiologists independently read all images obtained in each cycle. Cycle 1 consisted of 1103 digitized hand images with demographic data. Five cases for each younger age group (1–9 years) and 10 cases for each older age group (10–18 years) were included. The sample sizes were chosen to achieve a precision of approximately 0.20 for all age groups, with a 95% confidence interval when using the digital hand atlas to compare bone age with chronologic age. Precision is defined as the confidence interval width divided by the estimated mean value of chronologic age. Subjects younger than 1 year were considered infants, and their data were not used for analysis.

In order to study the active growth period in children aged 5–14 years more carefully to yield better statistics,

Figure 1

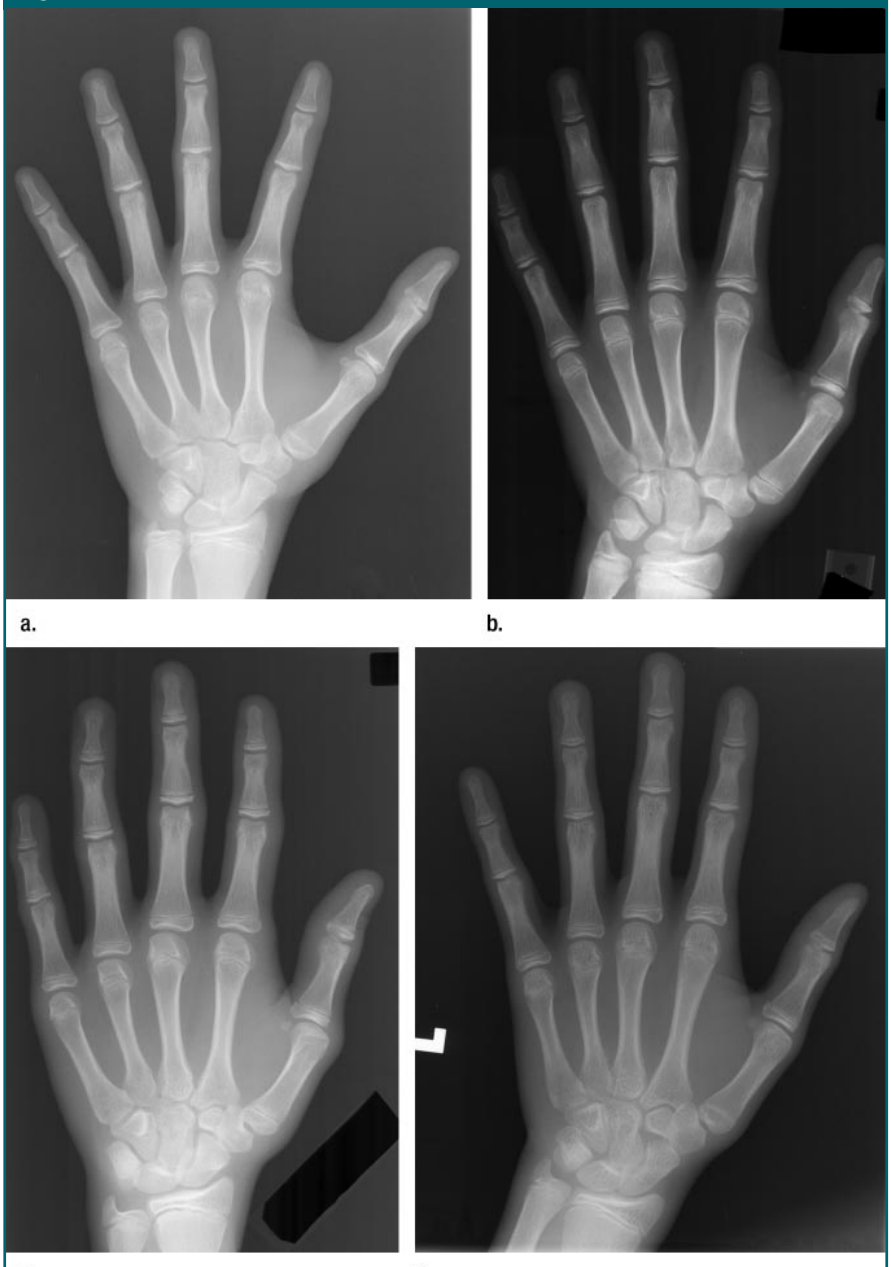

Figure 1: Examples of radiographs obtained in **(a)** a 14.13-year-old Asian boy, **(b)** a 14.46-year-old African American boy, **(c)** a 14.79-year-old white boy, and **(d)** a 14.64-year-old Hispanic boy. Corresponding demographic data and bone age, as assigned by two radiologists, are included in the DICOM image header (Table 1).

data were collected in 287 subjects during the second cycle after the first cycle had been completed. Thus, a total of 1390 cases were included in the DHA. The breakdown of cases was as follows: 167 Asian girls, 167 Asian boys, 174 African American girls, 184 African American boys, 166 white girls, 167 white boys, 183 Hispanic girls, and 182 Hispanic boys. These 1390 cases were used to derive the results described in this article.

Figure 2

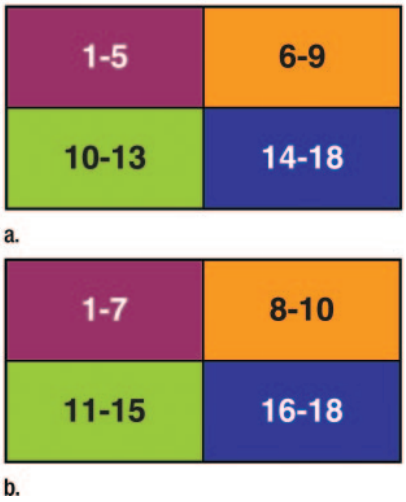

Figure 2: Charts show the four divided age subsets for **(a)** girls and **(b)** boys. These charts provide a road map for use in the study of racial differences during different growth periods. In **a**, purple indicates 1–5 years of age; orange, 6–9 years of age; green, 10–13 years of age; and blue, 14–18 years of age. In **b**, purple indicates 1–7 years of age; orange, 8–10 years of age; green, 11–15 years of age; and blue, 16–18 years of age.

Statistical Analysis

Statistical analysis was performed with computer software (SPSS, version 15.0 for Windows; SPSS, Chicago, Ill). Graphs were generated with third-party software (KaleidaGraph 3.5; Synergy Software, Reading, Pa). Two types of analysis, the paired-samples *t* test and analysis of variance, were performed by using chronologic age as the reference standard. Data from subjects in the newborn group were not used for analysis. $P \leq .05$ indicated a significant difference.

Data acquired in both cycles for each race and a given sex were combined with data for the entire age range (1–18 years), and the paired-samples *t* test was performed on a case-by-case basis to find the mean difference between the average bone age of two readings and the chronologic age. This resulted in eight categories for comparison: Asian boys, Asian girls, African American boys, African American girls, white boys, white girls, Hispanic boys, and Hispanic girls, each depicting the overall view of differences between the radiologists' average bone age reading against the chronologic age for subjects of each race and sex.

On the basis of the effects of the growth factor and sexual hormones, as well as our observations in the phalangeal, carpal, and wrist joint regions (9–15), we divided the entire growth age ranging from 1 year to 18 years into four age subsets, as shown in Figure 2. These subsets were used to study differences in growth patterns of children of different races in a given subset. Analysis of variance was used to study the cross-racial comparisons for a given subset of growth range on the basis of differences between chronologic age and bone age.

Results

Radiologist Interpretation

Table 2 shows the mean difference in age between the average bone age as-

Table 2

Mean Difference between Bone Age Assigned by Radiologists and Chronologic Age according to Race and Sex

	Asian		African American		White		Hispanic	
Characteristic	Girls	Boys	Girls	Boys	Girls	Boys	Girls	Boys
Mean difference between bone age assigned by radiologists and chronologic age (y)	0.24*	0.41*	0.03	−0.02	−0.15*	0.01	0.24*	0.30*
No. of cases†	166	165	170	179	163	164	182	178

* Mean difference between bone age assigned by radiologists and chronologic age was significant ($P \leq .05$).

† Infants (patients younger than 1 year) were excluded from analysis.

Table 1

Pertinent Information in Four 14-year-old Boys of Different Races

Subject No.	Race	Sex	Birth Date	Examination Date	Chronologic Age (y)	Tanner Maturity Index Score	Height (cm)	Trunk Height (cm)	Weight (kg)	Bone Age Assigned by Reader 1 (y)	Bone Age Assigned by Reader 2 (y)
1	Asian	Male	May 26, 1987	July 12, 2001	14.13	5	170.00	88.90	55.50	15.75	15.50
2	African American	Male	June 18, 1981	December 3, 1995	14.46	3.5	168.00	82.55	49.30	13.25	14.00
3	White	Male	July 05, 1979	April 19, 1994	14.79	4	169.00	86.70	56.00	14.00	14.50
4	Hispanic	Male	September 13, 1983	May 6, 1998	14.64	5	168.40	83.82	51.60	15.00	15.00

Note.—The DICOM header includes the subject's demographic and health-related information, as well as the bone age assigned by the radiologists. These data, along with the corresponding image, can be retrieved from the Web-based DHA.

Figure 3

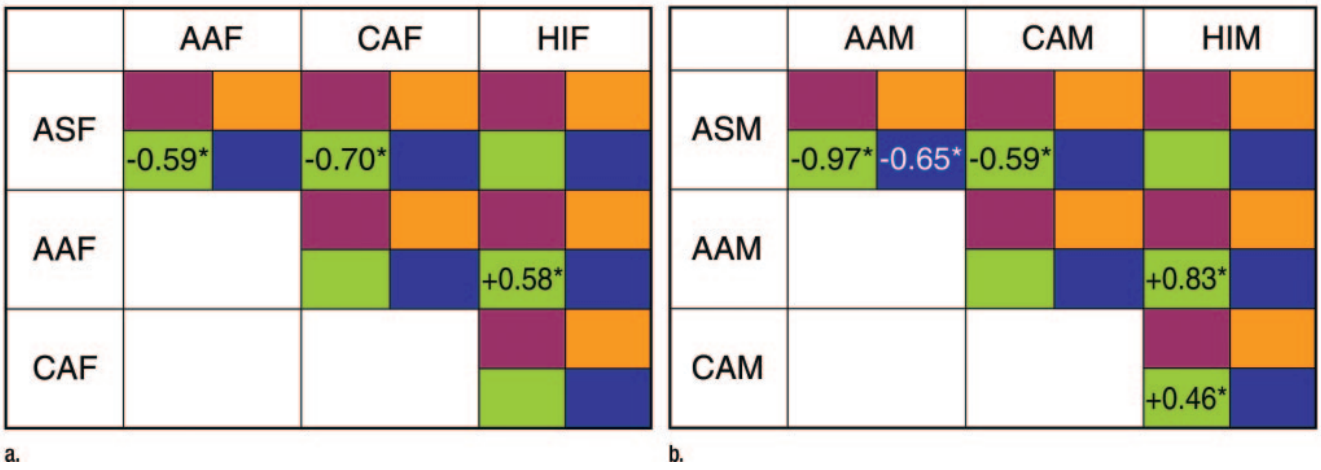

Figure 3: Charts show cross-racial comparisons of **(a)** girls and **(b)** boys. Data are shown only if differences are significant ($P \leq .05$). Each racial block was divided into four age groups, as described in Figure 2. The plus and minus signs indicate under- and overestimation of bone age, respectively, by radiologists in comparing rows with columns. *AAF* = African American girl, *AAM* = African American boy, *ASF* = Asian girl, *ASM* = Asian boy, *CAF* = white girl, *CAM* = white boy, *HIF* = Hispanic girl, *HIM* = Hispanic boy.

signed by two radiologists and the chronologic age for each of the eight categories separated by race and sex. Since we collected data in children with normal skeletal development, the differences with asterisks shown in Table 2 are within 2 standard deviations between the normal chronologic age and the average bone age (see the Case Selection Criteria section) and may not be important from a clinical perspective. However, we were able to conclude that the radiologists had a slight tendency, which was statistically significant, to overestimate bone age in the Asian and Hispanic populations as a whole.

Cross-racial Comparisons

The cross-racial differences assessed with analysis of variance among the four races in the four divided age subsets (Fig 2) are presented in Figure 3.

Figure 3a shows that in girls, significant mean differences of average reading between races were observed in the third age subset (10–13 years). Radiologists overestimated bone age in Asian girls in comparison with their African American and white peers by approximately 0.59 year and 0.70 year, respectively. Similarly, radiologists overestimated bone age by 0.58 year in Hispanic girls when compared with African American girls. Figure 4 shows plots of bone age versus chronologic age in Asian girls versus white girls, Asian girls versus African American girls, and Hispanic girls versus African American girls. In each comparison, the figure on the left covers the entire age range (1–18 years), whereas the figure on the right shows a close-up view of the third age subset (10–13 years).

Similar patterns were also observed in boys (Fig 3). In the third age subset (11–15 years), significant overestimation of bone age of 0.97 year and 0.83 year was observed in Asian and Hispanic boys, respectively, when compared with African American boys. Overestimation of 0.65 year continued until the fourth age subset (16–18 years) when Asian boys were compared with African American boys. Furthermore, comparison of white boys with Asian and Hispanic boys in the third age subset (11–15 years) resulted in significant overreading of 0.59 year and 0.46 year, respectively. Figure 5 shows bone age versus chronologic age in four racial pairs: *(a)* Hispanic boys versus African American boys, *(b)* Asian boys versus African American boys, *(c)* Asian boys versus white boys, and *(d)* Hispanic boys versus white boys.

Discussion

An up-to-date DHA for four ethnic groups has been developed with 1390 hand and wrist radiographs obtained in Asian, African American, white and Hispanic boys and girls with normal skeletal development aged between 1 day and 18 years. Each case was read by two pediatric radiologists working independently on the basis of the Greulich and Pyle atlas standard. The normality and consistency of the data were ensured by radiologists' readings and a rigorous quality assurance data collection protocol. Hand radiographs were digitized and stored in the DICOM format, which facilitates image viewing and transmission in the clinical environment for training and image-assisted daily clinical operation.

Previous studies, in which researchers examined the applicability of the Greulich and Pyle atlas for use in contemporary children, have been performed: Mora et al (7) examined 534 children of European and African de-

scent, and Ontell et al (5) collected data in 765 trauma patients of four races. Both of these studies are similar to our study in that they involved use and evaluation of the Greulich and Pyle atlas in each of the racial groups. However, in neither study did the authors compare cross-racial differences. Our study differed from the aforementioned studies in that our study consisted of a robustly designed database of 1390 carefully chosen healthy subjects and we compared cross-racial growth differences.

By using the DHA, we observed differences in the readings of two pediatric radiologists in subjects of four races on the basis of the Greulich and Pyle atlas standard, and we recorded these differences systematically. Our results show the cross-racial differences between skeletal growth patterns of Asian and Hispanic children and skeletal growth patterns of white and African American children. Radiologists assigned a bone age that was relatively close to the chronologic age of African American and white children. However, bone age and chronologic age were significantly different in Asian and Hispanic children. Cross-racial differences in four age subsets indicate that Asian and Hispanic children mature earlier than African American and white children. This holds true for girls and boys, especially those aged 10–13 years and 11–15 years, respectively.

Genetic differences, diet, and nutritional intake may influence variations in the bone growth pattern. This calls into question the applicability of the Greulich and Pyle atlas as a reference for children of different races. Our results suggest that bone age assessment in children can be improved by considering the ethnic population. An institutional review board–approved clinical validation study of the usefulness of the DHA is being performed at our institution (Los Angeles County Women's and Children's Hospital, Los Angeles, Calif).

Our study had limitations that should be considered in future research. First, all subjects enrolled in this study were from the Los Angeles metropolitan area. Further studies with data collection from different geographic regions are necessary to study regional factors in skeletal development. Second, mixed ethnicity was not considered. This issue should be addressed in future studies, with a view toward comparison of skeletal development in children with mixed ethnicity with that in children of their parents' ethnicities. Third, we investigated the effect of ethnicity in only those children whose skeletal development was considered normal on the basis of the Greulich and Pyle atlas. Fourth, a subject's ethnicity is usually unavailable in daily

Figure 4

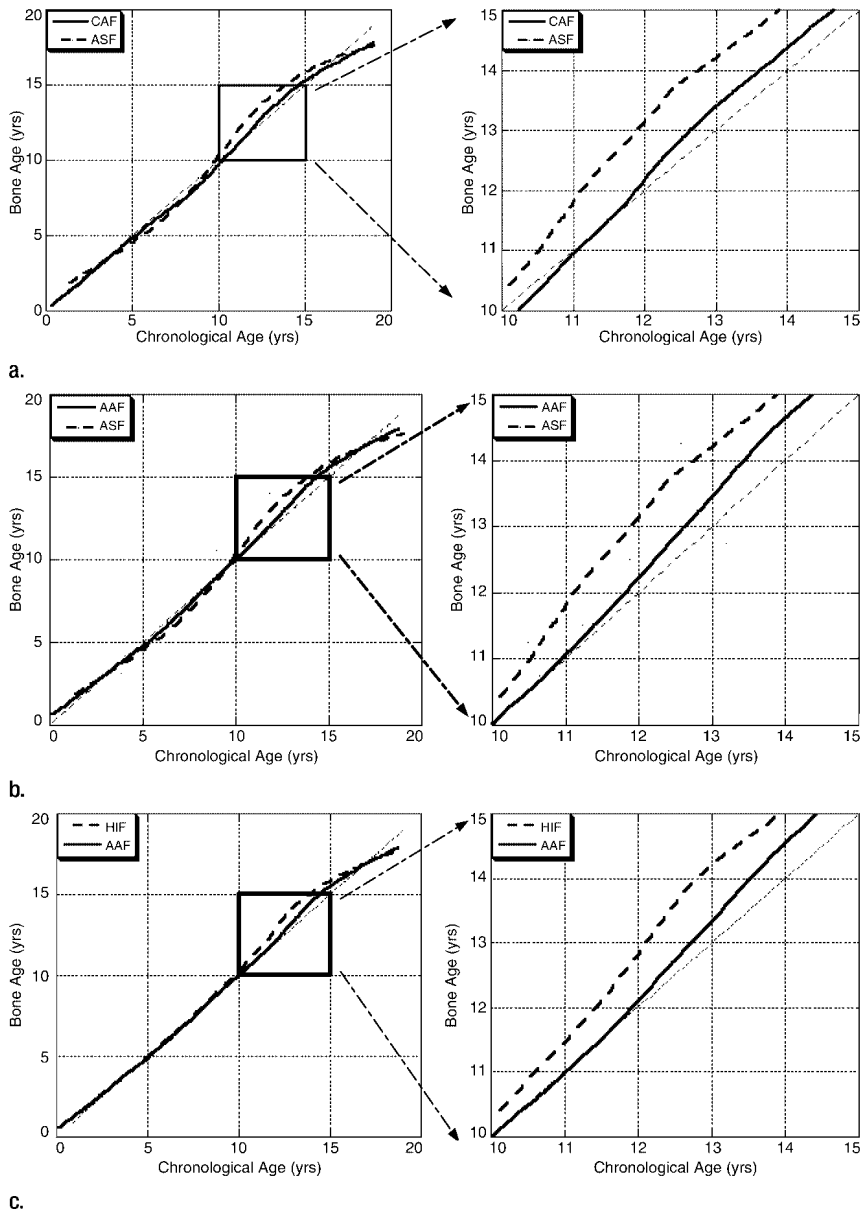

Figure 4: Graphs show comparisons of three racial pairs. The x-axis shows the chronologic age, the y-axis shows the average bone age, and the thin 45° dotted line shows the normal standard comparison in **(a)** Asian girls *(ASF)* versus white girls *(CAF),* **(b)** Asian girls versus African American girls *(AAF),* and **(c)** Hispanic girls *(HIF)* versus African American girls. The graphs on the left show the plots for the entire age range, whereas the graphs on the right are close-up plots for the third age subset (10–13 years).

practice. This limits future applications of the DHA in clinical practice. This issue needs to be addressed in patient care when enough attention has been brought to the racial factor in bone age assessment in children.

The DHA provides an up-to-date standard with which to classify normal bone growth and development in children. Currently, the DHA is accessible from the World Wide Web for online learning and teaching. Also, a computer-assisted bone age assessment system for use with the DHA has been developed and distributed to several international institutions (20) for use in a multicenter study.

Acknowledgments: We thank the National Institutes of Health for supporting this research; the Bone Development Group at the Childrens Hospital, Los Angeles, Calif, for data collection; and James Hill, MD, JD, for his assistance in the literature search and manuscript revision.

References

1. Tanner JM, Healy MJR, Goldstein H, Cameron N. Assessment of skeletal maturity and prediction of adult height (TW3 method). London, England: Saunders, 2001.
2. Kirks D. Practical pediatric imaging. In: Diagnostic radiology of infants and children. Boston, Mass: Little, Brown, 1984; 198–201.
3. Greulich WW, Pyle SI. Radiographic atlas of skeletal development of the hand and wrist. Stanford, Calif: Stanford University Press, 1959.
4. Roche AF, Roberts J, Harnill PV. Skeletal maturity of children 6–11 years: racial, geographic area and socioeconomic differentials. In: National Health Survey. Rockville, Md: Health Resources Administration, National Center for Health Statistics, 1975; 1–38.
5. Ontell FK, Ivanovic M, Ablin DS, Barlow TW. Bone age in children of diverse ethnicity. AJR Am J Roentgenol 1996;167:1395–1398.
6. Loder RT, Estle DT, Morrison K, et al. Applicability of the Greulich and Pyle skeletal age standards to black and white children of today. Am J Dis Child 1993;147:1329–1333.
7. Mora S, Boechat MI, Pietka E, Huang HK, Gilsanz V. Skeletal age determinations in children of European and African descent: applicability of the Greulich and Pyle standards. Pediatr Res 2001;50:624–628.

Figure 5

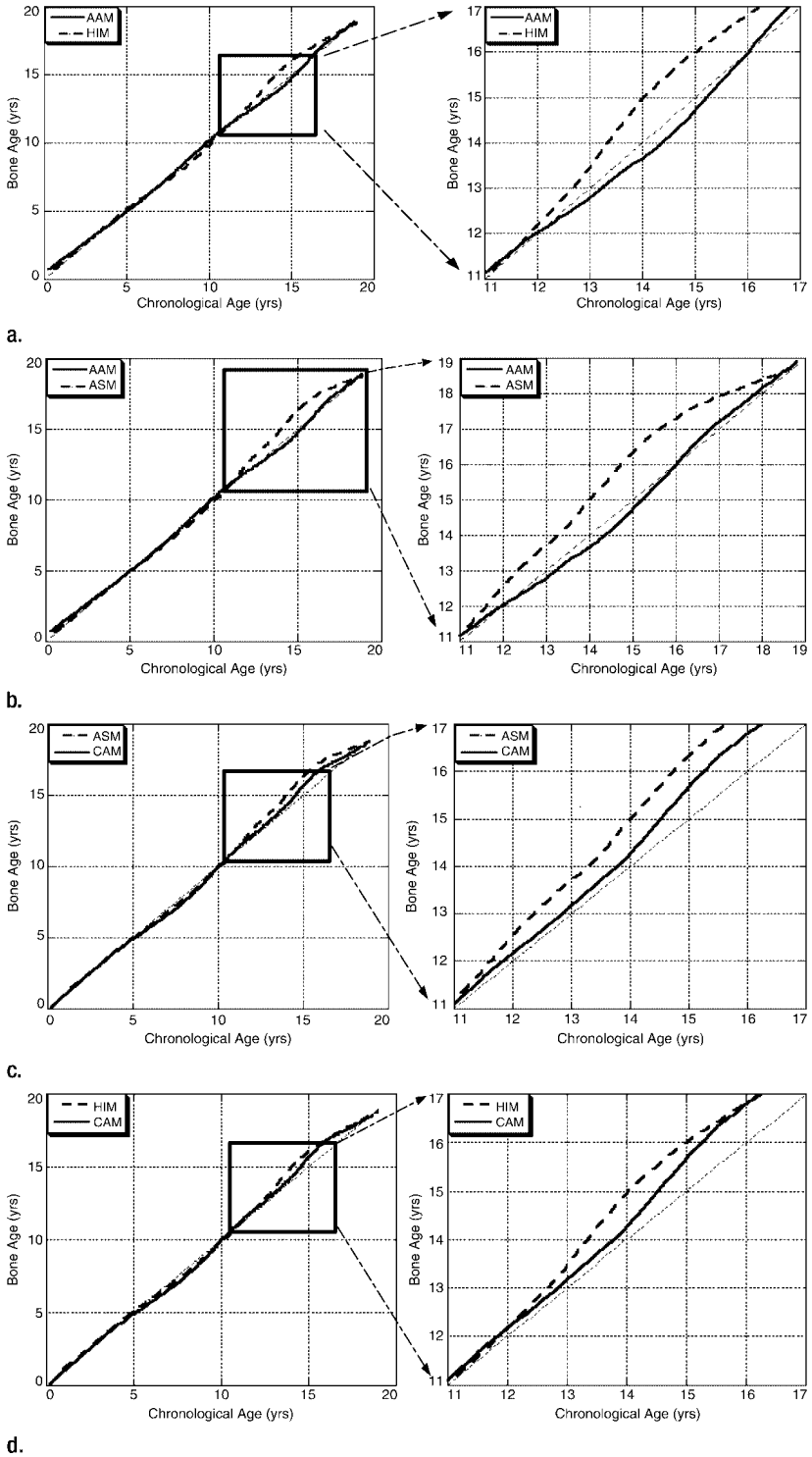

Figure 5: Comparisons (as in Fig 4) of **(a)** Hispanic *(HIM)* versus African American boys *(AAM),* **(b)** Asian *(ASM)* versus African American boys; **(c)** Asian versus white boys *(CAM);* and **(d)** Hispanic versus white boys. Left: entire age range. Right: third age subset (11–15 years) **(a, c, d)** and third and fourth age subsets (11–18 years) **(b)**.

8. Masse G, Hunt EE. Skeletal maturation of the hand and wrist in West African children. Hum Biol 1963;35:3–25.

9. Gertych A, Zhang A, Sayre J, Pospiech-Kurkowska S, Huang HK. Bone age assessment of children using a digital hand atlas. Comput Med Imaging Graph 2007;31:322–331.

10. Zhang A, Tsao S, Sayre J, Gertych A, Liu BJ, Huang HK. Is Greulich and Pyle atlas still a good reference for bone age assessment? In: Horii SC, Andriole KP, eds. Proceedings of SPIE: medical imaging 2007—PACS and imaging informatics. Vol 6516. Bellingham, Wash: International Society for Optical Engineering, 2007; 65161H.

11. Pietka E, Pospiech-Kurkowska S, Gertych A, Cao F, Huang HK. Computer-assisted bone age assessment: image analysis and fuzzy classification [abstr]. Radiology 2002;225(P):751.

12. Pietka BE, Pospiech S, Gertych A, Cao F, Huang HK, Gilsanz V. Computer automated approach to the extraction of epiphyseal regions in hand radiographs. J Digit Imaging 2001;14:165–172.

13. Zhang A, Gertych A, Liu BJ. Automatic bone age assessment for young children from newborn to 7-year-old using carpal bones. Comput Med Imaging Graph 2007;31:299–310.

14. Huang HK, Zhang A, Liu BJ, et al. Data grid for large-scale medical image archive and analysis. Proceedings of the 13th ACM International Conference on Multimedia. Singapore: Association for Computing Machinery, 2005; 1005–1013.

15. Zhang A, Gertych A, Liu BJ, Huang HK. Data mining and visualization of average images in a digital hand atlas. In: Ratib OM, Horii SC, eds. Proceedings of SPIE: medical imaging 2005—PACS and imaging informatics. Vol 5748. Bellingham, Wash: International Society for Optical Engineering, 2005; 65–72.

16. Tanner JM. Growth at adolescence. Oxford, England: Blackwell Scientific Publications, 1962.

17. Huang HK. PACS and imaging informatics: basic principles and applications. Hoboken, NJ: Wiley, 2004; 504–507.

18. Zhang A, Zhou Z, Gertych A, Liu BJ, Huang HK. Integration of bone age assessment CAD results with the PACS diagnostic workflow utilizing DICOM structure report [abstr]. In: Radiological Society of North America scientific assembly and annual meeting program. Oak Brook, Ill: Radiological Society of North America, 2006; 909.

19. Zhou Z, Liu BJ, Le AH. CAD-PACS integration tool kit based on DICOM secondary capture, structured report and IHE workflow profiles. Comput Med Imaging Graph 2007; 31:346–352.

20. Law M, Chan T, Tang FH, Lau TY, Huang HK, Zhang A. A retrospective study of bone age assessment of Chinese children in Hong Kong using a digital hand atlas [abstr]. In: Radiological Society of North America scientific assembly and annual meeting program. Oak Brook, Ill: Radiological Society of North America, 2006; 909.

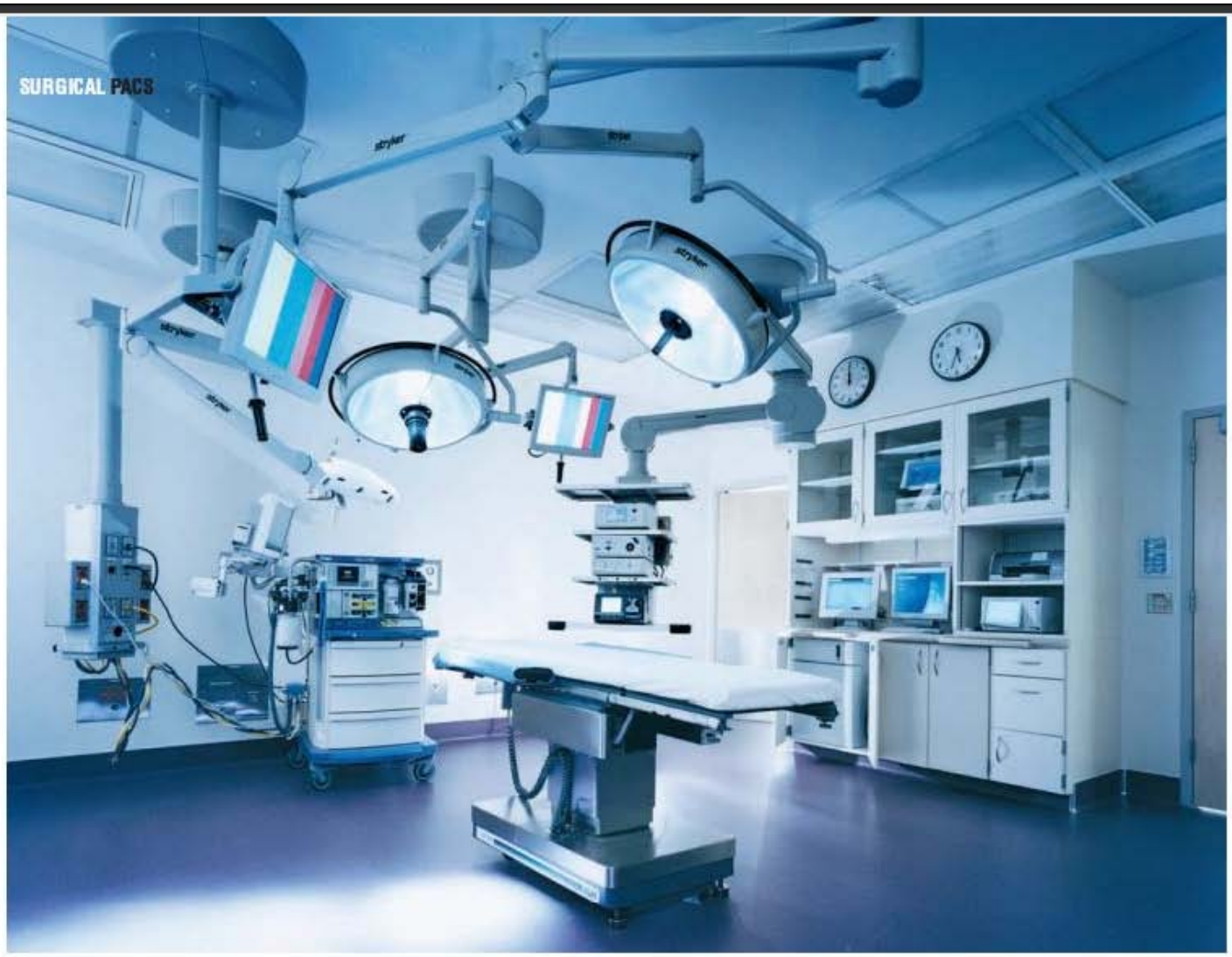

The Time for TIMMS

Enabling optimal workflow and comprehensive patient care in ORs and imaging-based interventional suites, surgical PACS can help your facility navigate complex digital infrastructures.

By Heinz U. Lemke, PhD, and Leonard Berliner, MD

A STATE-OF-THE-ART operating suite enables workflow management via data, image, information, model and tool communication. ***photo/courtesy Stryker***

Excellent patient care and efficient workflow require far more than skilled hands and savvy prioritization in the operating room (OR). Just ask any surgeon. While those elements are important, their end result is dulled without successful interchange among surgical system components.

This exchange can't occur if information and communication technology (ICT) and mechatronic systems (MTs) don't possess infrastructure and interface standards such as specialized extensions of DICOM. Enter the concept of surgical PACS (S-PACS)—more accurately termed therapy imaging and model management systems (TIMMS).

A TIMMS should support essential functions that enable and advance image-guided therapy (IGT)—and eventually, a more comprehensive form of patient-model-guided therapy.[1] Within this concept, the "image-centric worldview" of classical PACS is complemented by an IT "model-centric worldview." This worldview is founded ▸

in the special patient modeling needs of an increasing number of surgical interventions rather than the imaging-intensive mode of diagnostic radiology, for which PACS was conceptualized and developed.

OR workflow: problems and solutions

Since the OR and imaging-based interventional suites are a hospital's most cost-intensive sectors, workflow optimization is a priority for health care providers, managers and administrators. Understanding and managing workflow should become an integral part of planning and integrating complex digital infrastructures that support diagnostic and interventional procedures such as interventional radiology, minimally invasive surgery, computer-assisted surgery (CAS) and IGT.

Workflow and OR infrastructure issues include:[2]

- inefficient, ineffective and redundant processes;
- inflexible "systems" of operation;
- ergonomic deficiencies that hinder workflow;
- inadequate data (text, 1-D, 2-D, 3-D, 4-D) presentations (e.g., intraoperative and perioperative);
- soft knowledge (infomation and action strategy) presentation unavailable;
- scheduling (and tracking/radiofrequency identification) of patients, personnel, ORs and equipment not being facilitated or coordinated (often resulting in scheduling problems);
- lengthy setup times for image-guided and robotic surgery;
- lack of consistent guidelines or workflows (the hospital as a high-risk, high-velocity "production" environment isn't scripted enough, resulting in excessive behavioral diversity);
- no standardized integration of surgical devices and systems;
- lack of quantified information on workflow and error handling;
- inadequate interdisciplinary communication (for example, radiology and surgery); and
- lack of integrated and automated patient safety mechanisms and processes.

Possible solutions include:

- improving situational awareness;
- ensuring availability of real-time information regarding peri- and operative processes to respond to best practices and variances in patient care; and
- developing standard interfaces to seamlessly integrate ICT and MT systems into the OR by accounting for the special needs of imaging and modeling tools within the surgical workflow.

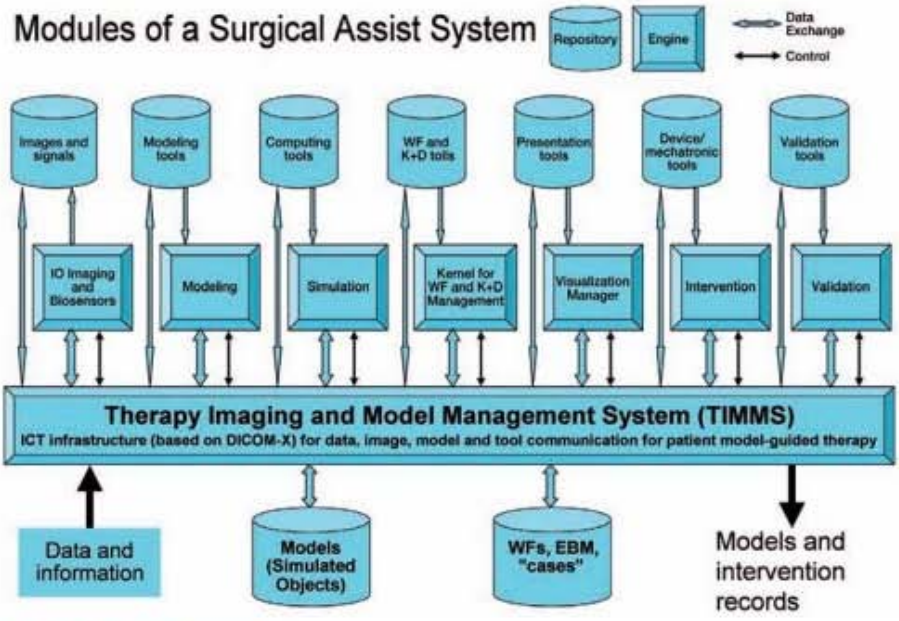

A META-ARCHITECTURE concept of a high-level SAS modular structure. ***graphic/ courtesy Dr. Lemke***

> The TIMMS approach to medical imaging extends far beyond images, integrating a wide variety of information and enabling a comprehensive, robust view of the patient, or a patient-specific model.

These potential solutions have led us to the concept of an ICT-supported OR—an S-PACS or TIMMS. This system provides the ICT-based infrastructure necessary for surgical/interventional workflow management of the modern digital operation room (DOR). A TIMMS infrastructure—based, for example, on a suitable DICOM extension—is geared toward significantly improving patient care as well as ergonomic and health-economic progress in the OR through data, image, information, model and tool communication.

Taking into account modern software engineering principles such as service-oriented architecture (SOA), a properly designed TIMMS will clarify the correct position of interfaces and relevant standards for a surgical assist system (SAS). Several research and development (R&D) institutions are designing and implementing these systems.

TIMMS components

Engineering ICT systems for surgery encompasses the specification, design, implementation and testing of CAS or IGT systems. System components developed in academic and industrial settings are applied across surgical disciplines. In most cases, however, they're standalone systems with specific ad hoc propriety or vendor interfaces—"islands" of IT technologies with varying degrees of modularization and interconnection.

The figure above illustrates a meta-architecture concept of a high-level SAS modular structure. The high-level modules are abstracted from specific, recently developed CAS/IGT systems. Most R&D and commercial SAS systems are limited to proprietary implementations of some of these functionalities. The TIMMS "kernel for workflow and knowledge and decision ▸

management" provides strategic intelligence for preoperative planning and intraoperative execution. Often, this module (or parts of it) is integrated into other engines.

Modular, scalable and distributable TIMMS components act synergistically to provide functionality and utility that exceed the sum of their parts. These components include:

- seven "engines"—or software modules that can be executed on an appropriate computing machine—that work independently and dependently to account for all facets of complex medical and surgical procedures. (The engines are intraoperative imaging and biosensors; modeling; simulation; kernel for workflow and knowledge and decision management; visualization representation management; intervention; and validation engines.);
- associated repositories—integrated hardware and software structure that stores and makes available data and/or data processing tools—linked to each of the seven engines; and
- additional repositories, including models (defined as simulated objects and potentially representing patient-specific information, implants, etc.) and references such as workflow models, evidence-based medical data and case-based medical data.

During surgery, the system enables real-time data mining from these repositories. The workflow and knowledge and decision management engine is the central computing kernel or "brain." It may use different forms of logic, database structuring, adaptable software agents and other forms of intelligence, depending on the procedure and its applications. Adaptable software agents are software modules that contain some form of artificial intelligence—which, with some autonomy and adaptability, can perform essential functions.

An ICT infrastructure enables intercommunication and interactivity among all TIMMS or S-PACS components. The engines, tools, repositories, ICT infrastructure and data sources—including the operative team—are linked through a distributed network, providing full functionality of TIMMS, including planning, guidance, learning, and data mining and processing.

Patient-specific model

The traditional imaging approach applied to patient care's clinical aspects—known as the "image-centric worldview"—has been limited to the images themselves. The model-centric worldview approach of TIMMS, however, extends far beyond images: A wide variety of patient information can be integrated with the images, making all relevant data available for surgical interventions and enabling a comprehensive, robust view of the patient, or a patient-specific model.[3]

Standards relating to medical imaging and communication for non-real-time diagnostic and related activities are an integral part of TIMMS and well-defined by DICOM. Most of the image and presentation states' information object definitions (IODs) defined in DICOM are also relevant to surgery. Until now, models haven't been considered extensively in DICOM, aside from work done in DICOM WG 07, WG 17 and WG 22. However, surgical modeling and simulation are key SAS functions. Interfacing of tools that support these functions is a relatively new scope for DICOM (DICOM Working Group 24, which issued the report "DICOM in Surgery," is addressing this issue). Therefore, in addition to defining mechanisms to enable real-time communication, standardization efforts will need to create an agreed-upon list of relevant models for DICOM IODs (see box).

> Modular, scalable and distributable TIMMS components act synergistically to provide functionality and utility that exceed the sum of their parts.

By extension

TIMMS provides a process for a comprehensive SAS, combing and integrating all necessary information and communication technology—workflow analysis, data processing and synthesis, interactive interfaces between surgeon and mechatronic devices, and adaptable software agents—to provide comprehensive assistance and guidance through complex procedures such as image- and model-guided surgeries. TIMMS fulfills the concept of extending diagnostic radiological PACS to surgical PACS, accounting for the OR's fundamentally different workflow requirements. ■

EXAMPLES OF MODELING TOOLS AND ASPECTS

Derived from a wide variety of surgical workflows, these DICOM IOD modules and services are under consideration for future use:

- geometric modeling, including volume and surface representations
- properties of cells and tissue
- segmentation and reconstruction
- biomechanics and damage
- tissue growth
- tissue shift
- prosthesis modeling
- fabrication model for custom prosthesis
- properties of biomaterials
- atlas-based anatomic modeling
- template modeling
- finite element models (FEMs) of medical devices and anatomic tissue
- collision response strategies for constraint deformable objects
- variety of virtual human models
- lifelike physiology and anatomy
- modeling of the biologic continuum
- animated models
- multiscale modeling
- fusion/integration of data/images
- registration between different models, including patient, equipment and OR
- workflow modeling
- real-time, intraoperative imaging and accompanying patient-specific information

References

1. Lemke, H.U., & Vannier, M.W. (2006). The operating room and the need for an IT infrastructure and standards. *International Journal of CARS, Springer*, 1(3).

2. Pentacost, M. (2004). Review of the operating room of the future, OR-2020, UCLA Seminar on Imaging and Informatics, Oct. 4-6.

3. Lemke, H.U., & Berliner, L. (2008). *Model-guided therapy, patient specific model and model-based therapy.* Health Academy, Dresden (in German).

Heinz U. Lemke, PhD, is research professor of radiology at the University of Southern California, Los Angeles, and Leonard Berliner, MD, is chief of interventional radiology at New York Methodist Hospital, Brooklyn, N.Y.

Int J Colorectal Dis (2008) 23:493–497
DOI 10.1007/s00384-007-0432-6

ORIGINAL ARTICLE

Fecal incontinence among morbid obese women seeking for weight loss surgery: an underappreciated association with adverse impact on quality of life

Nir Wasserberg · Mark Haney · Patrizio Petrone · Peter Crookes · Jason Rosca · Manfred Ritter · Howard S. Kaufman

Accepted: 13 December 2007 / Published online: 29 January 2008

Abstract
Purpose Morbid obesity is associated with urinary incontinence (UI). The study purpose was to determine the prevalence of fecal incontinence (FI), its associated risk factors, and its impact on quality of life (QOL) in morbidly obese women.
Materials and methods A questionnaire-based study on morbidly obese women [body mass index (BMI)≥35 m/kg^2], attending a bariatric surgery seminar, was conducted. Data included demographics, past medical, surgical and obstetric history, and obesity-related co-morbidities. Patients who reported of FI, completed the Cleveland Clinic Foundation Fecal Incontinence scale (CCF-FI) and the Fecal Incontinence Quality of Life scale (FIQL).
Results Participants included 256 women [median age 45 years (19–70)] and mean BMI of 49.3±9.4 m/kg^2. FI was reported in 63%. History of obstetric injury (OR: 2.4, 95% CI: 1.33–4.3; $p<0.001$) and UI (OR: 1.2, 95% CI: 1.1–1.4; $p<0.001$) were significantly associated with FI. There was no association with age, BMI, parity, and presence of diabetes or hypertension. Median CCF-FI score was 7 (1–20); 34.5% scored ≥10. Incontinence for gas was the most frequent type (87%) of FI, followed by incontinence for liquids (80%), which also had the highest impact on QOL ($p<0.01$). Mean FIQL scores were >3 for all four domains studied. CCF-FI scores were significantly correlated with FIQL scores in all domains ($p=0.02$).
Comment The prevalence of FI among morbidly obese women may be much higher than the rates reported in the general population. FI has adverse effects on QOL. Its correlation with UI suggests that morbid obesity may pose a risk of global pelvic floor dysfunction.

Keywords Fecal incontinence · Morbid obesity · Urinary incontinence · Quality of life

N. Wasserberg · M. Haney · P. Petrone · P. Crookes · J. Rosca · M. Ritter · H. S. Kaufman
Division of Colorectal and Pelvic Floor Surgery,
Department of Surgery, Keck School of Medicine,
University of Southern California,
Los Angeles, CA 90033, USA

N. Wasserberg (✉)
Department of Surgery B, Rabin Medical Center,
Beilinson Campus,
Petah Tiqwa 49100, Israel
e-mail: nwasserberg@gmail.com

Introduction

Incontinence for flatus or liquid or solid stool is a disturbing condition with an immense physical, psychological, and social impact on the patient's quality of life [1]. Estimated rates of fecal incontinence (FI) in the general population range from 4% to 19%; the wide variation is attributed to patient's reluctance to report the symptom, and to the physician's reluctance to inquire about it [1, 2]. FI is caused by multiple mechanisms, including impaired rectal capacity, changes in stool consistency, pelvic floor abnormalities, and anal sphincter dysfunction [3], all of which are greatly affected by age and gender [4]. The prevalence is higher in women than men, probably because of obstetric factors such as pregnancy, multiparity, and obstetrical injuries [5–7].

Morbid obesity is significantly associated with co-morbidities that impair general health and interfere with basic activities of daily living [8]. Among these, urinary incontinence (UI) of all types has been related to excessive weight in many studies [9, 10]. The possible mechanisms

that underlie the contribution of central obesity to UI include chronically increased intra-abdominal pressure [11] and obesity-related nerve conduction abnormalities and intervertebral disc herniation [12].

Data on the association between obesity and FI, however, are still limited, although correlational evidence is emerging. In a Canadian population-based epidemiology study, Alnaif and Drutz [13] noted that FI was associated with urinary stress incontinence and greater body weight in young women. Similar findings were reported in a recent study of morbidly obese women [14].

The objective of the present study was to determine the prevalence of FI in morbidly obese women and its impact on quality of life. We also sought to evaluate the influence of other contributory risk factors on the severity of fecal incontinence.

Materials and methods

Morbidly obese women, defined as having a body mass index (BMI)≥35 m/kg^2, who were attending seminars at the University of Southern California Bariatric Surgery Program to seek information on surgical weight loss between October 2003 and April 2005 were asked to participate in the study. All completed a questionnaire on demographics (age, weight, height) and past medical, surgical, and obstetric history. Participants were then questioned particularly about the presence of other obesity-related comorbidities, including diabetes mellitus and hypertension. The presence of UI was determined by the response to the question: "Have you experienced any involuntary urine leakage in the last three months?" The presence of FI was determined by the question: "Have you experienced any accidental leakage of stool or gas in the last 3 months?"

Participants who responded "No" to the last question were defined as not having FI symptoms and included in the No FI group. Participants who responded positively were included in the FI group and were requested to complete the Cleveland Clinic Foundation Fecal Incontinence score (CCF-FI) [3] and the Fecal Incontinence Quality of Life scale (FIQL) [15]. These instruments have been validated for the evaluation of the severity of FI symptoms and estimation of its effect on lifestyle, coping behavior, depression, and embarrassment. Women with a BMI smaller than 35 kg/m^2, history of chronic diarrhea, inflammatory bowel disease, major non-obstetric anal sphincter trauma, paraplegia/paresis, or previous (non-obstetric) anorectal surgery (other than hemorrhoidectomy) were excluded. Because the FIQL includes items on depression, women who were previously treated for depression were excluded as well. The study protocol was approved by the Institutional Review Board.

Statistical analysis

The chi-square test was used to analyze differences in categorical variables between the groups, and analysis of variance, for continuous variables. Variables for which differences had a p value of <0.2 were entered into a multiple logistic regression model. Quality of life correlations were estimated using the Pearson correlation coefficient. A value of $p<0.5$ was considered significant.

Results

Of the 285 women who completed the questionnaires, 31 were excluded (four with depression), for a final sample of 256. Median age was 45 years (range 19–70 years) and mean BMI was 49.3±9.4 kg/m^2. One hundred sixty-two women (63%) responded positively to the question on FI. Of these, five had a surgical history of hemorrhoids, one of cystocele repair, and two of hysterectomy.

The background characteristics of the patients with and without FI are shown in Table 1. There were no differences between the groups in age distribution, weight, or BMI. Univariate analysis revealed that history of complicated

Table 1 Risk factors associated with fecal incontinence—univariate analysis

Variable	No FI	FI	p value
Number (%)	97 (37)	162 (63)	–
Age (median, range)	49 (19–67)	45 (23–70)	0.9
Weight (lb) (mean ± SD)	301.1±62	291±56	0.2
BMI (kg/m^2) (mean ± SD)	49.9±9.7	49.3±9.4	0.6
History of diabetes mellitus (%)	21 (21)	56 (34)	0.03
History of hypertension (%)	31 (32)	68 (42)	0.14
History of IBS (%)	8 (8)	23 (14)	0.2
History of urinary incontinence (%)	65 (67)	147 (89)	<0.001
>1 vaginal delivery (%)	13 (13)	20 (12)	0.9
History of complicated delivery (%)	19 (19)	60 (37)	<0.01

delivery (obstetric injury and/or instrumental delivery) and UI were the only risk factors associated with fecal incontinence ($p<0.01$ and $p<0.001$, respectively; Table 1). On multiple regression analyses, history of complicated delivery (OR: 2.4, 95% CI: 1.33–4.3; $p<0.001$) and UI (OR: 1. 2, 95% CI: 1.1–1.4, $p<0.001$) remained statistically significant. None of the other factors studied (age, high BMI, multiparity, diabetes, hypertension, and history of irritable bowel syndrome) was significantly associated with fecal incontinence (Table 2). Eighty-nine percent of the women with any type of FI also reported UI (double incontinence).

Median score on the CCF-FI was 7 (range 1–20); 34.5% of the morbidly obese women had a score of ≥10, and 10% had a score of ≥15.

The frequency of the various FI symptoms is shown in Fig. 1. Of women reporting any FI, incontinence for gas was the most frequent type (87%), followed by incontinence for liquids (80%). Only 19% had incontinence for solid stool, and none of them reported experiencing it on a daily basis.

Mean scores on the FIQL by domain were as follows: embarrassment, 3.4±0.8; depression, 3.5±0.8; coping, 3.2±0.8; and lifestyle, 3.5±0.7 (Fig. 2). Correlation analysis of type of incontinence with total CCF-FI score and with scores on each of the FIQL domains revealed that a high score on the CCF-FI was significantly correlated with a high score on the FIQL in all domains ($p=0.02$). Incontinence for liquid stools had the greatest impact upon quality of life ($p<0.01$). Flatal incontinence significantly correlated only with embarrassment and depression ($p<0.04$ and $p<0.02$, respectively). There was no correlation of solid stool incontinence with any of the FIQL domains.

Discussion

The increased adiposity, inflammatory response, and direct mass effect of obesity can lead to hypertension, diabetes mellitus, sleep apnea, and musculoskeletal disease [16]. Although the association of obesity with UI has been well described [9, 12], its role in FI is less clear. In the present study, 63% of the obese women had fecal incontinence,

Table 2 Risk factors associated with fecal incontinence—multivariate analysis

Variable	OR	95% CI	*p* value
Weight	–	–	0.3
History of diabetes mellitus	–	–	0.1
History of hypertension	–	–	0.25
History of IBS	–	–	0.17
History of urinary incontinence	1.2	1.1–1.4	<0.001
History of complicated delivery	2.4	1.33–4.3	<0.001

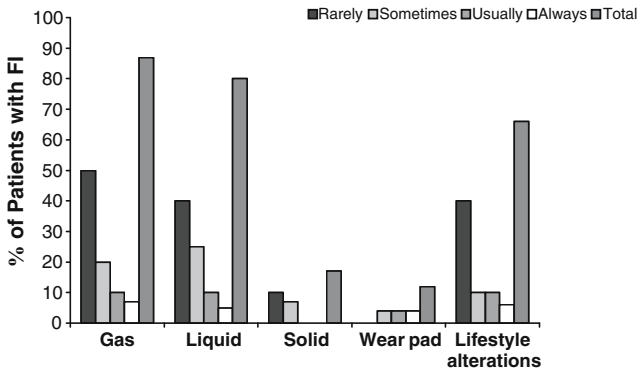

Fig. 1 Frequency of symptoms based upon Cleveland Clinic Foundation Fecal Incontinence score (CCF-FI)

which is a much higher rate than the 4–19% rate reported in the general population [17]. These results are in agreement with other publications [13, 14, 18]. Abramov et al. [19], to control for genetic variance, asked 271 identical twin sister pairs to complete the validated Colorectal Anal Distress Inventory questionnaire. A significant detrimental effect of obesity (BMI>30) was noted (mean difference, 5.18; $p=0.007$). The etiology of FI in obese subjects is likely multifactorial [20]. Chronically increased abdominal pressure due to the excess weight may cause pudendal nerve injury and damage to the pelvic musculature. Furthermore, other obesity-related conditions, such as diabetic neuropathy and intervertebral disc herniation, may contribute to pelvic floor dysfunction [12]. This assumption is supported by studies demonstrating an association between weight loss and alleviation of symptoms of pelvic floor dysfunction [21, 22].

We found a significant association with urinary and fecal incontinence in 89% of the patients. In a recent study by Meschia et al. [23], FI was reported in 20% of patients presenting with UI and pelvic organ prolapse. Others reported a correlation among disorders of pelvic support and individual pelvic floor problems [24, 25]. Because FI and UI share many causative factors, including neurological disorders, aging, and

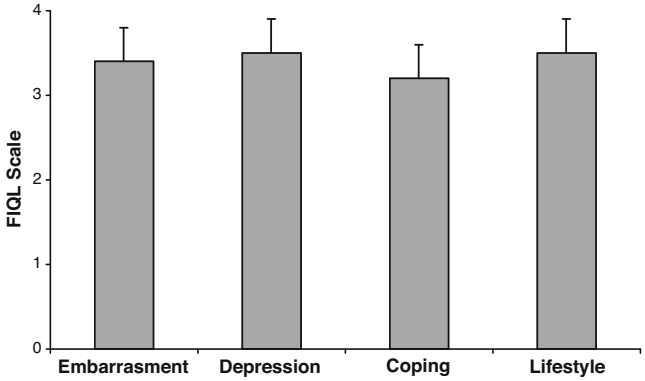

Fig. 2 Mean scores on Fecal Incontinence Quality of Life Scale (FIQL) by domain

obstetric trauma, it is conceivable that they may often co-exist. Our findings suggest that clinicians take a global pelvic floor approach to these cases instead of a segmented one that compartmentalizes pelvic anatomy and function.

Interestingly, increased BMI was not identified as a risk factor for fecal incontinence in the present study. Although one previous study noted an association of increased BMI with severity of UI [26], it was not confirmed in a more recent analysis of obese women [14]. The latter authors suggested the possibility of a threshold effect, wherein there is no symptomatic contribution of a BMI that is greater than 40. Although we based our study on the validated CCF-FI, this scale may be insufficiently sensitive to identify symptoms of FI in morbidly obese women whose BMI exceeds 40 kg/m^2.

Obstetric injury and difficult delivery are well-described risk factors for fecal incontinence [5–7]. It is not surprising, therefore, that history of complicated delivery was strongly correlated with FI in our sample. However, it is possible that the category of complicated delivery included obstetric injuries, instrumental deliveries, and high birth weight of vaginally delivered infants, all factors with higher than normal rates in morbidly obese women.

The degree of FI is based on type (solid liquid or gas), frequency, and duration. According to the severity of symptoms, FI can be classified as major or minor incontinence. Major FI is the involuntary loss of stool, and minor incontinence consists of the loss of control of gas or occasional liquid soiling [3]. However, while minor seepage of liquid stool, or occasional involuntary gas leek may not bother an 80-year-old sedentary reclusive patient, it may be devastating for a young corporate executive. Consequently, the CCF-FI includes items of lifestyle alterations. Sixty-three percent of the participants in the current study responded positively to the index question on anal incontinence of any nature. The median CCF-FI score was 7 (range 1–20) suggesting that most of the participants should be categorized as having minor FI. However, the score was greater than 10 in 34.5% and greater than 15 in 10% of the women, indicating more frequent symptoms with greater impact on lifestyle. The most frequent type of incontinence was flatal incontinence, found in 87% of affected patients. Incontinence for gas significantly contributed to embarrassment and depression. However, these findings may be limited, because the FIQL has not been validated for flatal incontinence [15, 27]. Incontinence for liquid stool, found in 80% of our patients, significantly correlated with the FIQL scores in all measured domains. These results indicate a significant impact of FI on quality of life. Although some previous studies reported a correlation between obesity and anal incontinence, ours is the first to distinguish among types of incontinence and to describe their impact on quality of life. Boreham et al. [27] reported that 25.6% of women presenting for gynecologic care have incontinence for gas, and 12.9% have incontinence for liquids. They, too, found that liquid incontinence had the greater impact on quality of life.

It is noteworthy that our cohort was limited to symptomatic obese patients seeking surgical weight reduction, so that our findings may not be generalizable to the entire population of morbidly obese patients. This study calls attention to the high incidence of FI and its negative impact on quality of life among a specific obese population. Further studies are needed to establish the degree of FI in the general obese population. The association of FI with UI suggests that morbid obesity may pose a still unrecognized risk of global pelvic floor dysfunction that merits additional research.

References

1. Johanson JF, Lafferty J (1996) Epidemiology of fecal incontinence: the silent affliction. Am J Gastroenterol 91(1):33–36
2. Giebel GD, Lefering R, Troidl H, Blochl H (1998) Prevalence of fecal incontinence: what can be expected? Int J Colorectal Dis 13 (2):73–77
3. Jorge JM, Wexner SD (1993) Etiology and management of fecal incontinence. Dis Colon Rectum 36(1):77–97
4. Nelson R, Norton N, Cautley E, Furner S (1995) Community-based prevalence of anal incontinence. JAMA 274(7):559–561
5. Lal M, H Mann C, Callender R, Radley S (2003) Does cesarean delivery prevent anal incontinence? Obstet Gynecol 101(2):305–312
6. Zetterstrom J, Lopez A, Anzen B, Norman M, Holmstrom B, Mellgren A (1999) Anal sphincter tears at vaginal delivery: risk factors and clinical outcome of primary repair. Obstet Gynecol 94 (1):21–28
7. Richter HE, Brumfield CG, Cliver SP, Burgio KL, Neely CL, Varner RE (2002) Risk factors associated with anal sphincter injury: a comparison of primiparous patients, vaginal births after cesarean deliveries, and patients with previous vaginal delivery. Am J Obstet Gynecol 187(5):1194–1198
8. Han TS, Tijhuis MA, Lean ME, Seidell JC (1998) Quality of life in relation to overweight and body fat distribution. Am J Public Health 88(12):1814–1820
9. Elia G, Dye TD, Scariati PD (2001) Body mass index and urinary symptoms in women. Int Urogynecol J Pelvic Floor Dysfunct 12 (6):366–369
10. Dwyer PL, Lee ET, Hay DM (1988) Obesity and urinary incontinence in women. Br J Obstet Gynaecol 95(1):91–96
11. Sugerman H, Windsor A, Bessos M, Wolfe L (1997) Intra-abdominal pressure, sagittal abdominal diameter and obesity comorbidity. J Intern Med 241(1):71–79
12. Cummings JM, Rodning CB (2000) Urinary stress incontinence among obese women: review of pathophysiology therapy. Int Urogynecol J Pelvic Floor Dysfunct 11(1):41–44
13. Alnaif B, Drutz HP (2001) The prevalence of urinary and fecal incontinence in Canadian secondary school teenage girls: questionnaire study and review of the literature. Int Urogynecol J Pelvic Floor Dysfunct 12(2):134–137
14. Richter HE, Burgio KL, Clements RH, Goode PS, Redden DT, Varner RE (2005) Urinary and anal incontinence in morbidly obese women considering weight loss surgery. Obstet Gynecol 106(6):1272–1277
15. Rockwood TH, Church JM, Fleshman JW, Kane RL, Mavrantonis C, Thorson AG, Wexner SD, Bliss D, Lowry AC (2000) Fecal

Incontinence Quality of Life Scale: quality of life instrument for patients with fecal incontinence. Dis Colon Rectum 43(1):9–16
16. Pender JR, Pories WJ (2005) Epidemiology of obesity in the United States. Gastroenterol Clin North Am 34(1):1–7
17. Johanson JF, Lafferty J (1996) Epidemiology of fecal incontinence: the silent affliction. Am J Gastroenterol 91(1):33–36
18. Kapoor DS, Davila GW, Rosenthal RJ, Ghoniem GM (2004) Pelvic floor dysfunction in morbidly obese women: pilot study. Obes Res 12(7):1104–1107
19. Abramov Y, Sand PK, Botros SM, Gandhi S, Miller JJ, Nickolov A, Goldberg RP (2005) Risk factors for female anal incontinence: new insight through the Evanston-Northwestern twin sisters' study. Obstet Gynecol 106(4):726–732
20. Bharucha AE, Fletcher JG, Harper CM, Hough D, Daube JR, Stevens C, Seide B, Riederer SJ, Zinsmeister AR (2005) Relationship between symptoms and disordered continence mechanisms in women with idiopathic faecal incontinence. Gut 54(4):546–555
21. Sugerman H, Windsor A, Bessos M, Kellum J, Reines H, DeMaria E (1998) Effects of surgically induced weight loss on urinary bladder pressure, sagittal abdominal diameter and obesity co-morbidity. Int J Obes Relat Metab Disord 22(3):230–235
22. Bump RC, Sugerman HJ, Fantl JA, McClish DK (1992) Obesity and lower urinary tract function in women: effect of surgically induced weight loss. Am J Obstet Gynecol 167(2):392–399
23. Meschia M, Buonaguidi A, Pifarotti P, Somigliana E, Spennacchio M, Amicarelli F (2002) Prevalence of anal incontinence in women with symptoms of urinary incontinence and genital prolapse. Obstet Gynecol 100(4):719–723
24. Jackson SL, Weber AM, Hull TL, Mitchinson AR, Walters MD (1997) Fecal incontinence in women with urinary incontinence and pelvic organ prolapse. Obstet Gynecol 89(3):423–427
25. Klingele CJ, Bharucha AE, Fletcher JG, Gebhart JB, Riederer SG, Zinsmeister AR (2005) Pelvic organ prolapse in defecatory disorders. Obstet Gynecol 106(2):315–320
26. Melville JL, Katon W, Delaney K, Newton K (2005) Urinary incontinence in US women: A population-based study. Arch Intern Med 165(5):537–542
27. Boreham MK, Richter HE, Kenton KS, Nager CW, Gregory WT, Aronson MP, Vogt VY, McIntire DD, Schaffer JI (2005) Anal incontinence in women presenting for gynecologic care: prevalence, risk factors, and impact upon quality of life. Am J Obstet Gynecol 192(5):1637–1642

Effect of Surgically Induced Weight Loss on Pelvic Floor Disorders in Morbidly Obese Women

Nir Wasserberg, MD, Patrizio Petrone, MD,* Mark Haney, MD,* Peter F. Crookes, MD,† and Howard S. Kaufman, MD, MBA*†*

Objective: To evaluate the effect of surgically induced weight loss on pelvic floor disorders (PFD) in morbidly obese women.

Summary Background Data: Although bariatric surgery may lead to the improvement of some obesity-related comorbidities, the resolution of global PFD has not been well described.

Methods: Women with a body mass index (BMI) of 35 kg/m^2 or more who were considering bariatric surgery were asked to complete 2 validated condition-specific questionnaires assessing the distress/quality of life impact of PFD, total and by domain (pelvic organ prolapse, colorectal-anal, and urogenital). Women who achieved a ≥50% excess body weight loss after surgery were asked to complete the same questionnaires for comparison.

Results: Of the 178 women who underwent surgery, 46 completed the postoperative questionnaires. Mean age of this group was 45 years (range, 20–67), and mean preoperative BMI was 45 kg/m^2 (range, 35–75). The prevalence of PFD symptoms improved from 87% before surgery to 65% after surgery (P = 0.02, 95% CI: 0.05%–53%). There was a significant reduction in total mean distress scores after surgery (P = 0.015, 95% CI: 3.3–32.9), which was attributed mainly to the significant decrease in urinary symptoms (P = 0.0002, 95% CI: 8.2–22.7). Reductions in the scores were noted for the other PFD domains as well. Quality of life total scores improved (P = 0.002, 95% CI: 4.8–27.1), as did scores in the urinary domain (P = 0.0005, 95% CI: 3.8–13.5) and the pelvic organ prolapse domain (P = 0.015, 95% CI: 0.6–9.5). Age, parity, history of complicated delivery, percent excess body weight loss, BMI, type of weight loss procedure and presence of diabetes mellitus and hypertension had no predictive value for postoperative outcomes.

Conclusion: Surgically induced weight loss has a beneficial effect on symptoms of PFD in morbidly obese women.

(*Ann Surg* 2009;249: 72–76)

More than 50% of all women in the United States are overweight (body mass index (BMI) greater than 25 kg/m^2) or obese (BMI greater than 30 kg/m^2),[1] and the prevalence of obesity is increasing by 6% yearly.[2] Morbid obesity is a well-described risk factor for urinary incontinence.[3] Pelvic floor disorders (PFDs) include a number of conditions besides urinary incontinence (and obstruction), such as anorectal dysfunction including fecal incontinence and constipation, pelvic organ prolapse (POP), chronic pelvic pain, and sexual dysfunction. Recent publications also report a strong correlation between morbid obesity and other types of pelvic floor disorders,[4–7] namely fecal incontinence[8,9] and POP.[4] Given that many patients affected by PFDs have more than one pelvic floor problem, the pelvic floor might be regarded as a global anatomic and physiological unit.[10,11]

The pathophysiology underlying the contribution of obesity to pelvic floor dysfunction is probably multifactorial, related to the increase in intra-abdominal pressure, and other obesity-related conditions such as nerve-conduction abnormalities, diabetes, and intervertebral disc herniation.[12] The finding of a significant relationship between BMI and intra-abdominal pressure[13] suggested that overweight may stress the pelvic floor secondary to a chronic state of elevated pressure. Previous data showed that the increase in intra-abdominal pressure is proportional to the increase in sagittal abdominal diameter and that decreasing the abdominal diameter by surgically induced weight loss also reduces the intra-abdominal and urinary bladder pressures.[14]

The finding that surgically induced weight loss can result in a dramatic improvement in obesity-associated comorbidities, such as diabetes and hypertension,[15] has led to the assumption that because weight is a modifiable risk factor for incontinence, weight reduction may be an effective treatment for loss of bowel and urinary control. This hypothesis has been supported by studies showing a significant reduction in urinary incontinence in women after weight loss surgery.[16,17] In addition, in a prospective study of incontinent obese women on a dietary weight-loss program, Subak et al reported a 50% reduction in incontinence frequency after only a 5% decrease in weight.[18] Others demonstrated an improvement in both stress and urge urinary incontinence after both surgical and nonsurgical weight reduction in moderately and morbidly obese women.[13,16–19] The objective of the present study was to evaluate the effect of surgically induced weight loss on global pelvic floor dysfunction in morbidly obese women.

PATIENTS AND METHODS

The study group included women with a BMI of ≥35 kg/m^2 attending the University of Southern California Bariatric Surgery Program from December 2003 to December 2005 for information on potential weight-loss surgery. All were asked to sign an informed consent and to complete 2 validated questionnaires of pelvic floor dysfunction in addition to a survey including questions on demographics and pertinent medical, surgical, and obstetric history. Patients who underwent bariatric surgery were followed at the outpatient clinic.

The patients who underwent surgery during the study period and achieved a ≥50% excess body weight loss (EBWL) postoperatively were asked to complete the same questionnaires and to return them either by post or during a clinic follow-up visit. The study was approved by the Institutional Review Board of the University of Southern California.

Instruments

For the present study, we used the pelvic floor distress inventory (PFDI-20) and the pelvic floor impact (PFIQ-7) questionnaires,[20] both validated short forms of 2 PDF-specific questionnaires on the distress caused by PDF and its adverse impact on quality of life. Three main domains are assessed: pelvic organ prolapse, colorectal-anal, and urogenital. The PFDI-20 includes 20 questions

From the *Division of Colorectal and Pelvic Floor Surgery and †Bariatric Surgery Program, Department of Surgery, Keck School of Medicine, University of Southern California, Los Angeles, California.

Reprints: Nir Wasserberg, MD, Department of Surgery B, Rabin Medical Center, Beilinson Campus, Petah Tiqwa 49100, Israel. E-mail: nwasserberg@gmail.com.

ISSN: 0003-4932/09/24901-0072
DOI: 10.1097/SLA.0b013e31818c7082

regarding subjective feelings of pelvic heaviness and pelvic organ prolapse, urinary incontinence and obstruction, fecal incontinence and obstruction, pain, and the need to manually assist with elimination of urine and/or stool. If any symptoms are present, respondents are asked to rate the "bother" associated with each symptom as "not at all, somewhat, moderately, or quite a bit." The same scales are used in the PFIQ-7 (Fig. 1), which asks the respondent to rate the impact of bladder, bowel, and vaginal/pelvic symptoms on acts of daily living, physical activity, and emotional well-being, The 3 domains of the PFDI-20 assessment are: pelvic organ prolapse distress inventory, colorectal-anal distress inventory, and urogenital distress inventory. The PFIQ-7 output domains are pelvic organ prolapse impact questionnaire, colorectal-anal impact questionnaire, and incontinence impact questionnaire. Possible scores for each domain range from 1 to 100, with higher scores indicating more severe symptoms. Both instruments are designed to detect initial prevalence and treatment outcome.

Statistical Analysis

Variables are presented as mean ± SD. The preoperative and postoperative scores were compared by paired 2-tailed Student *t* test and χ^2 was used to compare proportions. Analysis of variance was used for multiple comparisons. Pearson correlation, Student *t* test, Mann-Whitney *U* test, and χ^2, were used, as appropriate, to correlate clinical data with postoperative outcome. A *P* value of ≤ 0.05 was considered statistically significant.

RESULTS

Of the 400 female patients who filled the initial questionnaires during the study period, 178 underwent weight-reduction surgery by surgical faculty of the USC Bariatric Surgery Program. Of these, 82 achieved ≥50% EBWL during follow-up of 18.6 months (range, 6–34 months) and 46 (56%) patients agreed to repeat the questionnaires. Weight loss procedures for these patients included the duodenal switch (DS) (n = 22), Roux-en-Y gastric bypass (n = 21), and sleeve gastrectomy (SG) (n = 3). Their preoperative and postoperative characteristics are shown in Table 1.

At evaluation on entry to the program, 87% of the patients were found to have various degrees of PFDs. There was a statistically significant correlation between the self-reported distress caused by the PFD and the adverse impact on quality of life, both by domain and by total scores ($r = 0.35$, $P = 0.015$). The prevalence of any PFD symptom decreased significantly from 87% before surgery to 65% after surgery ($P = 0.02$). The decrease in the prevalence of PFD symptoms was mainly attributed to a significant reduction in the prevalence of urinary symptoms from 71% before surgery to 39% after surgery ($P = 0.003$). There was also a trend toward reductions in the prevalence of pelvic organ prolapse and colorectal symptoms that did not reach statistical significance (Table 2).

Pre and postoperative scores for the PFDI-20 and PFIQ-7 are shown in Figures 2 and 3, respectively. The total distress and urinary

Instructions: Some women find that bladder, bowel or vaginal symptoms affect their activities, relationships, and feelings. For each question, place an **X** in the response that best describes how much your activities, relationships or feelings have been affected by your bladder, bowel or vaginal symptoms or conditions **over the last 3 months**. Please be sure to mark an answer in **all 3 columns** for each question. Thank you for your cooperation.

How do symptoms or conditions related to the following usually affect your ↓ →→→→	*Bladder or urine*	*Bowel or rectum*	*Vagina or Pelvis*
1. ability to do household chores (cooking, housecleaning, laundry)?	☐ Not at all ☐ Somewhat ☐ Moderately ☐ Quite a bit	☐ Not at all ☐ Somewhat ☐ Moderately ☐ Quite a bit	☐ Not at all ☐ Somewhat ☐ Moderately ☐ Quite a bit
2. ability to do physical activities such as walking, swimming, or other exercise?	☐ Not at all ☐ Somewhat ☐ Moderately ☐ Quite a bit	☐ Not at all ☐ Somewhat ☐ Moderately ☐ Quite a bit	☐ Not at all ☐ Somewhat ☐ Moderately ☐ Quite a bit
3. entertainment activities such as going to a movie or concert?	☐ Not at all ☐ Somewhat ☐ Moderately ☐ Quite a bit	☐ Not at all ☐ Somewhat ☐ Moderately ☐ Quite a bit	☐ Not at all ☐ Somewhat ☐ Moderately ☐ Quite a bit
4. ability to travel by car or bus for a distance greater than 30 minutes away from home?	☐ Not at all ☐ Somewhat ☐ Moderately ☐ Quite a bit	☐ Not at all ☐ Somewhat ☐ Moderately ☐ Quite a bit	☐ Not at all ☐ Somewhat ☐ Moderately ☐ Quite a bit
5. participating in social activities outside your home?	☐ Not at all ☐ Somewhat ☐ Moderately ☐ Quite a bit	☐ Not at all ☐ Somewhat ☐ Moderately ☐ Quite a bit	☐ Not at all ☐ Somewhat ☐ Moderately ☐ Quite a bit
6. emotional health (nervousness, depression, etc.)?	☐ Not at all ☐ Somewhat ☐ Moderately ☐ Quite a bit	☐ Not at all ☐ Somewhat ☐ Moderately ☐ Quite a bit	☐ Not at all ☐ Somewhat ☐ Moderately ☐ Quite a bit
7. feeling frustrated?	☐ Not at all ☐ Somewhat ☐ Moderately ☐ Quite a bit	☐ Not at all ☐ Somewhat ☐ Moderately ☐ Quite a bit	☐ Not at all ☐ Somewhat ☐ Moderately ☐ Quite a bit

FIGURE 1. Pelvic floor impact (PFIQ-7) questionnaire.

TABLE 1. Patient Characteristics

	Preoperative	Postoperative
Number	46	46
Median age	45 (20–67)	
Type of surgery, n (%)		
Roux-en-Y gastric bypass	21 (46)	
Duodenal switch	22 (47)	
Sleeve gastrectomy	3 (7)	
Median weight (kg)	128 (82–198)	79 (58–116)
Median BMI (kg/m^2)	45 (35–75)	28 (22–44)
% EBWL		82 (49–129)
Co-morbidities (%)		
Diabetes	12 (26)	4 (8)
Hypertension	7 (15)	3 (6)
Vaginal deliveries (%)		
0	12 (26)	
1	9 (19)	
>1	25 (55)	
Complicated vaginal delivery	10 (20)	

BMI indicates body mass index; EBWL, excess body weight loss.

TABLE 2. Changes in Prevalence of Pelvic Floor Distress Before and After Surgical Weight Loss

Variable	Before Surgery (%)	After Surgery (%)	*P* Value	95% Confidence Interval (%)
UDI-6	71.3	39	0.003	12–54
CRADI-8	69.1	54.7	0.14	−.04–3
POPDI-6	54.2	43	0.4	−.09–3
Total	87.4	65.2	0.02	.05–53

UDI-6 indicates urogenital distress inventory; CRADI-8, colorectal-anal distress inventory; POPDI-6, pelvic organ prolapse distress inventory.

distress scores showed statistically significant decrease after surgery-induced weight loss. The PF impact scores also showed significant improvements after surgery in the total (combined) quality of life score and individual domains of pelvic organ prolapse and urinary incontinence impact.

There was no relationship of any of the distress/impact scores in any of the domains with age, parity, history of complicated delivery, BMI before or after surgery, or with % EBWL after surgery. There was no correlation between presence of preoperative hypertension and diabetes mellitus or between reversal of diabetes mellitus and/or reversal of hypertension with postoperative PFD scores. Procedure-specific data for absolute weight loss, percent excess body weight loss, and changes in individual domains and total scores for both questionnaires are displayed in Table 3. Colorectal-anal distress scores were higher after the DS and SG; however, this difference did not reach statistical significance. Moreover, there were no significant correlations between the type of bariatric surgical procedure and reductions in postoperative PFD distress/impact in any individual or all domains.

DISCUSSION

Obesity has been directly related to numerous health problems because of the inflammatory/metabolic effects of increased adiposity as well as the increased mass and pressure effects on the pulmonary system, bones, joints, and connective tissue, with an immense impact on quality of life.[5] The present study evaluated the effect of surgically induced weight loss on a spectrum of PFD symptoms using carefully validated instruments. Our results demonstrate that patients with a >50% EBWL after bariatric surgery report significantly less distress because of urinary incontinence, pelvic organ prolapse, and a corresponding improvement in quality of life related to PFDs. These findings agree with the study of Subak et al[21] in moderately obese women enrolled in a nonsurgical weight-reduction program, where patients who lost as little as 5%–10% of their baseline weight had an improvement in urinary incontinence. Moreover, these improvements with limited weight loss were associated with a significant correlation with objective urodynamic findings. Bump et al[16] evaluated 12 obese women with urinary incontinence and found a significant improvement in urinary incontinence after surgically induced weight loss. Like Subak et al,[22] they documented a reduction in bladder pressure and in waist circumference, both of which proved to be independent predictors of postoperative improvement in urinary incontinence.[12] These findings are further supported by more recent publications[17,22] that have reported

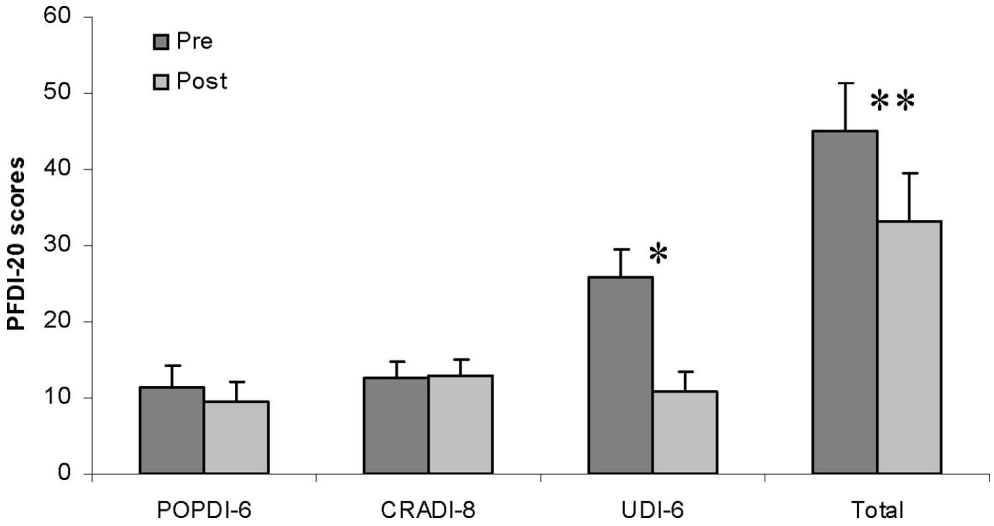

FIGURE 2. Pelvic floor disorder inventory–20 scores before and after surgery. *, $P = 0.0002$; **, $P < 0.015$. POPDI-6: pelvic organ prolapse distress inventory, CRADI-8: colorectal-anal distress inventory, UDI-6: urogenital distress inventory.

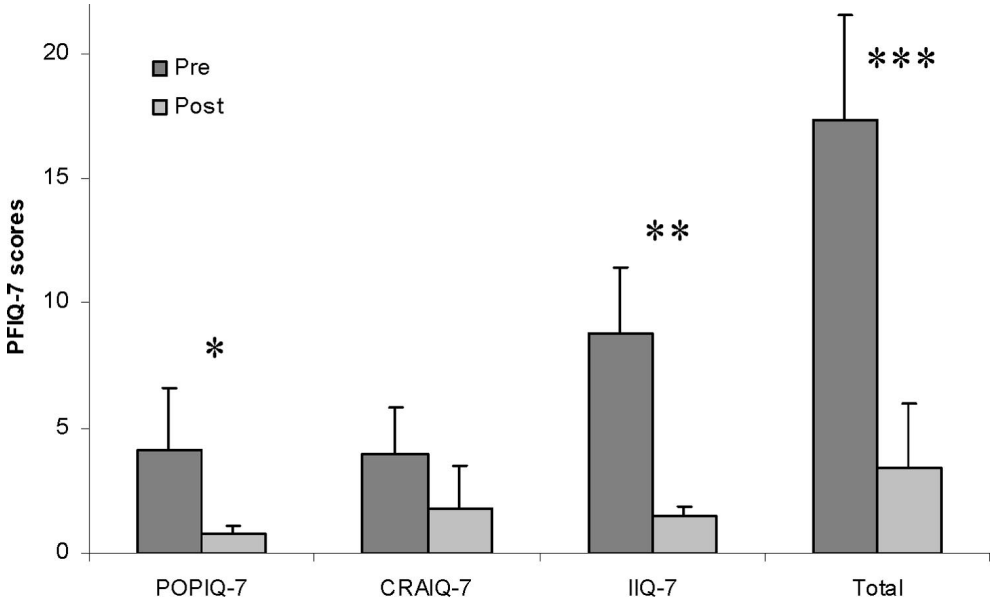

FIGURE 3. PFIQ-7scores before and after surgery. *, $P = 0.015$; **, $P = 0.0005$; ***, $P = 0.002$.POPIQ-7: pelvic organ prolapse impact questionnaire, CRAIQ-7: colorectal-anal impact questionnaire, and IIQ-7: incontinence impact questionnaire.

TABLE 3. Results by Type of Procedure

	RYGB (n = 21)	DS (n = 22)	SG (n = 3)	*P* Value*
Median age (years)	43 (19–67)	45 (35–60)	34 (12–58)	0.55
Median EBW (kg)	49 (29–96)	63 (24–133)	63 (34–107)	0.22
Median %EBWL	90 (56–120)	78 (49–108)	79 (59–89)	0.08
Change in scores† (Mean ± SD)				
IIQ-7	−12.4 ± 17.7	−6.2 ± 15.7	0	0.3
CRAIQ-7	−1.81 ± 6.8	−3 ± 21.1	0	0.9
POPIQ-7	−3.9 ± 10	−6.9 ± 19.5	0	0.6
Total-7	−18 ± 27.5	−16.1 ± 47.7	0	0.7
UDI-6	−19.5 ± 27	−13.6 ± 22.4	−1.3 ± 15	0.4
CRADI-8	−6.9 ± 15.4	2.1 ± 17.2	15.6 ± 27	0.055
PODI-6	−7.5 ± 25.8	0.5 ± 10.4	15.3 ± 33.7	0.16
Total –20	−31.2 ± 54.4	−13 ± 38.2	29.6 ± 74	0.1

*By one way ANOVA.

†Negative changes reflect decreased postoperative scores with improved outcomes and positive changes reflect increased postoperative scores with worsening outcomes.

RYGB indicates Roux-en-Y gastric bypass; DS, duodenal switch; SG, sleeve gastrectomy; POPIQ-7, pelvic organ prolapse impact questionnaire; CRAIQ-7, colorectal–anal impact questionnaire; IIQ-7, incontinence impact questionnaire; POPDI-6, pelvic organ prolapse distress inventory; CRADI-8, colorectal–anal distress inventory; UDI-6, urogenital distress inventory.

a significant reductions in the prevalence and severity of urinary incontinence after bariatric surgery.

The benefits of surgery targeted to correct urinary incontinence in obese women have been supported by some studies,[23,24] whereas others found obesity to correlate with poor outcomes.[24,25] However, all of these authors agreed that urologic surgery is more challenging in obese patients and carries a greater risk. Successful weight reduction before surgery in these cases may itself improve the urinary symptoms and obviate the need for further incontinence interventions. Therefore, we suggest that weight loss should be considered in morbidly obese women before surgical procedures to correct urinary incontinence are offered.

Several studies have indicated that increased BMI plays a role in the development of pelvic organ prolapse.[27–29] Hendrix et al[28] reported that morbid obesity (BMI ≥40 kg/m^2) was associated with significant increase in the occurrence of uterine prolapse (40%), rectocele (75%), and cystocele (57%). However, to our knowledge, there are no previous reports demonstrating an improvement in global pelvic organ prolapse symptoms after weight loss. Pelvic organ prolapse is the result of a disruption or dysfunction of the levator ani muscle complex and the endopelvic fascia, which provide the main support to the pelvic viscera. Chronic straining during defecation and pregnancy with vaginal delivery have been associated with stretching of the levator muscles and associated neuropathic injury.[30] The improvement in pelvic organ prolapse symptoms that was demonstrated after weight-reduction surgery in the current study, may be related to a decrease in abdominal pressure causing muscle and/or fascial weakness or stretch or a nerve stretch injury.

Colorectal and anal symptoms have also been associated with excessive weight.[5,8] Bowel symptoms related to PFD may vary from some forms of fecal/gas incontinence and urgency to obstructed defecation or full-thickness rectal prolapse. The mechanisms by which excessive weight affects colorectal symptoms may be related to chronic pressure on the pelvic floor, on the pudendal nerves and on the sphincter mechanism.[4] Burgio et al,[22] studied changes in fecal incontinence symptoms in 99 women who underwent laparoscopic Roux-en-Y gastric bypass for weight loss and reported a significant reduction in loss of liquid and solid stool from 19.2% before surgery to 8.6% after surgery. However, there was a significant increase in the prevalence of incontinence to flatus after surgery (12.9% to 30.1%), and an increase in fecal incontinence symptoms when solid stools, liquid stools, and flatus were combined. We found no significant improvement in colorectal distress/impact scores, or prevalence after weight loss. Our negative results may have been because of the nature of the instruments that we used, which group together colorectal symptoms. Although we found no correlation between surgery type and PFD outcome, the type of surgery may still directly affect bowel symptoms.[31] Furthermore, the level of weight reduction (>50%EBWL) used in our study for reevaluation may not be sensitive enough to detect changes in

colorectal symptoms. Nevertheless, although weight reduction alone may not be sufficient to relieve symptoms in women with predominantly colorectal problems, it should be considered before a specific pelvic floor intervention.[32]

Age, parity, obstetrical trauma, and increased BMI are all recognized risk factors for PFD,[33–35] but surprisingly, none of these correlated with the PFD distress/ impact scores after weight loss in our series. Data correlating PFD outcome with preoperative and postoperative diabetes mellitus and hypertension were insufficient to reach conclusions regarding the roles of these factors in the prediction of PFD outcomes after bariatric surgery.

Bowel habits after surgical weight loss are often worse after the DS procedure because of malabsorbtion.[36] In our study, there was a nonsignificant trend toward a worsening of colorectal-anal distress after DS. POP distress and colorectal-anal distress were also worse after the SG; however, the limited number of patients who underwent SG was too small to allow for a meaningful analysis. The recent enthusiasm for the SG should provide further opportunities for studying potential improvements pelvic floor dysfunction after weight loss via the SG.

There are other limitations to our study. First, there was no comparison with objective parameters such as pelvic floor-oriented physical examination and physiologic and radiologic studies. Second, only 56% of the study group completed the postoperative questionnaire, a disappointing compliance rate that may represent a selection bias. Finally, we did not design the study to evaluate PFD symptoms and impact at lower thresholds of weight loss, and therefore these results cannot be used to advise patients as to when they might expect to realize improvements in pelvic floor function after bariatric surgery.

Nonetheless, this study is important because of its use of validated instruments, unbiased comparisons, and global pelvic floor evaluation. The findings suggest that the distress because of PFD symptoms and their adverse impact on quality of life may improve after weight-reduction surgery. In morbidly obese women, weight loss should be considered as a treatment option for PFDs before other interventions. Further studies that include objective pelvic floor measurement on physical examination and larger groups are warranted.

REFERENCES

1. Ogden CL, Carroll MD, Curtin LR, et al. Prevalence of overweight and obesity in the United States, 1999–2004. *JAMA*. 2006;295:1549–1555.
2. Mokdad AH, Ford ES, Bowman BA, et al. Prevalence of obesity, diabetes, and obesity-related health risk factors, 2001. *JAMA*. 2003;289:76–79.
3. Elia G, Dye TD, Scariati PD. Body mass index and urinary symptoms in women. *Int Urogynecol J Pelvic Floor Dysfunct*. 2001;12:366–369.
4. Uustal Fornell E, Wingren G, Kjolhede P. Factors associated with pelvic floor dysfunction with emphasis on urinary and fecal incontinence and genital prolapse: an epidemiological study. *Acta Obstet Gynecol Scand*. 2004;83: 383–389.
5. Pender JR, Pories WJ. Epidemiology of obesity in the United States. *Gastroenterol Clin North Am*. 2005;34:1–7.
6. Melville JL, Fan MY, Newton K, et al. Fecal incontinence in US women: a population-based study. *Am J Obstet Gynecol*. 2005;193:2071–2076.
7. Kapoor DS, Davila GW, Rosenthal RJ, et al. Pelvic floor dysfunction in morbidly obese women: pilot study. *Obes Res*. 2004;12:1104–1107.
8. Richter HE, Burgio KL, Clements RH, et al. Urinary and anal incontinence in morbidly obese women considering weight loss surgery. *Obstet Gynecol*. 2005;106:1272–1277.
9. Altman D, Falconer C, Rossner S, et al. The risk of anal incontinence in obese women. *Int Urogynecol J Pelvic Floor Dysfunct*. 2007;18:1283–1289.
10. Klingele CJ, Bharucha AE, Fletcher JG, et al. Pelvic organ prolapse in defecatory disorders. *Obstet Gynecol*. 2005;106:315–320.
11. Wasserberg N, Haney M, Petrone P, et al. Morbid obesity adversely impacts pelvic floor function in females seeking attention for weight loss surgery. *Dis Colon Rectum*. 2007;50:2096–2103.
12. Cummings JM, Rodning CB. Urinary stress incontinence among obese women: review of pathophysiology therapy. *Int Urogynecol J Pelvic Floor Dysfunct*. 2000;11:41–44.
13. Noblett KL, Jensen JK, Ostergard DR. The relationship of body mass index to intra-abdominal pressure as measured by multichannel cystometry. *Int Urogynecol J Pelvic Floor Dysfunct*. 1997;8:323–326.
14. Sugerman H, Windsor A, Bessos M, et al. Effects of surgically induced weight loss on urinary bladder pressure, sagittal abdominal diameter and obesity co-morbidity. *Int J Obes Relat Metab Disord*. 1998;22:230–235.
15. Sugerman HJ, Wolfe LG, Sica DA, et al. Diabetes and hypertension in severe obesity and effects of gastric bypass-induced weight loss. *Ann Surg*. 2003; 237:751–756; discussion 757–758.
16. Bump RC, Sugerman HJ, Fantl JA, et al. Obesity and lower urinary tract function in women: effect of surgically induced weight loss. *Am J Obstet Gynecol*. 1992;167:392–397.
17. Kuruba R, Almahmeed T, Martinez F, et al. Bariatric surgery improves urinary incontinence in morbidly obese individuals. *Surg Obes Relat Dis*. 2007;3:586–590.
18. Subak LL, Johnson C, Whitcomb E, et al. Does weight loss improve incontinence in moderately obese women? *Int Urogynecol J Pelvic Floor Dysfunct*. 2002;13:40–43.
19. Brown JS, Wing R, Barrett-Connor E, et al. Diabetes Prevention Program Research Group. Lifestyle intervention is associated with lower prevalence of urinary incontinence: the Diabetes Prevention Program. *Diabetes Care*. 2006; 29:385–390.
20. Barber MD, Walters MD, Bump RC. Short forms of two condition-specific quality-of-life questionnaires for women with pelvic floor disorders (PFDI-20 and PFIQ-7). *Am J Obstet Gynecol*. 2005;193:103–113.
21. Subak LL, Whitcomb E, Shen H, et al. Weight loss: a novel and effective treatment for urinary incontinence. *J Urol*. 2005;174:190–195.
22. Burgio KL, Richter HE, Clements RH, et al. Changes in urinary and fecal incontinence symptoms with weight loss surgery in morbidly obese women. *Obstet Gynecol*. 2007;110:1034–1040.
23. Cummings JM, Boullier JA, Parra RO. Surgical correction of stress incontinence in morbidly obese women. *J Urol*. 1998;160(3 pt 1):754–745.
24. Rafii A, Darai E, Haab F, et al. Body mass index and outcome of tension-free vaginal tape. *Eur Urol*. 2003;43:288–292.
25. Brieger G, Korda A. The effect of obesity on the outcome of successful surgery for genuine stress incontinence. *Aust N Z J Obstet Gynaecol*. 1992; 32:71–72.
26. O'Sullivan DC, Chilton CP, Munson KW. Should Stamey colposuspension be our primary surgery for stress incontinence? *Br J Urol*. 1995;75:457–60.
27. Swift SE, Tate SB, Nicholas J. Correlation of symptoms with degree of pelvic organ support in a general population of women: what is pelvic organ prolapse? *Am J Obstet Gynecol*. 2003;189:372–377.
28. Hendrix SL, Clark A, Nygaard I, et al. Pelvic organ prolapse in the Women's Health Initiative: gravity and gravidity. *Am J Obstet Gynecol*. 2002;186: 1160–1166.
29. Moalli PA, Jones Ivy S, Meyn LA, et al. Risk factors associated with pelvic floor disorders in women undergoing surgical repair. *Obstet Gynecol*. 2003; 101:869–874.
30. Jelovsek JE, Maher C, Barber MD. Pelvic organ prolapse. *Lancet*. 2007;369: 1027–1038.
31. Foster A, Laws HL, Gonzalez QH, et al. Gastrointestinal symptomatic outcome after laparoscopic Roux-en-Y gastric bypass. *J Gastrointest Surg*. 2003;7:750–753.
32. Korsgen S, Deen KI, Keighley MR. Long-term results of total pelvic floor repair for postobstetric fecal incontinence. *Dis Colon Rectum*. 1997;40:835–839.
33. MacLennan AH, Taylor AW, Wilson DH, et al. The prevalence of pelvic floor disorders and their relationship to gender, age, parity and mode of delivery. *BJOG*. 2000;107:1460–1470.
34. Rortveit G, Brown JS, Thom DH, et al. Symptomatic pelvic organ prolapse: prevalence and risk factors in a population-based, racially diverse cohort. *Obstet Gynecol*. 2007;109:1396–1403.
35. Varma MG, Brown JS, Creasman JM, et al. Reproductive Risks for Incontinence Study at Kaiser (RRISK) Research Group. Fecal incontinence in females older than aged 40 years: who is at risk? *Dis Colon Rectum*. 2006;49:841–851.
36. Dolan K, Hatzifotis M, Newbury L, et al. A clinical and nutritional comparison of biliopancreatic diversion with and without duodenal switch. *Ann Surg*. 2004;240:51–56.

BOOK CHAPTER
REPRINTS AND PREPRINTS

CHAPTER 1

Introduction to Medical Imaging and Image Analysis: A Multidisciplinary Paradigm

Atam P Dhawan, HK Huang and Dae-Shik Kim

Recent advances in medical imaging with significant contributions from electrical and computer engineering, medical physics, chemistry, and computer science have witnessed a revolutionary growth in diagnostic radiology. Fast improvements in engineering and computing technologies have made it possible to acquire high-resolution multidimensional images of complex organs to analyze structural and functional information of human physiology for computer-assisted diagnosis, treatment evaluation, and intervention. Through large databases of vast amount of information such as standardized atlases of images, demographics, genomics, etc. new knowledge about physiological processes and associated pathologies is continuously being derived to improve our understanding of critical diseases for better diagnosis and management. This chapter provides an introduction to this ongoing knowledge quest and the contents of the book.

1.1 INTRODUCTION

In a general sense, medical imaging refers to the process involving specialized instrumentation and techniques to create images or relevant information about the internal biological structures and functions of the body. Medical imaging is sometimes categorized, in a wider sense, as a part of radiological sciences. This is particularly

relevant because of its most common applications in diagnostic radiology. In clinical environment, medical images of a specific organ or part of the body are obtained for clinical examination for the diagnosis of a disease or pathology. However, medical imaging tests are also performed to obtain images and information to study anatomical and functional structures for research purposes with normal as well as pathological subjects. Such studies are very important to understand the characteristic behavior of physiological processes in human body to understand and detect the onset of a pathology. Such an understanding is extremely important for early diagnosis as well as developing a knowledge base to study the progression of a disease associated with the physiological processes that deviate from their normal counterparts. The significance of medical imaging paradigm is its direct impact on the healthcare through diagnosis, treatment evaluation, intervention and prognosis of a specific disease.

From a scientific point of view, medical imaging is highly multidisciplinary and interdisciplinary with a wide coverage of physical, biological, engineering and medical sciences. The overall technology requires direct involvement of expertise in physics, chemistry, biology, mathematics, engineering, computer science and medicine so that useful procedures and protocols for medical imaging tests with appropriate instrumentation can be developed. The development of a specific imaging modality system starts with the physiological understanding of the biological medium and its relationship to the targeted information to be obtained through imaging. Once such a relationship is determined, a method for obtaining the targeted information using a specific energy transformation process, often known as physics of imaging, is investigated. Once a method for imaging is established, proper instrumentation with energy source(s), detectors, and data acquisition systems are designed and integrated to physically build an imaging system for imaging patients to obtain target information in the context of a pathological investigation. For example, to obtain anatomical information about internal organs of the body, X-ray energy may be used. The X-ray energy, while transmitted through the body, goes through attenuation based on the density of the internal structures. Thus,

the attenuation of the X-ray energy carries the target information about the density of internal structures which is then displayed as a two-dimensional (in case of radiography or mammography) or multidimensional (3D in case computed tomography (CT); 4D in case of cine-CT) image. This information (image) can be directly interpreted by a radiologist or further processed by a computer for image processing and analysis for better interpretation.

With the evolutionary progress in engineering and computing technologies in the last century, medical imaging technologies have witnessed a tremendous growth that has made a major impact in diagnostic radiology. These advances have revolutionarized healthcare through fast imaging techniques; data acquisition, storage and analysis systems; high resolution picture archiving and communication systems; information mining with modeling and simulation capabilities to enhance our knowledge base about the diagnosis, treatment and management of critical diseases such as cancer, cardiac failure, brain tumors and cognitive disorders.

Figure 1 provides a conceptual notion of the medical imaging process from determination of principle of imaging based on the target pathological investigation to acquiring data for image reconstruction, processing and analysis for diagnostic, treatment evaluation, and/or research applications.

There are many medical imaging modalities and techniques that have been developed in the past years. Anatomical structures can be effectively imaged today with X-ray computed tomography (CT), magnetic resonance imaging (MRI), ultrasound, and optical imaging methods. Furthermore, information about physiological structures with respect to metabolism and/or functions, can be obtained through nuclear medicine [single photon emission computed tomography (SPECT) and positron emission tomography (PET)], ultrasound, optical fluorescence, and several derivative protocols of MRI such as fMRI, diffusion-tensor MRI, etc.

The selection of an appropriate medical imaging modality is important for obtaining the target information for a successful pathological investigation. For example, if information has to be obtained about the cardiac volumes and functions associated with

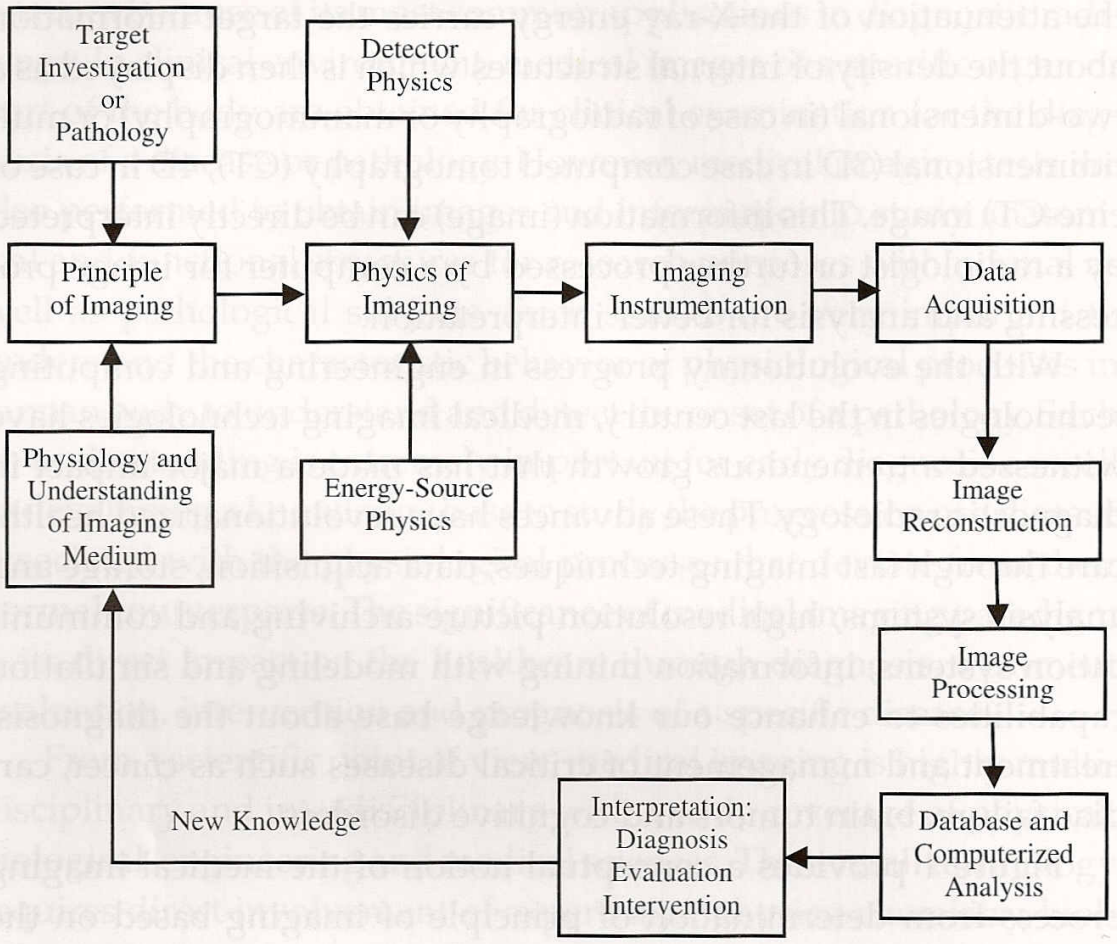

Fig. 1. A conceptual block diagram of medical imaging process for diagnostic, treatment evaluation and intervention applications.

a beating heart, one has to determine the requirements and limitations about the spatial and temporal resolution for the target set of images. It is also important to keep in mind the type of pathology being investigated for the imaging test. Depending on the investigation, such as metabolism of cardiac walls, or opening and closing measurements of mitral valve, a specific medical imaging modality (e.g. PET) or a combination of different modalities (e.g. stress-PET and ultrasound) can be selected.

1.1.1 Book Chapters

In this book, we present a collection of carefully written chapters to describe principles and recent advances of major medical imaging

modalities and techniques. Case studies and data analysis protocols are also described for investigating selected critical pathologies. We hope that this book will be useful for engineering as well as clinical students and researchers. The book presents a natural progression of technology development and applications through the chapters that are written by leading and renowned researchers and educators. The book is organized in three parts: Principles of Imaging and Image Analysis (Chapters 2–10); Recent Advances in Medical Imaging and Image Analysis (Chapters 11–23); and Medical Imaging Applications, Case Studies and Future Trends (Chapters 24–32).

Chapter 2 describes some basic principles of medical imaging and image formation. In this chapter, Atam Dhawan has focused on a basic mathematical model of image formation for a linear spatially invariant imaging system.

In Chapter 3, Brent Liu and HK Huang present basic principles of X-ray imaging modalities. X-ray radiography, mammography, computed tomography (CT) and more recent PET-XCT fusion imaging systems are described.

Principles of nuclear medicine imaging are described by Lionel Zuckier in Chapter 4 where he provides foundation and clinical applications of single photon emission tomography (SPECT) and positron emission tomography (PET).

In Chapter 5, Itamar Ronen and Dae-Shik Kim describes sophisticated principles and imaging techniques of Magnetic Resonance Imaging (MRI). Imaging parameters and pulse techniques for useful MR imaging are presented.

Elisa Konofagou presents the principles of ultrasound imaging in Chapter 6. Instrumentation and various imaging methods with examples are described.

In Chapter 7, Atam Dhawan describes the foundation of multidimensional image reconstruction methods. A brief introduction of different types of transform and estimation methods is presented.

Atam Dhawan presents a spectrum of image enhancement, restoration and filtering operations in Chapter 8. Image processing methods in spatial (image) domain as well as frequency (Fourier)

domain are described. In Chapter 9, Atam Dhawan describes basic image segmentation and feature extraction methods for representation of regions of interest for classification.

In Chapter 10, Atam Dhawan and Shuangshuang Dai present principles of pattern recognition and classification. Genetic algorithm based feature selection and nonparametric classification methods are also described for image/tissue classification for diagnostic applications.

Advances in MR imaging with respect to new methods and pulse sequences associated with functional imaging of brain are described by Dae-Shik Kim in Chapter 11. Diffusion and diffusion-tensor based magnetic resonance imaging methods are described by Dae-Shik Kim and Itamar Ronen in Chapter 12. These two chapters bring the most recent developments in functional brain imaging to investigate neuronal information including homodynamic response and axonal pathways.

Chapter 13 provides a spectrum of optical and fluorescence imaging for 3-D tomographic applications. Through specific contrast imaging methods, Sachin Patwardhan, Walter Akers and Sharon Bloch explore molecular imaging applications.

In Chapter 14, Qi Duan, Elsa Angelini, Shunichi Homma and Andrew Laine presents recent investigations in dynamic ultrasound image analysis for tracking endocardium in 4D cardiac imaging.

Chien-Min Kao, Emil Y. Sidky, Patrick LaRiviere, and Xiaochuan Pan describe recent advances in model based multidimensional image reconstruction methods for medical imaging applications in Chapter 15. These methods use multivariate statistical estimation methods in image reconstruction.

Shape-based optical image reconstruction of specific entities from multispectral images of skin lesions is presented by Song Wang and Atam Dhawan in Chapter 16.

Clinical multimodality image registration and fusion methods with nuclear medicine and optical imaging are described by Pat Zanzonico in Chapter 17. Pat emphasizes on clinical needs of localization of metabolic information with real time processing and efficiency requirements.

Recently wavelet transform has been extensively investigated for obtaining localized spatio-frequency information. The use of wavelet transform in medical image processing and analysis is described by Atam Dhawan in Chapter 18.

Medical image processing and analysis often require a multi-class characterization for image contents. Atam Dhawan presents a probabilistic multiclass tissue characterization method for MR brain images in Chapter 19.

In Chapter 20, Mathieu De Craene and Alejandro F Frangi present a review of advances in image registration methods for constructing standardized computational atlases.

In Chapter 21, HK Huang, Zheng Zhou and Brent Liu describe information processing and computational methods to deal with large image archiving and communication corresponding to large medical image databases.

Brent Lu, in Chapter 22, describes knowledge mining and decision making strategies for medical imaging applications in radiation therapy planning and treatment.

With large image archiving and communication systems linked with large image databases, information integrity becomes a critical issue. In Chapter 23, Zheng Zhou, HK Huang and Brent J Liu present lossless digital signature embedding methods in multidimensional medical images for authentification and integrity.

Medical imaging applications in intensity modulated radiation therapy (IMRT), a radiation treatment protocol, are discussed by Yulin Song in Chapter 24.

In Chapter 25, Maria Law presents the detailed role of medical imaging based computer assisted protocols for radiation treatment planning and delivery.

Recently developed fMR and diffusion-MR imaging methods provide overwhelming volumes of image data. A productive and useful analysis of targeted information extracted from such MR images of brain is a challenging problem. In Chapter 26, Angela Laird, Jack Lancaster and Peter Fox describe recently developed maximum likelihood estimation based "meta" analysis algorithms for the investigation of a specific pathology. In Chapter 27,

Christos Davatzikos presents dynamic brain mapping methods for analysis of patient specific information for better pathological characterization and diagnosis. Tianming Liu and Stephen Wong, in Chapter 28, explore a recently developed model-based image analysis algorithms for analyzing diffusion-tensor MR brain images for the characterization of neurological disorders.

Model-based intelligent analysis and decision-support tools are important in medical imaging for computer-assisted diagnosis and evaluation. Xiang Sean Zhou, in Chapter 29, presents specific challenges of intelligent medical image analysis, specifically for the interpretation of cardiac ultrasound images. However, the issues raised in this chapter could be extended to other modalities and applications. In Chapter 30, Yulin Song and Guang Li present an overview of future trends and challenges in radiation therapy methods that closely linked with high resolution multidimensional medical imaging.

Heinz U Lemke and Leonard Berliner, in Chapter 31, describes specific methods and information technology (IT) issues in dealing with image management systems involving very large databases and widely networked image communication systems.

To conclude, Chapter 32 presents a glimpse of future trends and challenges in high-resolution medical imaging, intelligent image analysis, and smart data management systems.

CHAPTER 25

Image Guidance in Radiation Therapy

Maria YY Law

Radiation therapy is one of the modalities for treating cancers. It has been image-based since its early stage of implementation. Medical images are used in radiation therapy for tumor diagnosis, tumor delineation, treatment planning and treatment verification. Computerization and advanced development in medical imaging have revolutionarized the practice of radiation therapy. The invention of computer-controlled multileaf collimators leads to the development of conformal radiation therapy and intensity modulated radiation therapy which enables the irradiated target volume to be more conformed to the shape of the tumor, sparing more surrounding normal tissue and thus decrease the probability of toxic effects to normal tissue. At the same time, a higher dose can be delivered to the tumor for better tumor control. However, systematic and random errors due to patient positioning and organ motion occur in a course of radiation therapy. They need to be monitored and accounted for by more stringent image guidance methods at times of tumor delineation, treatment planning and treatment delivery. This chapter describes the concept of image guidance in radiation therapy and reviews the different technologies adopted for image-guided radiation therapy.

25.1 INTRODUCTION

Radiation therapy is a treatment modality that uses ionizing radiation for treating a majority of cancers (malignant tumors). The ultimate goal of radiation therapy is to give as high a dose as possible to the tumor but as little dose as possible to the surrounding normal tissue. More accurate targeting of a tumor allows better tumor control. On the other hand increased dose to a non-tumor bearing

organ e.g. increased dose into the lung when treating a breast cancer, will increase the toxicity into the lung. Failure of achieving the goal would either lead to failure in tumor control or long-term complications in the surrounding tissues.

Basically radiation therapy consists of two major procedures, treatment planning and treatment delivery. Medical images are involved in many of the steps and have to a large extent, contributed to the evolution of treatment techniques in radiation therapy.

Treatment planning involves delineation of tumor target volume and critical structures (Fig. 1) nearby as well as arranging the radiation beams to achieve the best radiation dose distribution that will kill the tumor but spare the surrounding normal tissue as much as possible. It begins with imaging in the treatment simulator or CT simulator. The former produces 2D radiographic projectional images while the latter, like an ordinary CT scanner, produces cross-sectional images. CT images taken in treatment positions can be input into treatment planning system (TPS) for radiation beam planning. The beam arrangement will then be displayed in the TPS

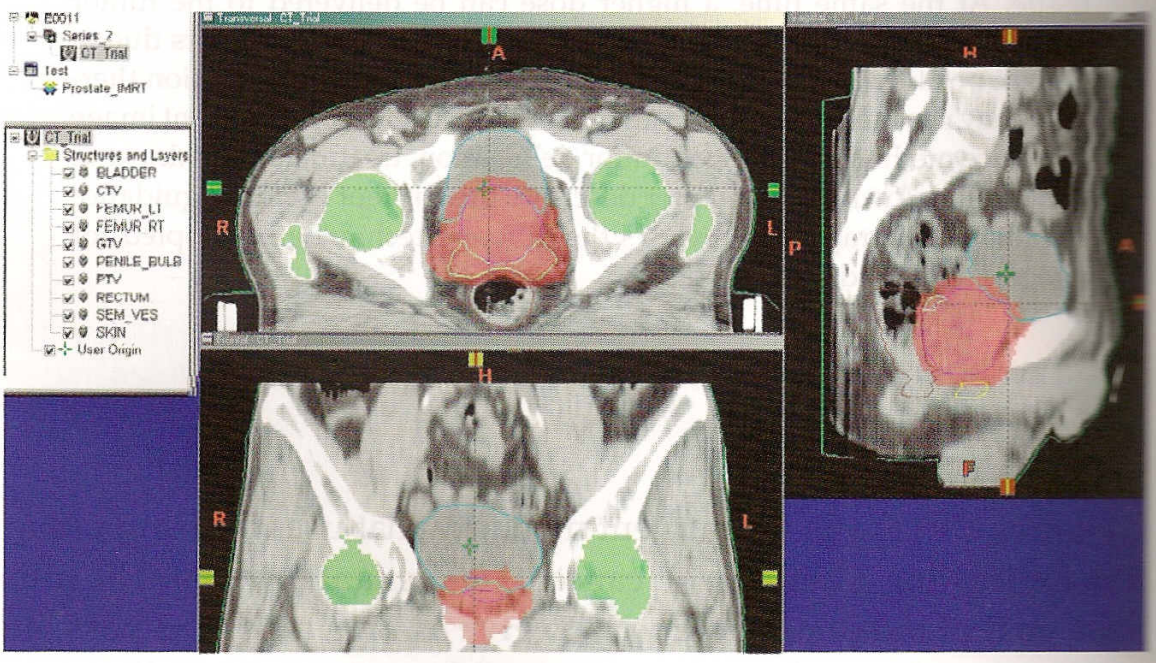

Fig. 1. Delineation of target volume (red) and organs at risk of a prostate cancer case for treatment planning. The cross-sectional CT images (upper left) can be reconstructed to different planes: coronal plane (bottom left) and sagittal plane (right).

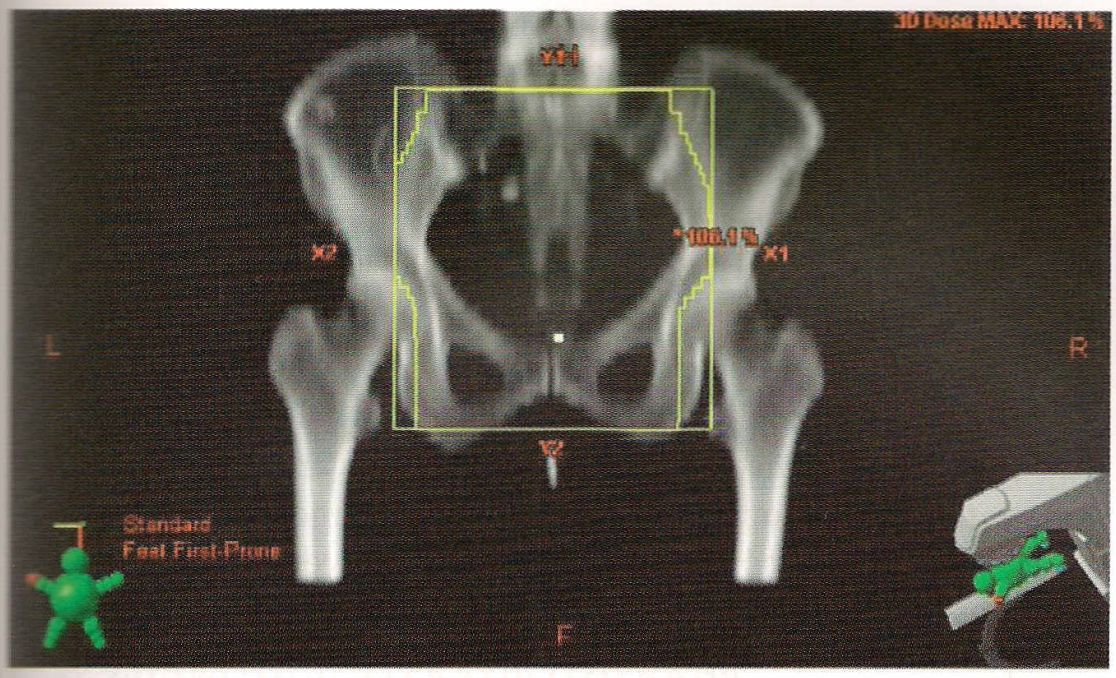

Fig. 2. DRR (digitally reconstructed radiograph) reconstructed from CT images for 2D treatment planning.

workstation with the resultant radiation dose distribution superimposed on the tumor and the surrounding structures. The graphical display of the tumor, critical structures around and the radiation dose distribution helps radiation oncologists to decide on the suitability of the treatment plan for the patient. Digitally reconstructed radiographs (DRR) can be generated from the set of CT images in the TPS for 2D treatment planning (Fig. 2). Simulator images or DRRs are planning images that also serve as reference images for set up verification later.

In treatment delivery, it is important to verify that the radiation beam is delivered as planned. Conventional verification involves the acquisition of 2D radiographic images on film or by electronic portal imaging device (EPID) from the megavoltage (MV) beam of the linear accelerator with the patient in treatment position. These images are called portal or verification images. Bony landmarks, which are the internal structures most visible on megavoltage images, are visually aligned with those on the planning or reference images to determine if the treatment portals match accurately with the treatment plans. Discrepancy between the images requires corrections or even

replanning on some occasions. It can be seen that radiation therapy has been an image-guided treatment modality from its early stage.

Computerization in medicine and digitization in medical imaging have revolutionarized radiation therapy and allowed the more intensive use of images. Different image processing techniques are deployed to aid in the visualization of the treatment plans. Segmentation is used to delineate the tumor and neighboring important body structures. For example, in planning a prostate tumor, other than delineating the tumor, the rectum behind the tumor or the bladder nearby need to be segmented for planning of the radiation beams. Surface or volume rendering are important methods for seeing the target tumor or body structures or even the level of radiation dose within the body. The dose-volume histogram (DVH) is an important tool for appraisal of a radiation treatment plan (Fig. 3). The combination of image processing methods provides the volume of segmented structure(s) or tumor and the treatment planning

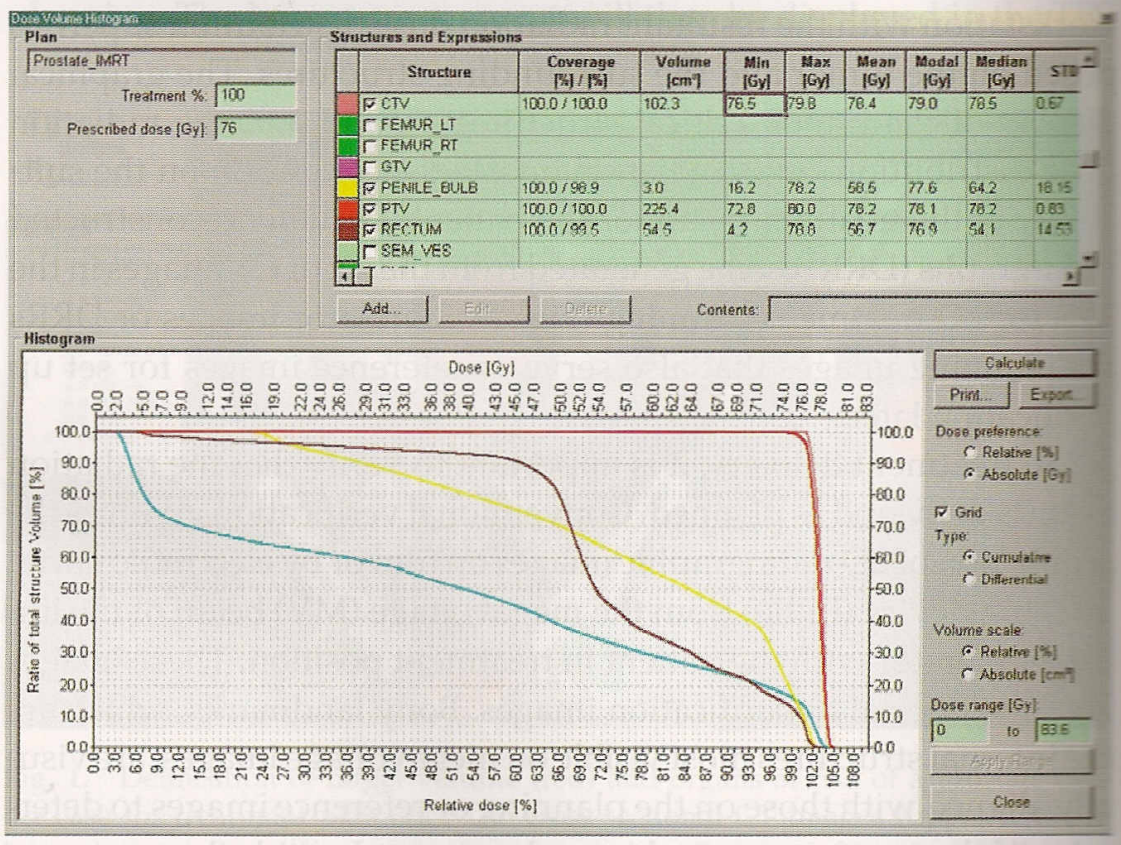

Fig. 3. Dose-volume histogram (DVH) for treatment plan evaluation.

algorithm provides the dose at different points within the irradiated volume. Together, they result in the formulation of the dose-volume histogram for medical decision on the appropriateness of the treatment plan. To improve the accuracy of tumor delineation, multimodality images such as CT and MRI or CT and PET can be variously aligned, registered and be mapped to each other or fused to obtain the maximum information from the combined images. PET/CT fusion images have shown to enhance tumor target volume definition and the registration algorithm is well established.[1] Image acquisition and image processing such as segmentation, registration and visualization are crucial to all procedures in radiation therapy.

25.2 IMAGE-GUIDED RADIOTHERAPY

A course of radiation treatment is normally delivered in many fractions of small doses. In the course of treatment, geometric uncertainties may arise between fractions (interfractional) or even within a fraction (intrafractional). Examples of such uncertainties include organ motion, variable filling of digestive or urinary organs, setup errors, tumor shrinkage and change in weight of patients (as the course may last for several weeks). To avoid marginal miss of the tumor, it is necessary to have a generous margin around the gross tumor volume (Fig. 4). The width of the margin depends on the estimated extent of tumor invasion, planning and setup errors, possible

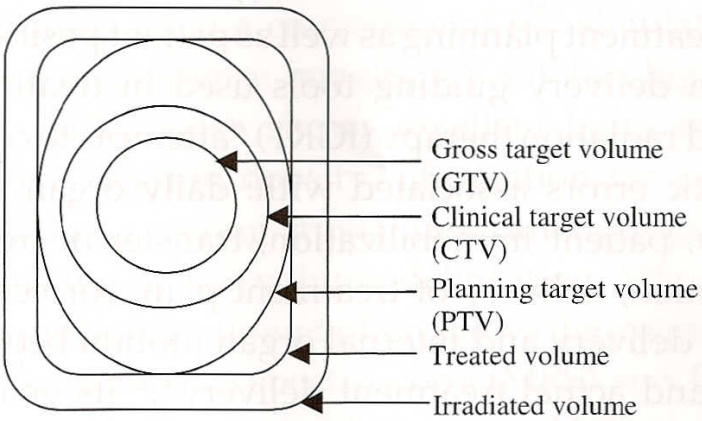

Fig. 4. Target volume definition (ICRU Report 50).

organ motion and the radiosensitivity of adjacent normal tissue. The wider the margin means the more surrounding normal tissue would be irradiated. In order to reduce complication to normal tissue, it is ideal to keep the margin to its minimum but at the same time to ensure that there is no geographical miss on the tumor. The evolvement of imaging technologies such as CT, MR, PET, advancement in planning software and computer-controlled radiation treatment delivery such as computerized collimator systems have all contributed to the delivery of a treatment that can be tightly conformed to the tumor, while the surrounding normal tissue can be spared more from the unwanted radiation.

The recent development of 3D conformal radiation therapy (3DCRT) and intensity modulated radiation therapy (IMRT) produces shaped radiation dose that closely conforms to the tumor dimensions. This means a tighter margin is allowed around the tumor target volume so that a higher radiation dose can be delivered (dose escalation) for tumor killing with reduced risk of complications to surrounding normal tissue. For example, using IMRT, a higher dose can be given to the prostate tumor which leads to better tumor control while the neighboring rectum received a minimal radiation dose and thus lowers the risk of rectal complications. These techniques call for a high degree of accuracy and precision of tumor delineation and beam targeting. These stringent requirements set off the scene for more sophisticated image guided technologies to cope with possible geometric uncertainties in radiation therapy. The technologies include image-based tumor localization methods in treatment planning as well as patient positioning devices and radiation delivery guiding tools used in treatment delivery. Image-guided radiation therapy (IGRT) "attempts to correct random and systematic errors associated with: daily organ motion, daily patient setup, patient immobilization, transfer of treatment planning information, delivery of treatment plan, corrections made to pretreatment delivery and internal organ motion between the time of planning and actual treatment delivery".[2] Its goal is "to manage both interfractional and intrafractional motion to improve the accuracy of treatment delivery".[3] In short, IGRT is the use of images

to visually confirm that the radiation treatment plan is accurately reproduced during radiation treatment. It is best adopted in situation where error is likely to result in large adverse consequence such as 3DCRT and IMRT and where large setup uncertainties are expected as in obese patients as well as for diseases in certain sites of the body e.g. head and neck, lung, liver or prostate.

25.3 IMAGE-GUIDED TECHNOLOGIES FOR RADIATION THERAPY

25.3.1 Imaging for Radiation Therapy Planning

Treatment planning starts with tumor volume delineation, the accuracy of which is vital to the subsequent procedures. Advanced imaging technologies contribute to the precision in target volume delineation which is crucial in reducing or eliminating uncertainties.

25.3.1.1 *Multimodality imaging*

CT scans are the most commonly used modality for tumor delineation as the dose calculation algorithms of TPSs are based on the electron density of CT images. Many radiation oncology departments have their own CT scanners with simulation functions. The patients are scanned in their immobilized treatment positions. The CT images acquired will be transferred in the DICOM format to the TPS, where the tumor is delineated. DRRs can be reconstructed for 2D visualization as in a conventional KV simulator and serve as the planning or reference images. KV CT has high spatial resolution (512 × 512 pixels), shows excellent bony structures and provides relative electron density information for radiation dose calculation.[1] Other imaging modalities can be registered to CT scans for enhancing tumor volume delineation. MRI shows better discrimination for soft tissue and often shows the extent of the tumor better. Magnetic resonance spectroscopy (MRS) and PET (positron emission tomography) can provide functional information unavailable from CT images. They show the spatial extent of the tumor

with its physiological movement about the tumor and normal tissue. Coregistration of images (image fusion) in the same setting from different imaging modalities e.g. CT and MRI, CT and PET will enhance target volume delineation.[4] Software for image registration is available in most TPSs nowadays. To improve the accuracy of delineating deforming organs e.g. liver or tumor in moving structures such as lung tumor, deformable registration techniques would be helpful. Multimodality anatomic imaging registration PET-CT does not only help in target delineation, but also in disease appraisal and assessment of therapy response.

25.3.1.2 *Imaging for organ motion*

Organ motion is a major source of error in beam targeting. A tumor in the lung and organs in the upper abdomen can move up to three centimeter with respiration.[3,5,6] Other internal organs such as pancreas, liver or prostate also move due to digestion, respiration or variation in filling from day to day. If the tumor is moved out of the planned range of the radiation beam, it will not receive the full radiation dose as planned and what is worse is a high dose will be delivered to the adjacent normal tissue instead. The situation will defeat the purpose of radiation therapy.

In tumors that are subject to motion, it is important to account for the motion. Methods include measuring the motion by different imaging modalities; reducing motion e.g. by applying compression on abdomen; eliminating motion during treatment e.g. by breath-holding; increasing the PTV thus providing a wider margin to accommodate the potential error; tracking the tumor position by continuous monitoring of internal anatomy or surrogates; and radiation beam gating to synchronize the beam with the moving target.

Organ motion can be visualized and assessed in fluoroscopy, which is a function in conventional KV treatment simulators or incorporated in recent MV treatment units. Traditional CT only shows the respiratory motion as artifacts and the tumor volume is shown to be distorted or larger than what it is. As such, information

in the fourth dimension — time is needed. 3D CT has to be extended to incorporate the fourth dimension, so that the changing position of the tumor over time can be visualized.

Multidetector CT scanners can show the temporal changes from breathing. The respiratory signal can be tracked and recorded e.g. by a camera over an external marker placed on the abdomen or by monitoring the chest expansion with a pneumatic bellow. CT data can be acquired over the whole respiratory cycle and then sorted based on the phase of the respiratory cycle. The series of CT images over several points in the respiratory cycle are then reconstructed. Images through the respiratory phases from end-inspiration to end-expiration can be scrolled through and be exported to TPS in DICOM format for geometric and dosimetric computation.

Other methods to counteract the artifacts caused by organ motion in radiation therapy are immobilization of the organs by repeated breath holds, respiration gating and 4D tumor tracking. The tumor is irradiated at the predetermined breathing interval when the tumor is at a constant position. Breath-hold techniques can be either active or passive. Deep inspiration breath-hold, active breathing control (inducing shallow breathing to minimize tumor motion) and self-held breath-hold are some of such techniques which have been reported in treating liver cancer,[7,8] Hodgkin's disease[9] and breast cancer. One of the most important steps of planning in IGRT is the accurate registration of the tumor position at the same phase of respiration as it is in treatment planning, hence such details need to be taken care of during planning.

Respiration gating is to match the radiation beam to the respiratory pattern. For monitoring the treatment, IGRT is coupled with respiratory control. The patient's breathing cycle is monitored by a gating system that uses an infrared camera to track a marker that is placed either on the patient's chest or abdomen. The radiation beam is triggered to turn on and off as the tumor moves in and out of the preset gating window respectively (Figs. 5 and 6). For planning purpose, 4D-CT images are acquired either prospectively or retrospectively. In the former, CT images are only acquired at one specific phase of the patient's normal breathing cycle. In the latter, multiple

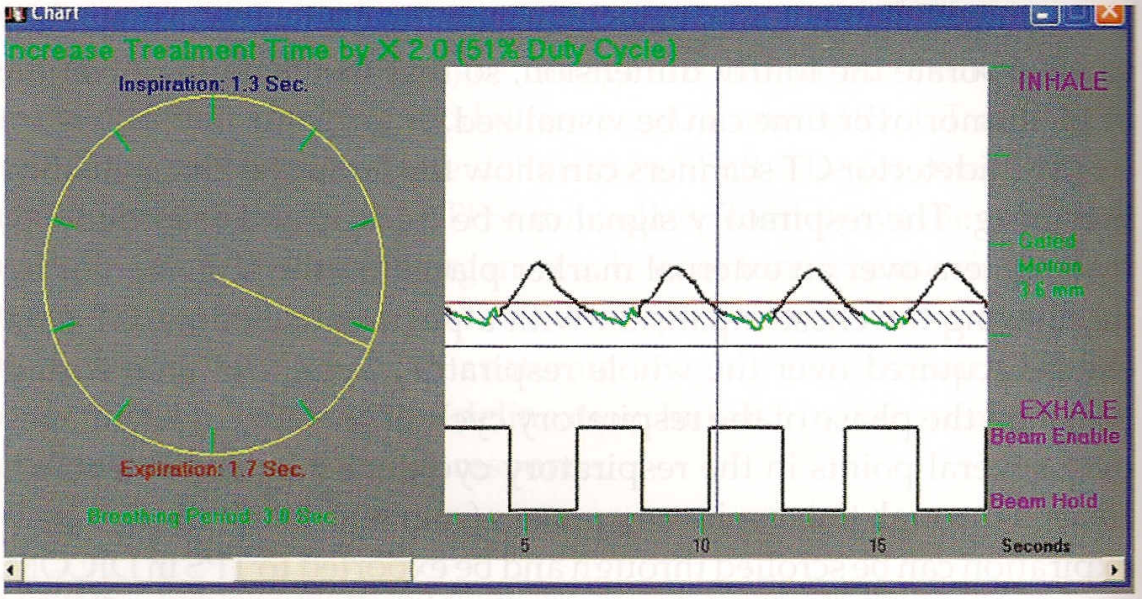

Fig. 5. Respiratory cycle of patient is tracked and recorded (upper curve) and is coupled with IGRT. Radiation beam is enabled at expiratory phase (lower curve).

volumetric CT images are acquired and then be sorted according to the patient's respiratory phases. The 4D-CT data can then be synchronized with the respiratory phase to show the exact location of the tumor at the specific respiratory phase.[3]

In 4D tumor tracking, fiducial markers are inserted into the irradiated site as an aid to visualization. CT images are taken for planning and the coordinates of the markers are registered. Before treatment starts, the marker coordinates are traced for one to two minutes (at a rate of 30 times per second) and recorded. Registration of the marker coordinates at the planning image and those at treatment will indicate if misalignment exists, and in which case, the treatment couch will be adjusted accordingly. Real-time tumor-tracking starts where radiation beam will only be turned on if the positions of the fiducial markers are within the gating window and turned off if they are not in the planed position.[10,11] While Shirato's group used only one set of CT for treatment planning, Keall and colleagues[12] developed a method of 4D treatment planning that involves a series of eight 3D CT image sets acquired at different respiratory phases for DMLC (dynamic multileaf collimator)-based respiratory motion tracking. Deformable image registration was used

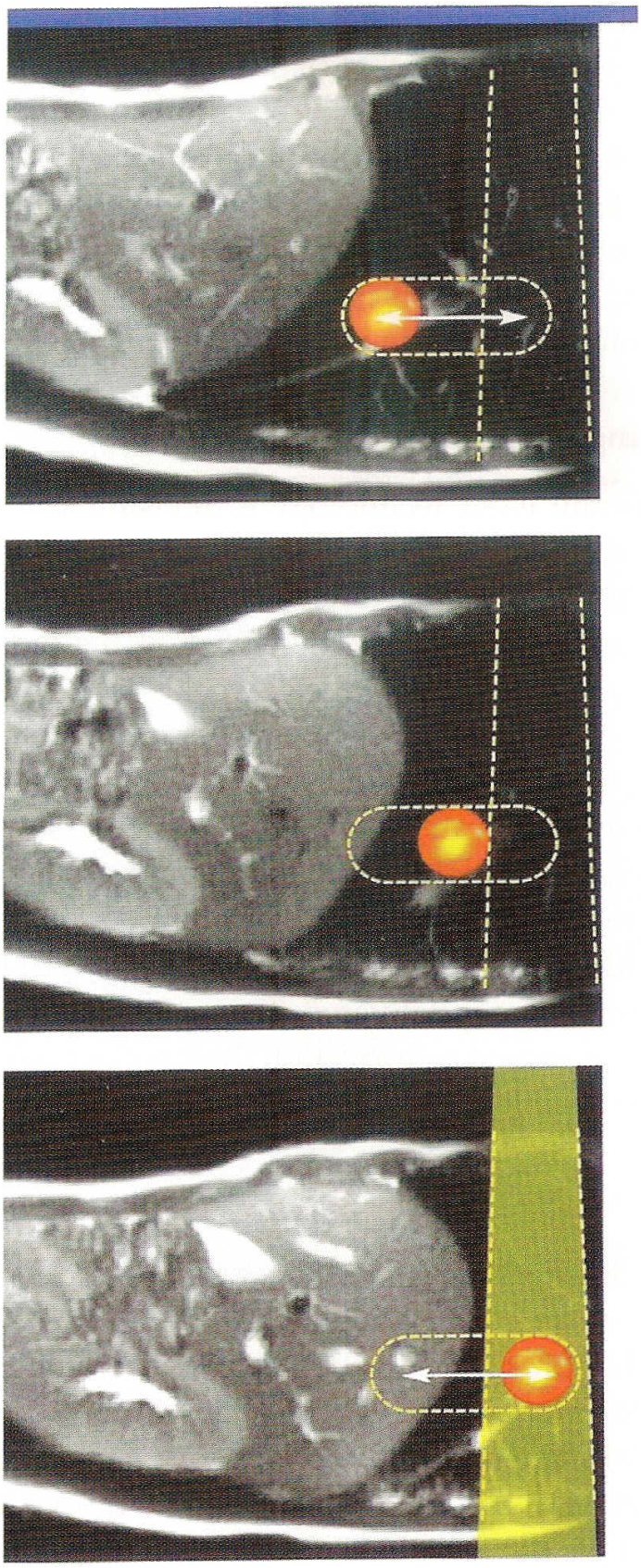

Fig. 6. Upper and middle: Beam off to spare normal tissue. Lower: Beam on when target volume is in the range of the radiation beam (Courtesy of BrainLab AG, Heimstetten, Germany).

in mapping CT sets from the peak-inhale respiratory phase to those of subsequent phases. Treatment planning was done on each of the eight CT sets with the MLC aperture conforming to the PTV (planning target volume). Dose distribution from each CT set was then mapped back to the CT of the peak-inhale phase for analysis. The goal of the 4D planning is to estimate the extent of the tumor motion and decide on appropriate measures to ensure accurate beam targeting at treatment.

25.3.2 Imaging for Treatment Delivery

Another important IGRT technology is devising accurate methods for treatment verification and radiation dose delivery during treatment. Conventionally, for treatment verification, 2D portal images whether on film or by EPID are taken before the radiation dose is delivered and at regular interval e.g. weekly thereafter, to be compared with the planning or reference images to confirm that the setup accurate as planned. Though many EPID systems offer computer-assisted tools for registration of anatomical features with the planning images and quantitative alignment analysis, errors if detected are corrected retrospectively because adjustments can only be made until the portal images are processed and reviewed, which is usually after the treatment is delivered. To improve treatment accuracy, it requires immediate error correction (before the treatment is delivered) and more frequent imaging such as daily.

25.3.2.1 *MV/KV 2D imaging*

MV EPIDs that generate digital images have been implemented for over a decade. An active matrix flat panel detector is installed opposite to the radiation source of the linear accelerator. Portal images of the irradiated area with patient in treatment position will be generated. Manual matching or template aided matching is normally used to determine the accuracy of the setup. However, the radiological properties of MV X-rays do not produce images of good contrast and is an issue when very high precision treatment verification is required. Also due to the higher radiation dose, MV imaging

precludes its daily use. On the other hand, KV X-rays generate higher contrast images with lower radiation dose and thus allow more frequent imaging. This has motivated the incorporation of KV X-ray tube systems in the treatment room that can be used for fluoroscopy, radiography and cone beam CT. Examples are the On-Board Imager™ (OBI) (Varian Medical System, Palo Alto, USA); XVI (X-ray Volume Imaging) system (Elekta®, Stockholm, Sweden); and ARTISTE system (Siemens AG, Munich, Germany). They are installed orthogonally to the MV treatment beam. The details of the cone beam CT will be described later while other KV X-ray systems for treatment verification purpose will be detailed in the next paragraph.

25.3.2.2 *Room mounted KV fluoroscopic imaging system*

For real-time tumor/position tracking, room mounted KV fluoroscopic units (two or more X-ray tubes paired with image intensifiers) are implemented[10,11,13] Such technique requires the insertion of markers in the soft tissue tumor to aid visualization. Planning CT will be acquired with the markers *in situ* and transferred to the specific planning software for dose planning. Positions of the markers in the reference images are registered with those in the fluoroscopy. In other similar systems, DRRs can also be reconstructed from planning CT for computer comparison with the real-time X-ray images acquired during treatment by registering the positions of the markers (Fig. 7). Deviations, as compared with the DRR are displayed and the computer-driven controller of the linear accelerator or treatment couch will automatically correct for the deviations up to a predetermined range. Another similar room mount KV X-ray system is the ExacTrac® X-ray 6D which uses two KV X-ray tubes with opposed amorphous silicon panel imaging detectors to acquire 2 orthogonal planar X-ray images (Fig. 8). The Cyberknife (Accuray, Sunnyvale, CA USA), a 6 MV linear accelerator with a moving robotic arm, capable of 6 degree of freedom movement, is another example of image guided system that is coupled with dynamic tracking software Synchrony.[14,15] Its localization system is also based on 2

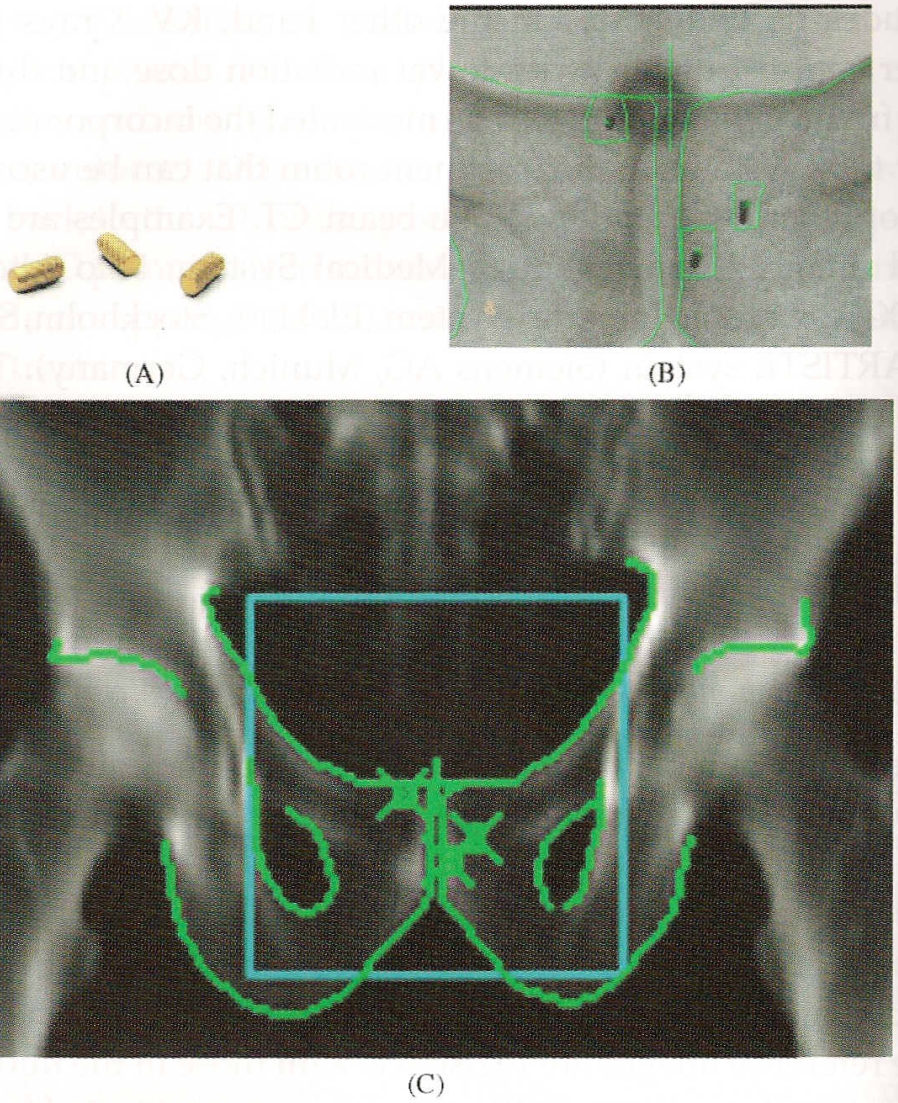

Fig. 7. (A) Fiducial markers; (B) Fiducial markers seen on KV radiographs; (C) Corresponding fiducial markers in DRR.

X-ray images generated by 2 X-ray tubes in orthogonal directions. By comparing the fiducial positions in these two images with those of the DRRs from the planning CT, the translation and rotation errors can be calculated and adjustment can be made to the treatment couch. The tracking in the Cyberknife is a continuous procedure at predetermined intervals throughout the treatment.

25.3.2.3 *Integrated CT/linear accelerator*

Reduction in geometric uncertainties requires the visualization of internal organs at treatment. CT images nowadays can be

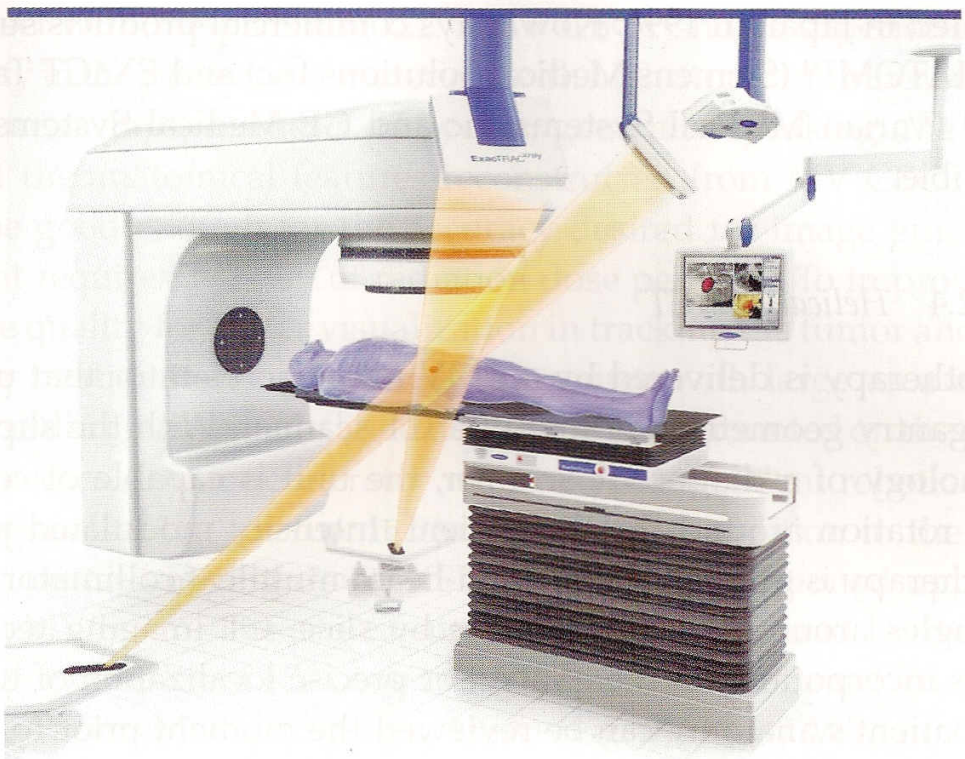

Fig. 8. ExacTrac X-ray 6D (Courtesy of BrainLAB AG, Heimstetten, Germany). The stereoscopic X-ray image sets generated allow detection of tumor movement 3-dimensionally.

reconstructed three or four dimensionally for radiation therapy. CT scan of patient in treatment position is the basis for radiation treatment planning and considered as the reference for treatment verification. A CT dataset obtained during treatment and reconstructed to similar views provides a straightforward comparison of the treatment delivered with the intended treatment plan. Therefore, more emphasis is now placed on introduction of facilities that can generate CT images in the radiation therapy treatment room.

To start with, bringing a CT scanner to the treatment room is the easiest solution. The CT scanner is mounted on rail in the treatment room and moves over the treatment couch of the linear accelerator. Patients can remain in the same position for imaging and treatment. The close proximity of the imaging CT and the treatment unit enables fine adjustments for changes in the size, shape or location of tumors and surrounding tissues by using CT images taken just before treatments are delivered. The first CT-on-rails was

installed in Japan in 1996. Nowadays commercial products such as PRIMATOM™ (Siemens Medical Solutions Inc) and EXaCT Targeting™ (Varian Medical Systems Inc and GE Medical Systems) are available.

25.3.2.4 *Helical MV CT*

Tomotherapy is delivered by a 6 MV linear accelerator that uses a ring gantry geometry like that of a CT scanner. With the slip ring technology of a diagnostic scanner, the unit is capable of continuous rotation around the the patient. Intensity modulated radiation therapy is given through a fan-beam multileaf collimator from all angles around the patient slice by slice. CT imaging technology is incorporated in the gantry for precise localization of tumor. The patient's anatomy can be reviewed the moment prior to treatment and the size, shape and intensity of the radiation beam can be adjusted to the precise location of the patient's tumor. The Hi Art System® (Tomotherapy Incorp, Middleton, WI USA) is a commercial tomotherapy unit. The energy fluence actually delivered to the patient can be computed and superimposed on a CT representation to be compared with the planned. Hence dose-guidance in addition to image-guidance is possible with tomotherapy. MV energy has the disadvantages of low inherent soft tissue contrast and poor detection efficiency of X-ray detectors.[16] Quantitative analysis of contour variations has shown to be inferior to KVCT for prostate delineation.[17]

25.3.2.5 *Cone beam CT (CBCT)*

In contrast to conventional fan-beam CT which acquires images slice by slice and in several rotations, CBCT captures a larger volume of tissue in one scan with a physically larger detector. It involves the reconstruction of 3D volumetric data from 2D projections. It works for either MV or KV X-ray beams. Example of MV Cone beam can be found in MVision™ Megavoltage Cone Beam (MVCB) (Siemens, AG, Munich, Germany). A maximization of mutual information algorithm is used to automatically register the MV CBCT

data set with the planning CT.[18] MV CBCT shows superior image quality in the presence of materials with high atomic number such as denture or hip prosthesis. However, generally speaking, the quality of the anatomical features reconstructed from MV CBCT may not be good enough for the accuracy desired for image guidance. Also it requires 1–2 cGy of radiation dose per scan. To improve the image quality for better visualization in tracking the tumor and verifying treatment setup, a KV X-ray source with large area amorphous silicon flat-panel digital detector is now mounted on the drum of a medical linear accelerator with two independent robotic arms orthogonal to the treatment beam. This is in addition to the electronic portal imaging devise (EPID) which is positioned opposite to the MV beam. The same centre of rotation is shared by the two beams. Examples of KV cone beam CT are the On-Board Imager™ (OBI) (Varian Medical System, USA) (Fig. 9), X-ray Volume Imaging (XVI) system (Synergy® Elekta Oncology, Stockholm, Sweden) and ARTISTE™ system (Siemens AG, Munich, Germany). They provide KV CT technologies for acquisition of data from cone-shaped beam of X-rays rather than from the conventional fan-beam. Images are taken at each degree of rotation. A total of 360 or more projections are collected over a thirty seconds to two minutes interval. The whole volume is reconstructed in one operation producing high resolution isotropic images instead of the conventional sliced image which are stacked after reconstruction.[19] Cone beam images have been used for body parts such as bladder, lung and prostate. After acquisition, software tools such as tile display or color wash display must be provided for processing of the images and for registration of the CBCT images with the planning CT images either manually or automatically (Fig. 10). Shifts in the x-, y- and x-direction and in the rotational direction need to be shown to indicate the corrections that should be applied to the patient setup. CBCT has shown to reveal setup error, anatomical deformation and physiological changes.[1] Other than longer acquisition times, registration is still a tedious and time-consuming procedure that deters the wide implementation of IGRT. Much effort is required to improve the efficiency of the volumetric image registration. Also, wide field scatter and the

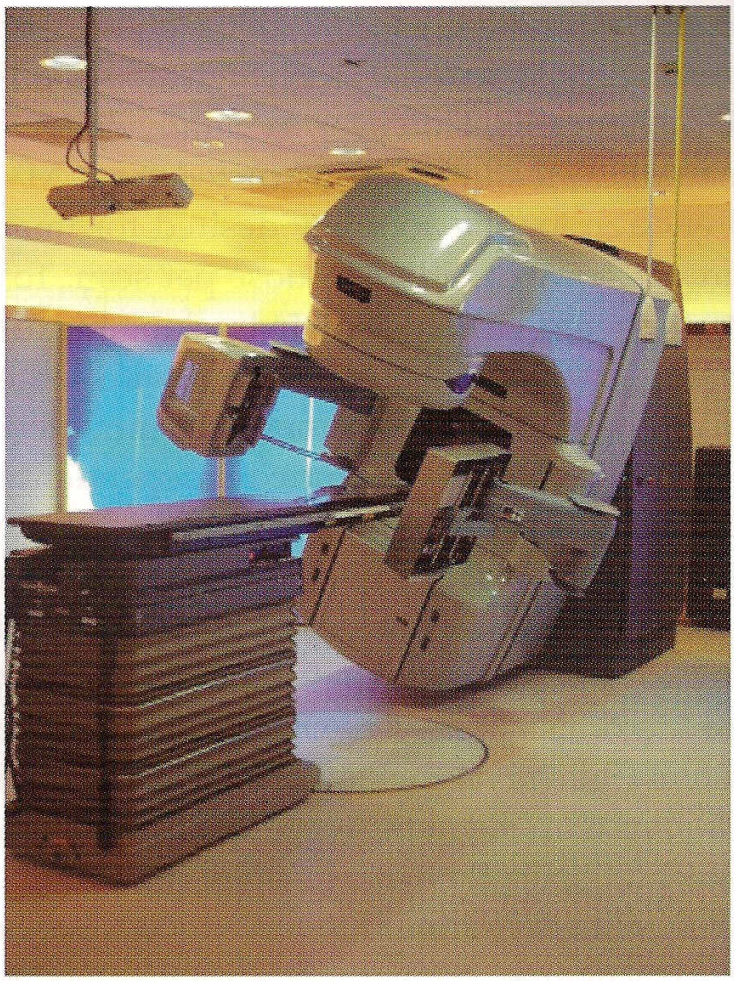

Fig. 9. A linear accelerator with an on-board imaging system orthogonal to the MV treatment beam.

slow gantry motion often introduces motion artifacts greater than conventional CT scanners.[20]

To test its accuracy, KV CBCT-based setup corrections were compared with orthogonal MV portal imaged-based corrections for patients with prostate cancer treated by external beam. The two methods correlated well using three intraprostate gold fiducial markers but less well for matching of soft tissue,[21] the visualization of which is being explored actively.

The role of CBCT has been extended to online planning and treatment delivery in a single step at the treatment unit for palliative spine metastases.[21,22] The cupping artifacts were greatly reduced by using image corrections and the accuracy of CBCT numbers was improved. Bony landmarks were sufficient for tumor definition.

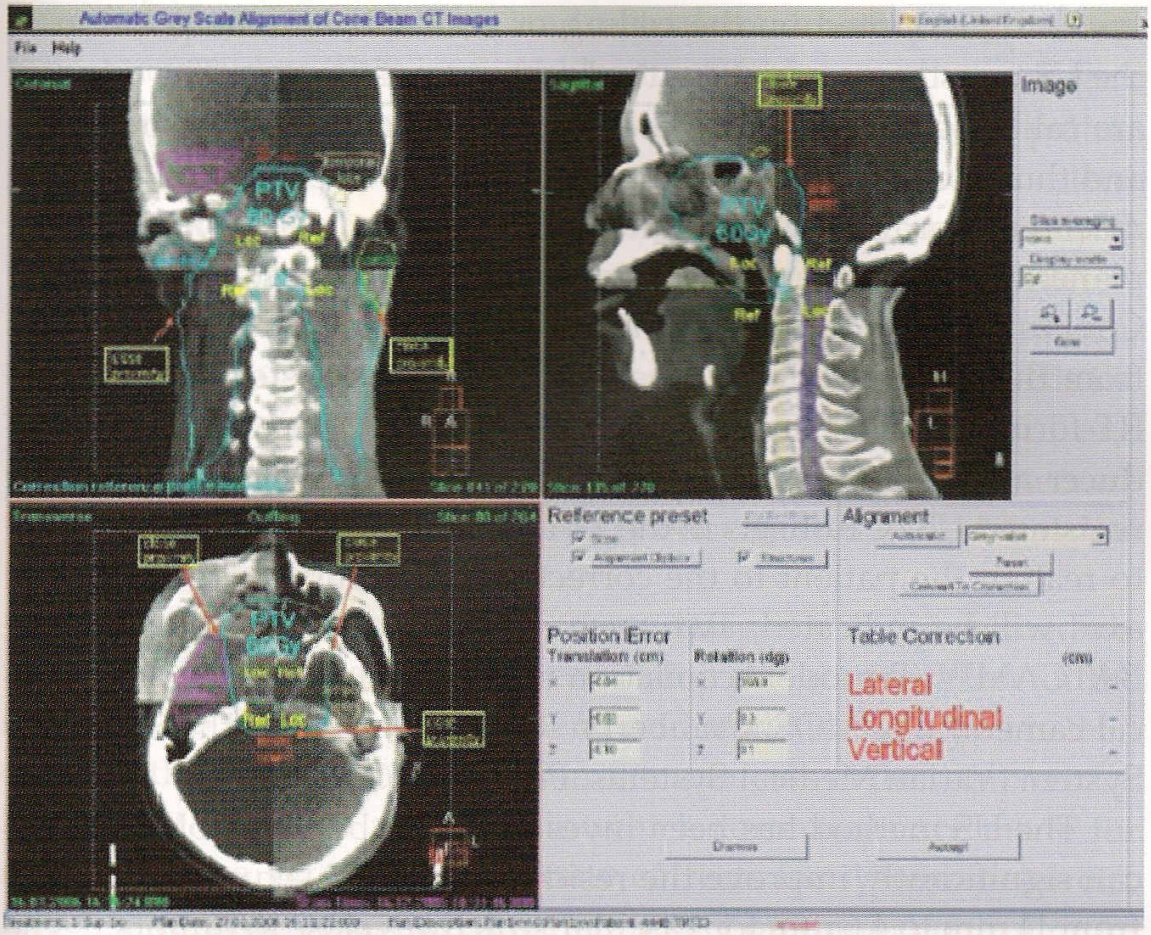

Fig. 10. CBCT/CT registration in tile display (Courtesy of Tuen Mun Hospital, Hong Kong).

Dose placement was in agreement as planned. IGRT using CT verification has proven to be a time efficient alternative to conventional verification practices and has the potential to further improve patient outcomes through better target volume localization.

25.3.2.6 *Ultrasound-guided radiation therapy*

Ultrasound (US) is a noninvasive, flexible and inexpensive imaging modality with no extra radiation dose to patients. It has a higher differential capability for soft tissues than X-ray imaging modalities. US IGRT targeting system can provide fast localization of a treatment target on a daily basis.

Such a targeting system combines US and a 3D tracking system with an interface to track tumor targets. An infrared optical camera

system is mounted on the ceiling or wall to track the position of the US transducer, which is attached to a tracking arm. The cameras are calibrated to recognize the isocenter of the treatment machine and thus the system allows the US images to be correlated with the machine coordinates. Real time US images in the axial and sagittal planes are acquired with patient at the time of treatment delivery. Contours of the tumor volume or surrounding critical structures from the planning CT, can be exported to the system in DICOM-RT format, and be superimposed onto the US images. The transducer and couch positions are calculated and correlated with the registered US/CT offsets in the X, Y, Z axes. 3D couch shift required to realign the patient to the correct position in the three principal axes will be indicated. Two such commercial US systems are the BATCAM™ (B-mode Acquisition and Targeting device with optical camera) (NOMOS, Cranberry Township, Pa) and the SonArray System (Varian Medical Systems, Palo Alto, Calif).

The US method has been investigated to be a feasible tool that can significantly improve the residual mean 3D setup error vector from 11 mm to 4.6 mm for vascular structures close to tumors.[23] The result was confirmed by repeat CT scans after repositioning. Hasan and colleagues[24] compared using the BAT™ transabdominal ultrasound system and fiducial markers with BrainLAB Exac Trac™ system for IGRT in a group of prostate cancer patients and found no difference in the acute toxicities. However, the US method is limited to abdominal and pelvic regions where no air cavities or less amount of bone is present. Interuser variation of the contour alignment was also found significant.[25,26] Potential for intrafractional treatment is limited.

25.3.3 Strategies for Error Correction

Setup variations can be separated into random and systematic components.[27] Random component is the daily variation including random patient movement and periodic movement such as breathing. Systematic component, on the other hand, is the deviation

between planning positions and actual treatment positions and repeats everyday. This is probably due to equipment inaccuracy, inaccurate outlining of target and the difference between patient positioning in CT planning and actual treatment in linear accelerator. The goal of image guidance is to improve treatment accuracy by correcting setup errors before the radiation treatment is delivered. This means imaging at the treatment room prior to each treatment and automatic or manual repositioning if misalignment exceeds the predefined tolerance upon comparison between planning CT and treatment CT. This is an online approach with immediate intervention based on predefined action level but requires more effort and time at treatment delivery.

The offline approach is to acquire images without immediate intervention. In this approach, verification images are taken for the first three to five days of treatment, and statistical analysis is then done for the systematic and random components of the setup errors. In contrast to online approach in which corrections are made for random errors, offline analysis only corrects for systematic errors, which is considered to have greater impact on tumor control probability because it may cause under dosage to the tumor volume at each fraction of the treatment. Corrections are made only at subsequent fraction. In offline approach, the treatment plan can be reoptimized to account for individual patient variations. A new plan can be developed based on the average position of the tumor or critical organs as estimated from the treatment images. Such practice is called adaptive radiation therapy (ART) and can be repeated several times during the course of radiation therapy.[28,29] Treatment parameters such as field margin, position of the MLC leaves, collimator rotation and treatment dose may be adjusted to help achieve a safe dose escalation. ART started as an offline method but can be brought online, which means based on the deviations obtained from the volumetric images, a new plan can be generated just prior to treatment delivery. Online replanning will significantly improve dose conformality and is the ultimate goal of IGRT.[30] ART is particular useful in cases of tumor regression during a course of radiation therapy.

25.3.4 Frequency of Imaging

IGRT for treatment delivery requires a change in the work pattern. Instead of taking images weekly during the treatment course, IGRT requires imaging to be done as frequently as daily or for every fraction. Also errors should be corrected immediately rather than retrospectively.

The frequency of image guidance on patients with head and neck cancer treated by a helical tomotherapy unit was evaluated.[31] Systematic setup errors are generally reduced with more frequent imaging but for fractions that were not imaged, random setup errors are not reduced. If every other treatment was imaged, about 11% of all treatments still subject to 3D setup errors of at least 5 mm. The residual setup errors could be reduced with increasing frequency of image guidance. The use of daily electronic portal imaging for improving precision in radiation therapy of prostate cancer was studied.[32] Interfraction prostate bed motion, setup error and total positional error were analyzed by comparing the location of intraprostate gold seed fiducials on the electronic portal images with those on the DRRs from the planning CT. Among the errors, the total positioning errors >5 mm were found in 14.1%, 38.7% and 28.2% of all treatment fractions in the left-right, superior-inferior and anterior-posterior axes respectively. This shows that daily imaging and immediate corrections are necessary for reduction of setup errors.

The online correction is normally based on a fixed action level. For example, correction should be done for errors >3 mm. Together with the daily imaging for verification, the workload is considerable and the procedure is costly.[33] Increasing the action levels to say 5 mm would reduce the workload but might not bring dose benefits to the organs at risk. Instead Keller and colleagues[34] proposed online correction strategies that aim for compliance with original treatment plan intent using dose volume histogram (DVH) and equivalent uniform dose (EUD) score. The new correction strategies were found to comply effectively with the initial treatment plan intent and could be tailored to individual patient. If IGRT were to be used for all conventional fractionation that requires 30–40 fractions for a full

course, the tradeoffs between benefits and cost would be a subject for debate. Considerations are now given to hypofractionation, i.e. using fewer fractions to save the setup time.[33,35]

25.4 CLINICAL RESULTS

Dose escalation to tumor will result in a rise in tumor control probability. A tighter margin around the target volume means a reduction in the volume of irradiation to normal tissue which will reduce the probability of normal tissue complications. With image guidance in a study on prostate cancer treatment, Ghilezan and colleagues[36] found that the target dose could be increased by 13% on average. Though advantage varies for individual patients, substantial dose escalation was possible in 32% of the patients. In a study by Ramsey and colleagues,[37] image-guided ART was used in a group of seven lung cancer patients to adjust the planning target volume (PTV) weekly based on the previous week's CT images used for image-guided setup. The gross target volume (GTV) was reduced by 60%–80% and the ipsilateral lung volume receiving 20 Gy can be reduced to an average of 21%. Redpath and Muren[38] found that use of IGRT in urinary bladder cancer treatment leads to significant reduction (from 30 mm to 16 mm) in the required margin for full volume coverage. Online CBCT guidance reduces the random errors in setup in partial breast irradiation when compared with the conventional method of using skin marks.[39] Preliminary geometric benefits support reduction in PTV margins in IGRT cases.[40] Whether such benefits can be translated to improvement in treatment outcome is an issue to be addressed by clinical trials.

25.5 FUTURE WORK

Research studies are ongoing evaluating the appropriateness of the image-guided technologies. The image-guided tools, whether equipment, accessories or software programs, should be able to review accurately the extent of errors that is likely to occur during

treatment and make automatic corrections. The accuracy of any new tool should be measured against the standard tools.

Current IGRT tool development is more focused on geometric precision of tumor and margins around it. Accuracy of the tools has proved acceptable. Biological and functional imaging may help provide the necessary information, not only for enhancing target definition and for treatment planning, but also to adapt the radiation dose distribution within the tumor so as to increase the tumor control probability. Image registration techniques are needed to link biological imaging with scans obtained at treatment. Methods for dose verification are also needed from IGRT tools to ensure that the delivered dose is the planned/prescribed dose.[41]

Image registration techniques for rigid transformation are well established. In IGRT, because of its varying imaging conditions and the multimodality imaging, the need for deformable image registration is on the increase and becomes a fundamental tool for image analysis. Organ deformation during respiration can be modeled[42] and organ motion or 4D planning[19] can be incorporated into the TPS. Currently, a robust and efficacious algorithm is still lacking though numerous existing methods are being validated. It is hoped that deformable registration can be a standard in radiation therapy treatment planning systems.

Thorson and Prosser[19] suggested storing the imaging data of patients with similar disease and technique for retrospective systematic analysis for better prediction of organ motion or status. For example, the bladder status at the time of treatment can be predicted from large amount of imaging data of the specific patient group for establishing treatment margin and doses. This predictive approach would provide guidelines for future IGRT planning.

25.6 SUMMARY

IGRT uses images for precise tumor and organ delineation specific for each patient and for the estimation of organ motion. Image acquisition, segmentation, registration and visualization are performed at

treatment planning. MR images can be registered to CT images and allow better target delineation. Before treatment, the target location or treatment setup is verified by different imaging technologies, the more popular one being CBCT. Registration of planning images with verification images provides the magnitude of deviations from the treatment plan intent for correction to be made or for replanning. For example, DRR from planning CT is registered with "live" 2D X-ray images taken at treatment using bony anatomy or fiducial markers or CT/CBCT 3D registration. The translation needed to register the image pairs is used to calculate a 3D setup error for the patient. For evaluation of target motion, 4D CT images are needed for planning and verification of beam gating treatment. The DRRs from 4D planning CT are to be correlated with the DRRs of CBCT on treatment unit for verification. A strong need for image registration at planning and treatment is indicated in IGRT.

References

1. Xing L, Thorndyke B, Schreibman E, Yang Y, *et al.*, Overview of image-guided radiation therapy, *Med Dosimet* **31**: 91–112, 2006.
2. Stinson, Image-guided radiation therapy, *Radiat Therapist* **15**: 139–156, 2006.
3. Huntzinger C, Munro P, Johnson S, Miettinen M, *et al.*, Dynamic targeting image-guided radiotherapy, *Med Dosimet* **31**: 113–125, 2006.
4. Heron DE, Smith RP, Andrade RS, Advances in image-guided radiation therapy — the role of PET-CT, *Med Dosimet* **31**: 3–11, 2006.
5. Dawson LA, Sharpe MB, Image-guided radiotherapy: Rationale, benefits, and limitations, *Lancet Oncol* **7**: 848–858, 2006.
6. Langen KM, Jones DTL, Organ motion and its management, *Int J Radiat Oncol Biol Phys* **50**: 265–278, 2006.
7. Dawson LA, Eccles C, Bissonnette JP, Brock KK, Accuracy of daily image guidance for hypofractionated liver radiotherapy with active breathing control, *Int J Radiat Oncol Biol Phys* **62**: 1247–1252, 2005.
8. Balter JM, Brock KK, Litzenberg DW, McShan DL, *et al.*, Daily targeting of intrahepatic tumors for radiotherapy, *Int J Radiat Oncol Biol Phys* **52**: 266–271, 2002.
9. Stromberg JS, Sharpe MB, Kim LH, Kini VR, *et al.*, Active breathing control (ABC) for Hodgkin's disease: Reduction in normal tissue

irradiation with deep inspiration and implications for treatment, *Int J Radiat Oncol Biol Phys* **48**: 797–806, 2000.
10. Shirato H, Shimizu S, Kitamura K, Nishioka T, *et al.*, Four-dimensional treatment planning and fluoroscopic real-time tumor tracking radiotherapy for moving tumor, *Int J Radiat Oncol Biol Phys* **48**: 435–442, 2000.
11. Shirato H, Shimizu S, Kunieda T, Kitamura K, *et al.*, Physical aspects of a real-time tumor-tracking system for gated radiotherapy, *Int J Radiat Oncol Biol Phys* **48**: 1187–1195, 2000.
12. Keall PJ, Joshi S, Vedam SS, Siebers JV, *et al.*, Four-dimensional radiotherapy planning for DMLC-based respiratory motion tracking, *Med Phys* **32**: 942–951, 2005.
13. Shirato H, Suzuki K, Sharp GC, Fujita K, *et al.*, Speed and amplitude of lung tumor motion precisely detected in four-dimensional setup and in real-time tumor-tracking radiotherapy, *Int J Radiat Oncol Biol Phys* **64**: 1229–1236, 2006.
14. Kuo JS, Yu C, Petrovich Z, Apuzzo MLJ, The cyberknife stereotactic radiosurgery system: Description, installation, and an initial evaluation of use and functionality, *Neurosurg* **53**: 1235–1239, 2003.
15. Cerszten PC, Ozhasoglu C, Burton SA, Vogel WJ, *et al.*, Cyberknife frameless stereotactic radiosurgery for spinal lesions: Clinical experience in 125 cases, *Neurosurg* **55**: 89–99, 2004.
16. Groh BA, Siewerdsen JH, Drake DG, Wong JW, *et al.*, A performance comparison of flat-panel imager-based MV and KV cone beam CT, *Med Phys* **29**: 967–975, 2002.
17. Song WY, Chiu B, Bauman GS, Lock M, *et al.*, Prostate contouring uncertainty in megavoltage computed tomography images acquired with a helical tomotherapy unit during image-guided radiation therapy, *Int J Radiat Oncol Biol Phys* **65**: 595–607, 2006.
18. Amies C, Bani-Hashemi A, Celi J, Grousset G, *et al.*, A multi-platform approach to image guided radiation therapy (IGRT), *Med Dosimet* **31**: 12–19, 2006.
19. Thorson T, Prosser T, X-ray volume imaging in image-guided radiotherapy, *Med Dosimet* **31**: 126–133, 2006.
20. Moore CJ, Amer A, Marchant T, Sykes JR, *et al.*, Developments in and experience of kilovoltage X-ray cone beam image-guided radiotherapy, *Br J Radiol* **79**: S66–S78, 2006.
21. Létourneau D, Wong R, Moseley D, Sharpe MB, *et al.*, Online planning and delivery technique for radiotherapy of spinal metastases using cone-beam CT: Image quality and system performance, *Int J Radiat Oncol Biol Phys* **67**: 1229–1237, 2007.

22. Yamada Y, Lovelock M, Bilsky MH, Image-guided intensity-modulated radiation therapy of spine tumours, *Current Neurology and Neuroscience Reports* **6**: 207–211, 2006.
23. Fuss M, Salter BJ, Cavanaugh SX, Fuss C, *et al.*, Daily ultrasound-based image-guided targeting for radiotherapy of upper abdominal malignancies, *Int J Radiat Oncol Biol Phys* **59**: 1245–1256, 2004.
24. Hasan IM, Reddy C, Mahadevan A, Comparison of acute toxicities when utilizing image guidance for prostate cancer external beam radiation — Ultrasound vs. fiducial markers, *J Radiat Oncol Biol Phys* **66**(3): S539–S591, 2006.
25. Langen KM, Pouliot J, Anezinos C, Aubin M, *et al.*, Evaluation of ultrasound-based prostate localization for image-guided radiotherapy, *Int J Radiat Oncol Biol Phys* **57**: 635–644, 2003.
26. Fuller CD, Thomas CR, Wong A, Cavanaugh SX, *et al.*, Image-guided intensity-modulated radiation therapy for gallbladder carcinoma, *Radioth Oncol* **81**: 65–72, 2006.
27. Bortfeld T, van Herk M, Jiang SB, When should systematic patient positioning errors in radiotherapy be corrected? *Phy Med Biol* **47**: N297–N302, 2002.
28. Yan D, Vicini F, Wong J, Martinez A, Adaptive radiation therapy, *Phy Med Biol* **42**: 123–132, 1997.
29. Yan D, Ziaja E, Jaffray D, Wong J, *et al.*, The use of adaptive radiation therapy to reduce setup error: A prospective clinical study, *Int J Radiat Oncol Biol Phys* **41**: 715–720, 1998.
30. Burgess L, Zhang T, Liang J, Wu Q, *et al.*, Image guided radiotherapy by online plan re-optimization: Studies of dosimetric benefits by treatment simulations, *Int J Radiat Oncol Biol Phys* **66**(3): S629–S630, 2006.
31. Zeidan OA, Langen KM, Meeks SL, Manon RR, *et al.*, Evaluation of image-guidance protocols in the treatment of head and neck cancers, *Int J Radiat Oncol Biol Phys* **67**: 670–677, 2007.
32. Schiffner DC, Gottschalk AR, Lometti M, Aubin M, *et al.*, Daily electronic portal imaging of implanted gold see fiducials in patients undergoing radiotherapy after radical prostatectomy, *Int J Radiat Oncol Biol Phys* **67**: 610–619, 2007.
33. Ling CC, Yorke E, Fuks Z, From IMRT to IGRT: Frontierland or Neverland? *Radiother Oncol* **78**: 119–122, 2006.
34. Keller H, Jaffray DA, Rosewall T, White E, Efficient online setup correction strategies using plan-intent, *Med Phys* **33**: 1388–1397, 2006.
35. Song WY, Schaly B, Bauman G, Battista JJ, *et al.*, Evaluation of image-guided radiation therapy (IGRT) technologies and their impact on the outcomes of hypofractionated prostate cancer treatments: A radiobiologic analysis, *Int J Radiat Oncol Biol Phys* **64**: 289–300, 2006.

36. Ghilezan M, Yan D, Liang J, Jaffray D, *et al.*, Online image-guided intensity modulated radiotherapy for prostate cancer: How much improvement can we expect? A theoretical assessment of clinical benefits and potential dose escalation by improving precision and accuracy of radiation delivery, *J Radiat Oncol Biol Phys* **60**: 1602–1610, 2004.
37. Ramsey CR, Langen KM, Kupelian PA, Scaperoth DD, *et al.*, A technique for adaptive image-guided helical tomotherapy for lung cancer, *Int J Radiat Oncol Biol Physics* **64**: 1237–1244, 2006.
38. Redpath AT, Muren LP, CT-guided intensity-modulated radiotherapy for bladder cancer: Isocentre shifts, margins and their impact on target dose, *Radiother Oncol* **81**: 276–283, 2006.
39. White EA, Lee G, Blackburn H, Nageeti T, *et al.*, ConeBeam CT guidance for daily setup of patients receiving accelerated partial breast irradiation, *J Radiat Oncol Biol Phys* **66**(3): 104, 2006.
40. Wong JR, Uematsu M, Chen T, Merrick S, *et al.*, Correction to target (PTV) underdose and rectal overdose_review of 1762 CT scans obtained during image- guided radiation therapy using an in room CT-on-rail with a linear accelerator for the treatment of prostate cancer, *J Radiat Oncol Biol Phys* **66**(3): S317–S318, 2006.
41. Wertz H, Boda-Heggemann J, Walter C, Dobler B, *et al.*, Image-guided in vivo dosimetry for quality assurance of IMRT treatment for prostate cancer, *J Radiat Oncol Biol Phys* **67**: 288–295, 2007.
42. Schreibmann E, Chen GTY, Xing L, Image interpolation in 4D CT using a BSpline deformable registration model, *Int J Radiat Oncol Biol Phys* **64**: 1537–1550, 2006.

CHAPTER 31

IT Architecture and Standards for a Therapy Imaging and Model Management System (TIMMS)

Heinz U Lemke and Leonard Berliner

Appropriate use of information and communication technology (ICT) and mechatronic (MT) systems is considered by many experts as a significant contribution to improve workflow and quality of care in the operating room (OR). This will require a suitable IT infrastructure as well as communication and interface standards, such as DICOM and suitable extensions, to allow data interchange between surgical system components in the OR. A conceptual design of such an infrastructure, i.e. a therapy imaging and model management system (TIMMS) will be introduced in this chapter.

A TIMMS should support the essential functions that enable and advance image, and in particular, patient model guided therapy. Within this concept, the image centric world view of the classical PACS technology is complemented by an IT model-centric world view. Such a view is founded in the special modeling needs of an increasing number of modern surgical interventions as compared to the imaging intensive working mode of diagnostic radiology, for which PACS was originally conceptualised and developed.

A proper design of a TIMMS, taking into account modern software engineering principles, such as service oriented architecture, will clarify the right position of interfaces and relevant standards for a surgical assist system (SAS) in general and their components specifically. Such a system needs to be designed to provide a highly modular structure. Modules may be defined on different granulation levels. A first list of components (e.g. high and low level modules) comprising engines and repositories of an SAS, which should be integrated by a TIMMS, will be introduced in this chapter.

31.1 INTRODUCTION

Since the OR and image-based interventional suites are the most cost-intensive sector in the hospital, the optimization of workflow processes has become of particular concern for healthcare providers, managers, and administrators. The understanding and management of workflows should become an integral part in the planning and implementation of complex digital infrastructures supporting diagnostic and interventional procedures (i.e. interventional radiology, minimal interventional surgery, computer assisted surgical procedures and image guided therapy (IGT)).

Examples of workflow and OR infrastructure related issues are[1]:

(1) Inefficient, ineffective and redundant processes.
(2) Inflexible "systems" of operation.
(3) Ergonomic deficiencies which hinder the workflow.
(4) Data (text, 1D, 2D, 3D, 4D) presentations not adequate, e.g. intraoperative and perioperative.
(5) Soft knowledge (info + action strategy) presentation not available.
(6) Scheduling (and tracking/RFIDing) of patients, personnel, operating rooms, equipment etc. not facilitated or coordinated (often the seeds of "busted" schedules).
(7) Too long set up times for image-guided and robotic surgery.
(8) Lack of consistent working practices/guidelines or workflows (the hospital as a high risk and high velocity "production" environment is not scripted enough, there is too much diversity of behavior).
(9) No standardized integration of surgical devices and systems.
(10) Lack of quantified information on workflow and error handling.
(11) Communication across disciplines not adequate, e.g. between radiology and surgery.

Possible solutions are:

(1) Improve situational awareness.

(2) Ensure availability of real time information regarding (peri) operative processes to respond to best practices and variances in actual patient care.
(3) Develop standard interfaces to integrate seamlessly ICT and MT systems into the OR by taking account of the special needs of imaging and modelling tools within the surgical workflow.

This leads to the concept of an ICT supported OR which may be named surgical PACS (S-PACS) or more specifically a "therapy imaging and model management system" (TIMMS). A TIMMS[2] should support the essential functions that enable and advance image, and in particular, patient model guided therapy. Within this concept, the image centric world view of the classical PACS technology is complemented by an IT model-centric world view. Such a view is founded in the special modelling needs of a number of modern surgical interventions as compared to the imaging intensive working mode of diagnostic radiology, for which PACS was originally conceptualized and developed.

A TIMMS provides the ICT based infrastructure necessary for surgical/interventional workflow management of the modern digital operation room (DOR). The concept and design of a TIMMS is based on the assumption that significant improvement in the quality of patient care, as well as ergonomic and health economic progress in the OR can only be achieved by means of an ICT infrastructure (based for example on a suitable DICOM extension) for data, image, information, model and tool communication. A proper design of a TIMMS, taking into account modern software engineering principles, such as service oriented architecture, will clarify the right position of interfaces and relevant standards for a surgical assist system (SAS) in general and their components specifically.

31.2 TIMMS AND ITS INTERFACES

Engineering of ICT systems for the assistance of surgical interventional activities implies the specification, design, implementation and testing of computer assisted surgery (CAS) or IGT systems.

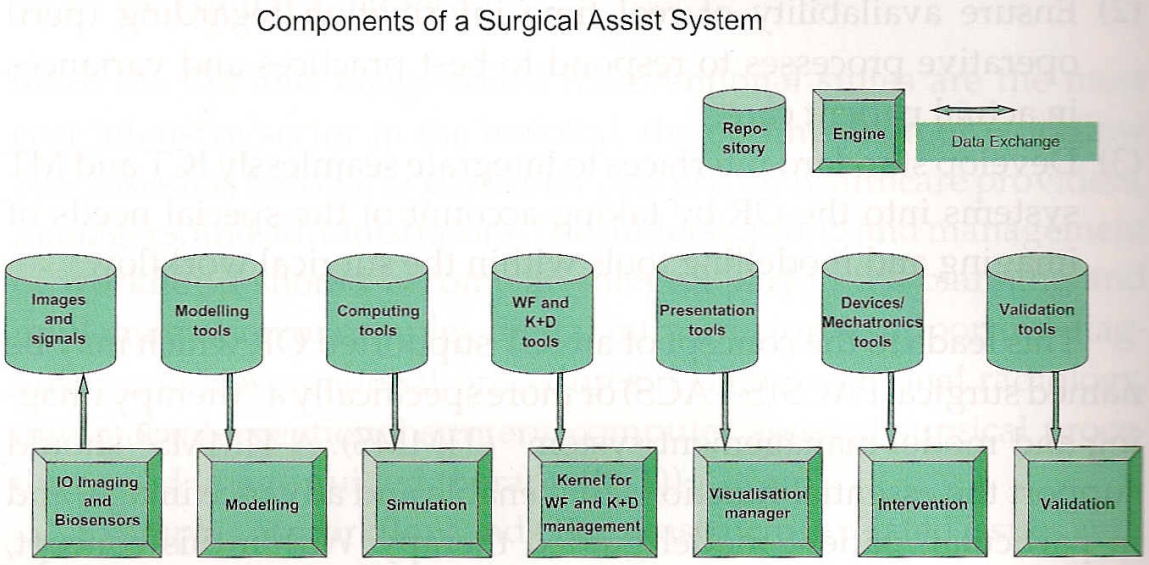

Fig. 1. Components of a surgical assist system.

A number of components for such systems have been developed in academic and industrial settings and are applied in various surgical disciplines. In most cases, however, they are stand alone systems with specific *ad hoc* propriety or vendor interfaces. They can be considered as islands of IT engines and repositories with varying degrees of modularization and interconnection.

Figure 1 shows an abstraction of seven engines with associated repositories, which may form part of an SAS. Ideally they should be integrated by a suitable TIMMS infrastructure.

Considering software engineering principles, such a system needs to be designed to provide a highly modular structure. Modules may be defined on different granulation levels. A first list of components (e.g. high and low level modules) comprising engines and repositories of an SAS, which should be integrated by a TIMMS, is currently being compiled in a number of R&D institutions and also within the DICOM "DICOM in surgery."

Figure 2 shows a concept (meta architecture) of a high level generic modular structure of a surgical assist system. The high level modules are abstracted from many specific CAS/IGT systems which have been developed in recent years. In general, a combination of these can be found in most R&D as well as commercial SAS systems.

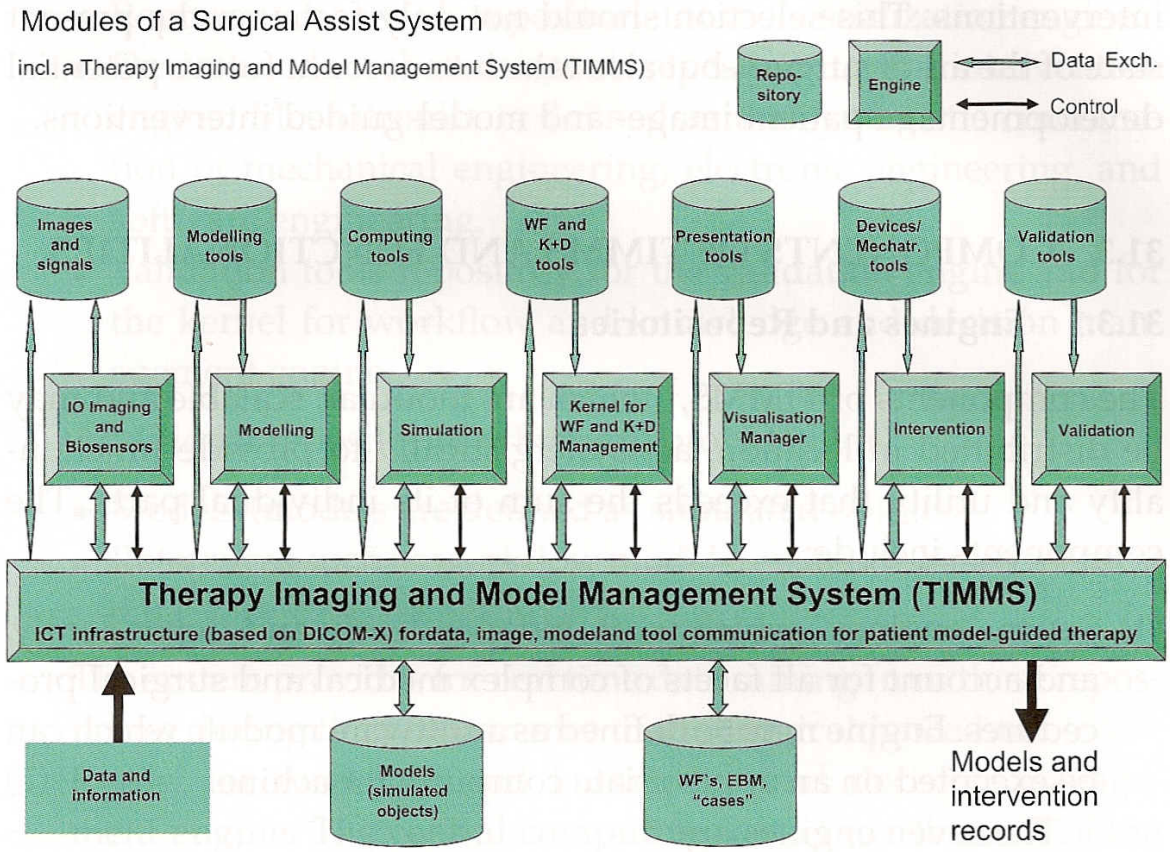

Fig. 2. Therapy imaging and model management system (TIMMS).

A central position in Fig. 2 is occupied by the "Kernel for workflow and knowledge and decision management." It provides the strategic intelligence for preoperative planning and intraoperative execution. Often this module (or parts thereof) is integrated into some of the other engines, as the need may have demanded.

Low level modules (LLM's) responsible for interfacing and communication are embedded in each of the engines and repositories given in Fig. 2. LLM's should be derived from a single or from a combination of several distinct surgical workflows. In the latter case, these are sometimes referred to as surgical integration profiles (SIP's). An LLM may be a surgical function or related activity using information objects, which ideally, may be part of different types of interventions. In order to identify LLM's which satisfy the above requirements, it is of critical importance to select a representative set of surgical/interventional workflows which cover the domain of interest for standardization of image and model-guided

interventions. This selection should not only focus on the present state of the art of surgery, but also take into account future potential developments of patient image- and model-guided interventions.

31.3 COMPONENTS OF TIMMS AND FUNCTIONALITIES

31.3.1 Engines and Repositories

The components of TIMMS,[3] which are modular, scalable and may be distributed in location, act synergistically to provide functionality and utility that exceeds the sum of its individual parts. The components include:

(1) Seven "engines" which work independently and dependently, and account for all facets of complex medical and surgical procedures. Engine may be defined as a software module which can be executed on an appropriate computing machine.

The seven engines are:

- Intraoperative imaging and biosensors engine
- Modelling engine
- Simulation engine
- Kernel for workflow and knowledge and decision management engine
- Visualization engine
- Intervention engine
- Validation engine.

(2) Associated repositories linked to each of the seven engines a repository may be defined as an integrated hardware and software structure which stores, and makes available, data and/or data processing tools.

- Images and signals repository for the intraoperative imaging and biosensors engine.
- Modelling tools repository for the modelling engine.
- Computing tools repository for the simulation engine.
- Workflow and knowledge and decision tools repository for the kernel for workflow and knowledge and decision management engine.

- Representation tools repository for the visualization engine.
- Devices and mechatronic tools repository for the intervention engine. Mechatronics is defined as the synergistic combination of mechanical engineering, electronic engineering, and software engineering.
- Validation tools repository for the validation engine and for the kernel for workflow and knowledge and decision management engine.

(3) Additional repositories which are provided for

- Models (models are defined as simulated objects).
- References such as workflow models, evidence-based medical data, case-based medical data.

The system provides for real time data mining from these repositories during the performance of the surgical procedure.

(4) Kernel for workflow and knowledge and decision management engine. The central computing kernel (or "brain") of the system may use different forms of logic, different database structuring, agents and other forms of artificial intelligence, depending on the specific applications of the procedure or procedures being performed. Agents may be defined as software modules, containing some form of intelligence, which, with some degree of autonomy and adaptability, carry out functions or tasks. Agents may be called by the workflow engine when executing a given activity component/element of a given workflow. In general, agents are part of the Kernel for workflow and knowledge and decision management, but they may also be part of and/or be accessible to the other engines of TIMMS.

(5) Information and communication technology infrastructure allowing for intercommunication and interactivity between all components of TIMMS. All of the engines, tools, repositories, ICT infrastructure, data sources, including the operative team are linked, through a distributed network, providing for the full functionality of TIMMS, including planning, guidance, learning, and data mining and processing.

The ICT infrastructure used by TIMMS includes structures, objects, processes and interfaces from well established sources, to ensure compatibility. This includes, but is not limited to:

- IHE
- HIS
- RIS
- PACS
- DICOM
- HL7

Interfaces are provided for the input of data and information from the outside world which are then processed and utilized by the functional components of TIMMS and stored within the repositories. A possible realization of interfaces required between major functional groups within and outside TIMMS is shown in Fig. 3.

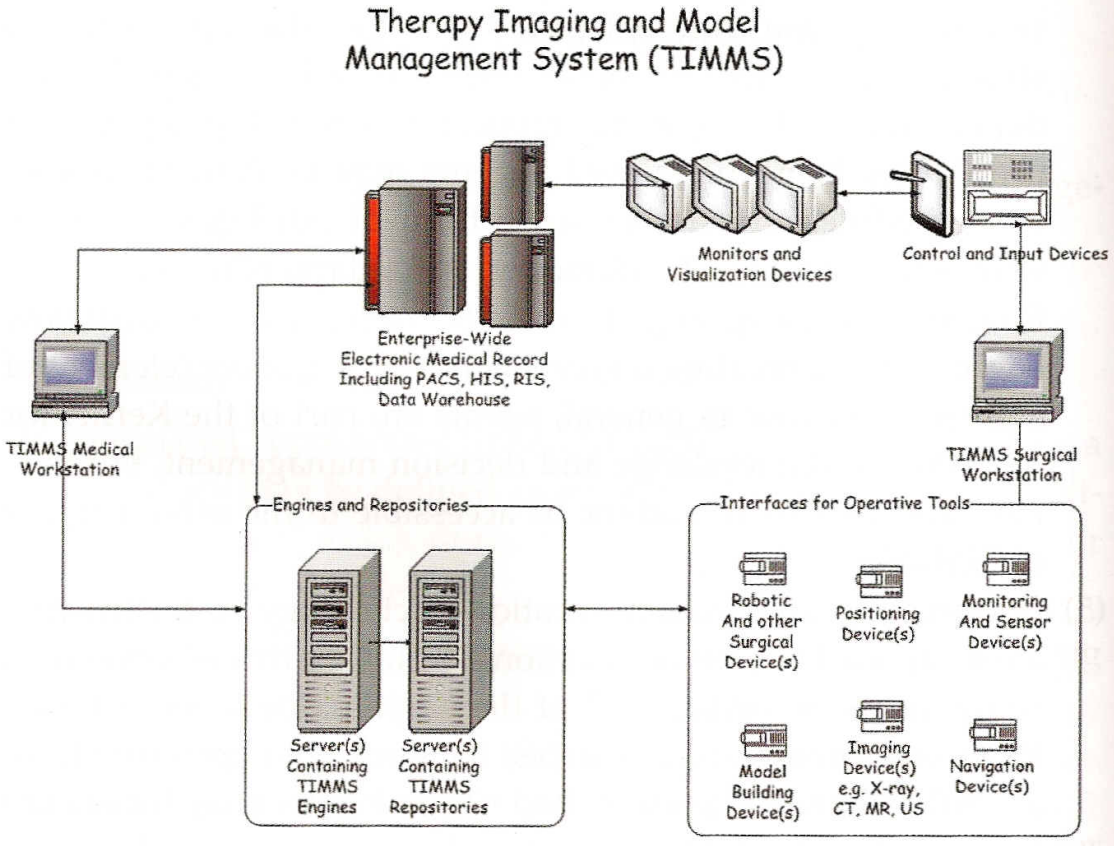

Fig. 3. Data interfaces of TIMMS.

Interfaces are also provided for the output of various models, intervention records, data and information that have been synthesized within the TIMMS structure.

31.3.2 Major Functionalities

31.3.2.1 *Patient specific modelling*

TIMMS is based on an underlying construct or approach to patient management entitled a model-centric view. Traditionally, the approach to medical imaging when applied to clinical aspects of patient care has been limited to the realm of the images themselves. This has been called the image-centric world view.

However, the approach to medical imaging employed by TIMMS is extended far beyond the realm of the images. In the model-centric world view a wide variety of information, relating to the patient, can be integrated with the images, providing a more comprehensive and robust view of the patient. TIMMS employs the model-centric world view, providing and utilizing all available data for surgical interventions.

31.3.2.2 *Adaptive workflow engines*

The incorporation and utilization of workflow processes, within the kernel for workflow and knowledge and decision management is central to the functioning of TIMMS. TIMMS employs an adaptive workflow engine that is flexible and capable of learning and providing guidance throughout the procedure. A reference workflow, which provides the basic framework for a surgical procedure, evolves into an executing workflow, which is patient specific and is based on the model-centric view of the patient that also evolves throughout the entire patient encounter. For example, modifications to the executing workflow may be based on feedback from physiologic monitoring of the patient, from the surgeon, from operative robots, from operative haptic devices, from stored data within repositories. Modifications to the executing workflow engine are in synchronization with updates to the patient model by the modelling

engine. The selected reference surgical workflows is extracted from the appropriate repository during the planning stage of the surgical procedure.

31.3.2.3 *Validation processes*

Data collection is automated for all aspects of the presurgical evaluation, intraoperative procedures, and postoperative evaluation. Methodology is provided for the application of statistical processes to the accumulated data.

The methodology for error handling and validation is built into the system so that variations in human performance, as well as machine performance, and patient response are factored in, and learned from, at any given step of the surgical procedure.

The system contains the functionality to achieve refinements in medical and surgical "best practices" and to facilitate quality improvement programs. Prospective medical research projects will be more easily achieved through the automated collection, monitoring and measuring of large volumes of data, with numerous variables.

Key aspects for the validation engine:

- Assess the surgical workflow activities, in particular the imaging, model and representations accuracy of the surgical intervention.
- Assess specific surgical domain data, information, knowledge and decision presentations, intervention protocols.
- Ascertain that the specific surgical workflow selected fulfils the purpose for which it is intended and is properly executed.
- Ascertain that selected critical activities, which imply given accuracy, precision, real time response, etc. are properly carried out.
- Ascertain that the appropriate tool sets selected from the repositories will provide the capabilities required.
- Secure that completeness and consistency checks produce the correct results.
- Ascertain that appropriate documentation and reporting for the intervention is carried out.

- Ascertain that the appropriate hardware and software devices required are online and functioning.

31.4 INCORPORATION OF SURGICAL WORKFLOW

Organized activities such as those observed in the operating room, regardless of complexity, may be better understood and characterized through the process of workflow analysis and diagramming. By analyzing, synthesizing and filtering multicomponent processes into their fundamental functional components, a workflow diagram may be generated. To provide consistency and reproducibility this process must utilize a uniform and consistent ontology. The workflow diagram thus generated may be viewed at different levels of granularity or orders. These may be described from the broadest categories (first-order processes) through the finest levels of the surgical procedure (n-order process).

The specific workflow diagrams generated through precise and analytic description of actual surgical procedures may be further distilled into generic, or reference, workflow diagrams for categories of procedures. The reference workflow diagrams thus generated provide the underlying roadmap to be followed by TIMMS throughout an entire operative procedure. This includes each of the three first-order processes: preoperative assessment and planning; operative procedure; and postoperative care.

The reference workflow diagram is a dynamic and flexible structure, designed to be transformed into a patient specific workflow, or executing workflow, by TIMMS throughout the entire procedure. The workflow Kernel and the various cognitive agents of TIMMS generate a patient-specific model from all of the available sources of data, such as imaging, physiological monitoring, EMR, data repositories, generated simulations, input and feedback from mechatronic devices. Furthermore, on the basis of changes in the patient model throughout the entire procedure, the executing workflow may be modified and updated as necessary. This provides the necessary flexibility required for a surgical procedure in which both minor and major variations are the norm. As variations or deviations from the

active executing workflow are encountered, the patient model and the executing workflow are updated as required. It should be noted that the patient specific model may be influenced by any and all factors directly impacting the procedure. These include factors that are both intrinsic and extrinsic to the patient, including the functions and status of surgical tools and devices, and activities of the operating surgeon and assistants.

As a surgical procedure progresses through the executing workflow, active links between the workflow engine and the TIMMS agents are activated in sequence in order to accomplish the tasks required for TIMMS to help facilitate the surgical process.

A reference workflow diagram for an hepatic tumor radiofrequency ablation procedure, which will be used to demonstrate the active links between workflow and TIMMS in Sec. 31.5, is presented in Figs. 4(A)–4(E).

31.5 EXAMPLE OF A TIMMS PROJECT

31.5.1 Active Links Between Surgical Workflow and TIMMS

A TIMMS project is designed to function throughout a surgical workflow at all levels of granularity of each of the three first-order processes: preoperative assessment and planning; operative procedure; and post-operative care, as described in Sec. 31.4. The initiation of a TIMMS project, in a clinical setting, may be considered to take place at the time a request for a procedure is received by the surgeon, and concludes when all post-operative care issues and post-operative quality assurance and archiving activities have been addressed.

An example of a TIMMS project (treatment for a solitary liver metastasis from a previous colon cancer with radiofrequency ablation) is presented in this section. The relationship between the workflow steps and accompanying TIMMS functions and actions are outlined in detail. Schematically, this will be represented as connections between the workflow steps and the TIMMS agents and engines which are accessed through the TIMMS network [Fig. 5(A)].

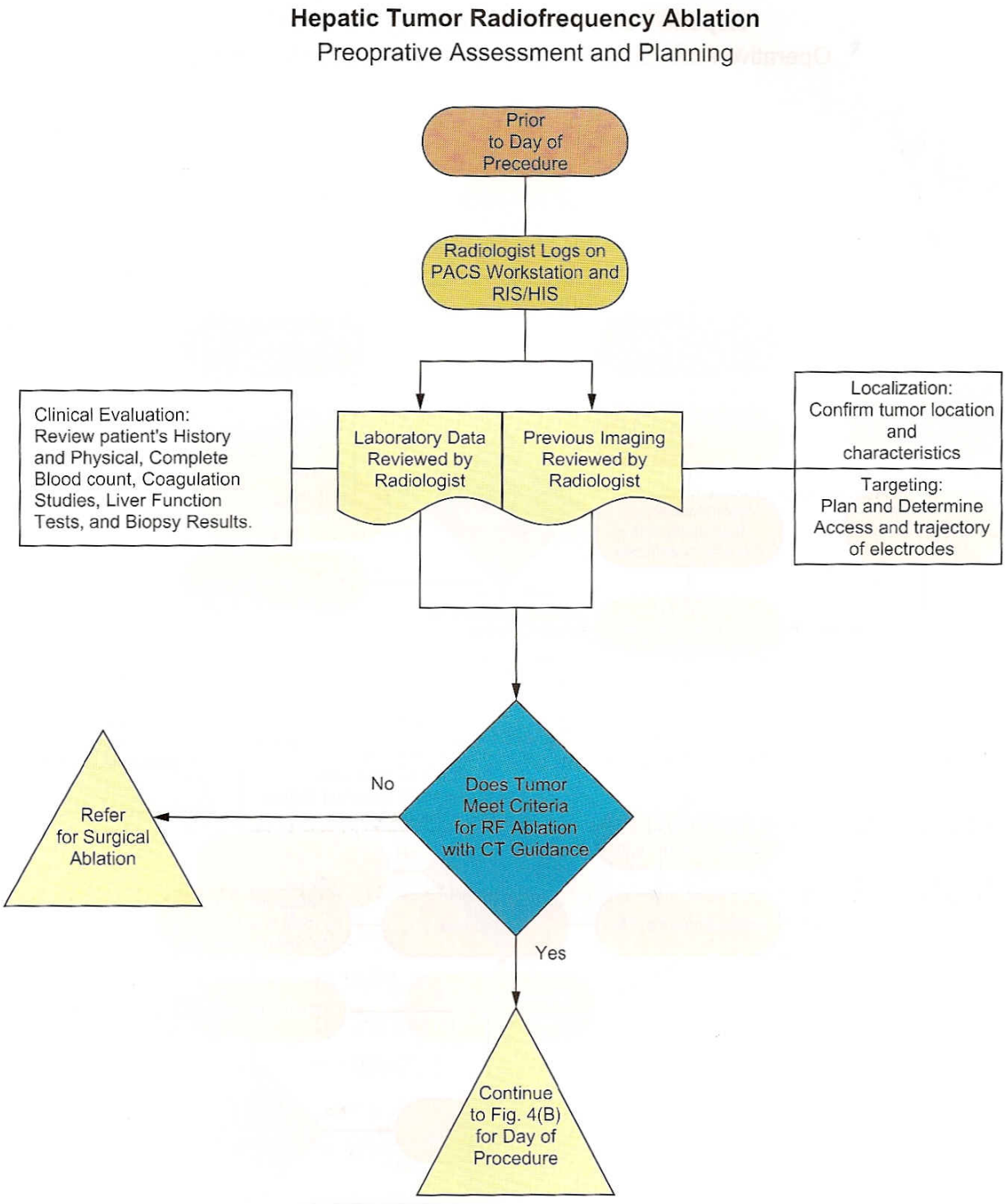

Fig. 4(A). The workflow steps involved in preoperative assessment and planning (the initial first-order process) for an hepatic tumor radiofrequency ablation procedure.

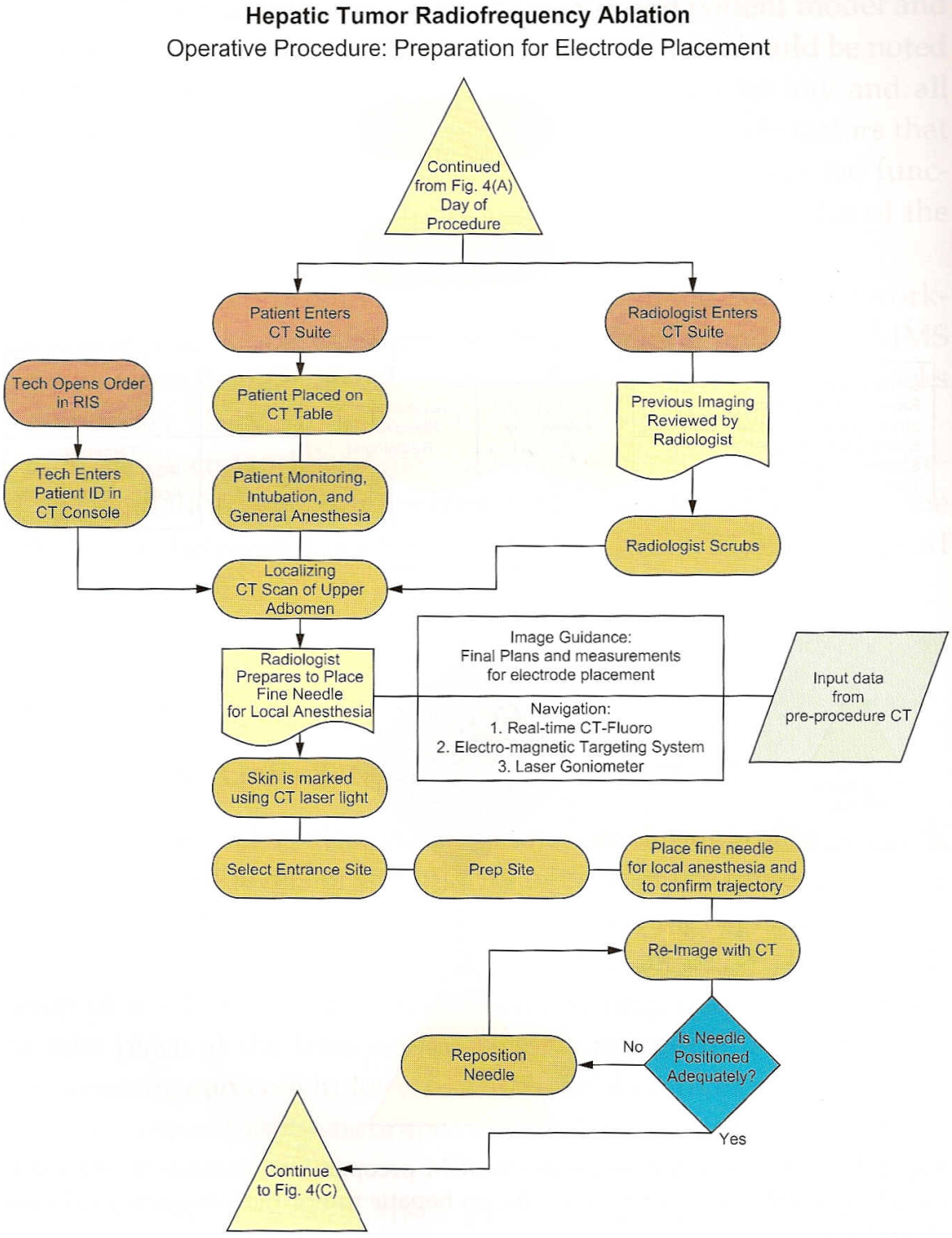

Fig. 4(B). The initial workflow steps involved in the operative procedure (the second first-order process) for an hepatic tumor radiofrequency ablation procedure. This portion of the workflow covers the preparatory steps required for placement of the radiofrequency electrode.

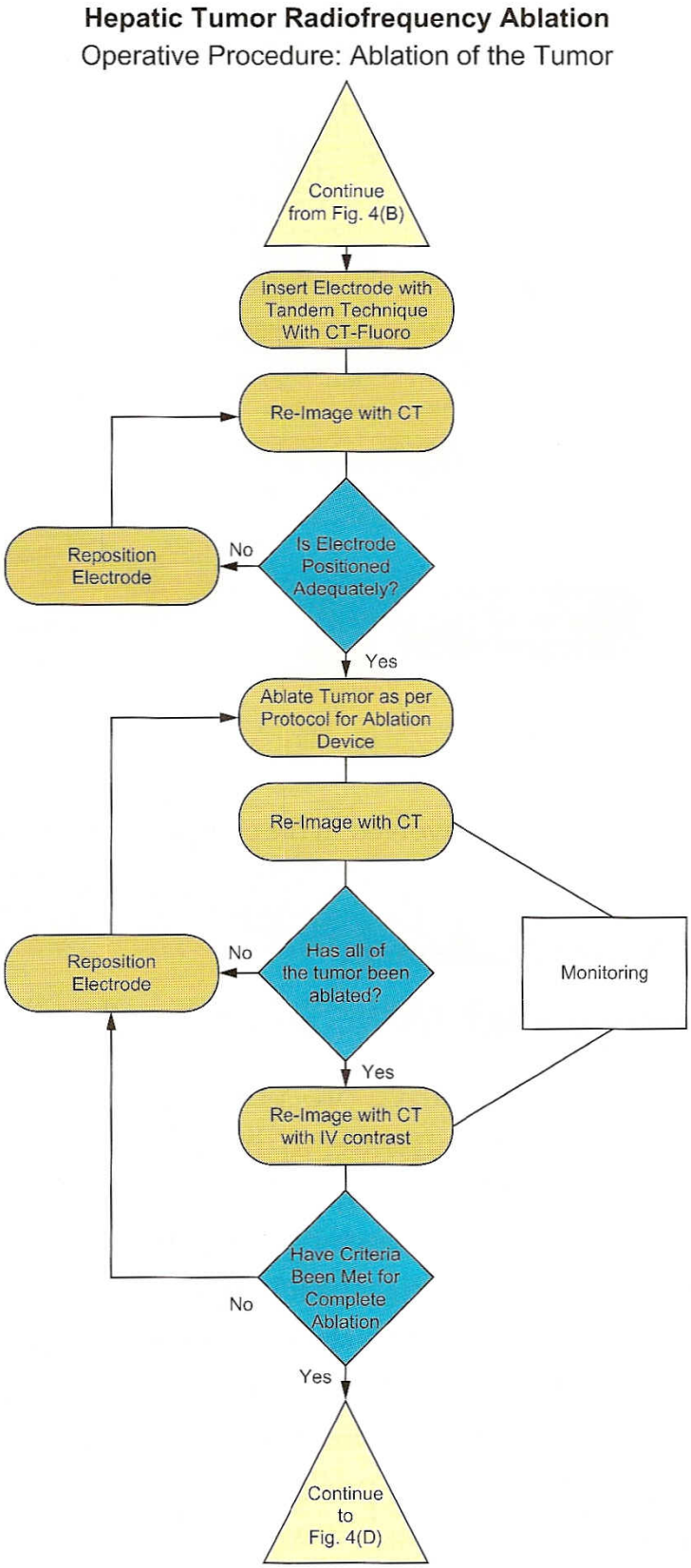

Fig. 4(C). The next workflow steps involved in the operative procedure for an hepatic tumor radiofrequency ablation procedure. These workflow steps are related to the ablation process.

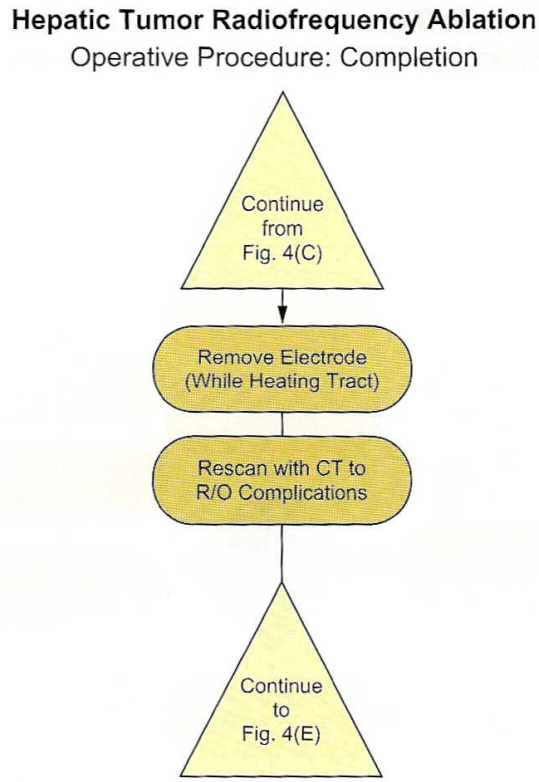

Fig. 4(D). The workflow steps involved in the completion of the ablation process.

31.5.2 Preoperative Assessment

31.5.2.1 *Initiation of a new TIMMS project*

When a request for an operative procedure is received, the surgeon may launch the TIMMS software to initialize a new project at a TIMMS medical workstation [Fig. 5(B)]. The TIMMS engines and repositories will start up and undergo an automated system check, and all of the engine activities which operate in the background will commence. At this time, the *validation engine* will check that all TIMMS software components are online and functioning properly. The default settings of all connected hardware and software devices will be initialized and their proper function will also be confirmed by the *validation engine. At this time, the surgeon may modify the specific connections* through the TIMMS computer interface.

The surgeon will then establish a new "TIMMS PROJECT" which will have its own unique *TIMMS Project ID Number and will enter* patient's name and medical record number. In order for TIMMS to

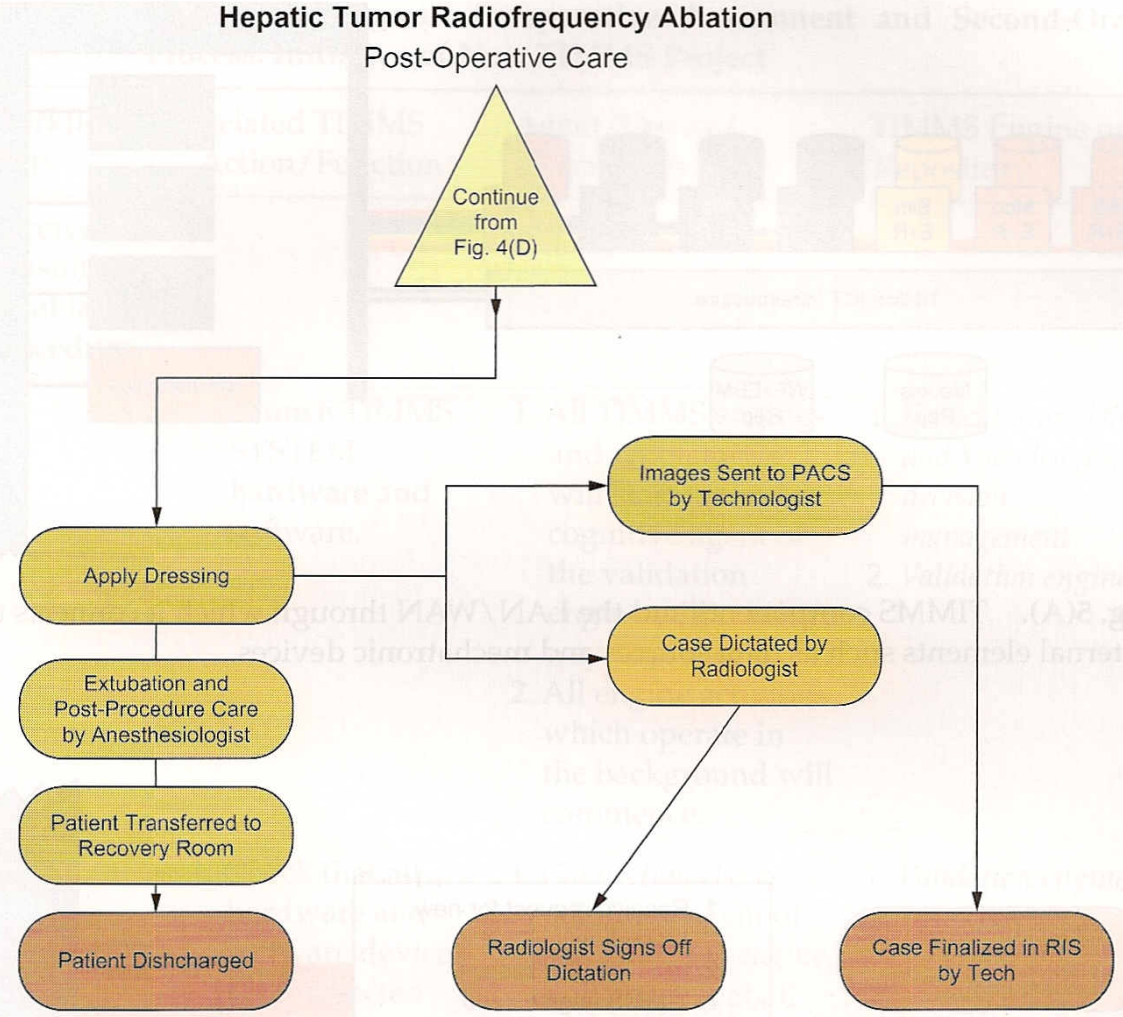

Fig. 4(E). The workflow steps involved in post-operative care (the third first-order process) for a hepatic tumor radiofrequency ablation procedure.

begin to select the appropriate reference workflow from the *workflow repository* and to perform the data mining from electronic medical records and *data repositories*, the surgeon will enter identifying features of the surgical procedure to be performed, such as a procedure class (radiofrequency ablation) and code (solitary liver metastasis from colon cancer). The reference workflow would be selected by a cognitive agent of the *kernel for workflow and knowledge and decision management* (*workflow kernel*). The data mining functions are mediated by the *electronic medical record* (*EMR*) *agent* of the *workflow kernel*. Patient information and images would be retrieved from sources including the radiology information system (RIS), hospital information system (HIS), picture archiving and communications system (PACS) and from TIMMS data repositories.

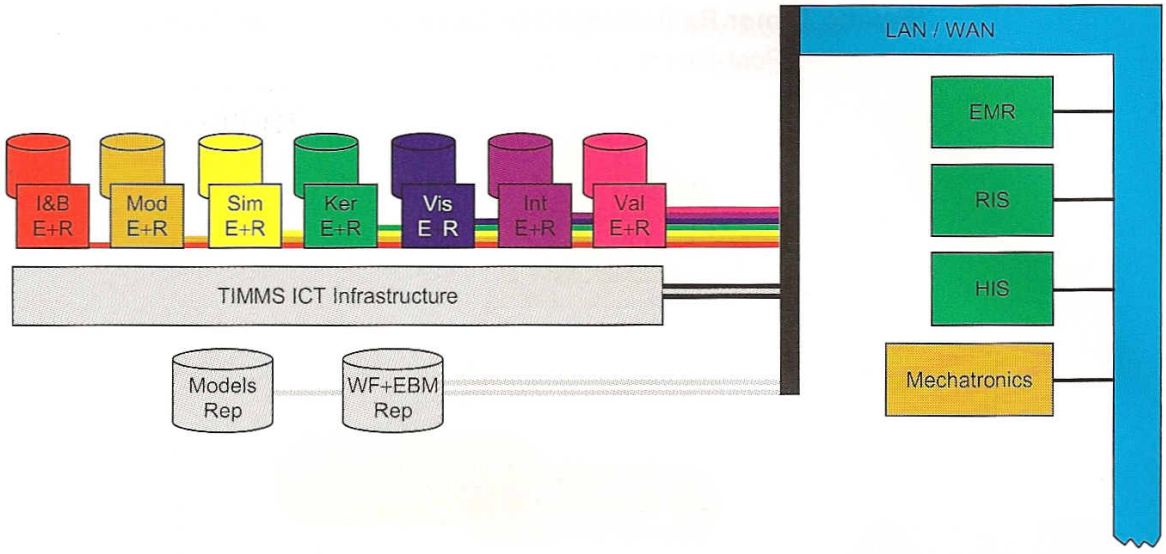

Fig. 5(A). TIMMS components and the LAN/WAN through which it connects to external elements such as data sources and mechatronic devices.

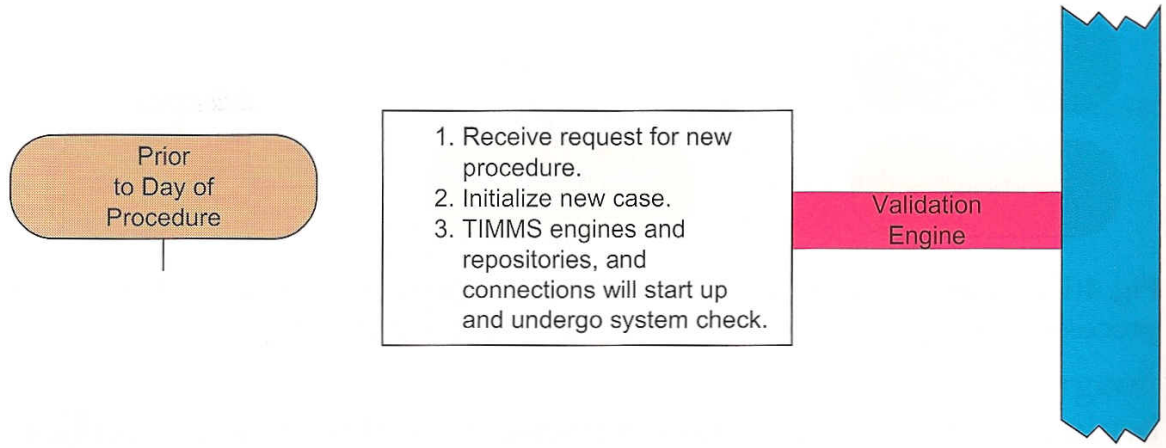

Fig. 5(B). The initial links between the surgical workflow and TIMMS when a request for a procedure is first received and the TIMMS software is started up.

31.5.2.2 *Collection of patient information and images*

A TIMMS cognitive agent, the *EMR Agent*, performs retrieval of data from the electronic medical record and the data repositories. This includes all relevant patient information, such as history and physical, past medical history, laboratory data, pathology reports, consultations, etc. The *imaging agent* of the TIMMS *Imaging and Biosensors Engine* will also retrieve and download pertinent medical imaging studies [Fig. 5(C)]. 149

Table 1. First-Order Process: Preoperative Assessment and Second-Order Process: Initiative of New TIMMS Project

Workflow Step	Related TIMMS Action/Function	Agent/Device/ Description	TIMMS Engine or Repository
Receive consult for RF ablation procedure.			
	1. Launch TIMMS SYSTEM hardware and software.	1. All TIMMS engines and repositories will start up and a cognitive agent of the validation engine will conduct a system check. 2. All engine activities which operate in the background will commence.	1. *Kernel for workflow and knowledge and decision management.* 2. *Validation engine.*
	1. Check that all hardware and software devices are connected and functioning.	1. *Connection checker,* a cognitive agent of the *validation engine,* will check that all external hardware and software devices are connected and functioning through the TIMMS infrastructure.	1. *Validation engine.*
Initialize new case.	1. Establish a new "TIMMS PROJECT" which will have its own unique TIMMS Project ID # . 2. Enter patient name, medical record number, procedure class (RFA) and code (liver metastasis).		

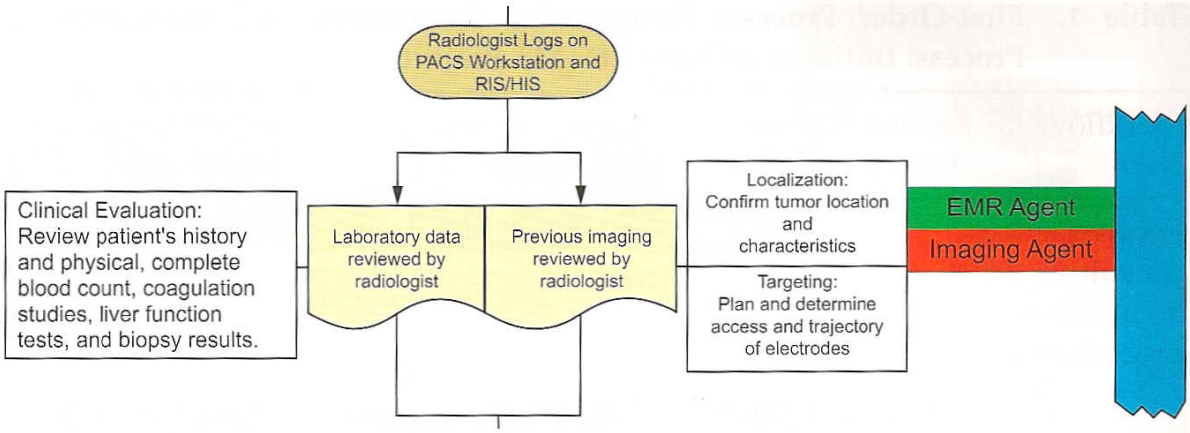

Fig. 5(C). The links between the surgical workflow and TIMMS for collecting the required clinical information and images from the electronic medical record (which may include PACS, HIS, and RIS systems, as well as TIMMS data repositories). This includes patient information and imaging data. The *Patient-Model Integrator* creates and updates the patent-model which is used by TIMMS throughout the operative procedure.

Table 2. First-Order Process: Preoperative Assessment, Second-Order Process: Collection of Patient Information and Images

Workflow Step	Related TIMMS Action/Function	Agent/Device/ Description	TIMMS Engine or Repository
Collect all known patient data.	1. Access the electronic medical record (EMR) to download all patient information; history and physical; lab data; pathology results.	1. *EMR agent* accesses HIS, and RIS systems, as well as TIMMS data repositories.	1. *Kernel for workflow and knowledge and decision management.* 2. *Data repository.*
Collect all known patient images.	1. Access the EMR to download all pertinent patient imaging studies.	1. *Imaging agent* accesses PACS and TIMMS data repositories.	1. *Imaging and biosensors engine.* 2. *Data repository.*

31.5.2.3 *Development of the patient model and treatment plan*

Once the required patient information and images are retrieved and made available, the next step is determining whether or not the metastatic tumor in the liver from a previous colon cancer, in this patient, meets criteria for treatment with radiofrequency ablation [Fig. 5(D)].

One of the core functions throughout the TIMMS project is the creation and maintenance of the patient-model [Fig. 5(D)]. A cognitive agent of the TIMMS *modeling engine*, the *Patient-model integrator*, which creates and updates the patient-model, will be activated. The information compiled in the patient-model is used to determine whether the patient is a suitable candidate for undergoing radiofrequency ablation and if the features of the lesion are favorable for radiofrequency ablation. Examples of parameters collected and analyzed would include the features of the tumor (histological characteristics; stage, grade, size/volume; shape; proximity to surface, diaphragm, vessels; portal vein patency and flow; proximity of diaphragm, gallbladder, colon, stomach); imaging features (CT, ultrasound, MRI, PET characteristics); and, previous treatment (systemic chemotherapy, surgery, chemoembolization). Information obtained from the previously retrieved images [Fig. 5(B)] would be used to determine feasibility of treatment based on location of

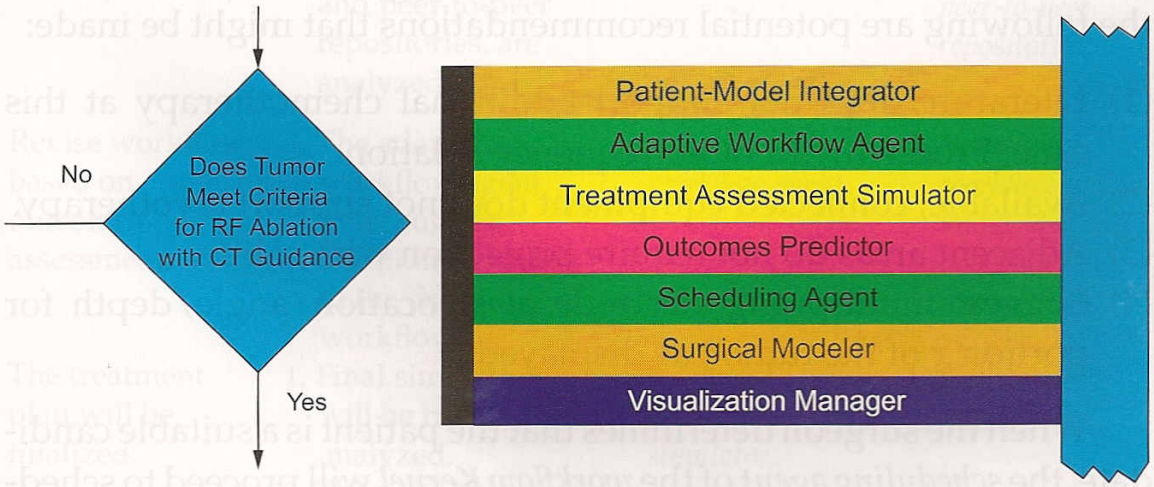

Fig. 5(D). TIMMS components that are called into play in order to create the patient model, to determine the feasibility of the proposed radiofrequency ablation treatment, and to specify the treatment plan.

the tumor, and, the access and trajectory of the electrodes to be employed.

Another of the core functions of a TIMMS project is the selection of the reference workflow and its modification into an executing workflow which is updated as changes in the patient-model are encountered. The *adaptive workflow agent* and the *treatment assessment simulator* of the *workflow kernel* and the *simulation engine*, respectively, would be instrumental in determining the suitability of radiofrequency ablation and in selecting the appropriate reference workflow, in this example, all available workflows for radiofrequency ablation of solitary hepatic metastasis from colon cancer would be considered [Fig. 5(D)]. A group of possible reference workflows would be selected, simulations would be conduct, and the "best-fit" reference workflow would be selected. The reference workflow would then be transformed into the executing workflow based on the specific features delineated in the patient-model. This executing workflow forms the basis for the treatment plan.

Cognitive agents of the *workflow kernel* and *validation engines*, such as the *outcomes predictor*, then perform data mining and outcomes predictions [Fig. 5(D)]. The patient-model, the executing workflow, and data mined from *data and peer-to-peer repositories*, are analyzed by the surgeon, assisted by the *workflow kernel*, to provide a prospective quantitative and qualitative assessment of the likelihood of technical success. If the outcomes prediction is favorable, the following are potential recommendations that might be made:

(1) Literature does not support additional chemotherapy at this time; Proceed with radiofrequency ablation.
(2) Available, connected equipment does not support cryotherapy.
(3) Adjacent areas do not require protection with saline.
(4) Suggest multi-prong electrode at x location/angle/depth for portion x of the tumor, as displayed.

When the surgeon determines that the patient is a suitable candidate, the *scheduling agent* of the *workflow Kernel* will proceed to schedule the procedure [Fig. 5(D)], and the TIMMS will continue to update the patient-model and executing workflow, in the background as

Table 3. First-Order Process: Preoperative Assessment, Second-Order Process: Development of Patient Model and Treatment Plan

Workflow Step	Related TIMMS Action/Function	Agent/Device/ Description	TIMMS Engine or Repository
Evaluation of whether the liver metastasis in this patient, meets criteria for treatment.	1. A comprehensive working patient model is constructed and maintained throughout the procedure.	1. *Patient-model integrator* creates and updates patent-model.	1. *Modeling engine.*
Select treatment plan.	1. A group of possible reference workflows are selected. 2. Conduct simulations. 3. Select "best-fit" "executing workflow."	1. Adaptive workflow agent. 2. *Treatment assessment simulator.*	1. *Kernel for workflow and knowledge and decision management.* 2. *Simulation engine.*
Assess feasibility; outcome probabilities; determine potential pitfalls.	1. Outcome prediction is performed. 2. The patient specific model, the executing workflow, data mined from data and peer-to-peer repositories, are analyzed.	1. *Outcomes predictor* perform data mining and outcomes predictions.	1. *Kernel for workflow and knowledge and decision management.* 2. *Validation engine.* 3. *Data and peer-to-peer repositories.*
Revise workflow based on outcomes assessment.	1. The adaptive workflow agent will "suggest" additional changes to the executing workflow.	1. *Adaptive workflow agent.*	1. *Kernel for workflow and knowledge and decision management.*
The treatment plan will be finalized.	1. Final simulation will be run and analyzed. 2. The final executing workflow is accepted.	1. *Treatment assessment simulator.*	1. *Simulation engine.*

(Continued)

Table 3. (*Continued*)

Workflow Step	Related TIMMS Action/Function	Agent/Device/ Description	TIMMS Engine or Repository
The procedure is scheduled.	1. The procedure is scheduled through the interface with RIS/HIS.	1. The *scheduling agent.*	1. *Kernel for workflow and knowledge and decision management.*
Patient undergoes presurgical laboratory testing and anesthesia assessment.	1. The patient model is updated with results from presurgical testing. 2. Simulation reassessed automatically. 3. Any changes are highlighted.	1. *EMR agent* retrieves patient data. 2. *Patient-model integrator* updates patent-model. 3. *Treatment assessment simulator* performs simulations.	1. *Kernel for workflow and knowledge and decision management.* 2. *Modeling engine.* 3. *Simulation engine.*
The executing workflow is revised if indicated.	1. The adaptive workflow agent will "suggest" changes to the executing workflow based on current data.	1. *Adaptive workflow agent* suggests revisions to executing workflow.	1. *Kernel for workflow and knowledge and decision management.*
3D illustrations and models may be constructed.	1. Preoperative 3D illustrations or models may be created to facilitate surgery.	1. Cognitive agents of the *modeling and visualization manager engines* are used to create required diagrams and illustrations.	1. *Visualization manager engine.* 2. *Modeling engine.*

any additional information, such as laboratory data collected during presurgical testing, is accumulated.

If needed, 3D illustrations or 3D models to facilitate surgery are created by the *visualization manager* and *surgical modeling engines* [Fig. 5(D)]. Through its infrastructure, TIMMS is capable of remotely

initiating the design and building of surgical 3D models by devices that are networked to TIMMS.

31.5.3 Operative Procedure

31.5.3.1 *Initiation of operation and patient assessment*

On the day of the operative procedure, after the TIMMS is started up and its functions and connections are checked and the physiological monitoring has been initiated, the *patient model integrator* updates patient-model from real time physiologic data. Revisions to workflow are suggested by the *adaptive workflow agent* of the *workflow engine* as the *patient model integrator* updates the patient-model [Fig. 5(E)].

Prior to the onset of the administration of anesthesia and the onset of the surgical procedure, preanesthesia assessment is required to ensure patient safety. Patient data is acquired by the efforts of the *imaging and biosensors engine* and the *patient safety agent* of the *validation engine*, and/or entered by operating room personnel. The procedure can only commence when the preanesthesia assessment is complete [Fig. 5(E)].

At the onset of the procedure the cognitive agents of the *workflow kernel* monitor, the procedure in parallel with the evolving executing workflow, recording the actual executing workflow ultimately used.

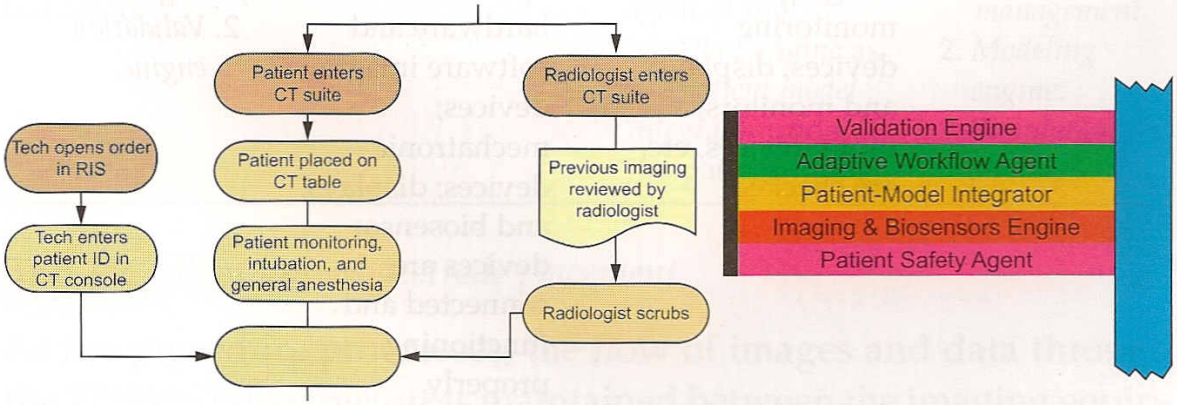

Fig. 5(E). TIMMS components utilized during the initiation of the operative procedure and during preanesthesia patient assessment.

Table 4. First-Order Process: Operative Procedure, Second-Order Process: Initiation of Operation and Preanesthesia Assessment

Workflow Step	Related TIMMS Action/Function	Agent/Device/ Description	TIMMS Engine or Repository
	Launch TIMMS SYSTEM hardware and software.	1. All TIMMS engines and repositories will start up and undergo system check. 2. All engine activities which operate in the background will commence.	*Validation engine.*
	1. Check that all TIMMS hardware and software devices are connected and functioning. 2. Use "default settings" or modify the specific connections. 3. Re-enter the unique TIMMS project ID #.	1. *Connection checker* confirms that all TIMMS hardware and software devices are connected and functioning.	*Validation engine.*
	1. Connections and links between imaging devices, monitoring devices, displays and monitors, input devices, etc. are checked.	1. Cognitive agents check that all operative hardware and software imaging devices; mechatronic devices; displays; and biosensor devices are connected and functioning properly.	1. *Imaging and biosensors engine.* 2. *Validation engine.*

(Continued)

Table 4. (*Continued*)

Workflow Step	Related TIMMS Action/Function	Agent/Device/ Description	TIMMS Engine or Repository
Workflow monitoring begins.	1. Initiate workflow.	1. *Adaptive workflow agent* monitors the progress of the executing workflow; any changes to the executing workflow are recorded.	1. *Kernel for workflow and knowledge and decision management.*
Patient monitoring begins.	1. The patient model is updated from real time physiologic data.	1. *Patient model integrator* update patient-model as the operation progresses.	1. *Imaging and biosensors engine.* 2. *Modeling engine.*
Preanesthesia assessmsnt.	1. To ensure patient safety, an indicator will be displayed and the procedure can continue, only when the preanesthesia assessment is complete.	1. *Patient safety agent* ensures that preanesthesia assessment is complete and within acceptable limits.	1. *Validation engine.* 2. *Workflow kernel.*
The executing workflow is revised if indicated.		1. Revisions to workflow are suggested by the *adaptive workflow agent* of the *workflow engine* as the *patient model integrator* updates the patient-model.	1. *Kernel for workflow and knowledge and decision management.* 2. *Modeling engine.* 3. *Simulation engine.*

31.5.3.2 *Planning of electrode placement*

As the procedure progresses, the flow of images and data through the *TIMMS Infrastructure* is maintained between the imaging equipment (e.g. the CT scanner and/or ultrasound) and the *registration and navigation agents* of the *intervention engine*. Mechatronic and

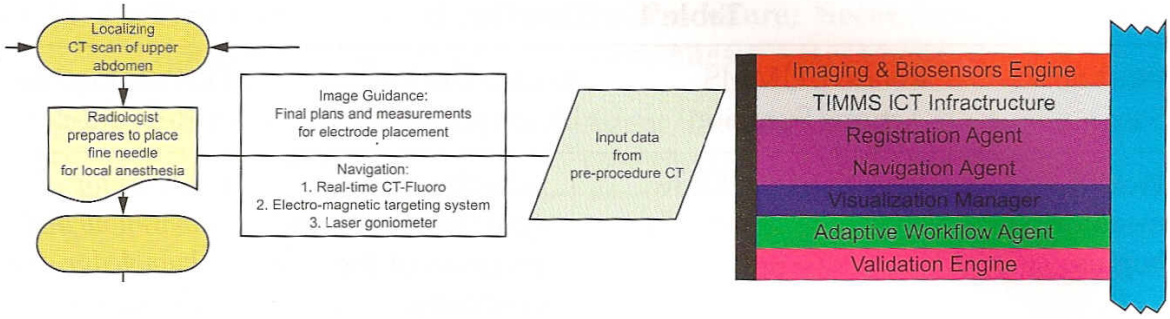

Fig. 5(F). TIMMS components in preparing for electrode placement.

navigation devices are brought online. All available imaging and physiologic data is fed through the *TIMMS infrastructure* to the mechatronic and navigation devices for maximum operative precision. This data is also assimilated by the *adaptive workflow agent* into the executing workflow [Fig. 5(F)].

Any additional visualization devices, such as stereoscopic overlay, are brought online, with all available data and images input from the *visualization manager engine*.

Once all available data has been processed by TIMMS, the *adaptive workflow agent* makes final revisions to the executing workflow, and the efficacy of the proposed treatment is confirmed through the *validation engine* [Fig. 5(F)].

31.5.3.3 *Placement of fine needle*

When the final, specified coordinates, angles, and depths of electrodes are calculated and displayed, the surgeon then proceeds with skin preparation and administration of anesthesia. A fine needle, long enough to extend from the skin to the tumor to be ablated, is deployed for two purposes. This needle will be used to administer local anesthesia and to verify adequacy of the planned electrode trajectory. This fine needle will also serve as a guiding needle for "tandem" placement of the radiofrequency (RF) electrode along side the fine needle.

Feedback from Navigational devices will dictate modifications to the executing workflow by the *adaptive workflow agent* [Fig. 5(G)].

Table 5. First-Order Process: Operative Procedure, Second-Order Process: Planning of Electrode Placement

Workflow Step	Related TIMMS Action/Function	Agent/Device/ Description	TIMMS Engine or Repository
Planning is made for electrode placement.	1. Imaging registration begins. 2. Technologist/ physician begin imaging the patient. 3. Feedback from the imaging modalities that are used, such as CT and/or ultrasound, are fed into TIMMS.	1. The flow of images and data through the TIMMS Infrastructure is maintained between the imaging equipment (e.g. the CT scanner and/or ultrasound) and the *registration and navigation agents.* 2. This data is then assimilated by the *adaptive workflow agent* into the executing workflow.	1. *Intervention engine.* 2. *Imaging and biosensors engine.* 3. *Workflow engine.*
Mechatronic set up (robotics, navigation).	1. Mechatronic and Navigation devices are brought online. 2. Feedback from the mechatronic and navigation devices are transmitted to TIMMS.	1. Flow of images and data is maintained between TIMMS and mechatronic and navigation devices. 2. This data is then assimilated by the *adaptive workflow agent* into the executing workflow.	*1. Intervention engine.* *2. Workflow engine.*
Visualization (such as stereoscopic overlay) set-up.	1. Additional visualization devices are brought online. 2. Data/images are input from TIMMS.	1. Flow of images and data is maintained between TIMMS and visualization hardware and software.	*1. Visualization manager engine.*
Final adjustments made to executing workflow.	1. Modification and acceptance of executing workflow.	1. *Adaptive workflow agent* makes final revisions to executing workflow. 2. Final coordinates, angles, depths of electrodes are displayed.	*1. Kernel for workflow and knowledge and decision management.* *2. Validation engine.*

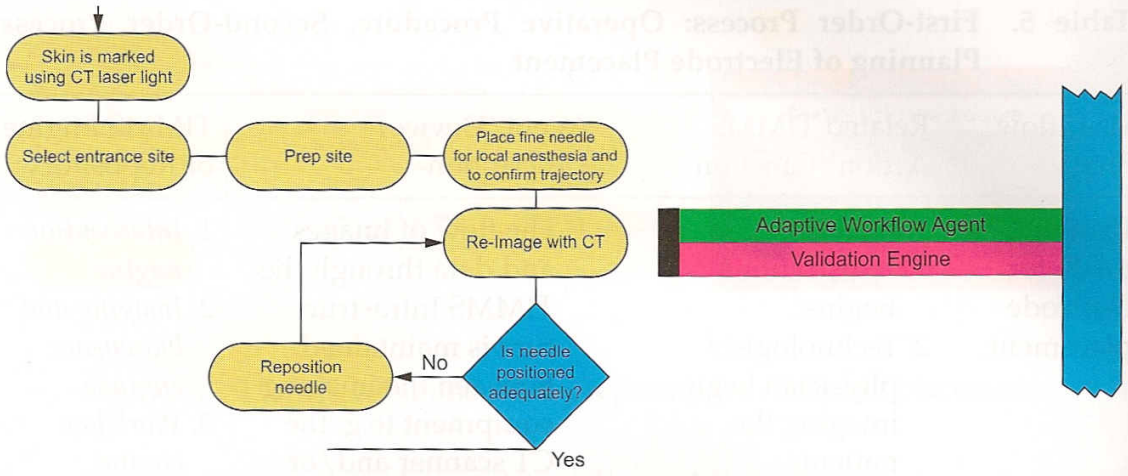

Fig. 5(G). TIMMS components for fine needle placement for local anesthesia. Adequacy of the trajectory of the fine needle will be confirmed, so that the radiofrequency electrode will be placed appropriately, in tandem, along side the fine needle.

Table 6. First-Order Process: Operative Procedure, Second-Order Process: Fine Needle Placement

Workflow Step	Related TIMMS Action/Function	Agent/Device/ Description	TIMMS Engine or Repository
Placement of fine needle for local anesthesia.	1. Adequacy of the trajectory of the fine needle will be confirmed, so that the radiofrequency electrode will be placed appropriately, in tandem, along side the fine needle.	1. Feedback from navigational devices will dictate modifications by the *adaptive workflow agent* to the executing workflow.	*1. Kernel for workflow and knowledge and decision management.* 2. *Validation engine.*

31.5.3.4 *Placement of radiofrequency electrode and ablation of tumor*

The radiofrequency (RF) electrode is deployed with the *biosensor and imaging, intervention, and validation engines* enabling coordinated, synchronized function of real time imaging devices (such as CT-fluoro or ultrasound), registration and navigation agents, and robotic devices. Once proper placement of the RF electrode is

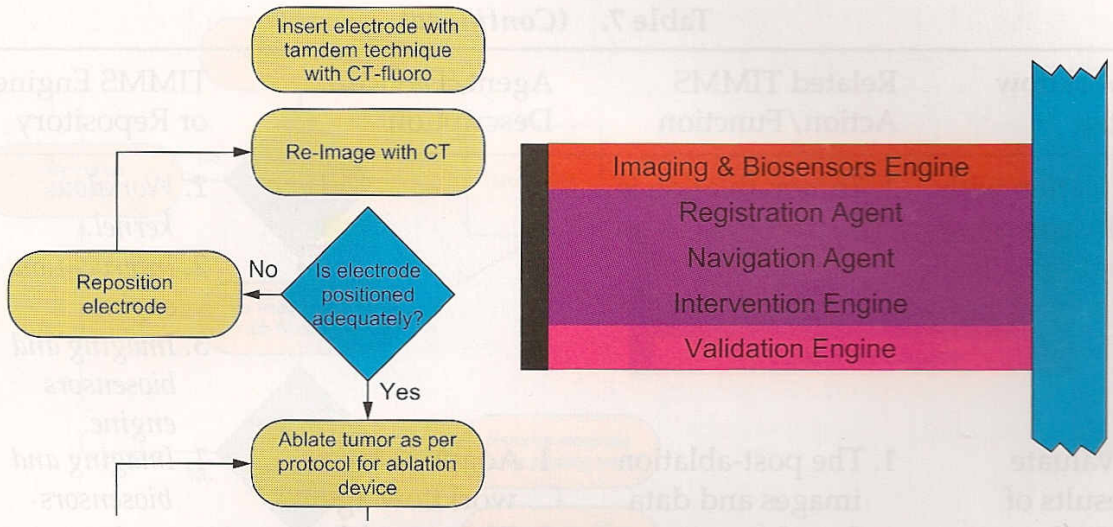

Fig. 5(H). TIMMS components for radiofrequency electrode placement and for ablation of the tumor.

confirmed, the RF generator may be activated and the tumor ablated via the *workflow kernel* and *intervention engines* [Fig. 5(H)].

31.5.3.5 *Assessment of initial ablation of tumor and completion of operation*

After the initial treatment, the results of the ablation are evaluated. The post-ablation images and data from biosensors will be analyzed and the patient model will be updated through a synchronized effort

Table 7. First-Order Process: Operative Procedure, Second-Order Process: Electrode Placement and Ablation

Workflow Step	Related TIMMS Action/Function	Agent/Device/ Description	TIMMS Engine or Repository
RF electrode insertion and feedback based adjustments.	1. The RF generator is brought online. 2. The RF electrode is deployed.	1. *Registration and navigation agents* provide coordinated, synchronized function with real time imaging.	1. *Intervention engine.* 2. *Imaging and biosensors engine.* 3. *Kernel for workflow and knowledge and decision management.* 4. *Validation engine.*

(*Continued*)

Table 7. (*Continued*)

Workflow Step	Related TIMMS Action/Function	Agent/Device/ Description	TIMMS Engine or Repository
Ablation with physiologic, and imaging feedback.	1. Tumor ablation is performed.		1. *Workflow kernel.* 2. *Intervention engine.* 3. *Imaging and biosensors engine.*
Evaluate results of initial ablation.	1. The post-ablation images and data from biosensors will be analyzed and the patient model will be updated. 2. The adaptive workflow agent will suggest changes to the executing workflow based on current data. 3. Need to repeat ablation will be indicated. 4. The planning steps will be repeated with development of new executing workflow.	1. Adaptive workflow agent. 2. *Patient model integrator.*	1. *Imaging and biosensors engine.* 2. *Modeling engine.* 3. *Workflow kernel.* 4. *Validation engine.*
Additional ablations performed with physiologic and imaging feedback if necessary.	1. Reposition RF electrode as indicated. 2. Perform additional tumor ablation.	1. *Registration and navigation agents* provide coordinated, synchronized function with real time imaging.	1. *Intervention engine.* 2. *Imaging and biosensors engine.* 3. *Kernel for workflow and knowledge and decision management.* 4. *Validation engine.*

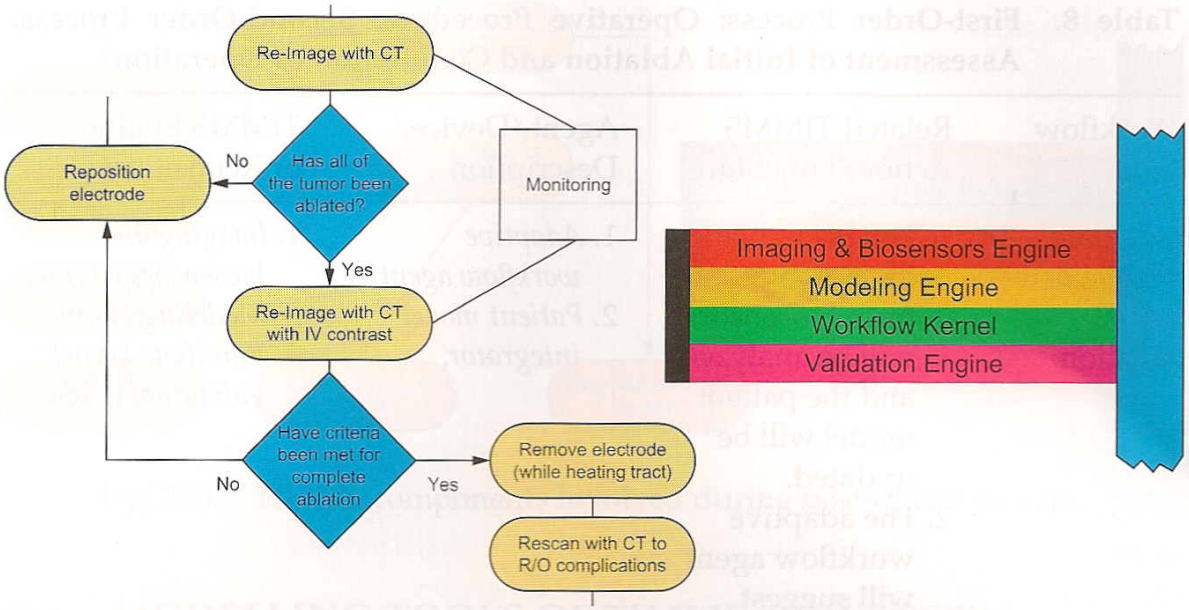

Fig. 5(I). TIMMS components for evaluating adequacy of tumor ablation, and for the completion of the operative procedure.

of the *imaging and biosensors engine*, the *modeling engine*, the *workflow kernel*, and the *validation engine*. If necessary, the *adaptive workflow agent* will suggest changes to the executing workflow based on current data, for a second ablation [Fig. 5(I)].

If all parameters indicate a successful ablation treatment, the electrode will be removed and a completion scan will be performed to rule out complications.

31.5.4 Post-Operative Care

31.5.4.1 *Completion of operation and patient assessment*

After the ablation procedure is completed, physiological monitoring continues, with the *imaging and biosensors engine* updating the patient model. The *EMR Agent* will update the patient's medical records with a report of the procedure and its outcome [Fig. 5(J)].

The *validation engine* will perform a variety of validation functions, including outcomes analysis, statistical evaluation, complication recording, etc. This data is sent to *repositories* and the EMR, and will be available for additional evaluation and research purposes. All required quality assurance procedures and documentation will be completed. When post-operative assessment indicates

Table 8. First-Order Process: Operative Procedure, Second-Order Process: Assessment of Initial Ablation and Completion of Operation

Workflow Step	Related TIMMS Action/Function	Agent/Device/ Description	TIMMS Engine or Repository
Evaluate results of initial ablation.	1. The post-ablation images and data from biosensors will be analyzed and the patient model will be updated. 2. The adaptive workflow agent will suggest changes to the executing workflow based on current data. 3. Need to repeat ablation will be indicated. 4. The planning steps will be repeated with development of new executing workflow.	1. *Adaptive workflow agent.* 2. *Patient model integrator.*	*1. Imaging and biosensors engine.* *2. Modeling engine.* *3. Workflow kernel.* *4. Validation engine.*
Additional ablations performed with physiologic and imaging feedback if necessary.	1. Reposition RF electrode as indicated. 2. Perform additional tumor ablation.	1. *Registration and navigation agents* provide coordinated, synchronized function with real time imaging.	*1. Intervention engine.* *2. Imaging and biosensors engine.* *3. Kernel for workflow and knowledge and decision management.* *4. Validation engine.*

that patient is stable and ready for transfer, and when validation procedures have been completed, the *patient safety agent* will indicate that the patient is ready for transfer to the recovery room [Fig. 5(J)].

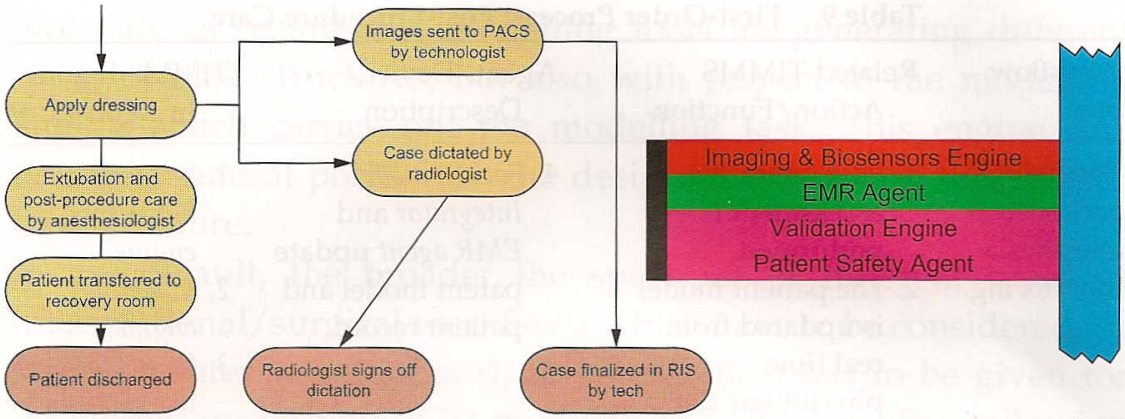

Fig. 5(J). TIMMS components involved during post-operative care.

31.6 MODELLING TOOLS OF TIMMS AND STEPS TOWARDS STANDARDS

Standards relating to medical imaging and communication for non-real time diagnostic and related activities are well defined by DICOM and are an integral part of TIMMS. Most of the image and presentation states IOD's, which are defined in DICOM, are also relevant to surgery.

Models and their associated management have not been considered in DICOM intensively, except through some work done in DICOM WG 07, WG 17 and WG 22. Modelling and simulation in surgery however, are key functions for SAS's pre- and intraoperatively. Interfacing of tools which support these functions comprises a relatively new scope for DICOM.

To define model and simulation, a definition by O Balci[4] may be used "A model is a representation or abstraction of something such as an entity, a system or an idea. Simulation is the act of experimenting with or exercising a model or a number of models under diverse objectives including acquisition, analysis and training." As indicated in Fig. 2, both modelling and simulation are critical components of an SAS, particularly for planning and intervention activities.

It will be a significant extension of current DICOM efforts to complement the image centric view with a model centric view for developing DICOM objects and services. Some IOD's which make use of the concept of a model are listed in DICOM PS 3.3 as part

Table 9. First-Order Process: Post-Procedure Care

Workflow Step	Related TIMMS Action/Function	Agent/Device/ Description	TIMMS Engine or Repository
Physiologic and post-anesthesia monitoring.	1. Post-operative assessment is performed. 2. The patient model is updated from real time physiologic data. 3. Orders for post-operative care are written.	1. *Patient model Integrator* and *EMR agent* update patent model and patient record.	1. *Imaging and biosensors engine.* 2. *Modeling engine.* 3. *Kernel for workflow and knowledge and decision management.*
Procedure validations.	1. Validation processes, including outcomes analysis, statistical evaluation, complication recording, etc. are performed. 2. Data sent to repositories and EMR.	Cognitive agents perform quality assurance procedures and *EMR agent* adds documentation to repositories and EMR.	1. *Validation engine.* 2. *Kernel for workflow and knowledge and decision management.*
Discharge patient to recovery room.	1. When post-operative assessment indicates that patient is stable and ready for transfer, and when validation procedures have been initiated, an indicator will light up.	1. *Patient safety agent.*	1. *Validation engine.*

of annex C 8.8. "radiotherapy modules." Currently, approximately 40 modules have been specified for radiation therapy. They imply a limited spectrum of data types and data structures with different degrees of complexity, e.g. simple lists or tree structures. In the context of a TIMMS, a more comprehensive view on modelling than for example in radiation therapy, will be necessary.

Not only as regards the modelling tools for generating different types of data structures, but also with respect to the modelling engine which carries out the modelling task. This engine will occupy a central position in the design of a SAS and the TIMMS infrastructure.

By default, the broader the spectrum of different types of interventional/surgical workflows which have to be considered for standard interfacing support, the more effort has to be given for designing appropriate IOD modules and services. The following list contains some examples of modelling tools and aspects, derived from different types of surgical workflows, which may have to be considered for future standard activities such as DICOM:

- Geometric modelling including volume and surface representations
- Properties of cells and tissue
- Segmentation and reconstruction
- Biomechanics and damage
- Tissue growth
- Tissue shift
- Prosthesis modelling
- Fabrication model for custom prosthesis
- Properties of biomaterials
- Atlas-based anatomic modelling
- Template modelling
- FEM of medical devices and anatomic tissue
- Collision response strategies for constraint deformable objects
- Variety of virtual human models
- Lifelike physiology and anatomy
- Modelling of the biologic continuum
- Animated models
- Multiscale modelling
- Fusion/integration of data/images
- Registration between different models including patient, equipment and OR
- Modelling of workflows

Real time aspects identified for imaging during intervention are equally applicable for the generation and management of these models. In addition to defining mechanisms to enable real time communication, it will also be one of the first tasks of standardization to agree on a list of relevant models to be considered for DICOM IOD's.

31.7 GENERAL MOTIVATION FOR STANDARDS IN SURGERY

31.7.1 Meetings

A number of special workshops and seminars which have addressed the medical, technical, economic and related problems of the OR have taken place in recent years in Europe and in the USA. The most notable recent meetings with a focus on IGT, surgical workflow and standards in the OR were:

(1) UCLA Seminars on Imaging and Informatics, September 22–25, 2003, Lake Arrowhead, CA, USA.[5]
(2) Leipzig University Forum, ICCAS, October 2003.[6]
(3) Workshop on "OR2020: Operating Room of the Future", March 18–20, 2004, Ellicott City, MA, USA.[7]
(4) CARS/SPIE "Joint meeting on Surgical Workflow, PACS and the OR of the Future," June 26, 2004, Chicago, IL, USA.[8]
(5) UCLA Seminars on Imaging and Informatics, October 4–6, 2004, Lake Arrowhead, CA, USA.[9]
(6) NCIGT and NA-MIC Workshop on Image Guided Therapy, Rockville, MD, October 19–20, 2006.[10]

Standards and interoperability of devices were a common theme of almost all of these meetings. Exemplary for this effort are the insight and results given by two working groups established for the OR 2020 Workshop.[7] It is worth noting that approximately one third of the participants of the OR 2020 Workshop were MD's, R&D PhD's and representatives from the industry and government institutions respectively. The problems which were identified before and then elaborated during the workshop by the two working groups, are summarized as follows:

31.7.1.1 *Working group 1: Operational efficiency and workflow*

This group focused on examining requirements for achieving increased efficiencies in the OR. These requirements focused on needed mechanisms for accessing and obtaining correct and current patient-related information and scheduling, and accessing use of correct surgical tools. The group also discussed developing surgical practice standards that define day-to-day, step-by-step surgical workflows. Four of the most critical technical needs which were identified for improving OR efficiencies and workflow are as follows:

(1) creating accessible "patient-centric" medical records,
(2) developing readable equipment locator/tracking mechanisms,
(3) resolving OR teamwork/personnel issues; and
(4) developing and following technical standards in the OR.

31.7.1.2 *Working group 2: Systems integration and technical standards*

This group focused on the need for interoperability among a broad range of devices that are used in the OR. To achieve seamless integration among devices, it was recommended, that a standard interface for interoperability among these technologies should be developed using a plug and play platform. This group also discussed the need for device standards that will enable configurability and easy use of these tools in the OR.

31.7.2 Recommendations

Many details have been listed by the two working groups as potential solutions to the above problems, here included as a summary recommendation[7]:

(1) Standards, standards, standards. If there was an overarching theme of the workshop, this was it. Standards are needed in all areas, and must be developed through a concerted effort involving companies, government agencies, academic institutions, and

perhaps standards organizations. Research studies of surgical workflow and efficiencies are required to develop practice standardization and thus realize improvements.

(2) Progress on the first recommendation will also enable progress on device interoperability. It is recommended that research be devoted to developing common user interfaces among medical devices, and that the device industry take the lead in performing this research with input for academic institutions and government agencies. A "plug and play" architecture for medical devices is also needed.

Of particular interest is here the statement that standards are needed in all areas and must be developed through a concerted effort involving companies, government agencies, academic institutions, and perhaps standards organizations. Motivating these players to work in a concerted effort towards standards can only be achieved, of course, if it is in their business interest. One of the critical questions which needs to be addressed is:

"Is the OR of the Future (ORF) a viable economic reality?"[11]

31.8 SURGICAL WORKFLOWS (WF) FOR MEDICAL IMAGING (MI) IN SURGERY

Standards for creating and integrating information about patients, equipment, and procedures are vitally needed at the outset in planning for an efficient ORF. To determine these standards, research is needed to define day-to-day, step-by-step surgical workflow practices and create surgery workflow models per procedures or per variable cases.

An example that might be used to better understand (and eventually improve on) or workflows and efficiencies is the recent work carried out by the integrating the healthcare enterprise (IHE) initiative and its definitions of work profiles and efficiencies in healthcare outside of the surgical room. This body of experts develops recommendations for the healthcare industry on how to implement

standards. (Note: IHE's members do not develop the standards themselves.)

Furthermore, the IHE initiative has developed "integration profiles" that enable consistent access to images and reports for certain medical specialties (such as radiology). Surgical profiles have not been developed yet, but they are needed (a widespread opinion expressed at the OR 2020 Workshop), as is a "surgical DICOM." Today's DICOM standard is not suitable for many imaging types and working modes that are needed in the or (e.g. it does not cover real time, and 3D and higher dimensional issues, nor does it address interactivity).

31.8.1 Recording of Workflows

With these objectives in focus, a detailed workflow analysis[12] has been carried out by the Technical University Berlin (TUB) and the Innovation Center for Computer Assisted Surgery (ICCAS) in Leipzig. The aim is to model and visualize surgical procedures in order

- to allow a correlation between workflows of different types of surgical procedures, e.g. to obtain a measure of similarity between workflows,
- to assist in identifying (e.g. through simulation, see Fig. 6), those parts of the same and between different workflows (Surgical Integration Profiles — SIP's) where a process redesign with automated activities may prove to be of a clinical and economic advantage,
- to provide concepts and data to assist in the specification, design, implementation and *in vivo* usage of new information and communication technology and mechatronic systems.

An important aspect when recording workflows is their modelling and representation technology. Amongst many possibilities and derived from the above work, the workflow management coalition standard is being recommended for workflow recording within WG24. Figure 7 shows an example of a surgical workflow in orthopedic surgery.

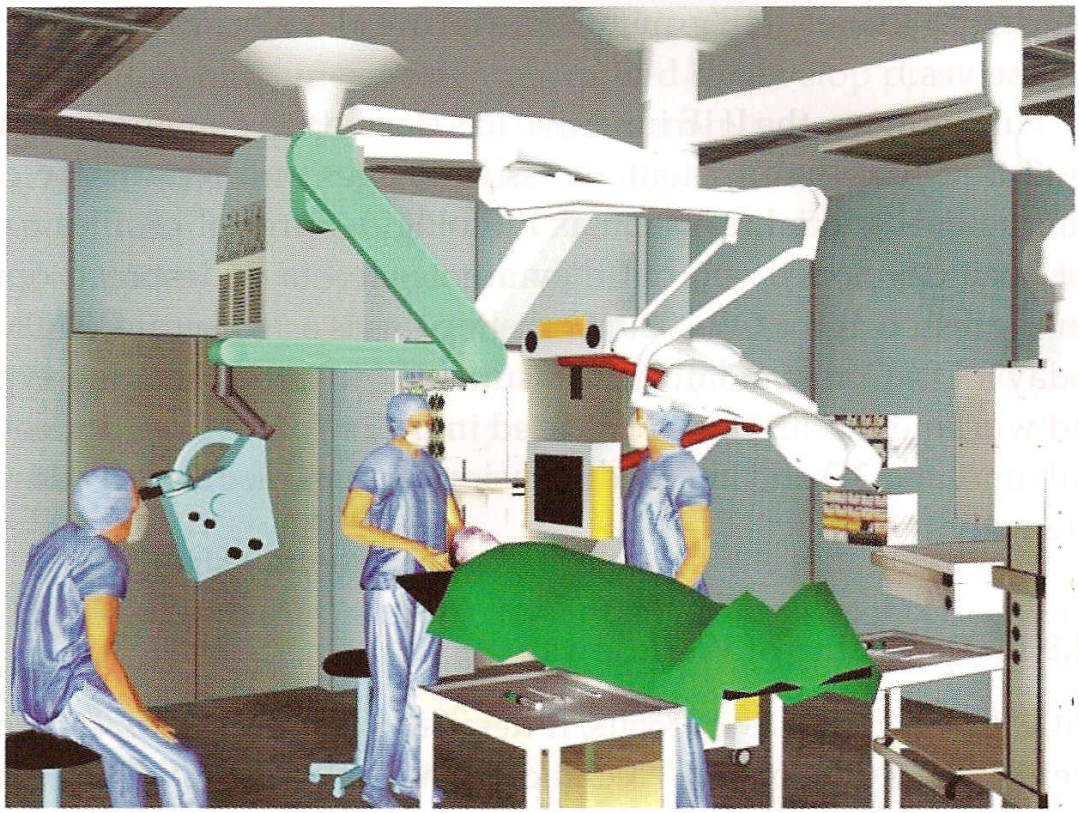

Fig. 6. Simulation of surgical workflow.

31.8.2 Dynamics of Workflows and the Model of the Patient

It is important to consider workflows to be dynamic entities. For WG24, they serve as reference (not best practiced!) workflows and are updated at regular intervals to detect within the workflows possible changes in imaging and patient modelling requirements. For example, it can be expected, that molecular imaging modalities will impact workflow for oncologic patients substantially.[13] Radiation resistant parts of a tumor may be defined with molecular imaging to a higher precision giving rise to include surgical/interventional ablation procedures combined with radiation therapy as a possible regimen.

A well defined workflow and a high fidelity patient model will be the base of activities for both, radiation therapy and surgery. Considering the present and future requirements for surgical planning and intervention, such a patient model must be n-dimensional, were n may include the spatial and temporal dimensions as well as a

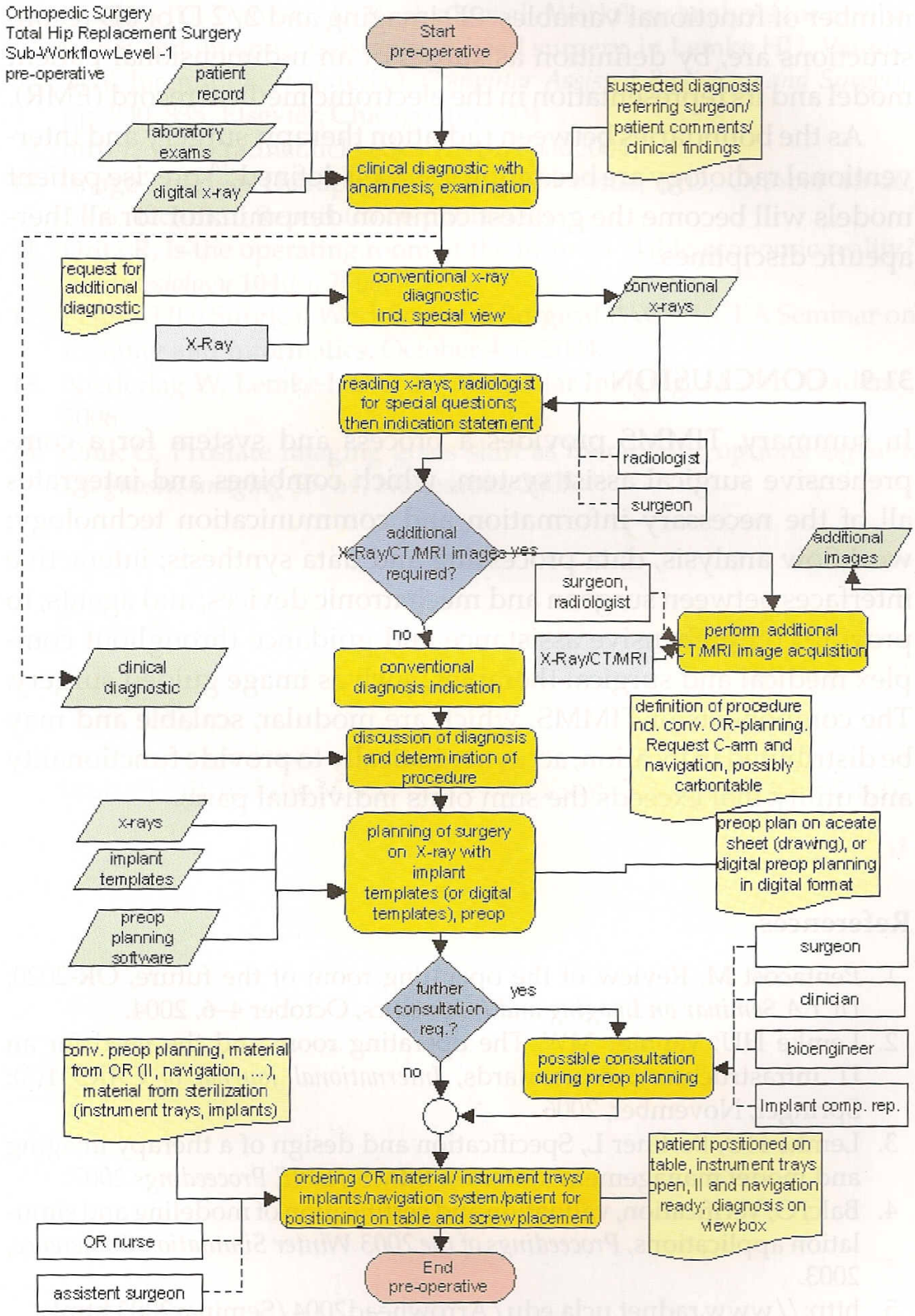

Fig. 7. A workflow example in orthopedic surgery.

number of functional variables. 2D imaging and 2/2 D or 3D reconstructions are, by definition as subset of an n-dimensional patient model and its representation in the electronic medical record (EMR).

As the boundaries between radiation therapy, surgery and interventional radiology are becoming less well defined,[14] precise patient models will become the greatest common denominator for all therapeutic disciplines.

31.9 CONCLUSION

In summary, TIMMS provides a process and system for a comprehensive surgical assist system, which combines and integrates all of the necessary information and communication technology; workflow analysis, data processing and data synthesis; interactive interfaces between surgeon and mechatronic devices; and agents; to provide comprehensive assistance and guidance throughout complex medical and surgical therapies, such as image guided surgery. The components of TIMMS, which are modular, scalable and may be distributed in location, act synergistically to provide functionality and utility that exceeds the sum of its individual parts.

References

1. Pentacost M, Review of the operating room of the future, OR-2020, *UCLA Seminar on Imaging and Informatics*, October 4–6, 2004.
2. Lemke HU, Vannier MW, The operating room and the need for an IT infrastructue and standards, *International Journal of CARS* **1**(3): Springer, November, 2006.
3. Lemke HU, Berliner L, Specification and design of a therapy imaging and model management system (TIMMS), *SPIE Proceedings 2007*.
4. Balci O, Verification, validation and certification of modeling and simulation applications, *Proceedings of the 2003 Winter Simulation Conference*, 2003.
5. http://www.radnet.ucla.edu/Arrowhead2004/Seminar2003.html.
6. Leipzig University Forum 2003 (Technical Report).
7. Cleary K, Kinsella A, OR 2020: The operating room of the future, *J Laproendosc Adv Surg Tech A* **15**(5): 497–573, 2005.

8. Lemke HU, Trantakis C, Kochy K *et al.*, Workflow analysis for mechatronic and imaging assistance in head surgery, in Lemke HU, Vannier MW, Inamura K *et al.* (eds.), *Computer Assisted Radiology and Surgery*, pp. 830–835, Elsevier, Chicago, IL, 2004.
9. http://www.radnet.ucla.edu/Arrowhead2004/.
10. Image Guided Therapy Workshop, Rockville, MD, October 19–20, 2006, Technical Report (to be published).
11. Dritz R, Is the operating room of the future a viable economic reality? *Anesthesiology* **104**(6), 2006.
12. Lemke HU, Surgical Workflow and Surgical PACS, UCLA Seminar on Imaging and Informatics, October 4–6, 2004.
13. Niederlag W, Lemke HU *et al.*, Molecular Imaging, Health Academy, 2006.
14. Onik G, Prostate imaging goals shift as therapeutic options expand, *Diagnostic imaging* 55–64, November, 2005.

CHAPTER 32

Future Trends in Medical and Molecular Imaging

Atam P Dhawan, HK Huang and Dae-Shik Kim

Recent advances in computerized medical imaging and associated areas of basic and applied sciences, engineering, medicine and computing technologies have created a synergy among researchers and scientists to explore complex issues related to the onset of critical diseases for better understanding of physiological processes from molecular to organ and behavioral levels. Future trends are expected to continue to develop more complex and sophisticated tools in the investigation of biological functional and pathologies associated with the onset of critical diseases for early diagnosis, treatment, evaluation and interventional protocols. This chapter points out some areas and challenges of future technology development with potential applications.

32.1 FUTURE TRENDS WITH SYNERGY IN MEDICAL IMAGING APPLICATIONS

In recent years, clinical medicine and healthcare have been revolutionarized through multidisciplinary technological advances. Critical health care technologies including diagnostic radiology, surgery and rehabilitation extensively use computerized systems to continuously improve diagnosis, treatment and prognosis. These technological advances have emerged from a synergy of many specialized areas including engineering, computer science, mathematics, and other basic, applied and social sciences. Today, we can critically measure neurological signals of the brain with under a

millimeter spatial resolution over a fraction of second to diagnose and characterize neurological disorders and diseases. As the technological contributions are impacting medicine and clinical practice, higher goals and standards are being established to achieve better diagnosis, treatment and healthcare. The synergy of advanced technologies such as computerized medical imaging, high volume data storage and database architecture, picture archiving and communications systems, wireless networking, and display technology is leading to better patient care with more computer processing, modeling and analysis, leaving less room for guesswork.

Medical imaging technologies provide complimentary information from molecular to organ levels. Current and future trends in fMR, diffusion-MR, positron emission tomography (PET), ultrasound, and optical imaging are targeted towards obtaining molecular information from the cellular structure of tissue.

Advanced imaging techniques are expected to explore biological investigations to develop signatures and models for understanding physiological processes associated with "presymptomatic" conditions leading to specific diseases and pathologies. Future technological developments in multimodal molecular and cellular imaging should allow early detection of cellular/neurological deviations in critical diseases such as Alzheimer's disease, autism, or multiple sclerosis, before the first symptomatic sign(s). This is of great importance given the fact that sometimes many neurological diseases (such as Alzheimer's disease, where several decades can pass between the initial neurological deviations and observed behavioral changes) have exceedingly long incubation periods. Current imaging paradigms rely on the expression of the first symptomatic sign(s), scientists then try to correlate, on an *ad hoc* basis, the observed signs with cellular and/or neurological deviations. The problem is that by the time the symptoms are expressed, the disease is probably already in a relatively advanced stage (e.g. shrinkage of the brain in the case of Alzheimer's disease). Therefore, it is important to improve the patient care that the future imaging methods and protocols must be able to detect critical diseases in a presymptomatic stage for better preventive treatment, and at the same time provide

robust, efficient and reliable support for early diagnosis, treatment, evaluation and intervention protocols.

32.1.1 Trends in Targeted Imaging and Image Fusion

Targeted imaging provides a systematic investigation into a physiological process for the assessment of the nature and extent of pathology through multilevel analysis of information from molecular to organ levels. Recent discoveries in molecular science and medical imaging contrast agents are setting up future trends in designing specific contrast agents for multidimensional medical imaging modalities such as ultrasound, PET, fMR and optical fluorescence imaging to study molecular interactions defining abnormal physiological processes linked with the onset of a disease. Targeted contrast agents provide an opportunity to image physiology or pathology that might be otherwise difficult to distinguish from the surrounding tissue without targeted contrast enhancement. For example, encapsulated microbubbles in ultrasound imaging can provide information about activated neutrophil, a cell involved in the inflammatory response (www.ImaRx.com).

The technology of using specific contrast agent for targeted imaging can also be used for better drug delivery in critical therapeutic protocols. It is expected that future diagnostic, treatment-evaluation and therapeutic-intervention protocols will use specific multimodality targeted imaging with computerized analyses through models using molecular signatures of physiological processes. For example, tumor-induced angiogenesis is a complex process involving tumor cells, blood, and the stroma of the host tissue. Studies related to angiogenic growth factors linked with endothelial cells has shown that vascular integrin alpha v beta 3 may be a useful therapeutic target for diseases characterized by neovascularization.[1] Thus, $\alpha v\beta 3$ is a prime candidate for molecular targeting and can be monitored through advanced imaging methods.

Furthermore, nanoparticle conjugated novel MRI contrast agents can be used in order to directly observe gene expression,

metabolism and neurotransmission. The great advantage of these novel contrast agents is their ability to provide such information in a noninvasive fashion. This enables important cellular and metabolic processes to be observed for the first time from whole animals over repeated time periods.[2]

One of the major challenges in using several advanced technologies such as EKG, EEG, CT, MRI, fMRI, PET, etc. is how to integrate information from several complimentary technology instruments. The process of information fusion requires computer processing of large data files with a common standard and coordinate system so that information from different instruments can be easily read and integrated to target the specific region. Though efforts have been made in establishing common formats for images and data from different instruments, the files are usually transported to a common computing environment off-line after the images and measurements are acquired from corresponding instruments. Such systems provide large datasets to handle in the real-time on-demand environment. It is still a challenge for acquisition, storage, analysis, and communication of integrated information resulting from multimodality image fusion.

32.1.2 Image Fusion for Surgical Intervention

Real-time information fusion and analysis is critical for interactive surgical interventional protocols. Today, a surgeon studies every piece of available radiological and pathological information including 3-D images from X-ray CT, MRI, Nuclear medicine and ultrasound images, and pathology reports before planning a surgery. Computers are used to plan surgical or radiation procedure before a patient is brought into the operating room in piecemeal fashion. Computers are used to integrate all information from radiological imaging and diagnostic protocols but without a user friendly graphic user interface display mechanism. Computer-based modeling and simulations can also be used to predict the outcome to study and compare alternatives. Though this is a grand step forward in using technologies in surgery, this is just a beginning in

learning how a spectrum of technologies can be used to optimize the diagnosis, interactive surgery, treatment, and patient care.

However, the current operating rooms and instrumentation technologies do not allow an interactive surgical procedure in the operating room where the intermediate steps can be evaluated in real-time to ensure the success of the planned surgical procedure. The new goal in operating room of the future is to integrate technologies to facilitate interactive surgery with intervention procedures for minimally invasive surgery with completely/maximally possible successful outcome.

There are some leading clinical and research facilities where the operating rooms of the future are being designed. At MGH, Dr Warren Sandberg is designing an operating room of the future (ORF). Information is found on the internet (http://www.cimit.org/orfuture.html). Another ORF is being built to include MRI in the operating room at the University of Maryland Medical Center (http://www.umm.edu/news/releases/or_future_opening.html) (see Chapter 31 for additional details). These efforts are starting to realize the potential of interactive integrated information to perform minimally invasive surgery. However, defining specific sources of information needed for data acquisition and information fusion to be used during the surgery to evaluate surgical plan enroute with dynamics of the tissue response would be a key factor that would guide future design of ORs. The other issue is whether there should be one general ORF or they should be designed on the basis of specific categorical needs defining specific instrumentations for data fusion and analysis for the surgeon's use. The design of future operating room has to address challenges in the following three categories:

(1) **Architecture:** If the patient has to be examined through different complimentary diagnostic and radiological systems such as EKG, ECG, EMG, DF, CT, ultrasound, MRI and/or nuclear medicine before, and sometimes during the operation, the patient should remain on a stable operating table without much movement. Therefore, every instrument has to come to the

patient bed rather than having the patient moved into different rooms. Therefore, the first challenge is to have instrumentation and architecture of the operating room synchronized in such a way that any instrument needed for measurement or imaging can be easily slipped around the patient bed without obscuring the surgeon's access to the patient.

(2) **Networking and Information Fusion:** If there are several instruments that are being used to acquire complimentary information necessary to evaluate the surgical procedure and tissue response in real-time, all data files from different instruments must follow common format and standards for networking and communications to a central computer. Thus, data output, communication and networking among all equipment must be effective and without any noise interference. Such type of data acquisition and wireless communication environment require a very fast and high volume data throughput with common standards.

(3) **Human-Machine Interface:** The overall goal of bringing all technologies together is to help a surgeon in the continuous evaluation of the ongoing surgical procedure for any necessary modification to successfully perform minimally invasive surgery. This requires an enormous task of information fusion of high-volume data from several instruments, and analyses to filter out only the useful and necessary information that a surgeon needs to know to evaluate and revise the surgical plan. All of this has to be done in real-time with a proper and effective human-machine interface to the surgeon and in some cases, guiding the surgical instruments as well such as needed in robotic assisted surgery.

Even with the above conceptual description of the future operating room, it is quite clear that technologies and expertise from so many disciplines including architecture, engineering, computer science, basic and applied sciences, psychology and human perception have to work together to create a synergy to successfully develop an efficient operating room of the future.

32.2 TRENDS IN LARGE-SCALE MEDICAL IMAGE DATA STORAGE AND ANALYSIS

With the large amount of image data accumulated daily from medical imaging modalities, picture archiving and communication systems (PACS) in hospitals, we can take advantage of these resources to investigate the concept of imaging informatics. PACS-based medical imaging informatics is to use existing PACS resources including images and related data for systematic large-scale horizontal and longitudinal clinical service, education, and research applications that could not have been performed before because of insufficient data and unavailable tools.

32.2.1 PACS-Based Medical Imaging Informatics

Medical imaging informatics infrastructure (MIII) is the vehicle to facilitate the utilization of PACS in addition to its daily clinical service. Figure 1 illustrates MIII components and their logical relationship.[3] The PACS, Data Grid, Grid Computing, and CAD-PACS integration discussed in Chapter 21 are components in the MIII infrastructure. The integration of CAD-PACS, Data Grid and Grid Computing is an example of large-scale MIII components integration. Another example is the use of Data Grid and Computing Grid for image-based clinical trials to be discussed in the following

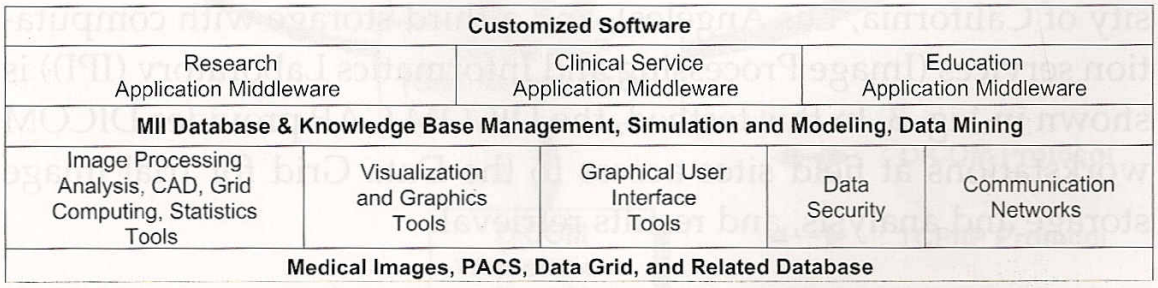

Fig. 1. MIII components and their logical relationship. The second layer from bottom are common tools in MIII; the third layer is general database, knowledge base, simulation and modeling, and data mining software packages; the fourth layer is application specific software; and the top layer is customized application software. CAD, PACS, data grid and grid computing facilities are components in each layer.

subsection. The use of MIII concept for other applications in large-scale medical image data storage and analysis will be continuously explored and solidified by researchers in medical imaging.

32.2.2 Data and Computing Grids for Image-Based Clinical Trials

Clinical trials play a crucial role in testing new drugs or devices in modern medicine. Medical imaging has also become an important tool in clinical trials because images provide a unique and fast diagnosis with visual observation and quantitative assessment. A typical imaging-based clinical trial consists of: (1) A well-defined rigorous clinical trial protocol; (2) a medical image core that has a quality control mechanism, image analysis, a biostatistics component, and a server for storing and distributing data and analysis results; and (3) many field sites that generate and send image studies to the medical imaging core. As the number of clinical trials increases, it becomes necessary for the core which services multiple trials to have a server robust enough to administrate and quickly distribute information to worldwide participants. The Data Grid can satisfy the aforementioned requirements of image-based clinical trials.[4] A general organization of an image-based clinical trial with responsibilities of each component is depicted in Fig. 2. An example of a fault-tolerant Data Grid with computational services testbed for image-based trials with two storage nodes (University of Southern California and University of California, Los Angeles), and a third storage with computation services (Image Processing and Informatics Laboratory (IPI)) is shown in Fig. 3. In this testbed, the DICOM GAP provides DICOM workstations at field sites access to the Data Grid for trial image storage and analysis, and results retrieval.

32.3 MEDICAL IMAGING TO BRIDGE THE GAP BETWEEN DIAGNOSIS AND TREATMENT

Most medical images have been used for diagnostic purpose. In order to communicate images from modalities to workstations for

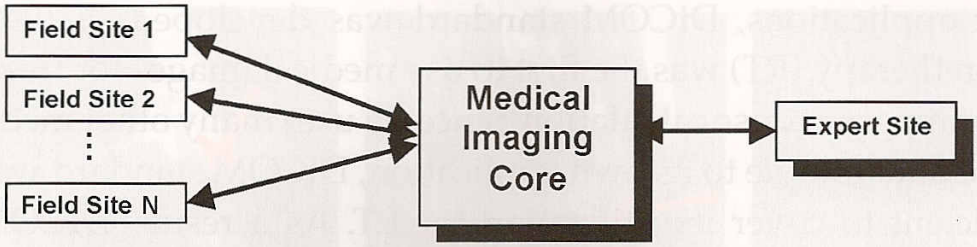

Field Site Responsibilities:

1. Recruit patients
2. Collect images

Core Responsibilities:

1. Perform quality control of images sent by field sites
2. Store images acquired by field sites
3. Distributes acquired images for analysis by experts
4. Distributes analysis back to appropriate field sites

Expert Site Responsibilities:

1. Analyze images sent by core
2. Sends analysis back to core for storage

Fig. 2. A generic image-based clinical trial organization layout and responsibilities of each component.

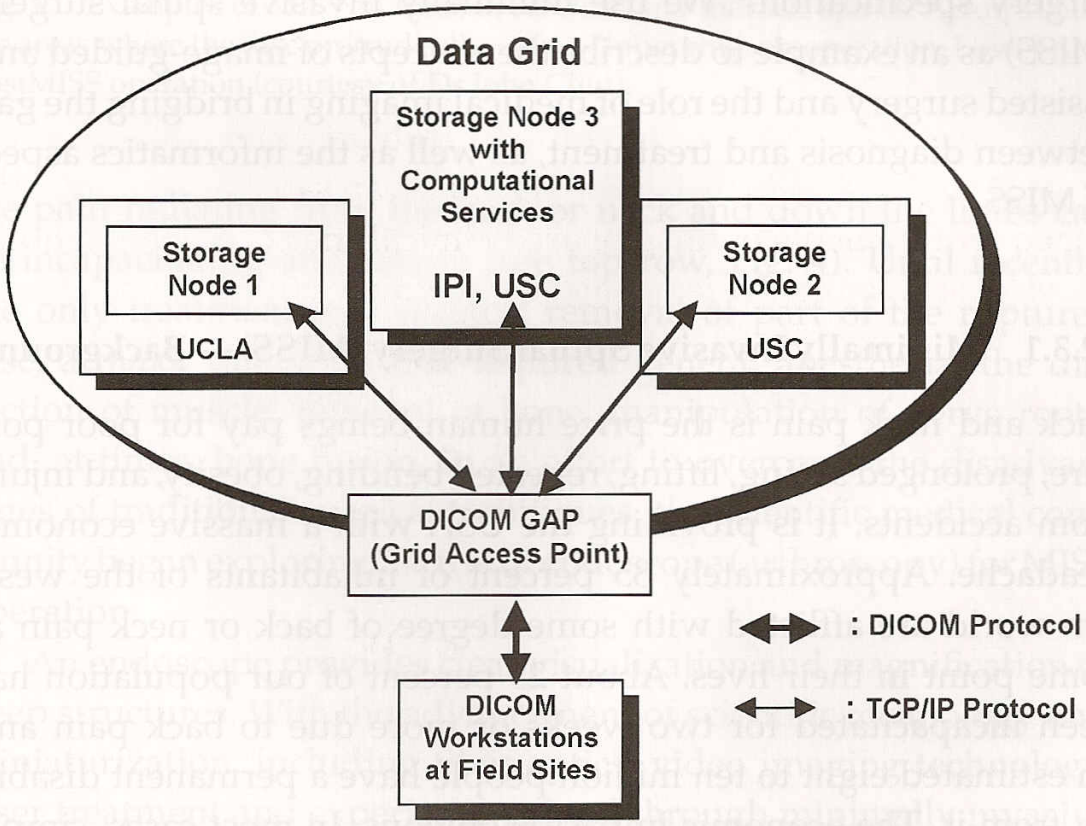

Fig. 3. An image-based clinical trial testbed with two storage nodes (USC, UCLA) and a third storage node with computational services (IPI, USC). The DICOM GAP provides access for DICOM workstations at filed sites to store, perform image analysis and retrieve results from the DICOM Data Grid.

different applications, DICOM standard was developed in 1992. Radiation therapy (RT) was the first to use medical images for treatment planning and dose calculation. Since RT uses many other medical image data unique to its own application, DICOM standard was not sufficient to cover its utilization for RT. As a result, DICOM RT was ratified with seven RT-specific DICOM objects in 1999.[5] Both DICOM and RT DICOM are evolving standards, new DCIOM objects and specifications are being developed and rectified continuously. During the past ten years, image-assisted and guided surgery has become popular. In order to perform image-assisted surgery successfully, it requires image communication and display as well as surgical workflow profiles. The results are the need of an extended DICOM standard for image-guided surgery. The new DICOM Working Group (WG24) with experts in both medical imaging and surgery has been formed to develop an image-assisted and guided surgery specification.[6] We use minimally invasive spinal surgery (MISS) as an example to describe the concepts of image-guided and assisted surgery and the role of medical imaging in bridging the gap between diagnosis and treatment, as well as the informatics aspect of MISS.

32.3.1 Minimally Invasive Spinal Surgery (MISS) — Background

Back and neck pain is the price human beings pay for poor posture, prolonged sitting, lifting, repeated bending, obesity, and injury from accidents. It is providing the USA with a massive economic headache. Approximately 85 percent of inhabitants of the western world are afflicted with some degree of back or neck pain at some point in their lives. About 25 percent of our population has been incapacitated for two weeks or more due to back pain and an estimated eight to ten million people have a permanent disability from it. The economic impact is obvious. In most cases, simple treatments such as bed rest, exercise, physiotherapy, and pain medication bring relief. Many sufferers are not so fortunate. If one or more of their vertebral discs ruptures and presses on nerve roots,

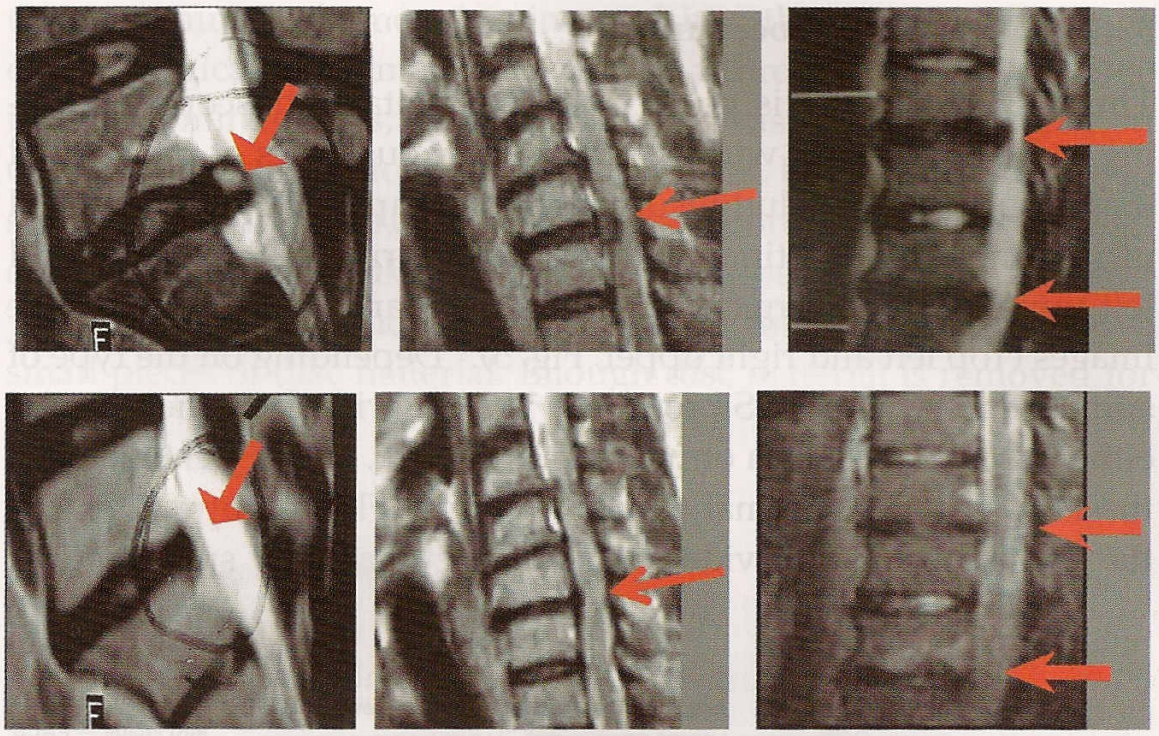

Fig. 4. Examples of MISS on lumbar, cervical, and thoracic spines. Arrows show the areas where the disc protrudes the spine. Upper row: preoperation, Lower row: postMISS operation (courtesy of Dr John Chiu).

the pain radiating from the back or neck and down the limbs can be incapacitating and severe (see top row, Fig. 4). Until recently, the only treatment was surgical removal of part of the ruptured disc, a major operation that required general anesthesia, the dissection of muscle, removal of bone, manipulation of nerve roots, and, at times, bone fusion. In an effort to overcome the disadvantages of traditional surgical techniques, the scientific medical community began exploring the use of endoscope (arthroscopy) for MISS operation.

An endoscope provides clear visualization and magnification of deep structures. With the advancement of scientific technology and miniaturization, including fiber optics, video imaging technology, laser treatment and experience gained through minimally invasive spinal surgery, there is a less traumatic discectomy procedure for some patients with disc problems. In the recent years, the development of image-guided surgery has improved the precision and reduced surgical tissue trauma.[7]

32.3.2 The MISS Procedure

The MISS procedure is performed in a digital endoscopic operating room (OR, Fig. 5) with an array of various types of presurgical diagnostic images including digital fluorography (DF), CT, MR, and ultrasound; and real-time vital sign waveforms (right bottom and left upper, Fig. 5), surgical images like DF and digital endoscopic images (Top left and right upper, Fig. 5).[8] Depending on the type of spinal surgery, the MISS procedure is done with the patient under either a local anesthesia or in some situations, a brief general anesthesia. Using the minimal exposure Digital Fluoroscopy (DF) and the endoscope digital video image for guidance, a small hollow

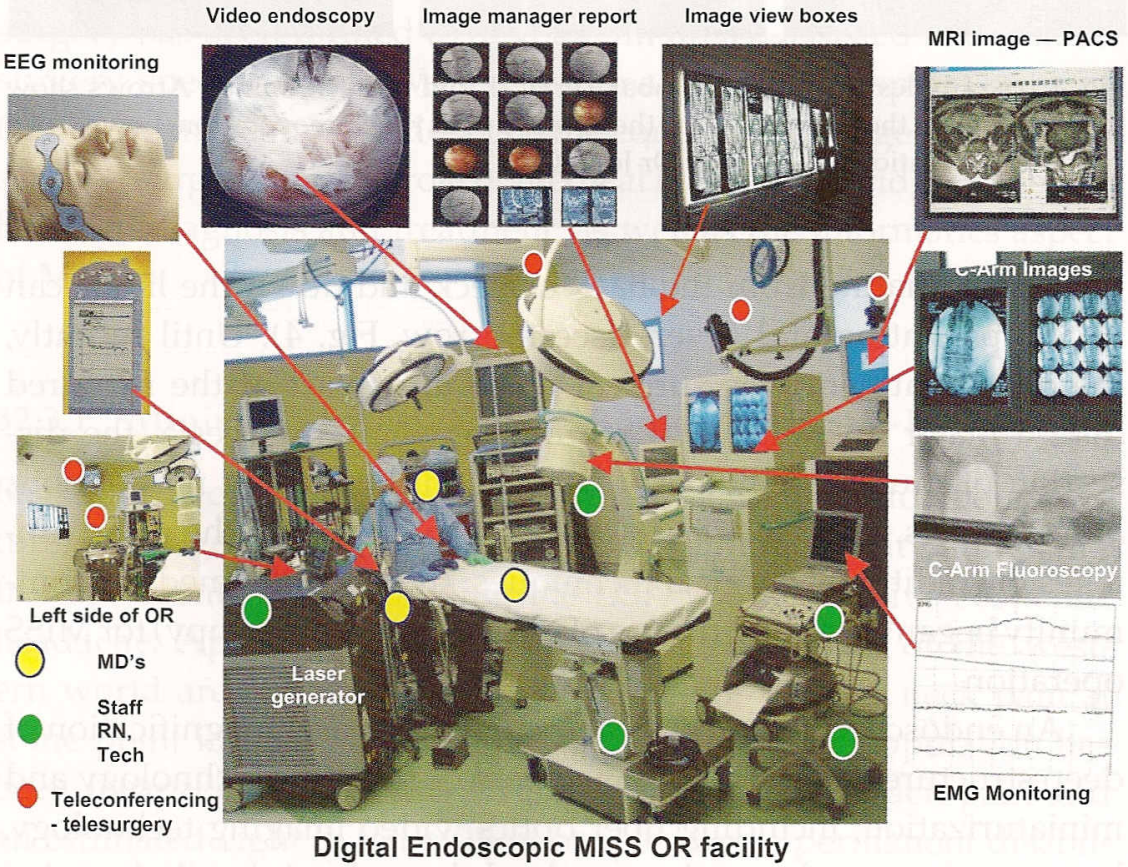

Fig. 5. A digital endoscopic OR for MISS operation of today with various images and waveform data scattering in the suite. With the design and implementation of the ePR, future MISS OR will have the benefit of streamlined patient pre and during surgical operation data to improve the efficiency and effectiveness of MISS (courtesy of Dr John Chiu).[9]

tube (~6 mm in diameter) is inserted into the disc space. A variety of surgical instruments can be used through the hollow tube including miniforceps, curettes, trephines, rasps, burrs, cutters, and other types of probes for disc decompression. Lasers are also used to shrink and tighten the disc and to remove portions of the protruded disc. The procedure takes about 15 minutes per disc on the average. The discectome, a hollow probe, is used to cut, suction and remove small pieces of disc material. Enough disc material is removed for

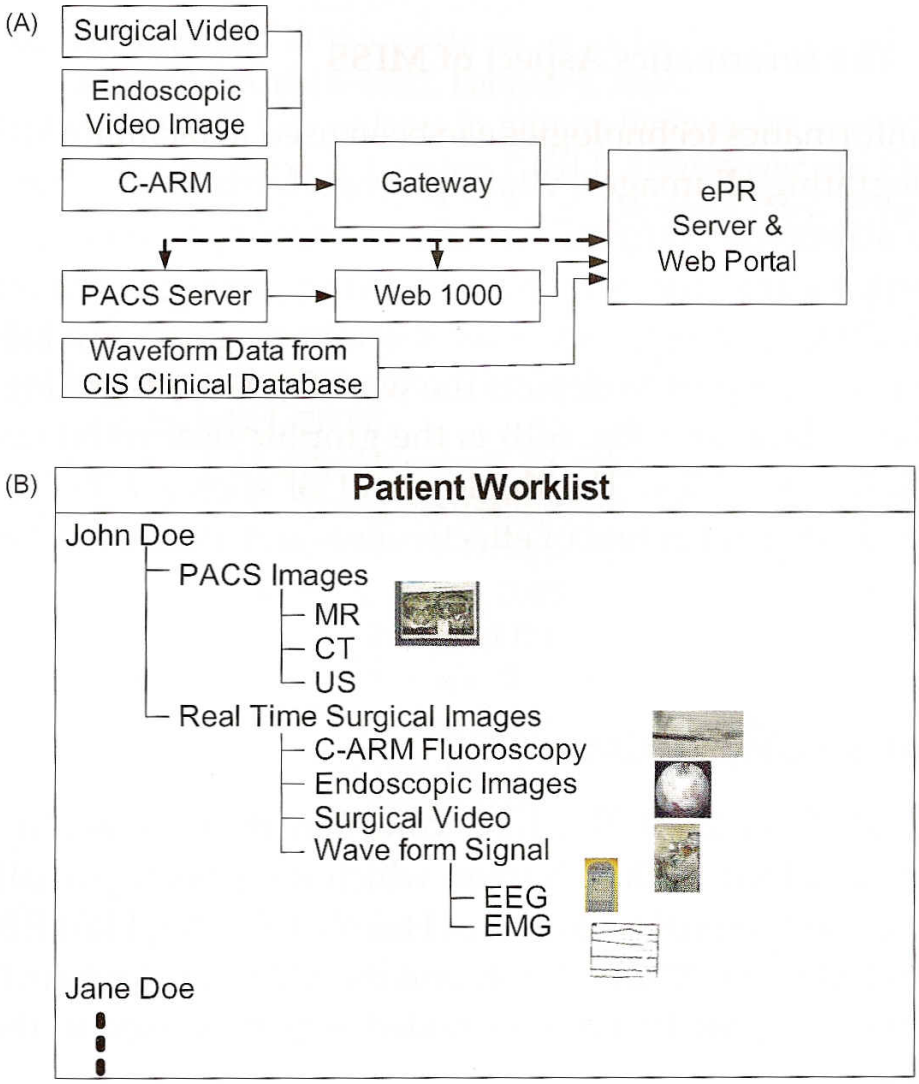

Fig. 6. (A) The infrastructure of a MISS ePR system showing the connections of various presurgical and during operation MISS images, waveforms and related clinical data (see also Fig. 5). (B) The patient worklist graphic user interface design of the ePR.

decompression of the nerve root. A laser is used to shrink and to tighten the disc. The supporting structure of the disc is not affected. Upon completion, sutures and a small band-aid are applied to the incision. This endoscopic procedure is also used currently for bony decompression in spinal stenosis. Overall, endoscopic spine surgery has a patient satisfaction score of 91 percent, and a 94 percent success rate (for a single level of disc problem). The complication rate is much less than 1 percent and mortality rate directly from spinal disc surgery is zero.[9] Figure 4 shows a cervical, thoracic and lumbar spine before and after MISS operations.

32.3.3 The Informatics Aspect of MISS

Image informatics technologies can been used to facilitate MISS[10] by first integrating all images, vital sign waveforms, and other related data to streamline surgical workflow; and implementing an ePR (electronic patient record) system for data management and outcome analysis. Figure 6 shows the work-in-progress of a MISS ePR system design; Fig. 6(A) depicts the workflow of integrating image and related data, and Fig. 6(B) is the graphic user interface of the MISS patient worklist. The deployment of such a MISS ePR will facilitate the improvement of effectiveness and efficiency of MISS of the future.[11]

32.4 ACKNOWLEDGMENT

Liu B and Zhou Z, at IPI, USC contributed substantially to the projects described in this chapter, which have been partially supported by the National Institutes of Health, USA: NIH R01 EB 00298, NIH R01 LM 07606, T32 EB00438; and the MII Corp. Dr John Chiu of the California Spine Institute provided materials used in the MISS operation.

References

1. Brooks PC, Clark RA, Cheresh DA, Requirement of vascular integrin alpha v beta 3 for angiogenesis, *Science* **264**(5158): 569–571, 1994.
2. Atanasijevic T, Shusteff M, Fam P, Jasanoff A, Calcium-sensitive MRI contrast agents based on superparamagnetic iron oxide nanoparticles and calmodulin, *Proc Natl Acad Sci USA* **103**: 14707–14712, 2006.
3. Huang HK, *PACS and Imaging Informatics: Principles and Applications* John Wiley & Sons, Hoboken, New Jersey, 2004.
4. Zheng Zhou, Marco A Gutierrez, Jorge Documet, Lawrence Chan, *et al.*, The role of a data grid in worldwide imaging-based clinical trials, *J High Speed Networks* 1–13, 2006.
5. Law MYY, A model of DICOM-based electronic patient record in radiation therapy, *J Comp Med Imag Graphics* **29**(2–3): 125–136, 2006.
6. Lemke H, Summary of the white paper of DICOM WG24, *Proc SPIE Medical Imaging*, pp. 6516–6522, February, 2007.
7. Chiu J, Savitz MH, Use of laser in minimally invasive spinal surgery and pain management, in Kambin P (ed.), *Arthroscopic and Endoscopic Spinal Surgery — Text and Atlas*, 2nd ed., Humana Press, New Jersey, Vol. 13, pp. 259–269, 2005.
8. Chiu J, Technological developments for computer assisted endoscopic minimally invasive spinal surgery (MISS), *Proceedings Computer Assisted Radiology and Surgery*, 20th International Congress, Osaka, Japan, June 28–July 1, 2006.
9. Chiu J, Savitz M, Multicenter study of percutaneous endoscopic discectomy, in Savitz M, Chiu J, Rauschning W, Yeung A (eds.), *The Practice of Minimally Invasive Spinal Technique*: 2005 Edition, AAMISS Press, New City, New York, pp. 622–626, 2005.
10. Huang HK, PACS, Informatics, and the neurosurgery command module, *J Mini Invasive Spinal Technique* **1**: 62–67, 2001.
11. Chiu JC, Savitz MH, Operating room of the future for spinal procedures, in Savitz MH, Chiu JC, Rauschning W, Yeung AT (eds.), *The Practice of Minimally Invasive Spinal Technique*, AAMISS Press, NY, pp. 645–648, 2005.